

JAERI - M
92-053

(INDC(JPN)-159 L)

COMPARISON OF
DOUBLE-DIFFERENTIAL NEUTRON EMISSION CROSS SECTIONS
CALCULATED FROM EVALUATED NUCLEAR DATA LIBRARIES
WITH EXPERIMENTAL DATA

April 1992

Tokio FUKAHORI, Satoshi CHIBA and Tetsuo ASAMI*

JAE RI-M reports are issued irregularly.
Inquiries about availability of the reports should be addressed to Information Division
Department of Technical Information, Japan Atomic Energy Research Institute, Tokaimura,
Naka-gun, Ibaraki-ken 319-11, Japan.

Comparison of
Double-differential Neutron Emission Cross Sections
Calculated from Evaluated Nuclear Data Libraries
with Experimental Data

Tokio FUKAHORI, Satoshi CHIBA and Tetsuo ASAMI^{*}

Department of Physics
Tokai Research Establishment
Japan Atomic Energy Research Institute
Tokai-mura, Naka-gun, Ibaraki-ken

(Received March 5, 1992)

The energy-angle double differential cross sections of emitted neutrons (DDXs) from neutron induced reactions are fundamental data for fusion neutronics calculation. The third version of Japanese Evaluated Nuclear Data Library (JENDL-3) was produced aiming at the applications related to the fission neutronics as well as fusion reactors. In order to check the reliability of the evaluated data, the DDX data for 32 elements from lithium to uranium calculated from JENDL-3 were compared with experimental data and values calculated from other two major evaluated nuclear data libraries, ENDF/B-VI and JEF-2. The comparison was made at the neutron incident energies of 4.2, 5.4, 6.0, 14.1 and 18.0 MeV, and at the angles of 30°, 60°, 90°, 120° and 150°. It was found that the DDX data calculated from JENDL-3 could reproduce overall trend of experimentally observed values. However, some discrepancies were also recognized.

Keywords: Nuclear Data, JENDL-3, Evaluation, Experimental Data, Neutron, Data Review, Double Differential Cross Section, Fusion Neutronics

* Nuclear Energy Data Center

中性子放出二重微分断面積の実験値と評価値の比較

日本原子力研究所東海研究所物理部

深堀 智生・千葉 敏・浅見 哲夫*

(1992年3月5日受理)

中性子放出二重微分断面積は核融合ニュートロニクス計算の基礎データとなる。わが国の評価済核データライブラリー第3版(JENDL-3)は核分裂だけでなく核融合も用にも使用できるよう作成された。JENDL-3の評価値の信頼度を検討するために、リチウムからウランまでの32元素の二重微分断面積についてENDF-B-VI及びJEFF-2とともにJENDL-3の評価済核データと実験データ比較を行った。比較を行った入射中性子のエネルギーは4.2, 5.4, 6.0, 14.1, 18.0MeV、放出角度は30°, 60°, 90°, 120°, 150°である。JENDL-3の評価済核データは大部分で実験値との良い一致を示したが、いくつかの相違点が確認された。

東海研究所：〒319-11 茨城県那珂郡東海村白方字白根2-4

* (財)原子力データセンター

Contents

1. Introduction	1
2. Brief Description of Data Processing	2
3. Graphs and Discussions	4
3.1 Lithium	5
3.2 Beryllium	27
3.3 Boron	31
3.4 Carbon	38
3.5 Nitrogen	45
3.6 Oxygen	51
3.7 Fluorine	58
3.8 Sodium	62
3.9 Magnesium	66
3.10 Aluminum	70
3.11 Silicon	77
3.12 Sulphur	81
3.13 Calcium	85
3.14 Titanium	89
3.15 Vanadium	93
3.16 Chromium	97
3.17 Manganese	101
3.18 Iron	105
3.19 Cobalt	112
3.20 Nickel	116
3.21 Copper	123
3.22 Zirconium	130
3.23 Niobium	137
3.24 Molybdenum	141
3.25 Tin	145
3.26 Antimony	149
3.27 Tantalum	153
3.28 Tungsten	157
3.29 Lead	161
3.30 Bismuth	165
3.31 Thorium	169
3.32 Uranium	183

4. Concluding Remarks	197
Acknowledgements	200
References	200
Appendix Brief Manual of Code 'PLDDX'	201

目 次

1. 緒 言	1
2. データ処理	2
3. 図及び議論	4
3. 1 リチウム	5
3. 2 ベリリウム	27
3. 3 ホウ素	31
3. 4 炭 素	38
3. 5 空 素	45
3. 6 酸 素	51
3. 7 フッ素	58
3. 8 ナトリウム	62
3. 9 マグネシウム	66
3.10 アルミニウム	70
3.11 硅 素	77
3.12 イオウ	81
3.13 カルシウム	85
3.14 チタン	89
3.15 バナジウム	93
3.16 クロム	97
3.17 マンガン	101
3.18 鉄	105
3.19 コバルト	112
3.20 ニッケル	116
3.21 銅	123
3.22 ジルコニウム	130
3.23 ニオブ	137
3.24 モリブデン	141
3.25 錫	145
3.26 アンチモン	149
3.27 タンタル	153
3.28 タングステン	157
3.29 鉛	161

3.30	ビスマス	165
3.31	トリウム	169
3.32	ウラン	183
4.	結 言	197
	謝 辞	200
	参考文献	200
付	録 PLDDX コードの簡易マニュアル	201

1. Introduction

Transport of high energy neutrons plays an important role in determining major characteristics of fusion reactor blankets and structural components: Aging due to radiation damage, nuclear heating distributions, accumulated activities, shielding capability and tritium breeding ratio are governed by nuclear reactions induced by fast neutrons. Double differential neutron emission cross sections (DDXs) of nuclear reactions induced by neutrons are fundamental and important data used in fusion neutronics calculations. Recent evaluated nuclear data libraries, e.g. JENDL-3¹⁾, ENDF/B-VI²⁾, JEF-2³⁾, have been produced to meet the above requirements. On the other hand, the DDXs have been actively measured by Osaka university and Tohoku university⁵⁻¹⁴⁾. Therefore, it is beneficial to make a comprehensive comparison of DDXs calculated from JENDL-3 with those from other evaluated nuclear data libraries and the experimental data. From these comparisons, it is expected that some information on the reliability and possible improvements of the data given in JENDL-3 will be derived.

A DDX data processing code, PLDDX, for the ENDF-4, -5 and -6 format data was developed in the present work. The DDXs calculated from JENDL-3 are compared with those from ENDF/B-VI and JEF-2, and the experimental data of Osaka and Tohoku universities. The considered elements and isotopes are ^{6,7}Li, ⁹Be, ^{10,11}B, C, N, ¹⁶O, ¹⁹F, ²³Na, Mg, ²⁷Al, Si, S, Ca, Ti, V, Cr, ⁵⁵Mn, Fe, Co, Ni, Cu, Zr, ⁹³Nb, Mo, Sn, Sb, W, ¹⁸¹Ta, Pb, ²⁰⁹Bi, Th and U. Five angles, 30°, 60°, 90°, 120°, and 150° in the laboratory system, are selected for the comparison, and the incident neutron energies are 4.2, 5.4 and 14.1 MeV for ⁶Li, 5.4, 6.0 and 14 MeV for ⁷Li, 14.1 and 18.0 MeV for C, ¹⁶O, ²⁷Al, Fe, Ni, Cu and Zr, 1.20, 2.03, 4.25, 6.10 and 14.1 MeV for Th and U, and 14 MeV for the others.

In chapter 2, the data processing method and the PLDDX code are briefly described. In chapter 3, graphs of DDXs are presented for each nuclide, and brief discussions are also given. Concluding remarks are given in the chapter 4.

2. Brief Description of Data Processing

Data processing was performed for the evaluated and experimental data. The data processing code, PLDDX, was developed to check validity of DDX stored in evaluated nuclear data libraries in a simple manner, without too much data processing work. This code has roughly two functions. One is process of evaluated data; to read the evaluated data and to calculate DDX with the method described below. The other function is experimental data handling; to read in experimental DDX data stored in the EXFOR-type format, and to write them onto a disk file in a special format called 'transmission format'. These outputs are used as input data of a plotting code, SPLINT⁴⁾, which was used to generate the graphs shown in this report.

The quantities of the evaluated data considered in PLDDX are the elastic scattering (MT=2), the discrete inelastic scattering (MT=51 to 90), the continuum inelastic scattering (MT=91), the ($n,2n$) reaction (MT=16), the ($n,3n$) reaction (MT=17), the ($n,n\alpha$) reaction (MT=22) and the (n,np) reaction (MT=28). For the fissionable nuclides, fission neutron spectra can be also considered. The evaluated data of cross sections (MF=3), angular distributions (MF=4), energy spectra (MF=5) and energy-angle distributions (MF=6) in the ENDF-4, -5 or -6 format file are used to calculate DDXs. The results of the DDX calculations are written onto a disk file with the same specifications as MF=3 of the ENDF-5 format.

Let $\sigma(E-E'',\mu)$ the DDX at incident energy E , secondary energy E'' and emission angle $\cos^{-1}(\mu)$ calculated from evaluated data by PLDDX. The resolution broadening is applied to this quantity to be compared with the experimental data, by the following relation;

$$\sigma_{\text{obs}}(E-E',\mu) = \int \sigma(E-E'',\mu) \cdot G(E',E'') \cdot dE'' \quad (1)$$

where $G(E',E'')$ denotes the normalized resolution function, $\sigma_{\text{obs}}(E-E',\mu)$ the 'observable' DDX affected by resolution broadening with the secondary neutron energy E' . In PLDDX, the function G has two components, corresponding to energy and timing resolutions of the time-of-flight experiments. Both are expressed by Gaussian functions centered at E'' , but the latter has a width varying with E'' . In this work, the widths were empirically determined to reproduce the width of the elastic scattering peak

measured at 90°.

The fission neutron spectra were considered only for uranium data of JENDL-3. Other details of data processing are described in each section of in chapter 3. A brief manual of the PLDDX code is given at appendix.

3. Graphs and Discussions

In this chapter, graphs of comparisons between the evaluated and experimental data are shown for each nuclides, and some discussion is given. In general, the DDXs calculated from JENDL-3, ENDF,-VI and JEF-2 are illustrated by solid, dotted and dashed lines, respectively, while the experimental data measured at Osaka and Tohoku universities are marked by circles and triangles, respectively.

3.1 Lithium

Comparisons of DDXs at the angles of 30° , 60° , 90° , 110° and 135° for ^6Li at the incident energies of 4.2 and 5.4 MeV are shown in Figs.1 and 2. The experimental data/CHIBA('84)/ exist only in the continuum region. The evaluated data reproduce the experimental data.

Figure 3 shows the DDXs of ^6Li at 30° , 60° , 90° , 120° and 150° at 14.1 MeV/MATSUYAMA+('89)/. At this incident energy, the JENDL-3 data agree with the experimental data at all angles excellently. The ENDF/B-VI data cannot reproduce lower part of the energy spectra at all the angles, while the JEF-2 data give small values in the 6-10 MeV region at the forward angles. On the contrary, the JEF-2 data are larger than the experimental data at the backward angles.

The DDXs of ^7Li at 5.4 and 6.0 MeV/CHIBA('84)/ at the emitted angles of 30° , 60° , 90° , 110° and 135° are shown in Figs.4 and 5. The experimental data exist only in the continuum region. The DDXs calculated from the three libraries can reproduce the experimental data.

The DDXs calculated from the evaluated data of ^7Li are compared with the experimental data at 30° , 60° , 75° , 120° and 150° for ^7Li /CHIBA('84)/ at the incident neutron energy of 14.2 MeV in Fig.6. Figure 7 shows those of 30° , 60° , 80° , 120° and 150° for ^{nat}Li /TAKAHASHI('86)/, whose incident energies change according to scattered angles. Both figures indicate that the data of JENDL-3 reproduce the experimental data at all the angles but other two libraries give small values in the neutron energy region just below the second peak (the first inelastic scattering peak) at the forward angles.

References for the Experimental Data in Figures

- CHIBA('84) : Chiba S., Baba M., Nakashima H., Ono M., Yabuta N., Yukinori S. and Hirakawa N., J. Nucl. Sci. Technol., 22, 771 (1985)
- MATSUYAMA+('89): Baba M., Matsuyama S., Fujisawa M., Iwasaki T., Iwasaki S. and Sakamoto R., JAERI-M 90-025, 383 (1990).
- TAKAHASHI+('86): Takahashi A., JAERI-M 86-029, 99 (1986).

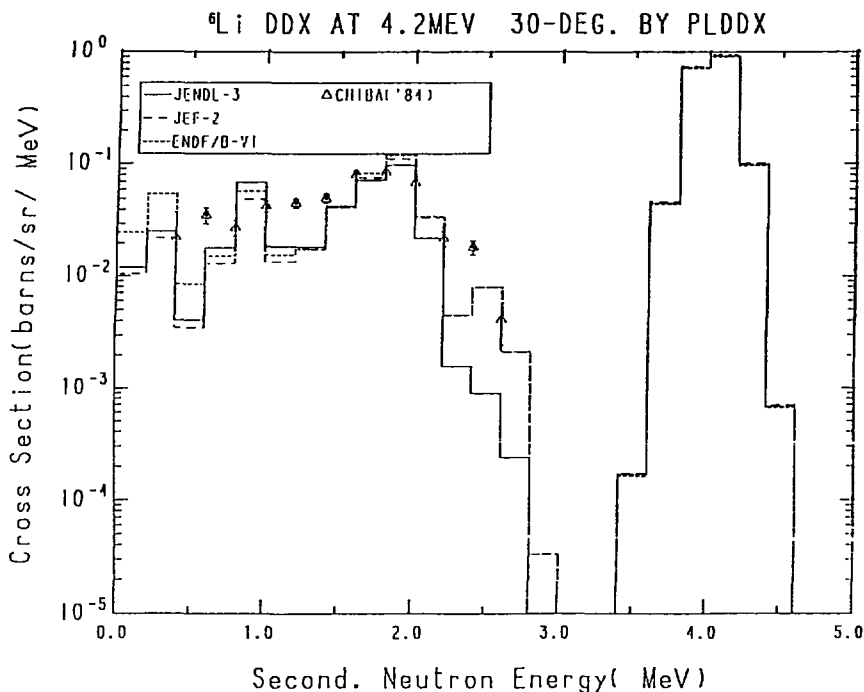


Fig. 1-1 The ${}^6\text{Li}$ Double Differential Cross Section at 4.2 MeV,
Emitted Angle = 30° in Laboratory System

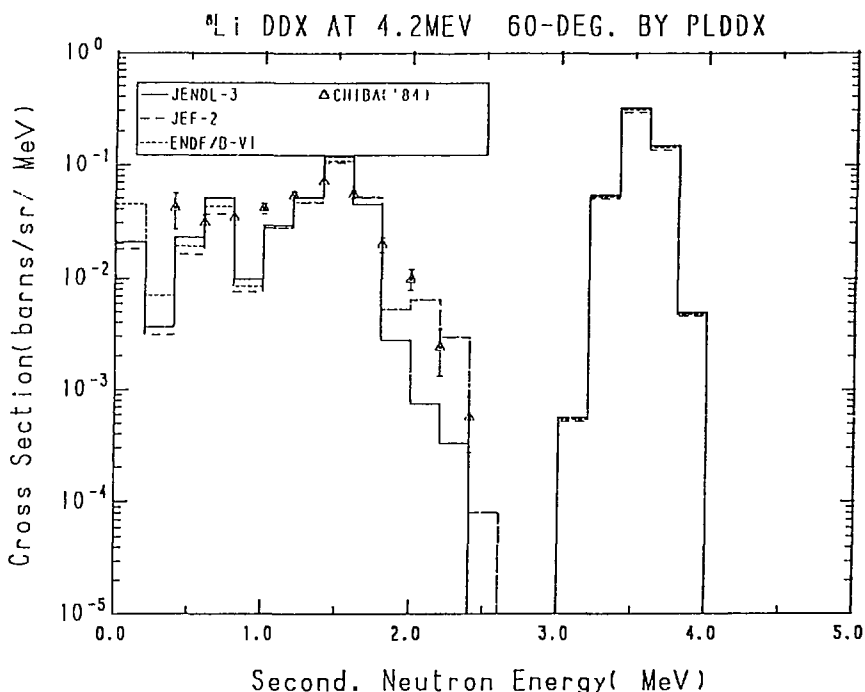


Fig. 1-2 The ${}^6\text{Li}$ Double Differential Cross Section at 4.2 MeV,
Emitted Angle = 60° in Laboratory System

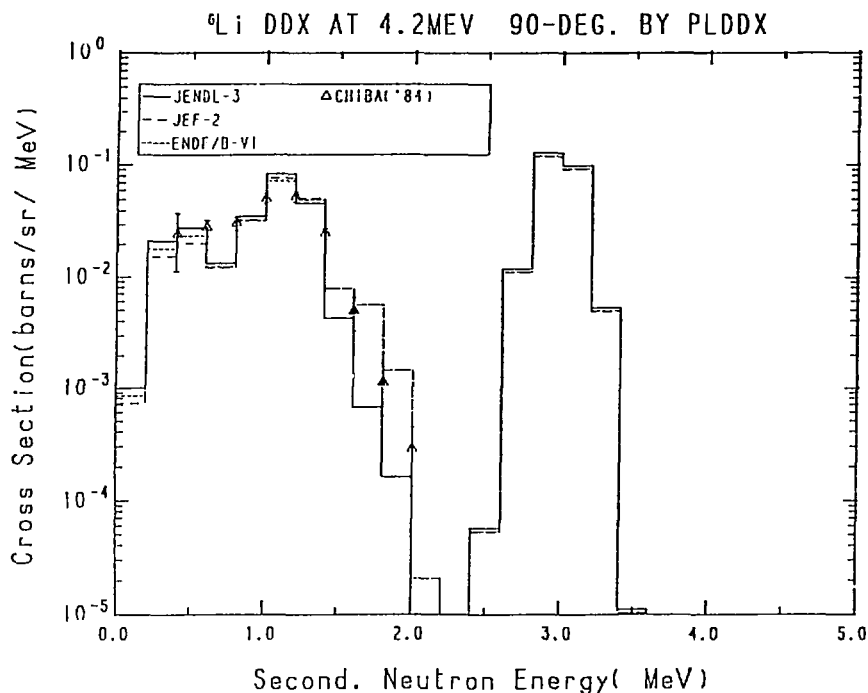


Fig. 1-3 The ${}^6\text{Li}$ Double Differential Cross Section at 4.2 MeV,
Emitted Angle = 90° in Laboratory System

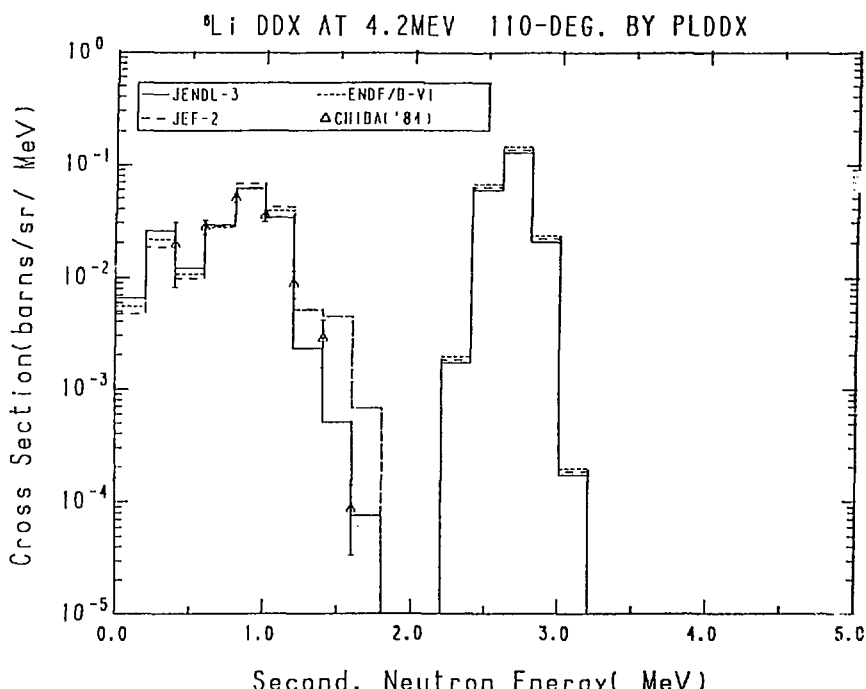


Fig. 1-4 The ${}^6\text{Li}$ Double Differential Cross Section at 4.2 MeV,
Emitted Angle = 110° in Laboratory System

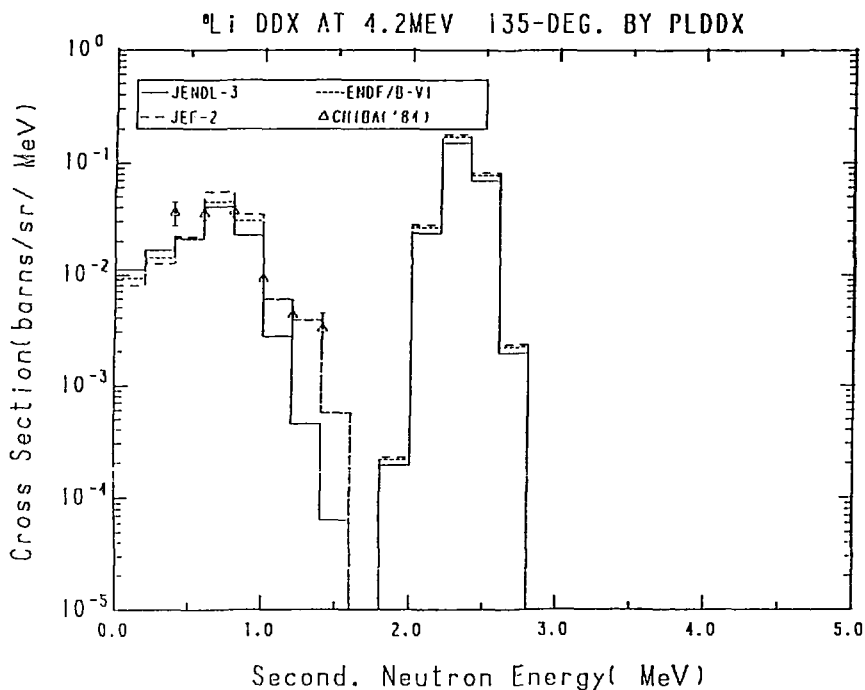


Fig. 1-5 The ^{6}Li Double Differential Cross Section at 4.2 MeV,
Emitted Angle = 135° in Laboratory System

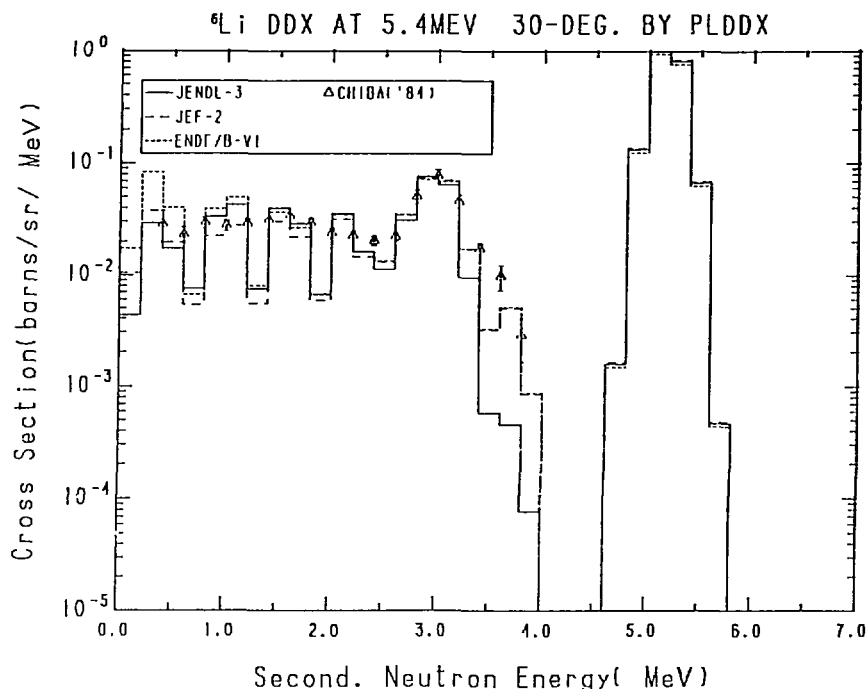


Fig. 2-1 The ${}^6\text{Li}$ Double Differential Cross Section at 5.4 MeV,
Emitted Angle = 30° in Laboratory System

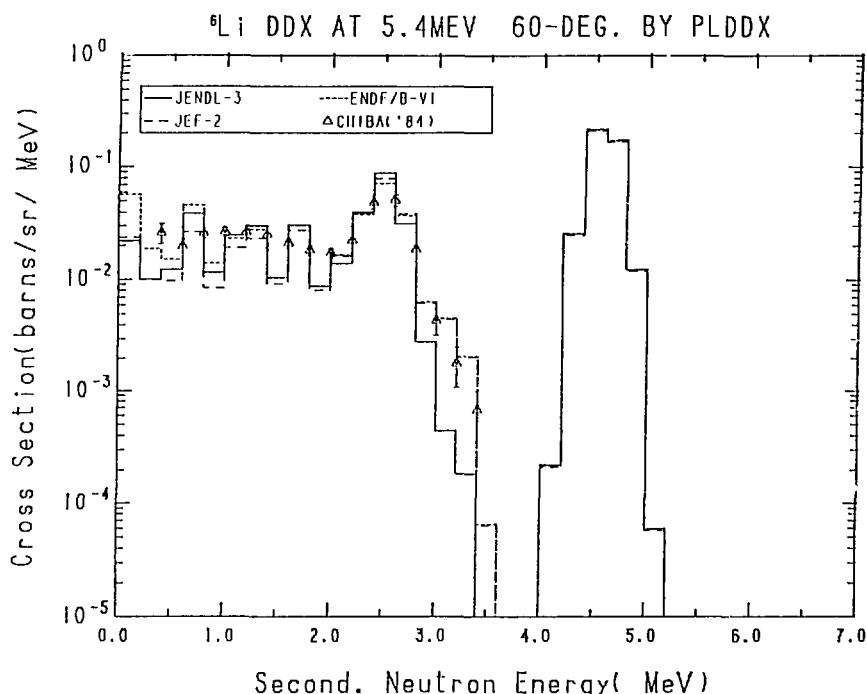


Fig. 2-2 The ${}^6\text{Li}$ Double Differential Cross Section at 5.4 MeV,
Emitted Angle = 60° in Laboratory System

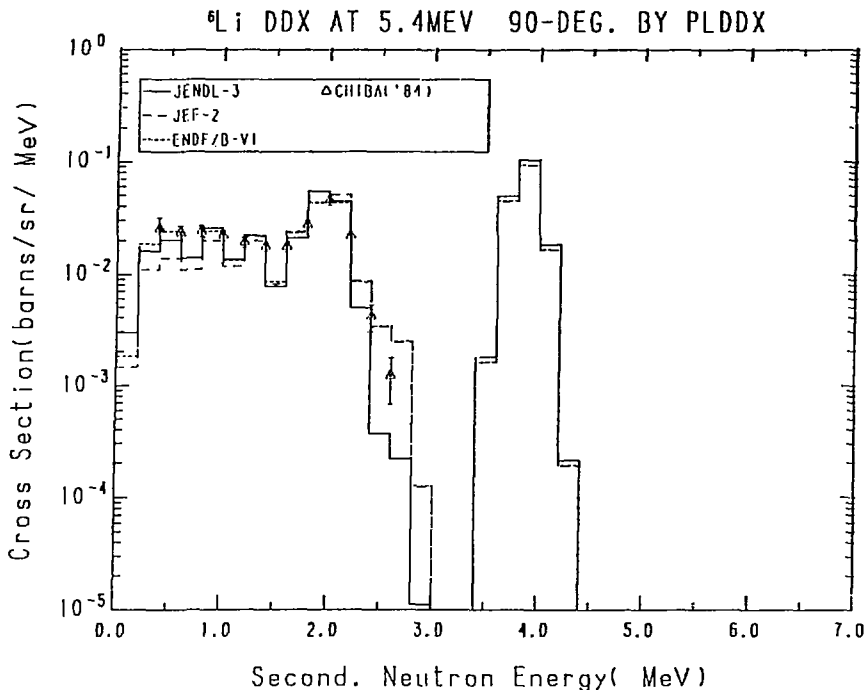


Fig. 2-3 The ${}^6\text{Li}$ Double Differential Cross Section at 5.4 MeV,
Emitted Angle = 90° in Laboratory System

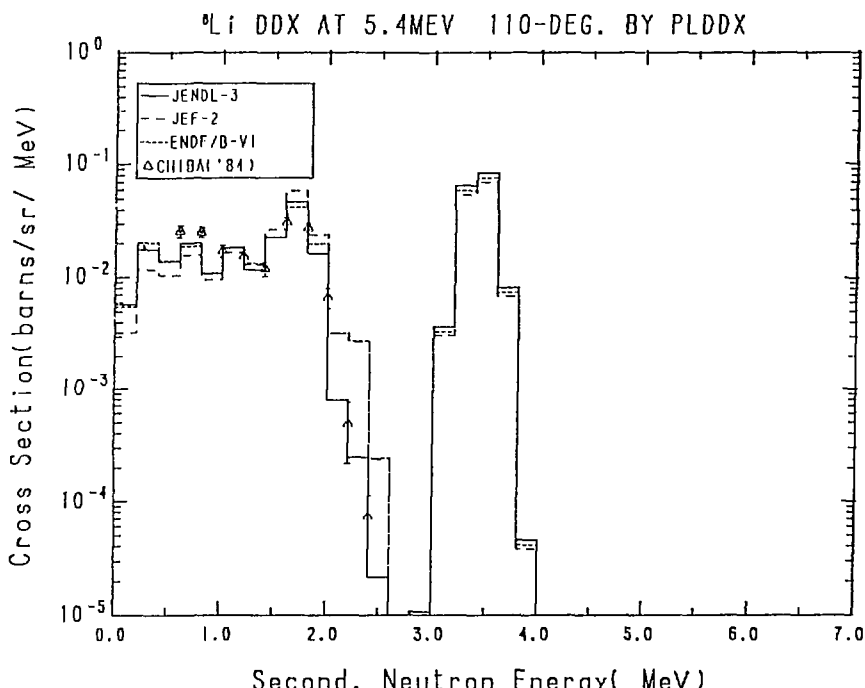


Fig. 2-4 The ${}^6\text{Li}$ Double Differential Cross Section at 5.4 MeV,
Emitted Angle = 110° in Laboratory System

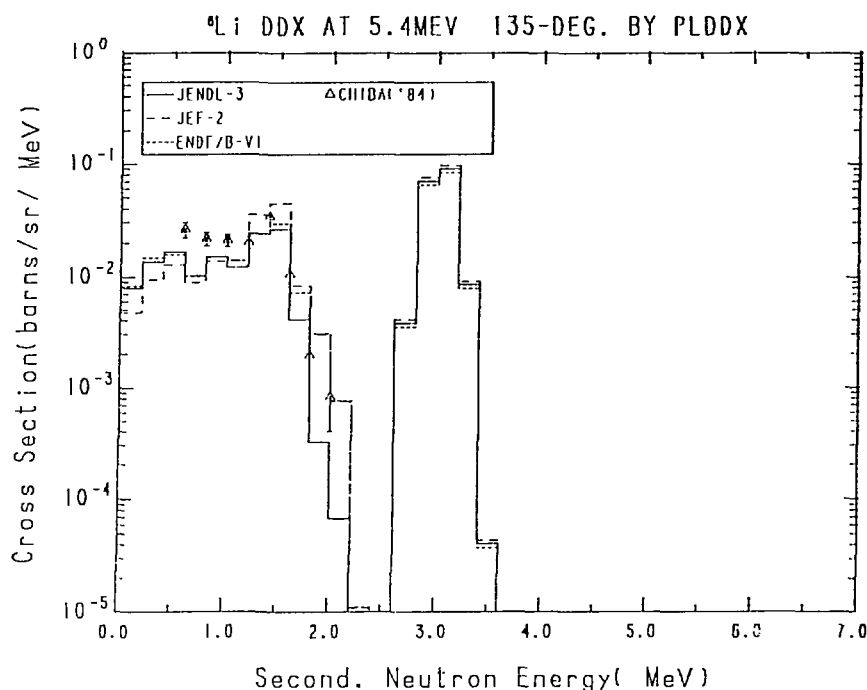


Fig. 2-5 The ${}^6\text{Li}$ Double Differential Cross Section at 5.4 MeV,
Emitted Angle = 135° in Laboratory System

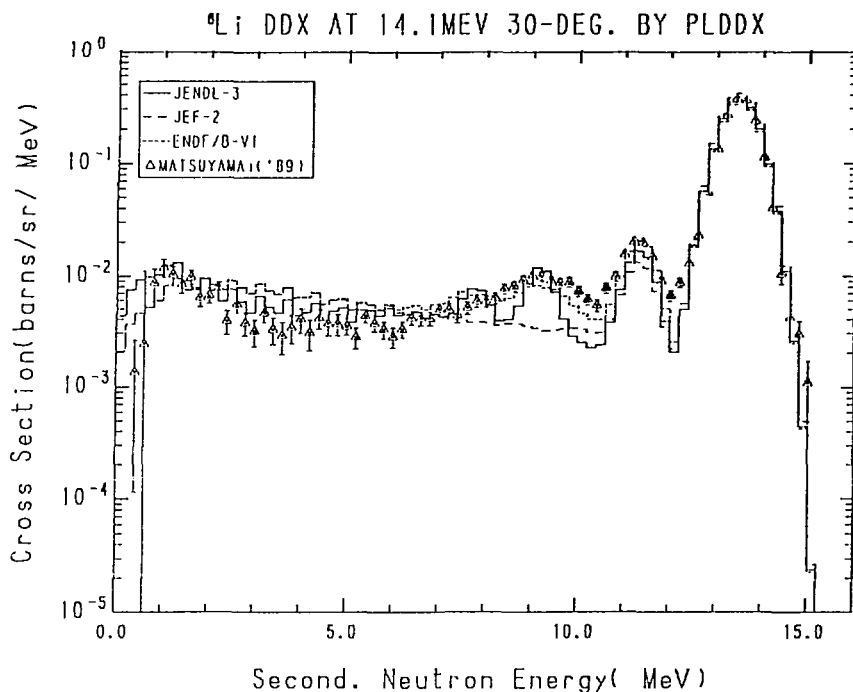


Fig. 3-1 The ${}^6\text{Li}$ Double Differential Cross Section at 14.1 MeV,
Emitted Angle = 30° in Laboratory System

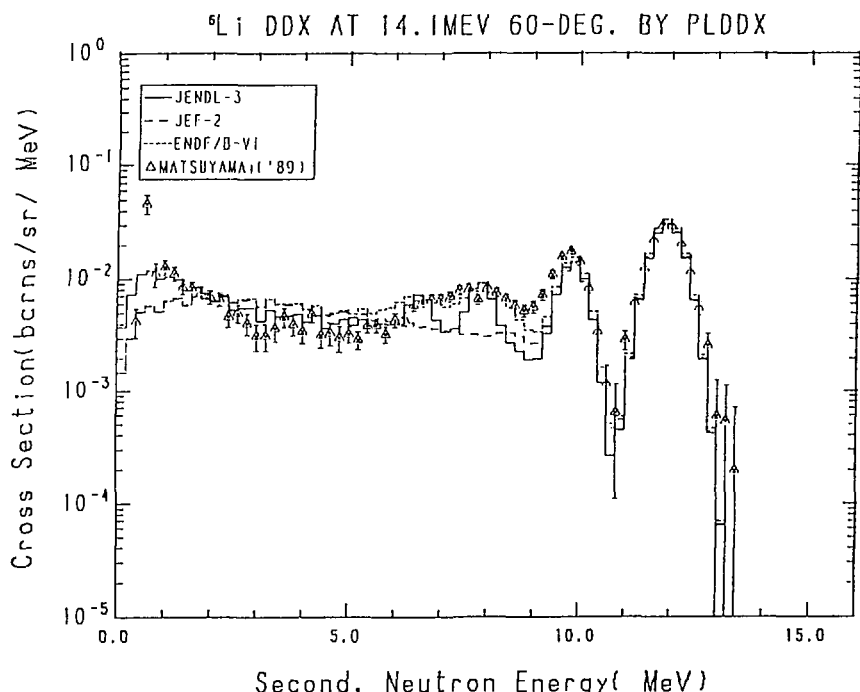


Fig. 3-2 The ${}^6\text{Li}$ Double Differential Cross Section at 14.1 MeV,
Emitted Angle = 60° in Laboratory System

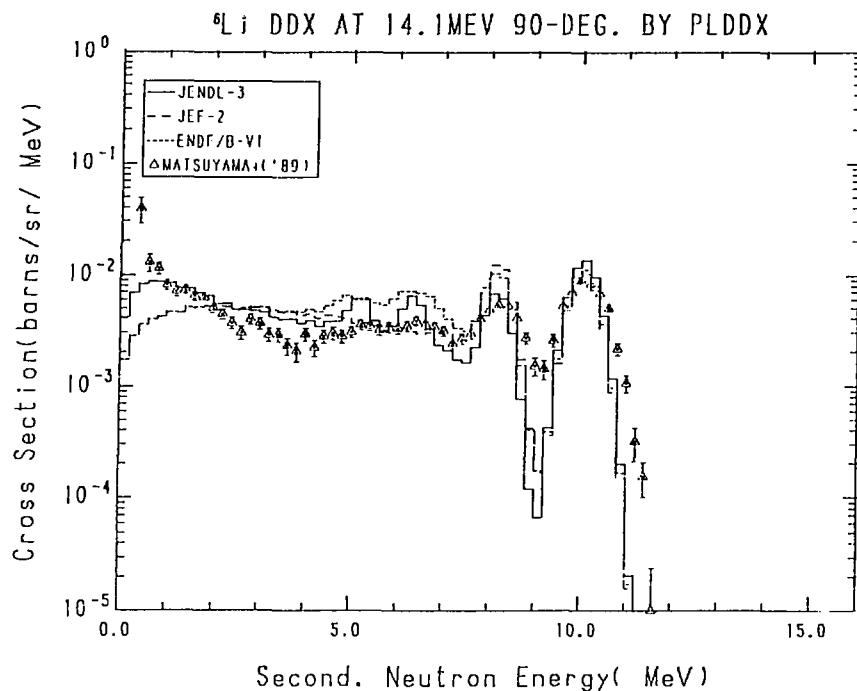


Fig. 3-3 The ${}^6\text{Li}$ Double Differential Cross Section at 14.1 MeV,
Emitted Angle = 90° in Laboratory System

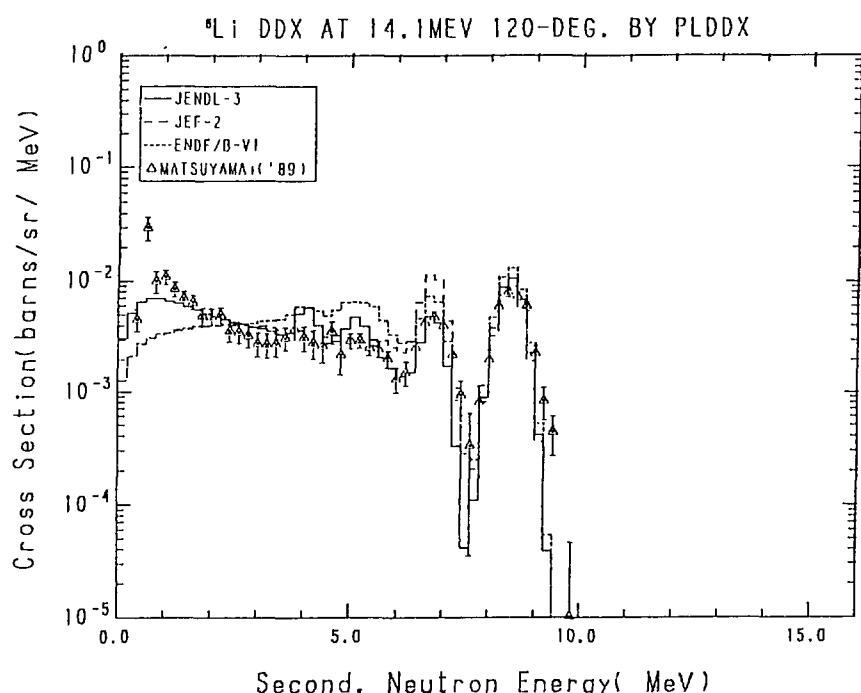


Fig. 3-4 The ${}^6\text{Li}$ Double Differential Cross Section at 14.1 MeV,
Emitted Angle = 120° in Laboratory System

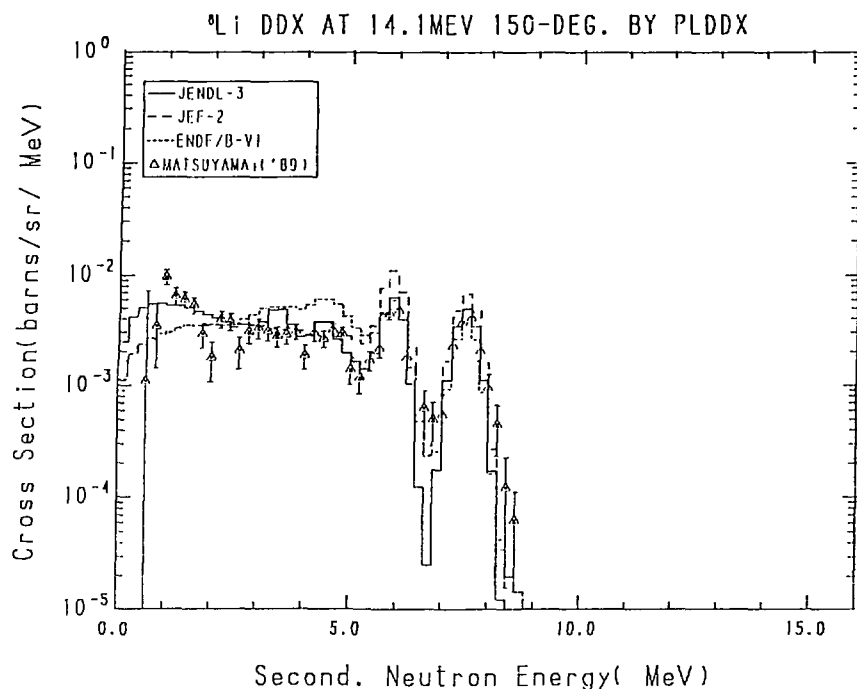


Fig. 3-5 The ${}^6\text{Li}$ Double Differential Cross Section at 14.1 MeV,
Emitted Angle = 150° in Laboratory System

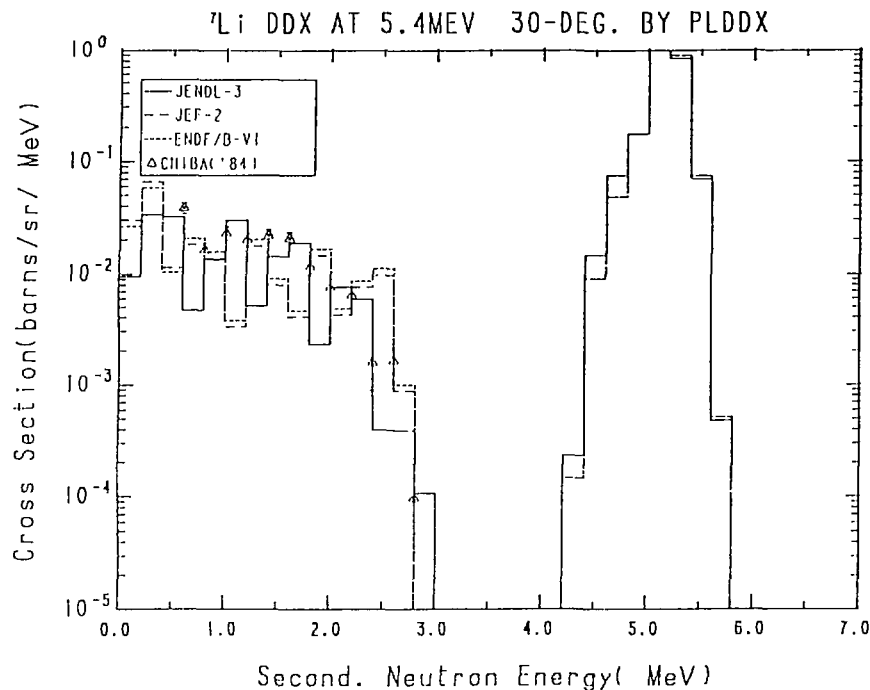


Fig. 4-1 The ${}^7\text{Li}$ Double Differential Cross Section at 5.4 MeV,
Emitted Angle = 30° in Laboratory System

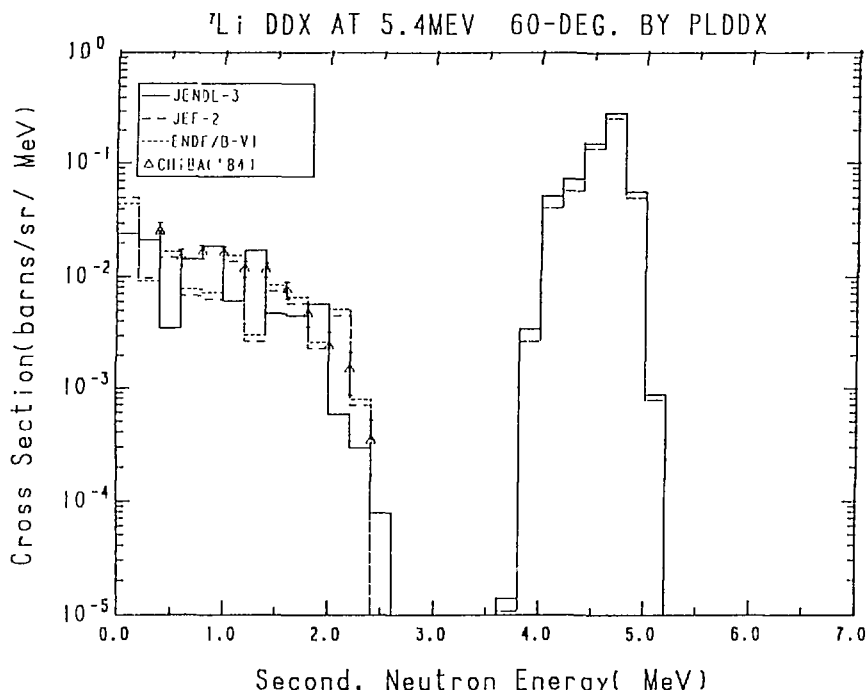


Fig. 4-2 The ${}^7\text{Li}$ Double Differential Cross Section at 5.4 MeV,
Emitted Angle = 60° in Laboratory System

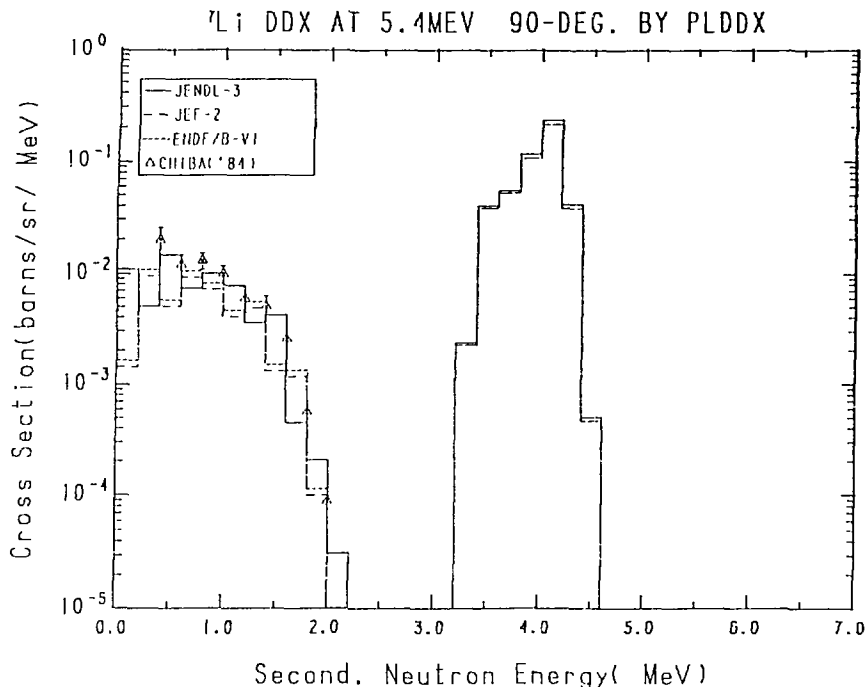


Fig. 4-3 The ${}^7\text{Li}$ Double Differential Cross Section at 5.4 MeV,
Emitted Angle = 90° in Laboratory System

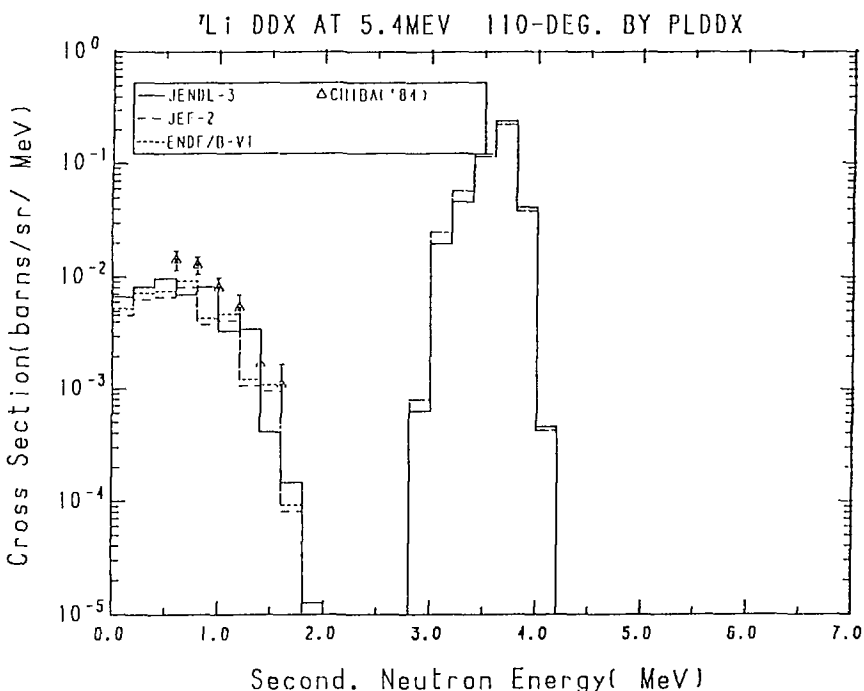


Fig. 4-4 The ${}^7\text{Li}$ Double Differential Cross Section at 5.4 MeV,
Emitted Angle = 110° in Laboratory System

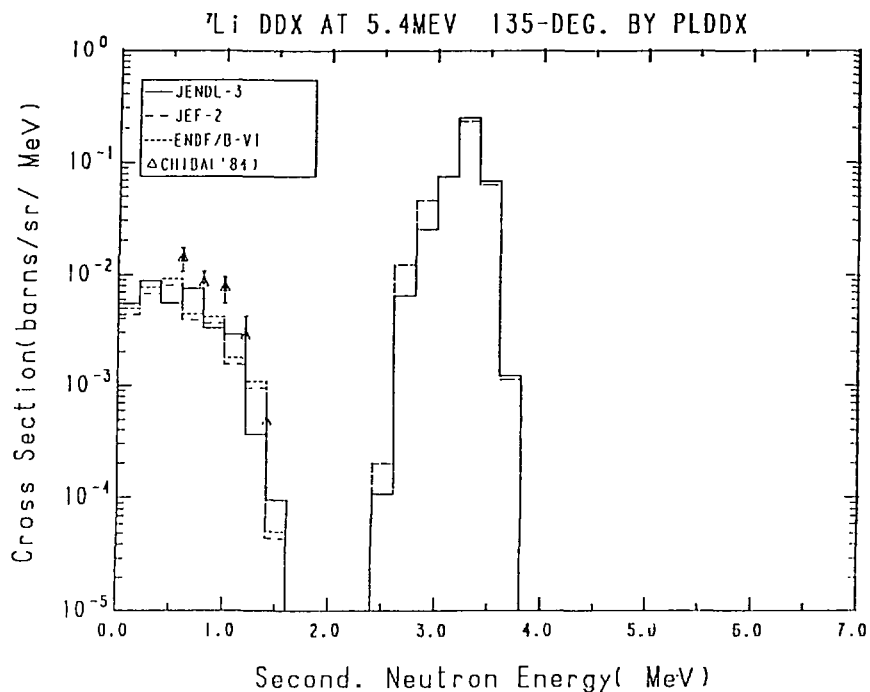


Fig. 4-5 The ^{7}Li Double Differential Cross Section at 5.4 MeV,
Emitted Angle = 135° in Laboratory System

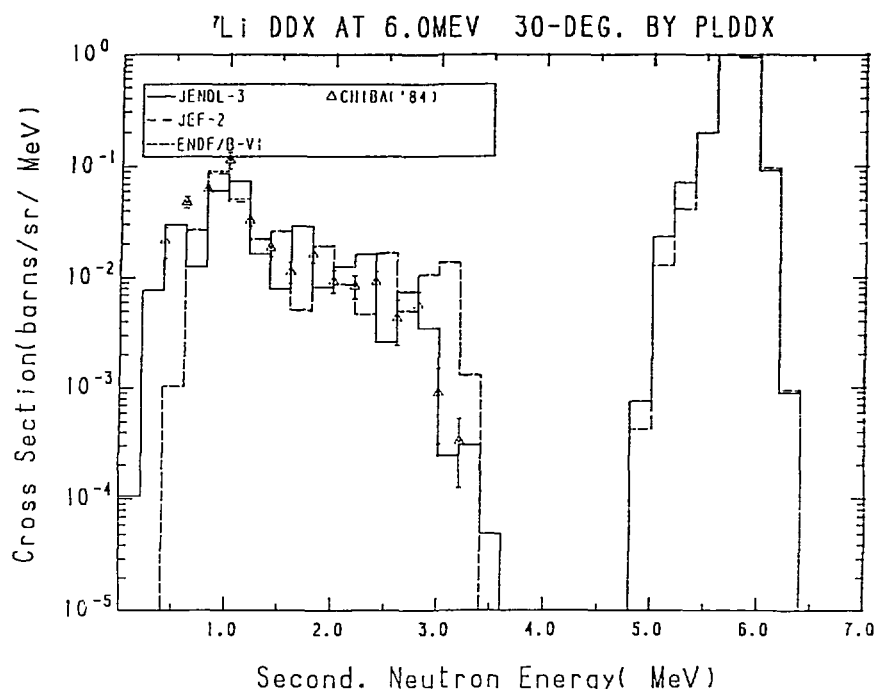


Fig. 5-1 The ${}^7\text{Li}$ Double Differential Cross Section at 6.0 MeV,
Emitted Angle = 30° in Laboratory System

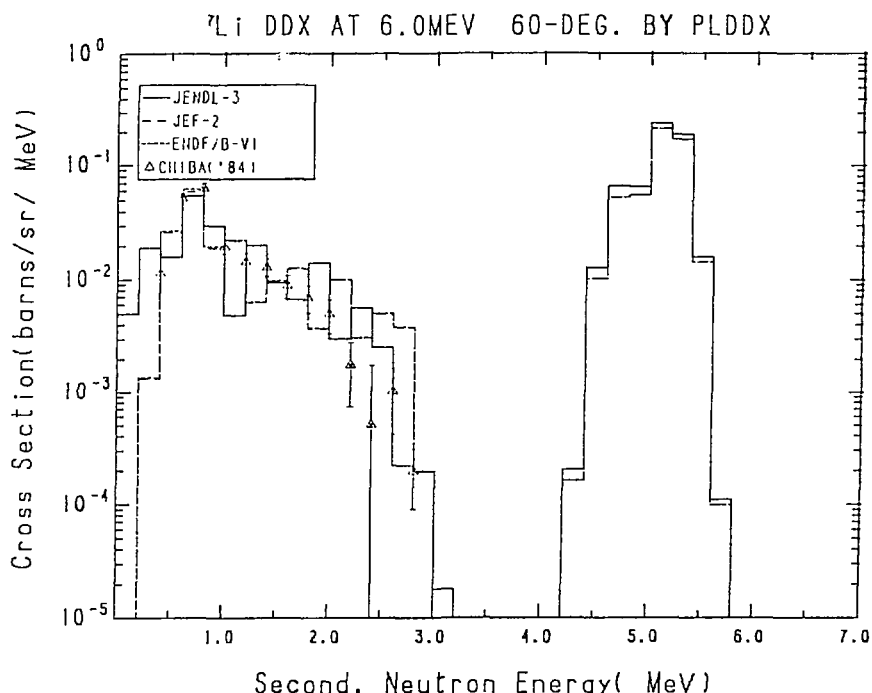


Fig. 5-2 The ${}^7\text{Li}$ Double Differential Cross Section at 6.0 MeV,
Emitted Angle = 60° in Laboratory System

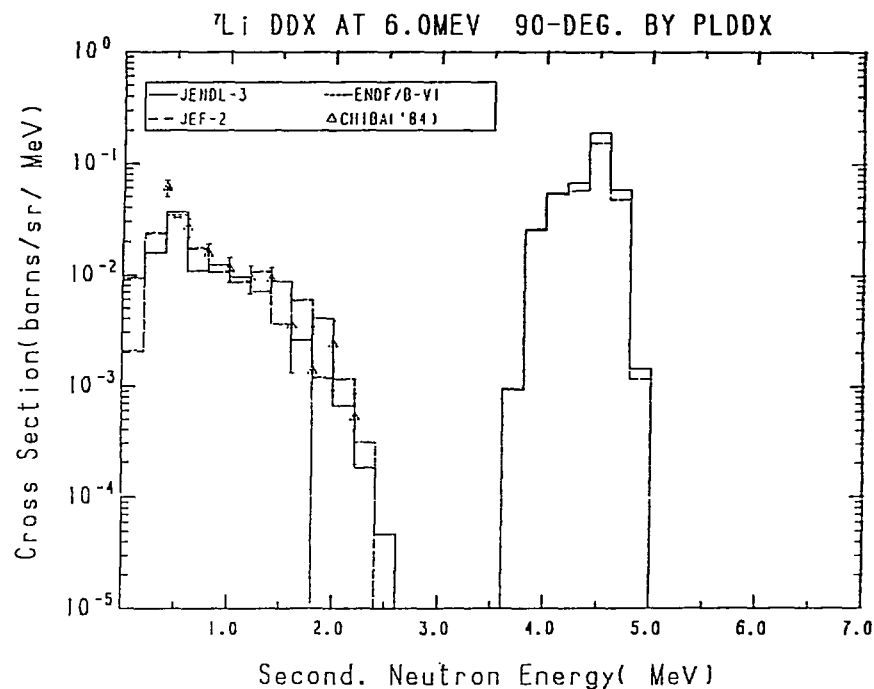


Fig. 5-3 The ^7Li Double Differential Cross Section at 6.0 MeV,
Emitted Angle = 90° in Laboratory System

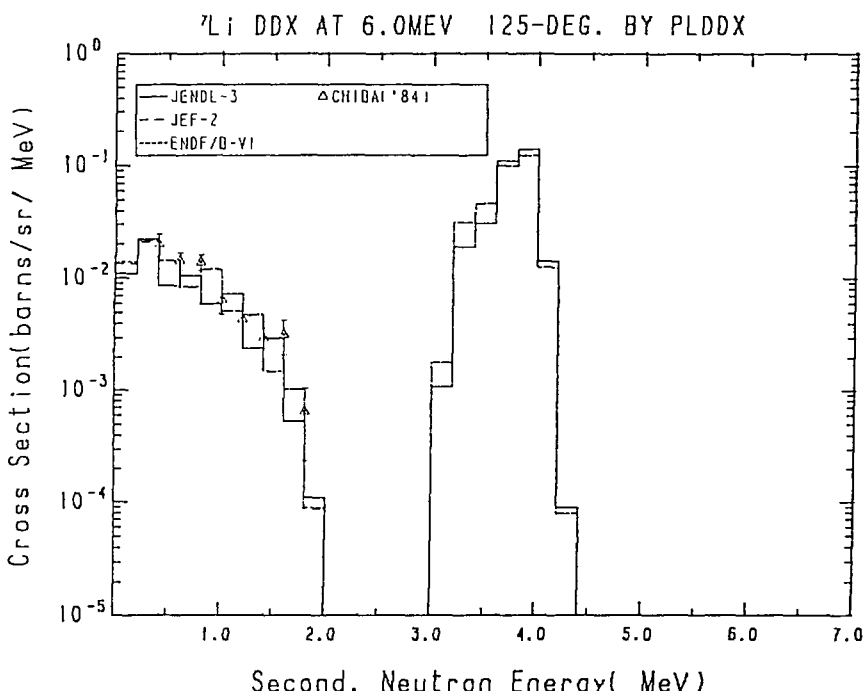


Fig. 5-4 The ^7Li Double Differential Cross Section at 6.0 MeV,
Emitted Angle = 125° in Laboratory System

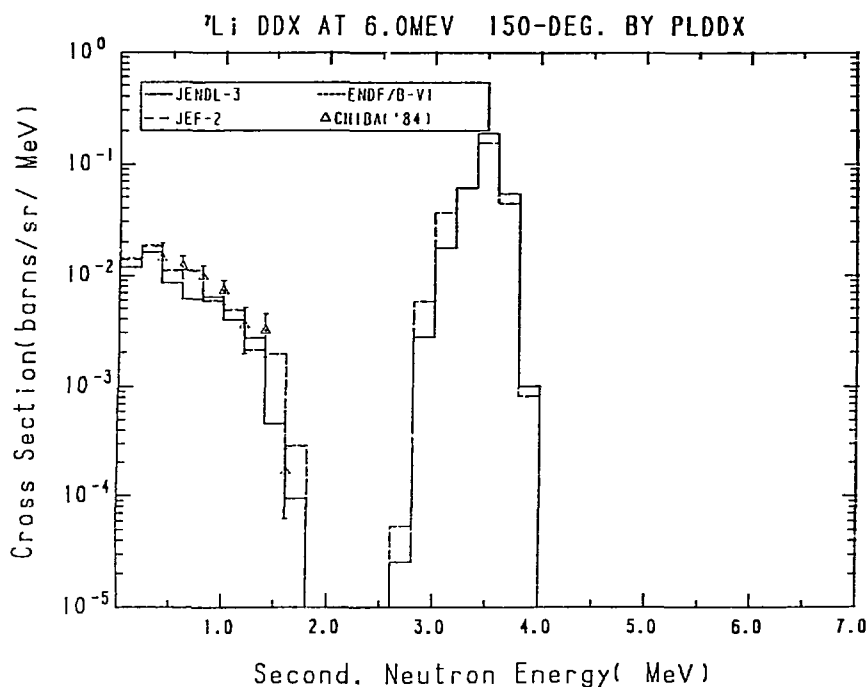


Fig. 5-5 The $^{7\text{Li}}$ Double Differential Cross Section at 6.0 MeV,
Emitted Angle = 150° in Laboratory System

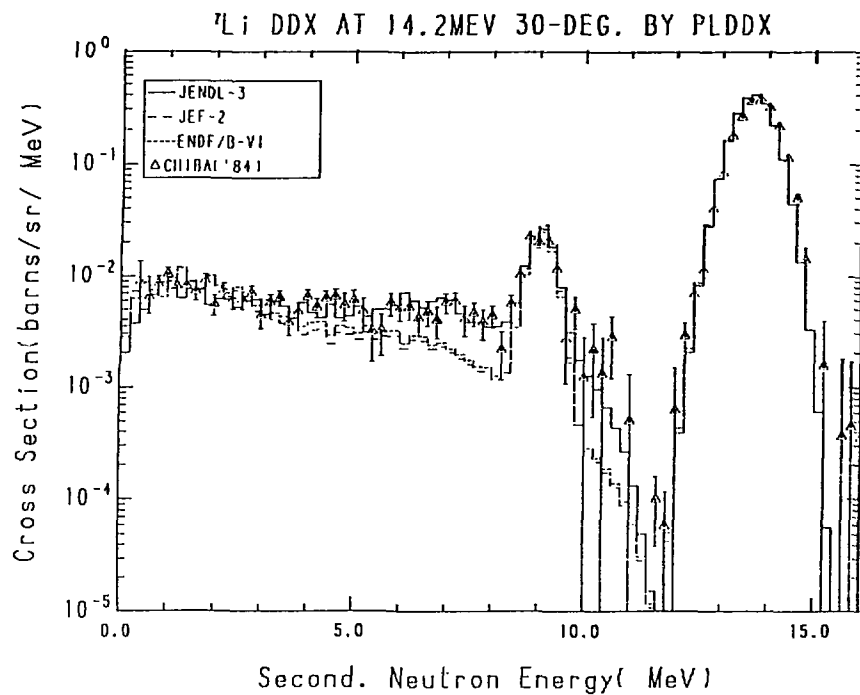


Fig. 6-1 The ^7Li Double Differential Cross Section at 14.2 MeV,
Emitted Angle = 30° in Laboratory System

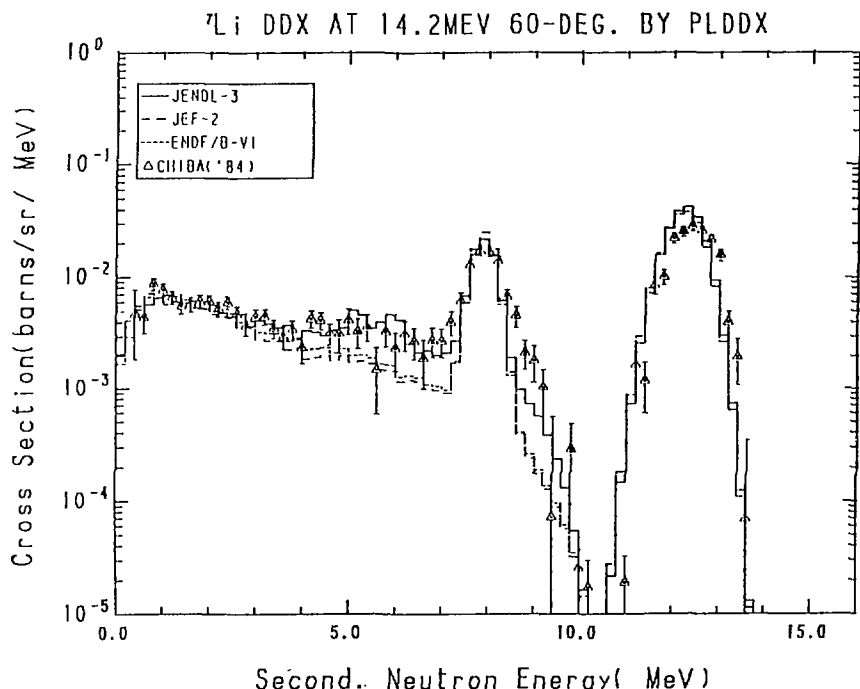


Fig. 6-2 The ^7Li Double Differential Cross Section at 14.2 MeV,
Emitted Angle = 60° in Laboratory System

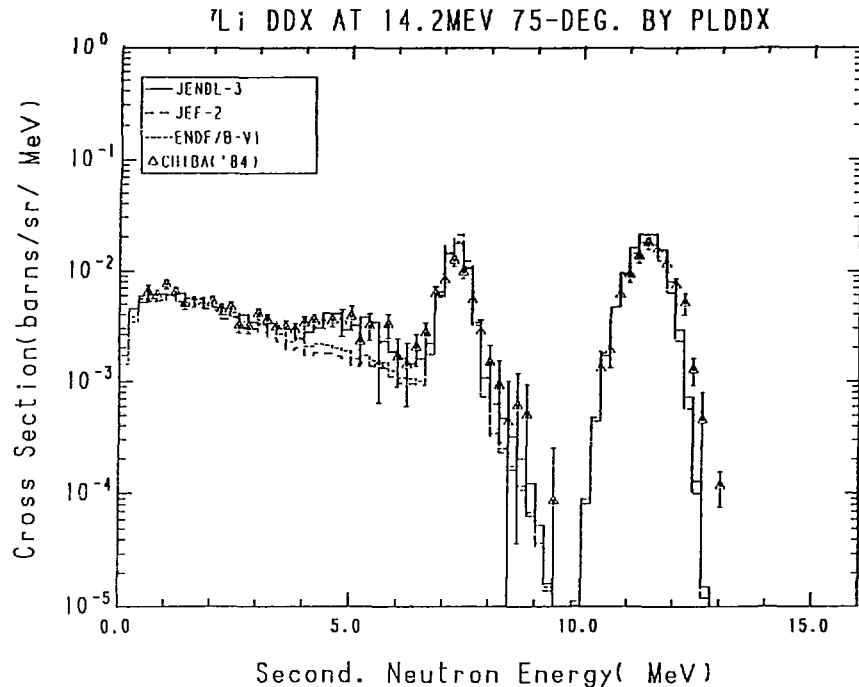


Fig. 6-3 The ^7Li Double Differential Cross Section at 14.2 MeV,
Emitted Angle = 75° in Laboratory System

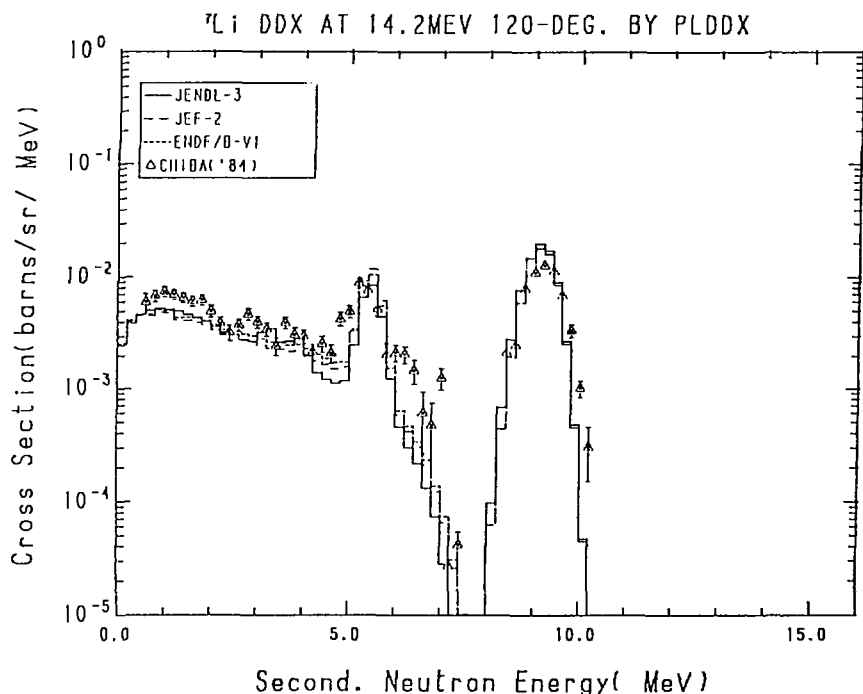


Fig. 6-4 The ^7Li Double Differential Cross Section at 14.2 MeV,
Emitted Angle = 120° in Laboratory System

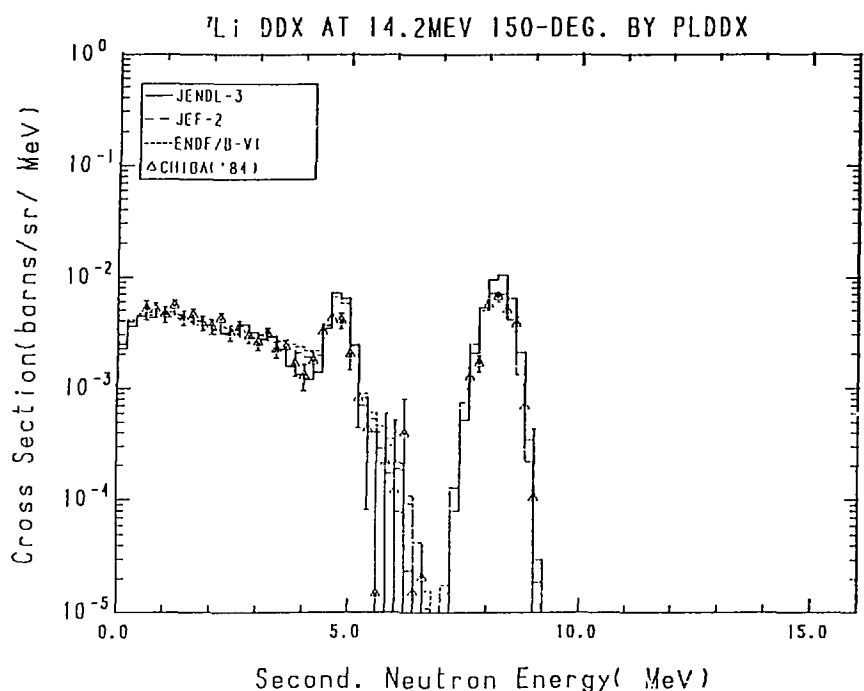


Fig. 6-5 The ^{7}Li Double Differential Cross Section at 14.2 MeV,
Emitted Angle = 150° in Laboratory System

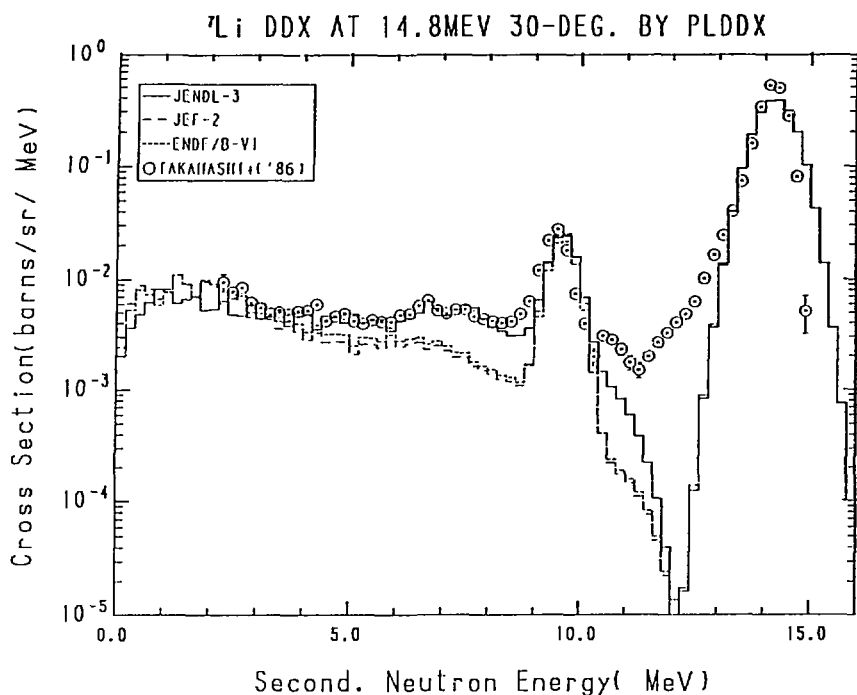


Fig. 7-1 The ${}^7\text{Li}$ Double Differential Cross Section,
Incident Energy = 14.8 MeV, Emitted Angle = 30°

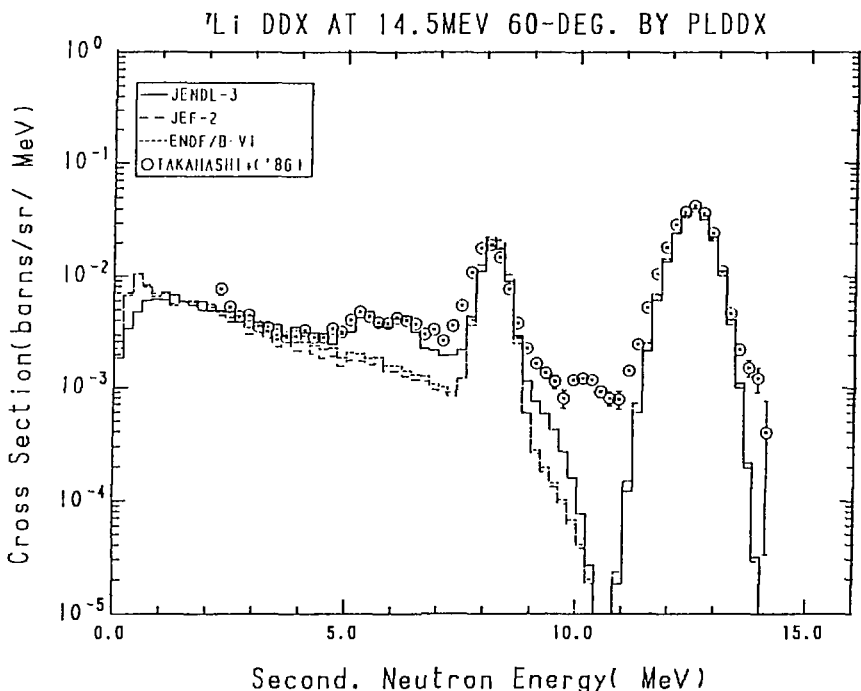


Fig. 7-2 The ${}^7\text{Li}$ Double Differential Cross Section,
Incident Energy = 14.5 MeV, Emitted Angle = 60°

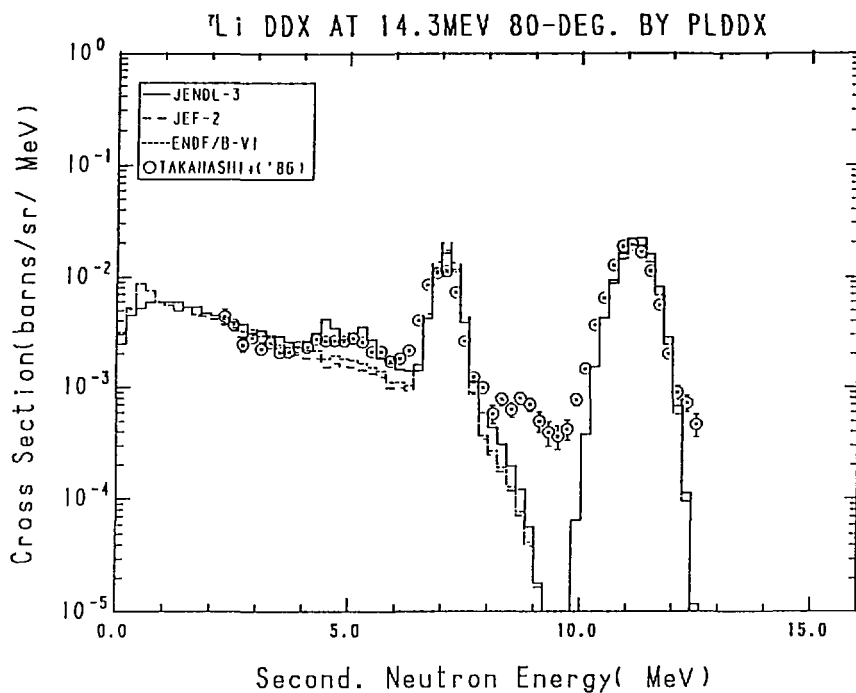


Fig. 7-3 The ^7Li Double Differential Cross Section,
Incident Energy = 14.3 MeV, Emitted Angle = 80°

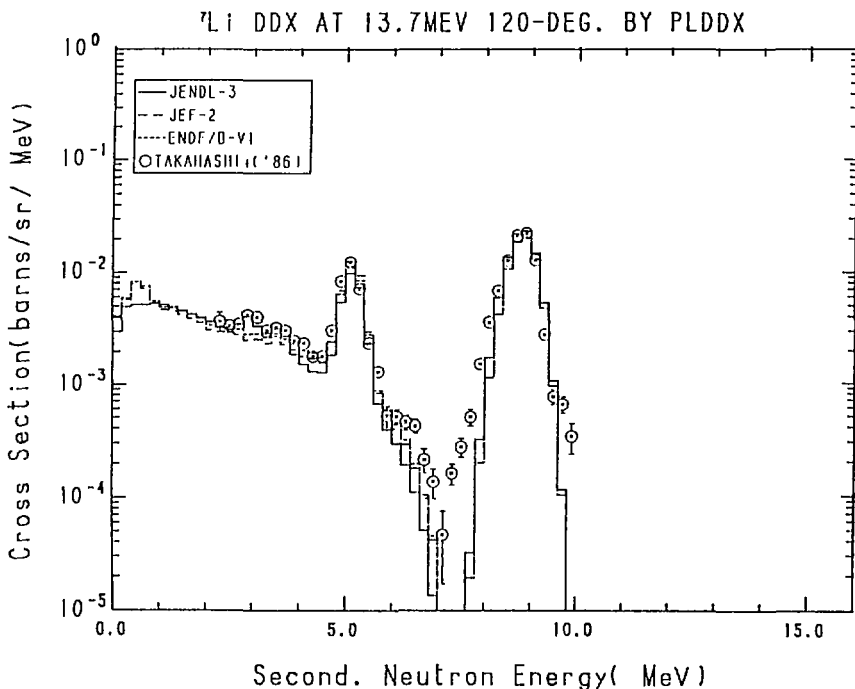


Fig. 7-4 The ^7Li Double Differential Cross Section,
Incident Energy = 13.7 MeV, Emitted Angle = 120°

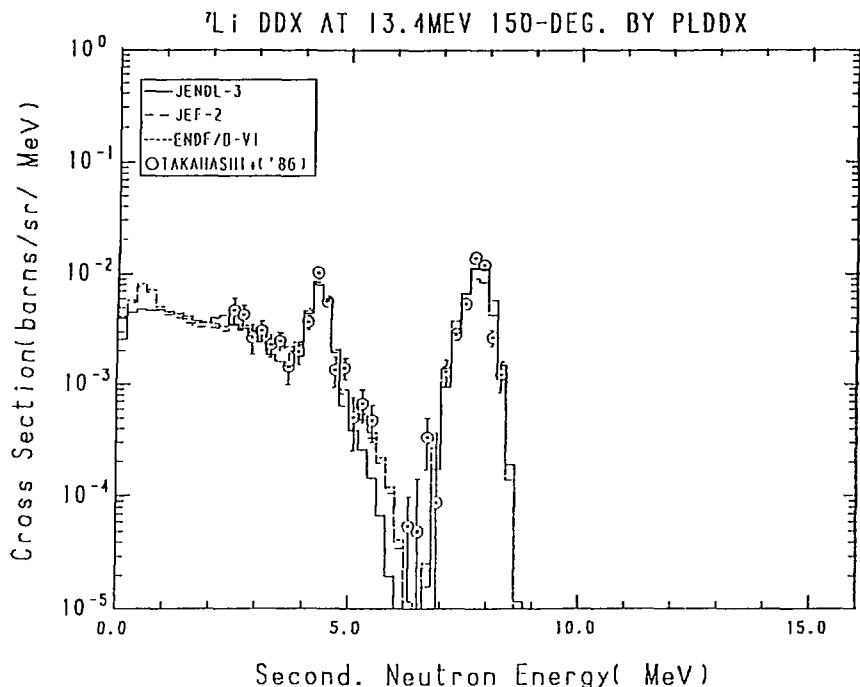


Fig. 7-5 The ${}^7\text{Li}$ Double Differential Cross Section,
Incident Energy = 13.4 MeV, Emitted Angle = 150°

3.2 Beryllium

The DDXs calculated from the evaluated data of ^9Be are compared with the experimental data at 30° , 60° , 100° , 120° and 150° at the incident neutron energy of 14.1 MeV/BABA+('88), TAKAHASHI+('87)/ in Fig.8. The JENDL-3 and ENDF/B-VI data agree with the experimental data satisfactorily, and the JEF-2 data underestimate at all the angles except for the elastic scattering peak. At the backward angles, a 'shoulder' appears above the elastic scattering peak in the DDXs calculated from JENDL-3. In JENDL-3, the continuum ($n, 2n$) neutron spectrum is given in MF=5, which cannot take account of the energy-angle correlation. Although it is shown that the data given in JENDL-3 can reproduce the overall trend of DDX for ^9Be , drawbacks of not employing MF=6 become clear.

References for the Experimental Data in Figures

- BABA+('88) : Baba M., Ishikawa M., Kikuchi T., Wakabayashi H. and Hirakawa N., Proc. of Int. Conf. on Nucl. Data for Sci. and Technol. at Mito in May 30- Jun. 3, p.209 (1988).
TAKAHASHI+('87): Takahashi A., private communication (1989).

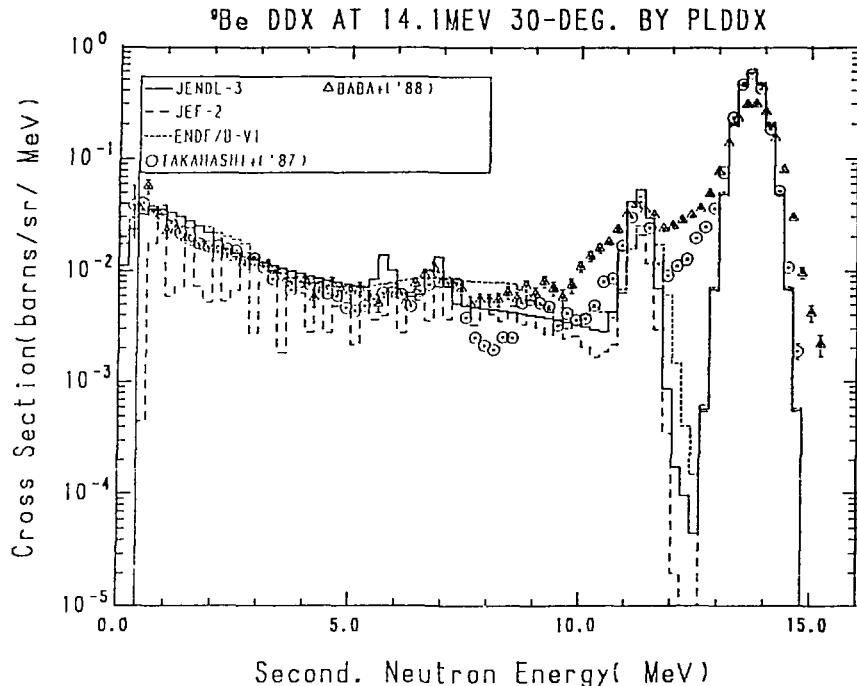


Fig. 8-1 The ${}^9\text{Be}$ Double Differential Cross Section at 14.1 MeV,
Emitted Angle = 30° in Laboratory System

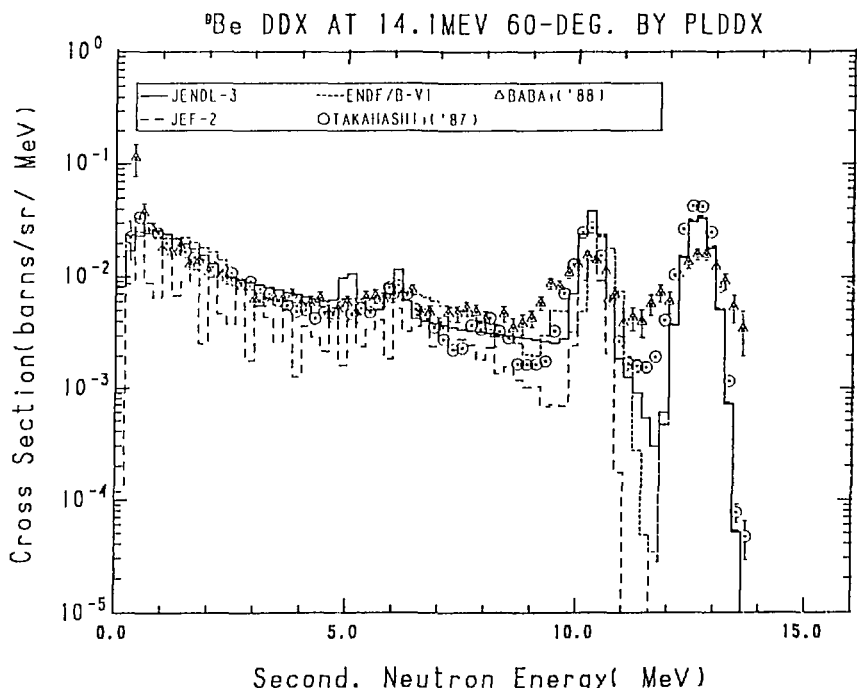


Fig. 8-2 The ${}^9\text{Be}$ Double Differential Cross Section at 14.1 MeV,
Emitted Angle = 60° in Laboratory System

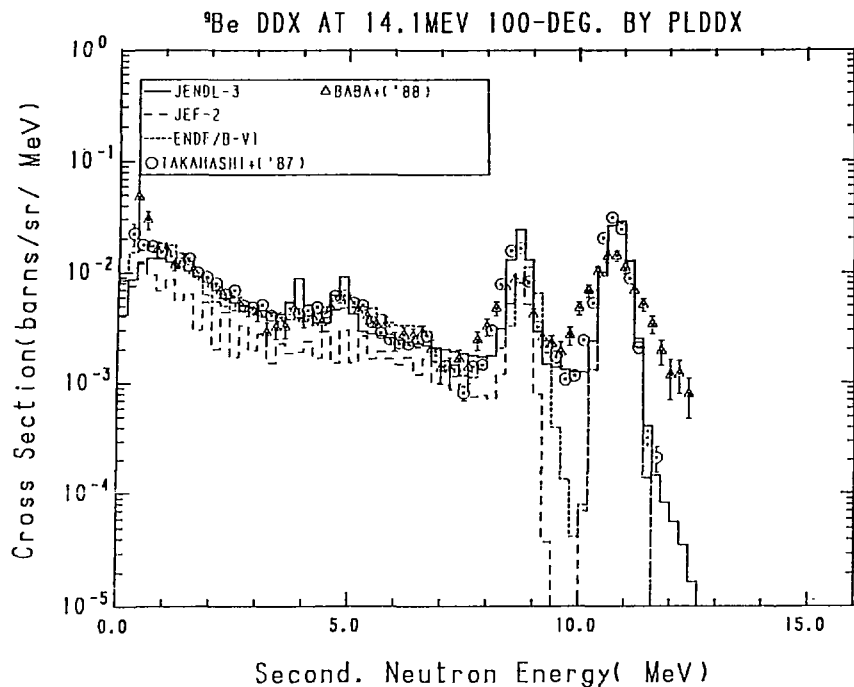


Fig. 8-3 The ⁹Be Double Differential Cross Section at 14.1 MeV,
Emitted Angle = 100° in Laboratory System

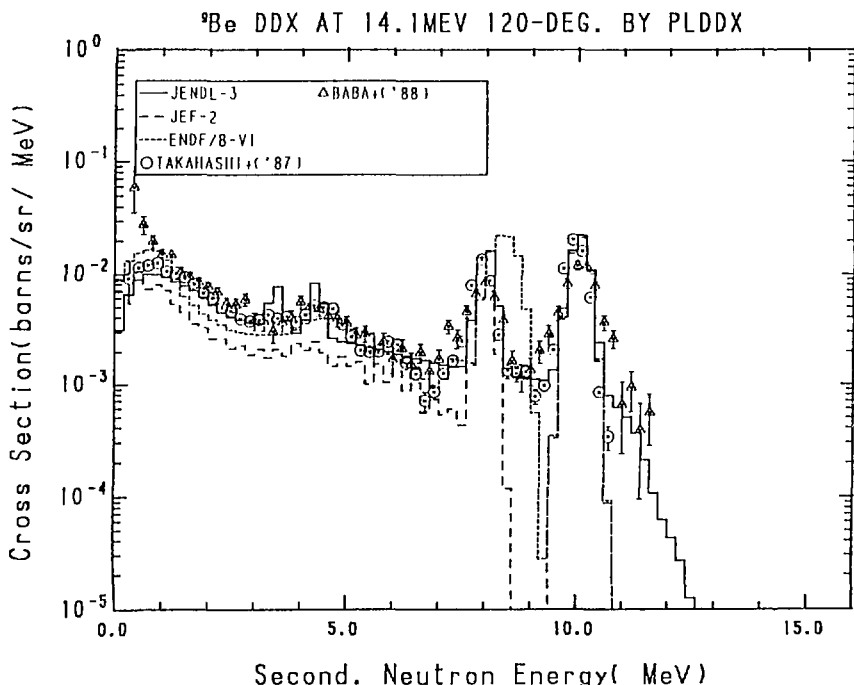


Fig. 8-4 The ⁹Be Double Differential Cross Section at 14.1 MeV,
Emitted Angle = 120° in Laboratory System

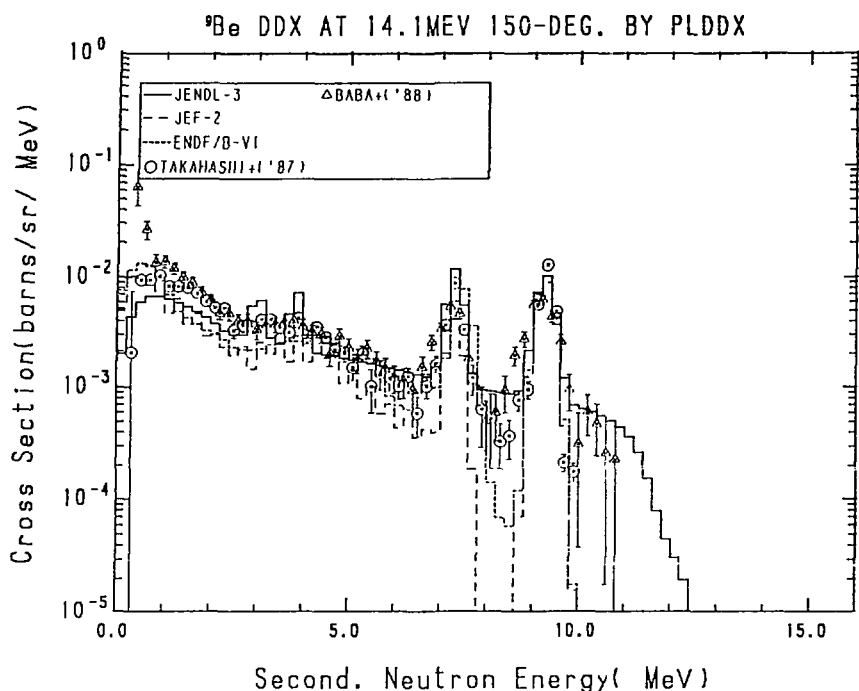


Fig. 8-5 The ⁹Be Double Differential Cross Section at 14.1 MeV,
Emitted Angle = 150° in Laboratory System

3.3 Boron

The DDXs calculated from the evaluated data of ^{10}B and ^{11}B at 30° , 60° , 100° , 120° and 150° at the incident neutron energy of 14.1 MeV are shown in Figs.9 and 10, respectively. Some discrepancies are observed between the two experimental data sets/BABA+('85),TAKAHASHI+('89)/. For ^{10}B , the elastic scattering peak of the data measured at Tohoku university is 0.5 MeV higher and broader than that of Osaka university and their magnitude significantly disagree with each other. The three evaluated data have almost the same trends and reproduce roughly the experimental data/ONO('85),TAKAHASHI+('88)/. For ^{11}B , the JENDL-3 data give lower values than the experimental data in the energy region below 2 MeV.

References for the Experimental Data in Figures

- BABA+('85) : Baba M., Ono M., Yabuta N., Kikuchi T. and Hirakawa N., Proc. of Int. Conf. on Nucl. Data for Basic and Applied Sci. at Santa Fe in May 13-17, p.223 (1985).
- ONO('85) : Baba M., Ono M., Yabuta N., Kikuchi T. and Hirakawa N., Proc. of Int. Conf. on Nucl. Data for Basic and Applied Sci. at Santa Fe in May 13-17, p.223 (1985).
- TAKAHASHI+('88): Takahashi A., private communication (1988).
- TAKAHASHI+('89): Takahashi A., private communication (1989).

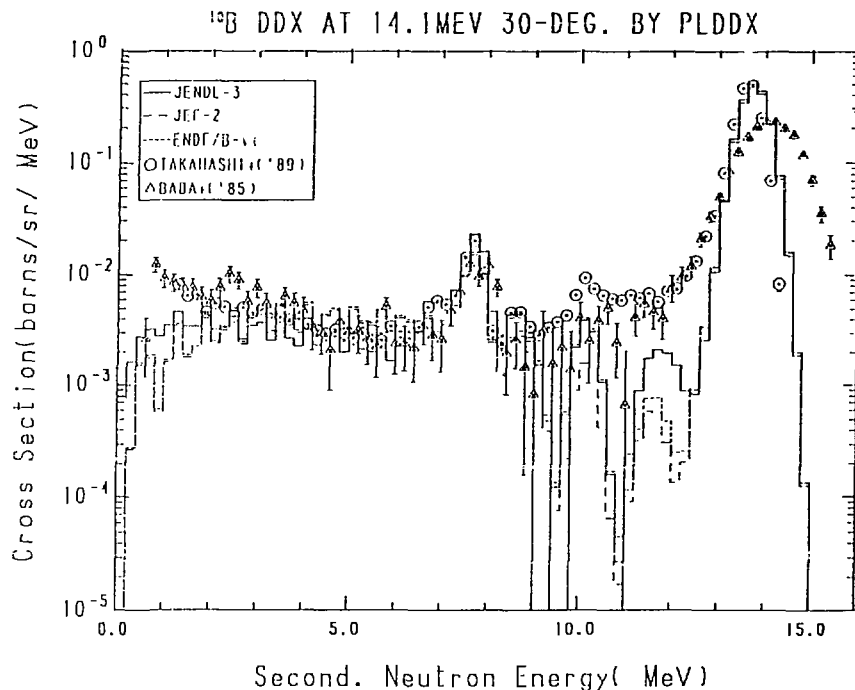


Fig. 9-1 The ^{10}B Double Differential Cross Section at 14.1 MeV,
Emitted Angle = 30° in Laboratory System

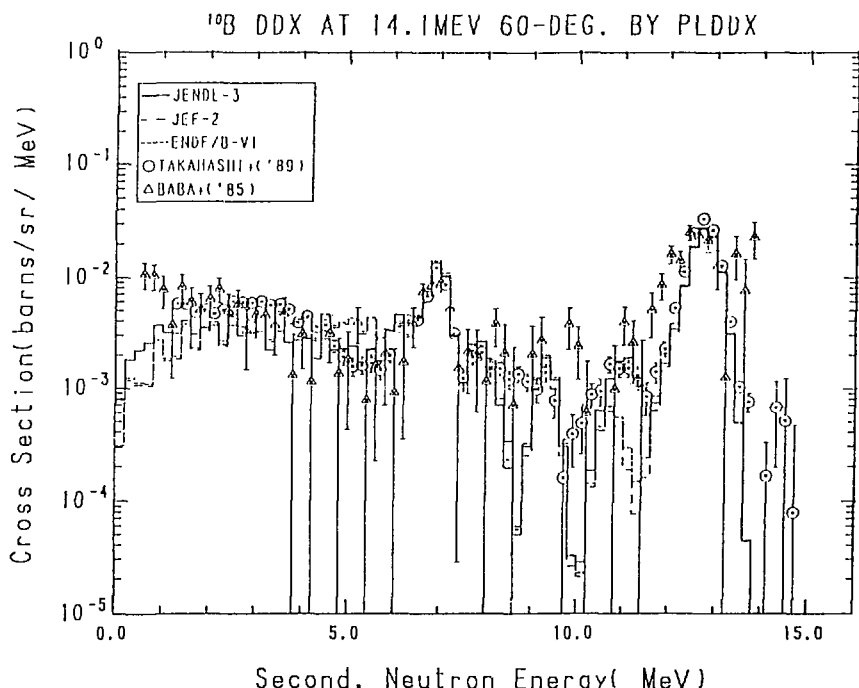


Fig. 9-2 The ^{10}B Double Differential Cross Section at 14.1 MeV,
Emitted Angle = 60° in Laboratory System

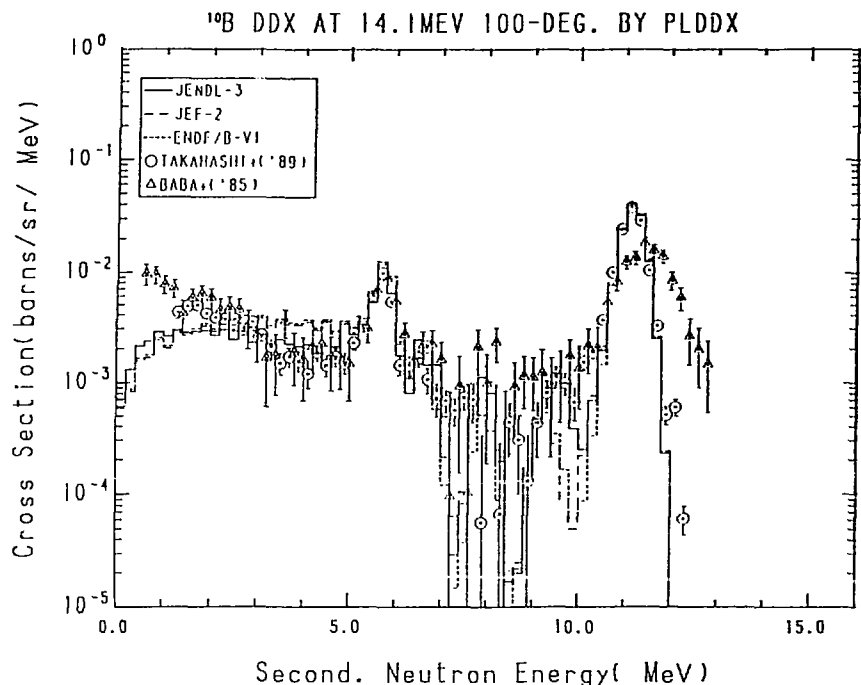


Fig. 9-3 The ^{10}B Double Differential Cross Section at 14.1 MeV,
Emitted Angle = 100° in Laboratory System

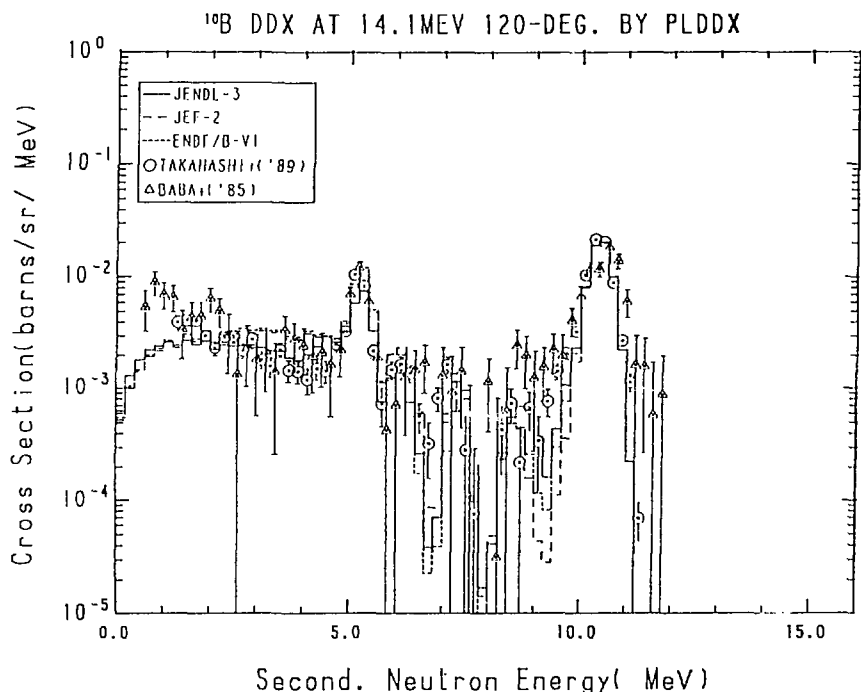


Fig. 9-4 The ^{10}B Double Differential Cross Section at 14.1 MeV,
Emitted Angle = 120° in Laboratory System

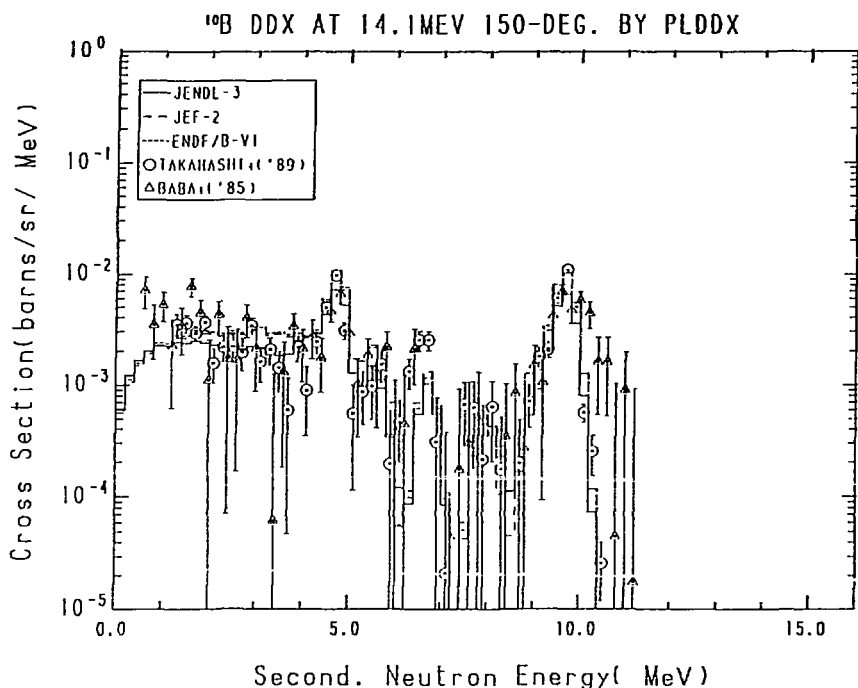


Fig. 9-5 The ^{10}B Double Differential Cross Section at 14.1 MeV,
Emitted Angle = 150° in Laboratory System

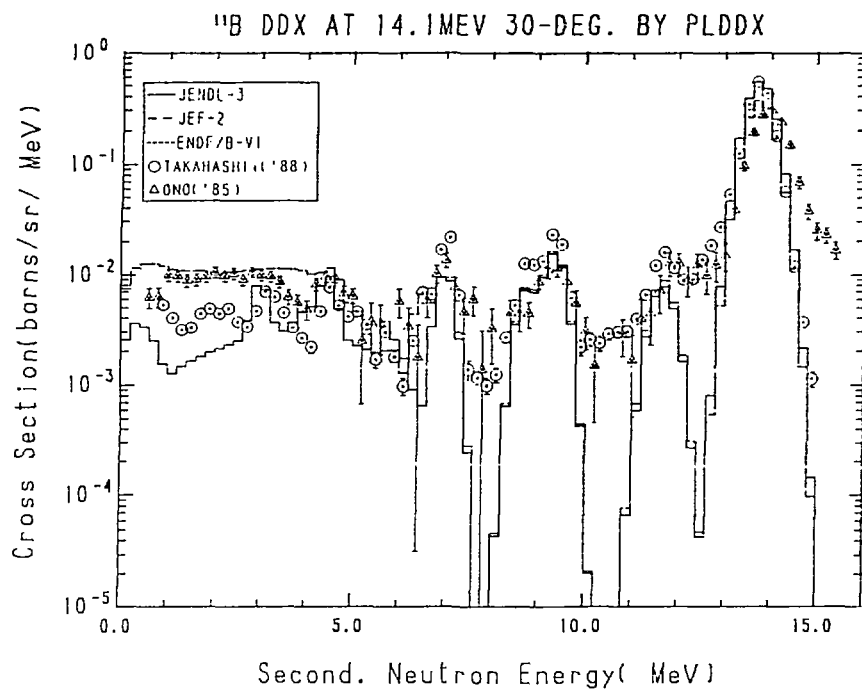


Fig. 10-1 The ^{11}B Double Differential Cross Section at 14.1 MeV,
Emitted Angle = 30° in Laboratory System

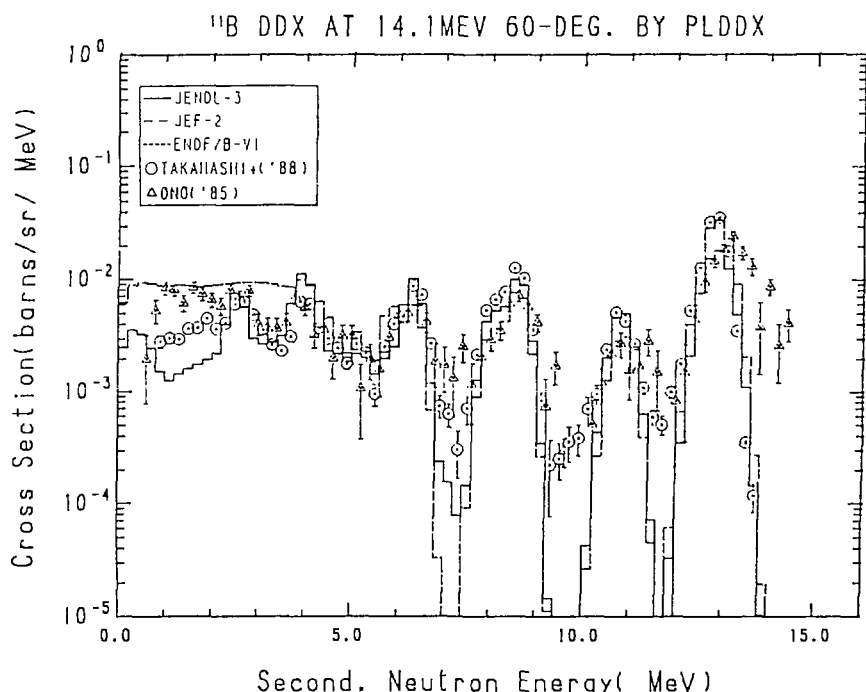


Fig. 10-2 The ^{11}B Double Differential Cross Section at 14.1 MeV,
Emitted Angle = 60° in Laboratory System

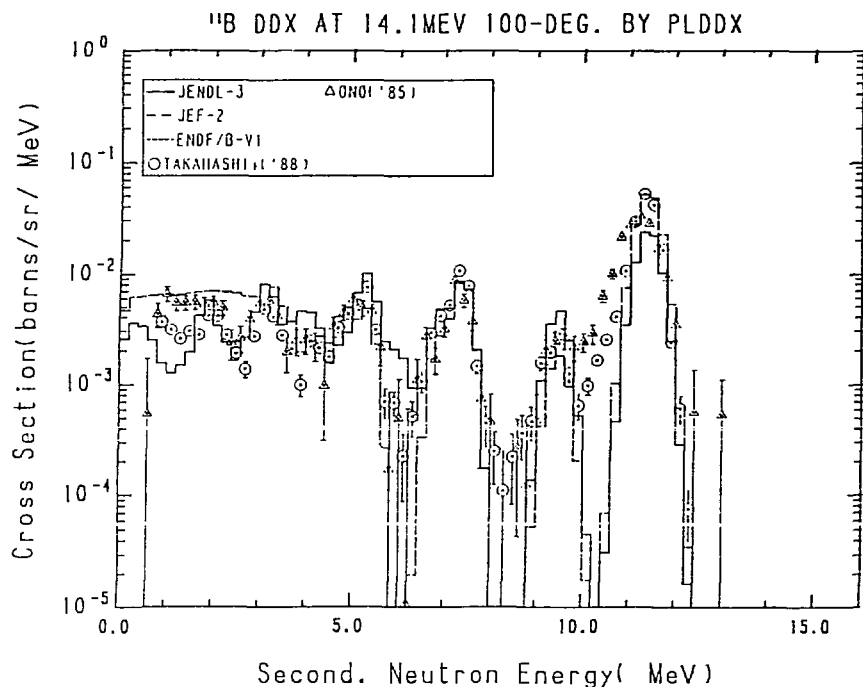


Fig. 10-3 The ^{11}B Double Differential Cross Section at 14.1 MeV,
Emitted Angle = 100° in Laboratory System

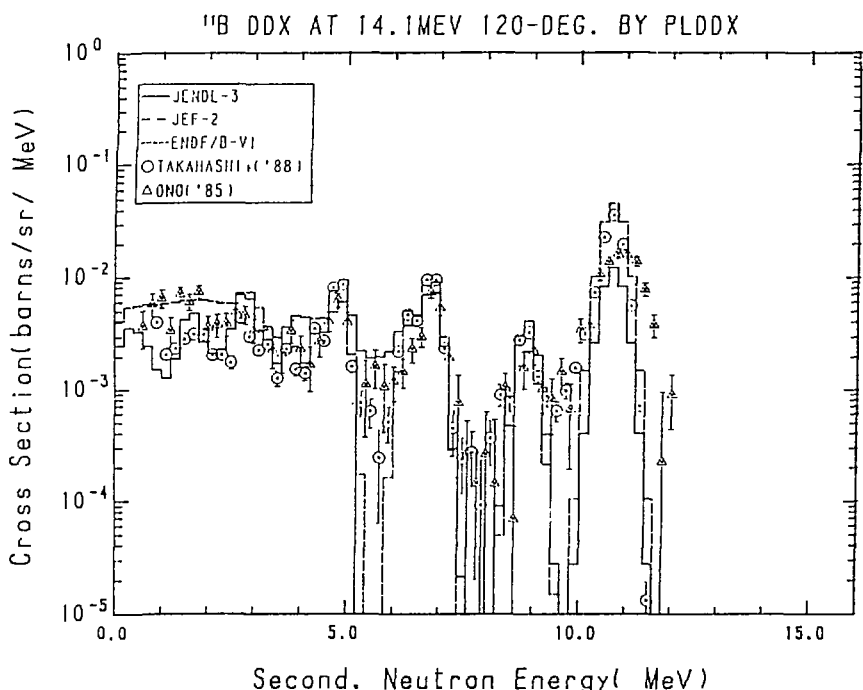


Fig. 10-4 The ^{11}B Double Differential Cross Section at 14.1 MeV,
Emitted Angle = 120° in Laboratory System

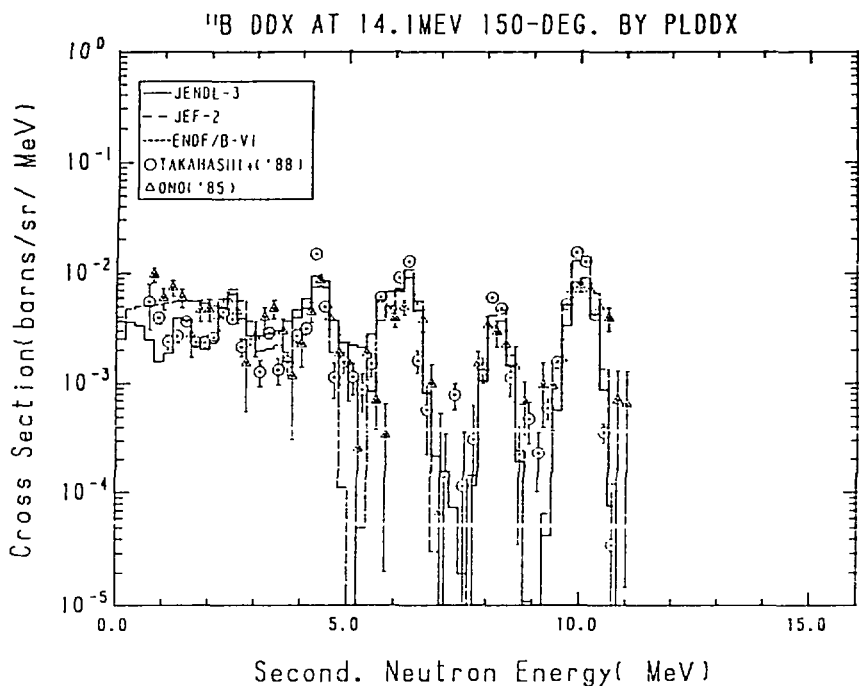


Fig. 10-5 The ¹¹B Double Differential Cross Section at 14.1 MeV,
Emitted Angle = 150° in Laboratory System

3.4 Carbon

The DDXs calculated from the evaluated data of ^{12}C at 30° , 60° , 90° , 120° and $145^\circ/155^\circ$ are displayed in Fig.11 together with the experimental data/ONO('85),TAKAHASHI+('88)/ at the incident neutron energy of 14.1 MeV and in Fig.12 together with those/MATSUYAMA+('90)/ at 18.0 MeV. The JENDL-3 data reproduce the experimental data excellently, but the data of the other two libraries have unphysical structures below the lowest peak region at both incident energies.

References for the Experimental Data in Figures

- MATSUYAMA+('90): Baba M., Matsuyama S., Fujisawa M., Iwasaki T., Iwasaki S. and Sakamoto R., JAERI-M 90-025, 383 (1990).
- ONO('85) : Ono M., private communication (1989).
- TAKAHASHI+('88): Takahashi A., Ichimura E., Sugimoto H. and Kato T., JAERI-M 86-080, 393 (1986).

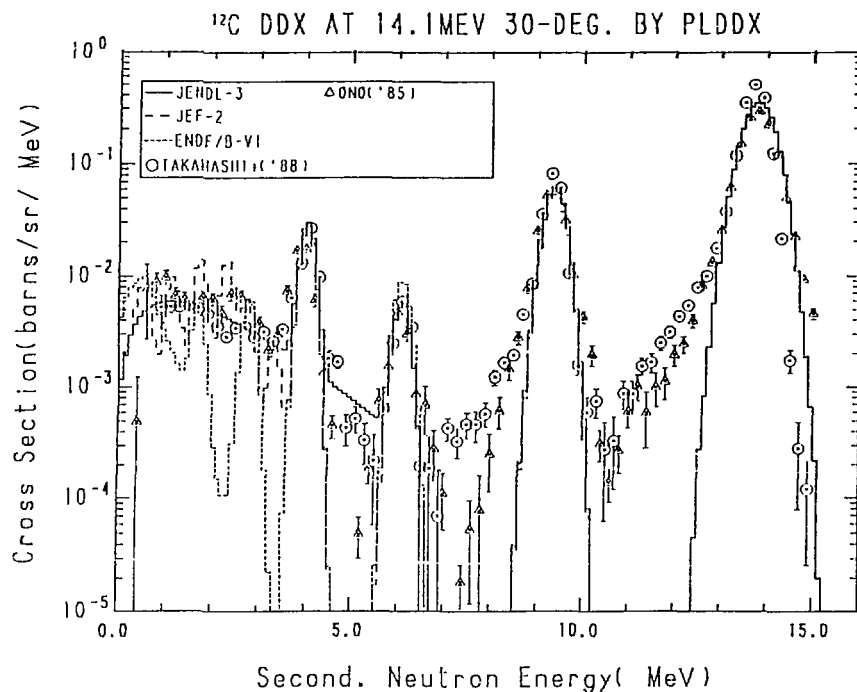


Fig. 11-1 The ^{12}C Double Differential Cross Section at 14.1 MeV,
Emitted Angle = 30° in Laboratory System

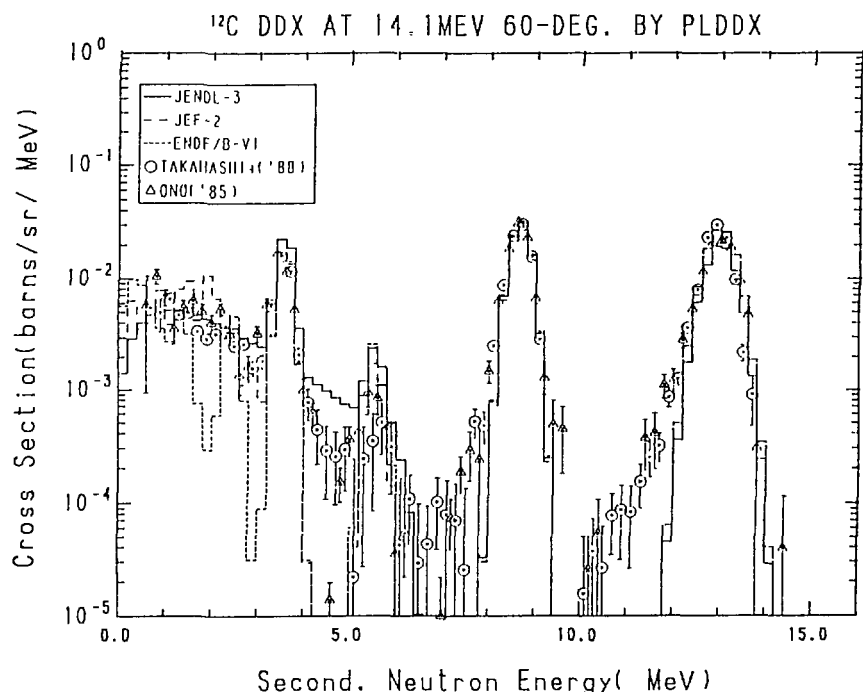


Fig. 11-2 The ^{12}C Double Differential Cross Section at 14.1 MeV,
Emitted Angle = 60° in Laboratory System

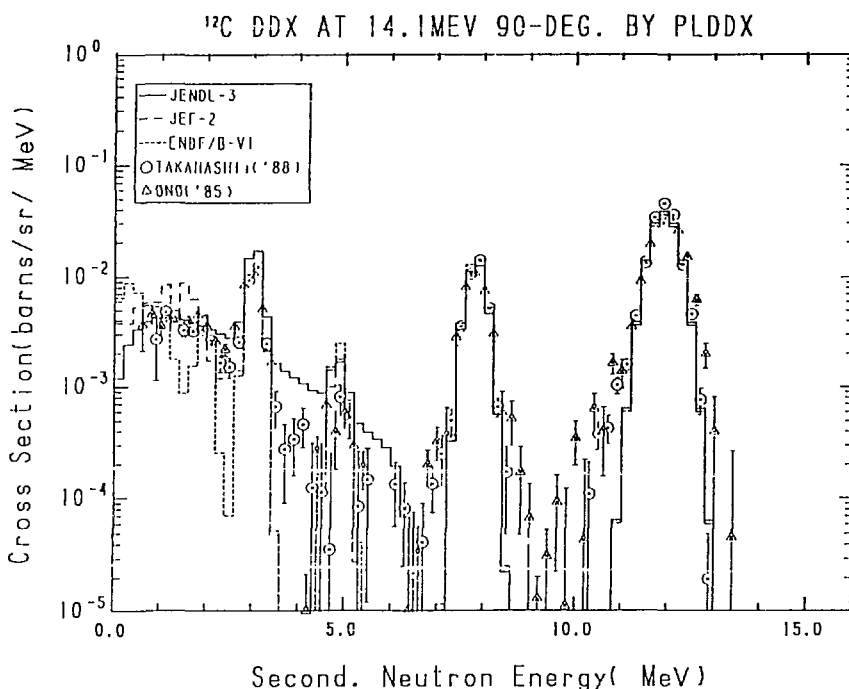


Fig. 11-3 The ^{12}C Double Differential Cross Section at 14.1 MeV,
Emitted Angle = 90° in Laboratory System

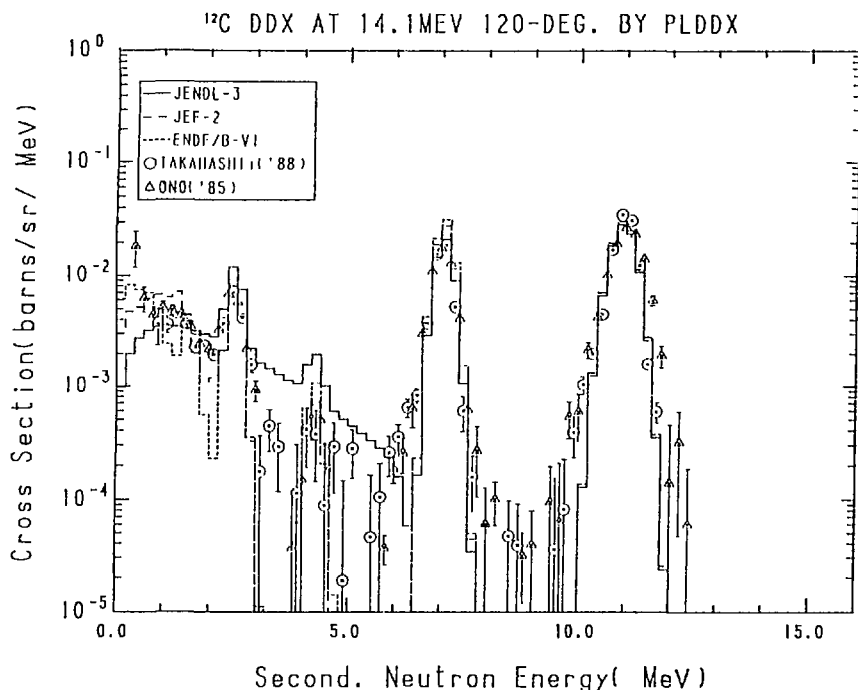


Fig. 11-4 The ^{12}C Double Differential Cross Section at 14.1 MeV,
Emitted Angle = 120° in Laboratory System

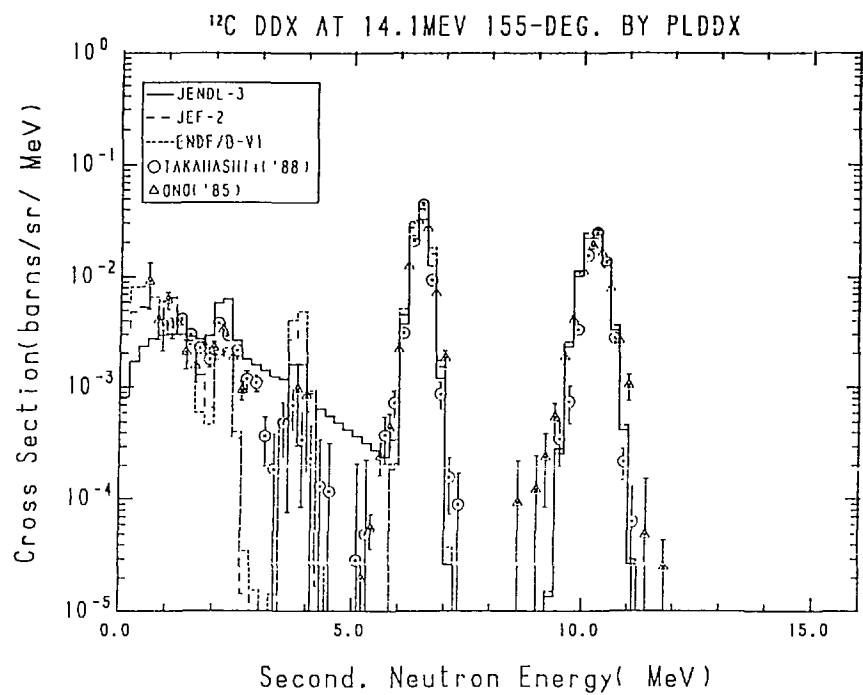


Fig. 11-5 The ^{12}C Double Differential Cross Section at 14.1 MeV,
Emitted Angle = 155° in Laboratory System

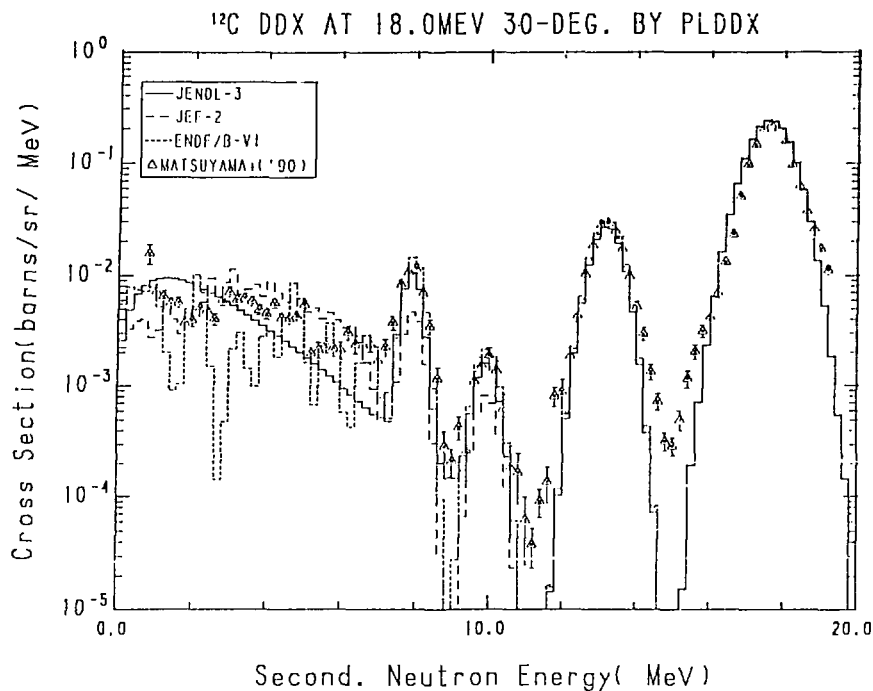


Fig. 12-1 The ^{12}C Double Differential Cross Section at 18.0 MeV,
Emitted Angle = 30° in Laboratory System

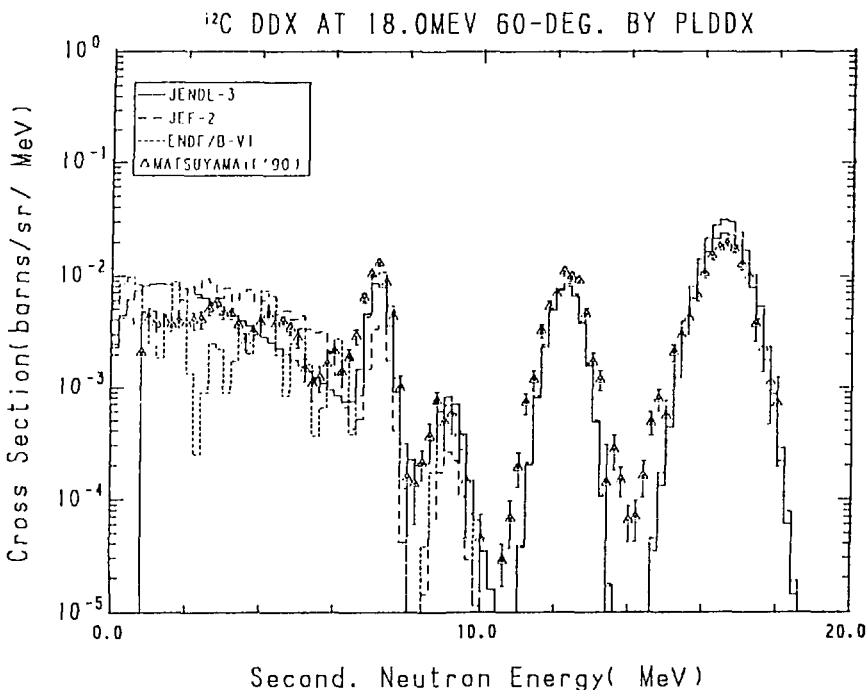


Fig. 12-2 The ^{12}C Double Differential Cross Section at 18.0 MeV,
Emitted Angle = 60° in Laboratory System

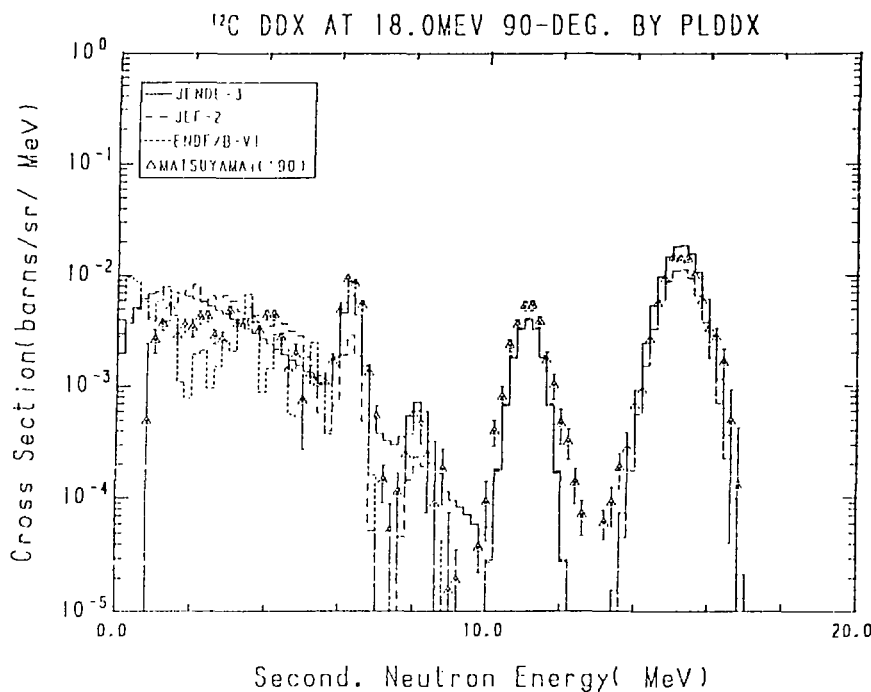


Fig. 12-3 The ^{12}C Double Differential Cross Section at 18.0 MeV,
Emitted Angle = 90° in Laboratory System

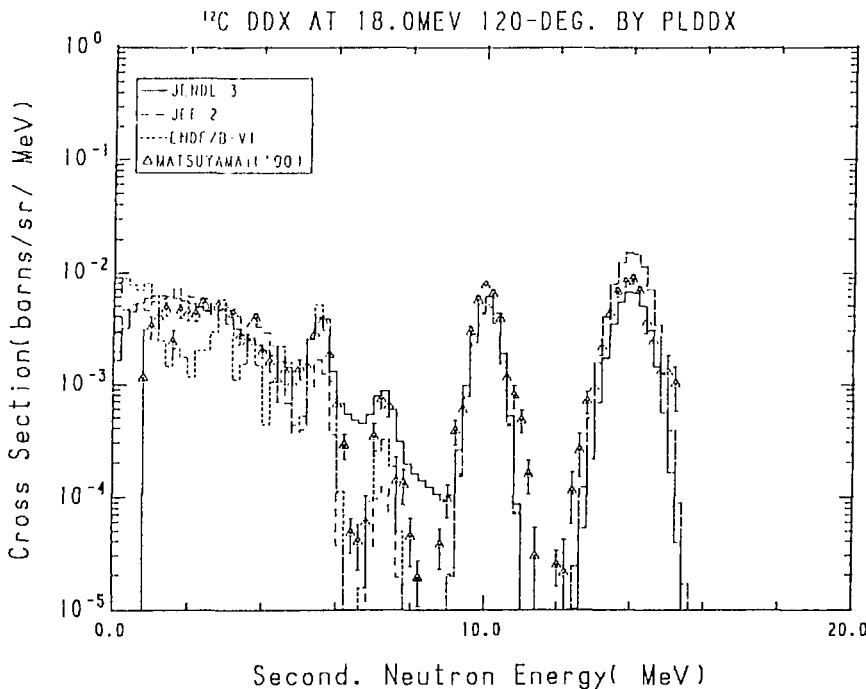


Fig. 12-4 The ^{12}C Double Differential Cross Section at 18.0 MeV,
Emitted Angle = 120° in Laboratory System

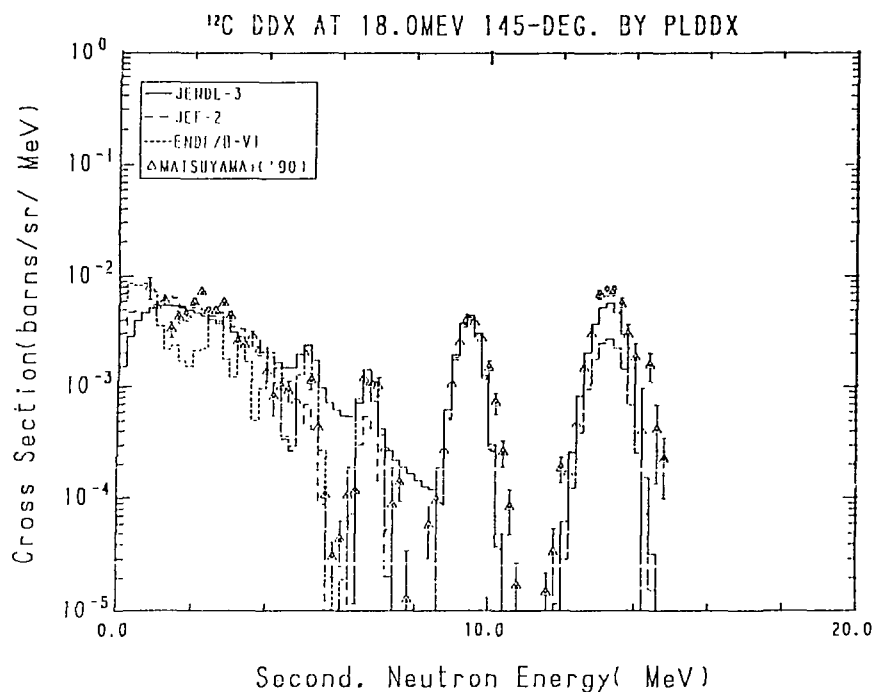


Fig. 12-5 The ¹²C Double Differential Cross Section at 18.0 MeV,
Emitted Angle = 145° in Laboratory System

3.5 Nitrogen

The DDXs calculated from the evaluated data of ^{14}N are compared with the experimental data/ONO('85)/ of 30° , 60° , 80° , 120° and 150° for ^{14}N at the incident neutron energy of 14.2 MeV in Fig.13, and those/TAKAHASHI+('86)/ of 30° , 60° , 80° and 120° for ^{nat}N at the incident energies from 13.7 to 14.8 MeV in Fig.14. The JENDL-3 data in the figures are the revised version of the current JENDL-3 which will be released in 1993, and reproduce the experimental data measured at Osaka university (Fig.14). The experimental data of Tohoku university are larger than the JENDL-3 data just below the elastic peak. Since those are not observed in the data measured at Osaka university, it might be a tail of the elastic scattering peak.

References for the Experimental Data in Figures

- ONO('85) : Baba M., Ono M., Yabuta N., Kikuchi T. and Hirakawa N., Proc. of Int. Conf. on Nucl. Data for Basic and Applied Sci. at Santa Fe in May 13-17, p.223 (1985).
- TAKAHASHI+('86): Takahashi A., JAERI-M 86-029, 99 (1986).

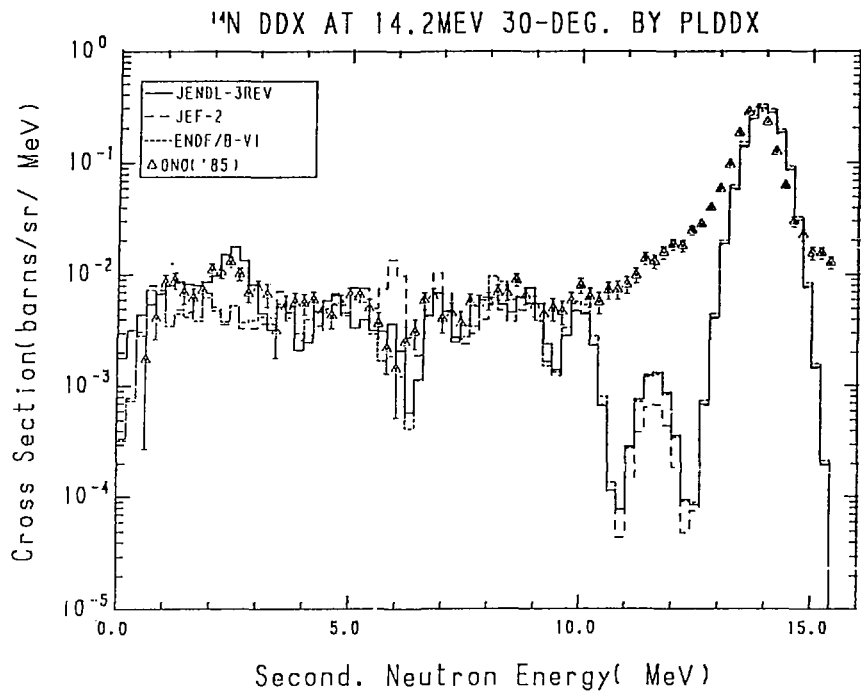


Fig. 13-1 The ^{14}N Double Differential Cross Section at 14.2 MeV,
Emitted Angle = 30° in Laboratory System

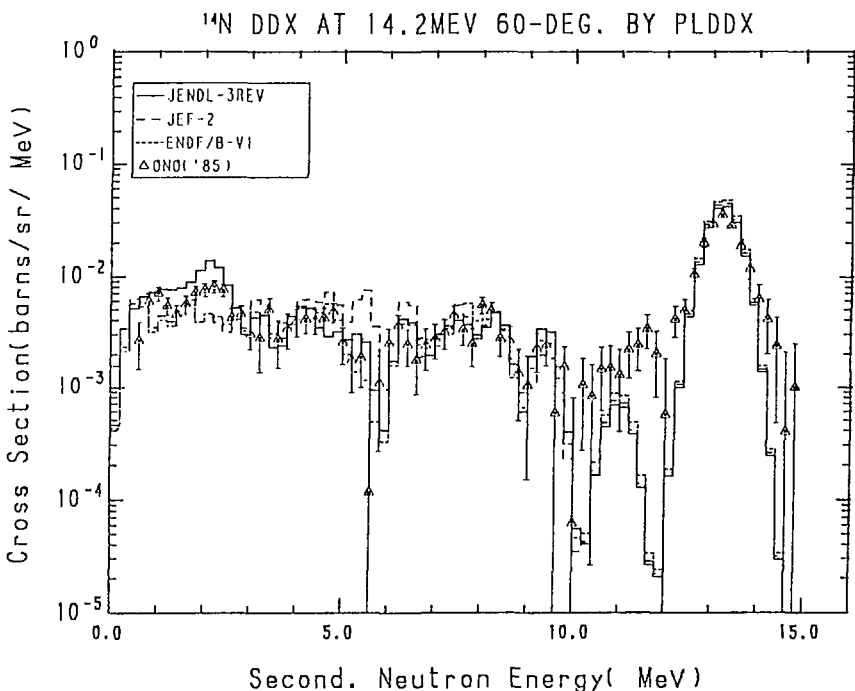


Fig. 13-2 The ^{14}N Double Differential Cross Section at 14.2 MeV,
Emitted Angle = 60° in Laboratory System

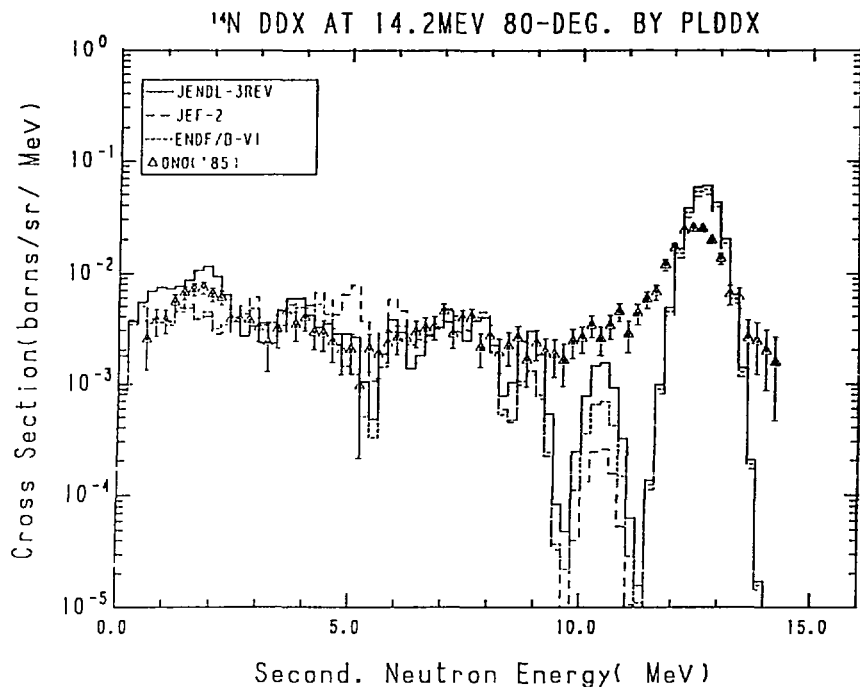


Fig. 13-3 The ^{14}N Double Differential Cross Section at 14.2 MeV,
Emitted Angle = 80° in Laboratory System

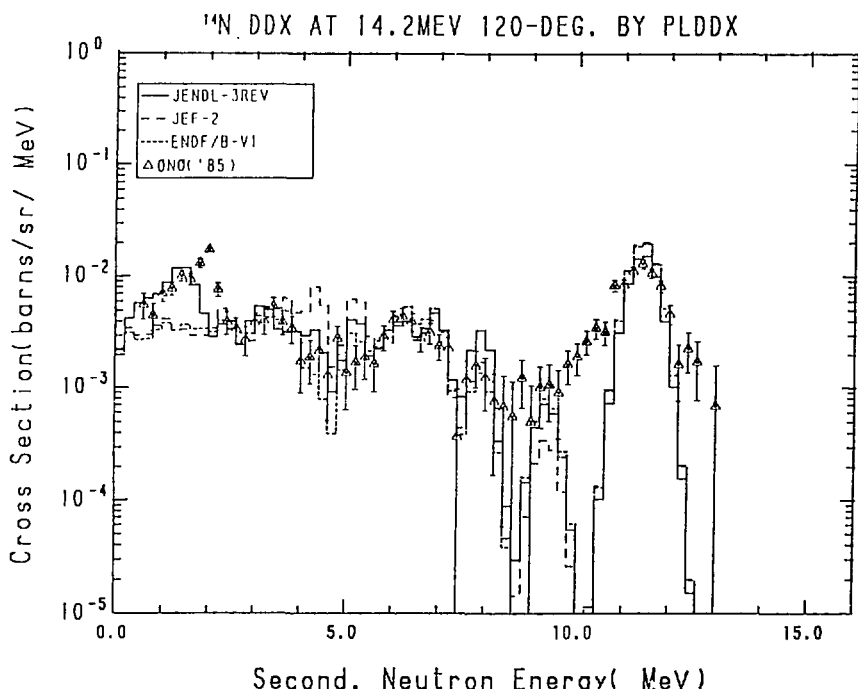


Fig. 13-4 The ^{14}N Double Differential Cross Section at 14.2 MeV,
Emitted Angle = 120° in Laboratory System

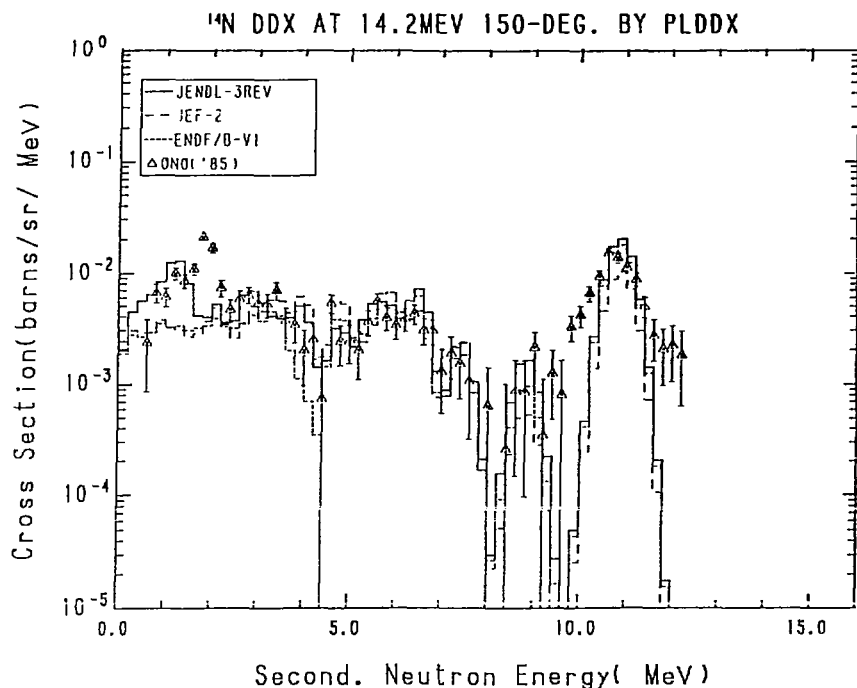


Fig. 13-5 The ^{14}N Double Differential Cross Section at 14.2 MeV,
Emitted Angle = 150° in Laboratory System

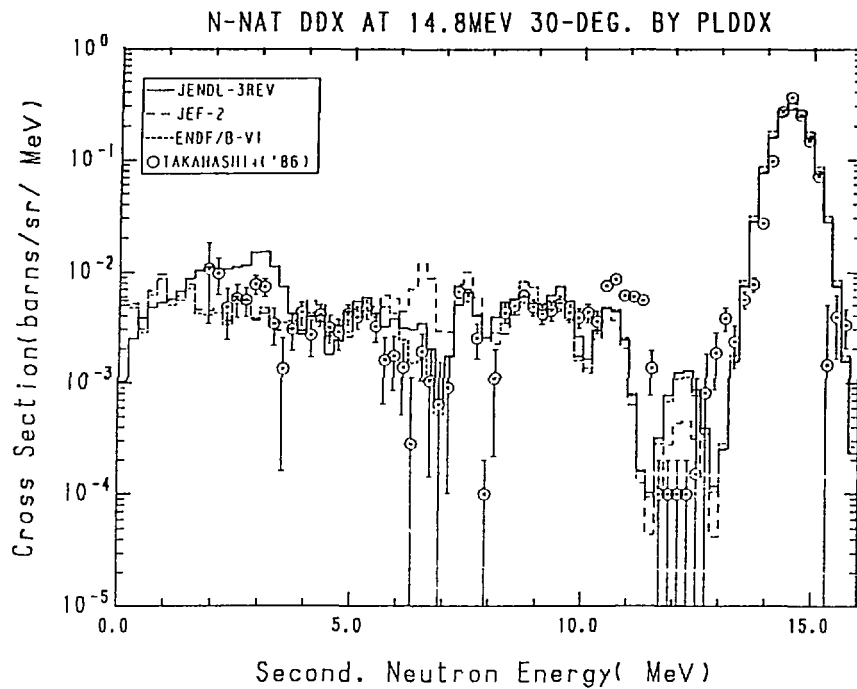


Fig. 14-1 The ^{nat}N Double Differential Cross Section,
Incident Energy = 14.8 MeV, Emitted Angle = 30°

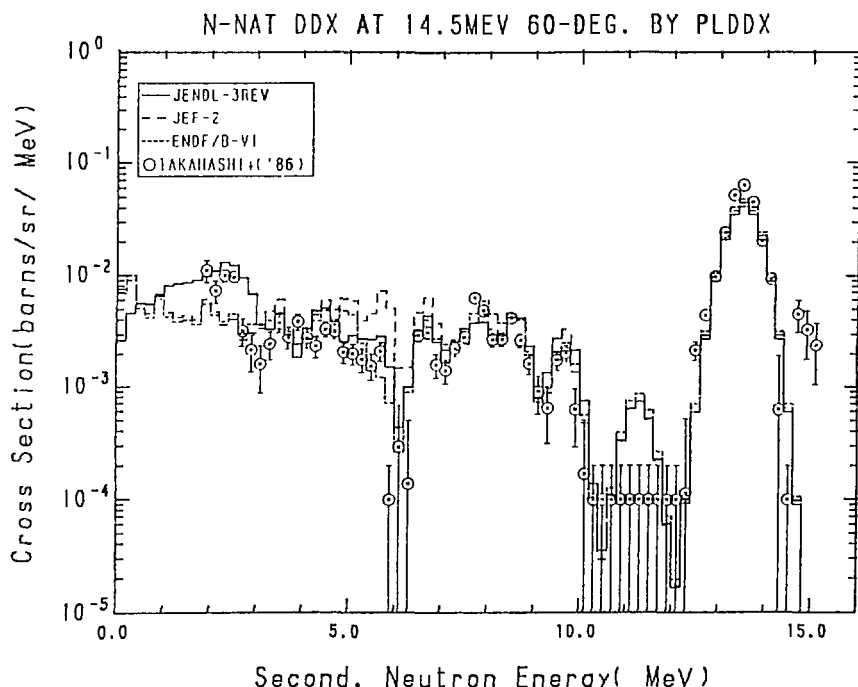


Fig. 14-2 The ^{nat}N Double Differential Cross Section,
Incident Energy = 14.5 MeV, Emitted Angle = 60°

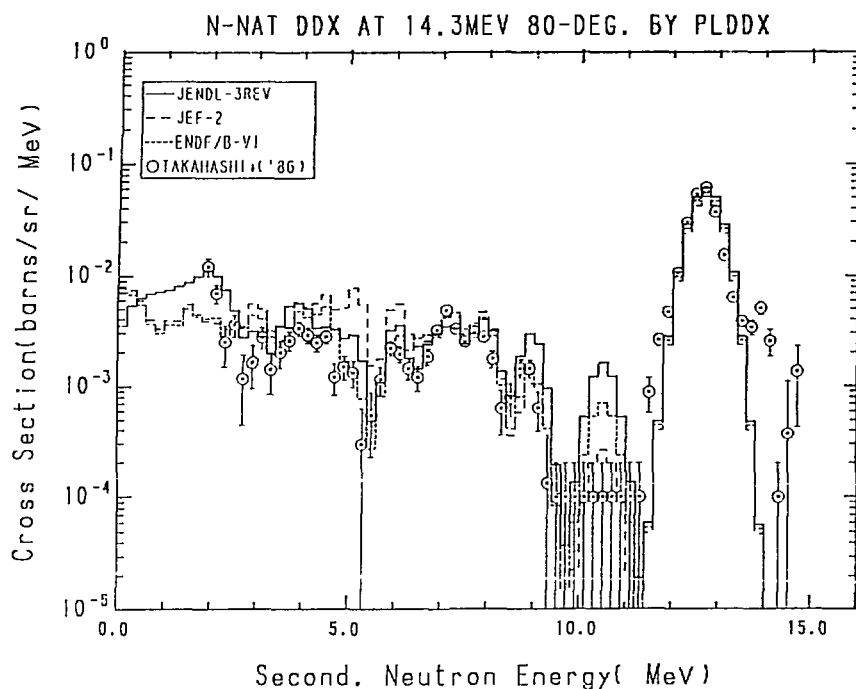


Fig. 14-3 The ^{nat}N Double Differential Cross Section,
Incident Energy = 14.3 MeV, Emitted Angle = 80°

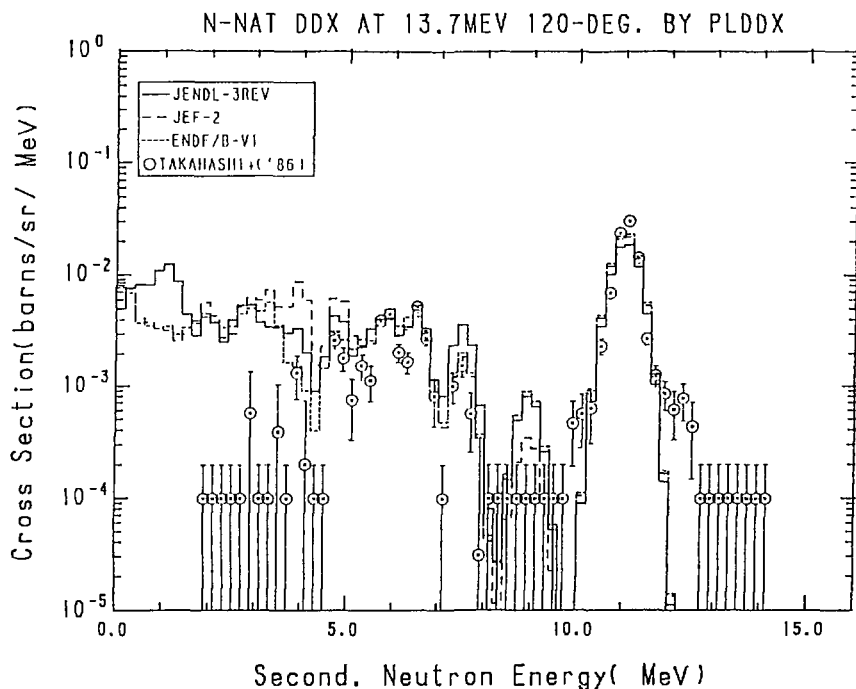


Fig. 14-4 The ^{nat}N Double Differential Cross Section,
Incident Energy = 13.7 MeV, Emitted Angle = 120°

3.6 Oxygen

The DDXs calculated from the evaluated data of ^{16}O are compared with the experimental data/BABA+('88),TAKAHASHI+('89)/ of 25° , 60° , 90° , 120° and 150° at the incident neutron energy of 14.1 MeV in Fig.15, and those/BABA+('88)/ at 18.0 MeV in Fig.16. The JEF-2 data are equivalent to the ENDF/B-VI data. The three libraries give similar results at 14.1 MeV (Fig.15) and underestimate just below the elastic scattering peak. Since there is no 'level' in ^{16}O corresponding to this region, it is speculated that the experimental data are affected by backgrounds. In the case of 18.0 MeV (Fig.16), the data of the three libraries have the same trends in the higher energy region. In the energy region below 10 MeV, however, they are discrepant. Below 4 MeV, the JENDL-3 data reproduce the experimental data at the forward angles, and give smaller values at the backward angles. The JENDL-3 data are significantly lower than the experimental data just below the second peak.

References for the Experimental Data in Figures

- BABA+('88) : Baba M., Ishikawa M., Kikuchi T., Wakabayashi H. and Hirakawa N., Proc. of Int. Conf. on Nucl. Data for Sci. and Technol. at Mito in May 30- Jun. 3, p.209 (1988).
 TAKAHASHI+('89): Takahashi A., private communication (1989).

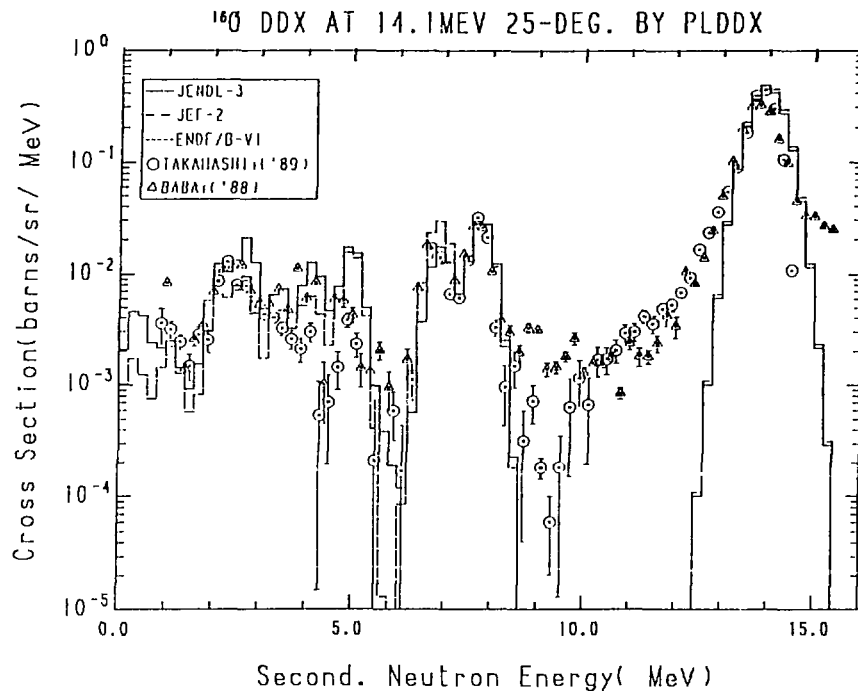


Fig. 15-1 The ^{160}O Double Differential Cross Section at 14.1 MeV,
Emitted Angle = 25° in Laboratory System

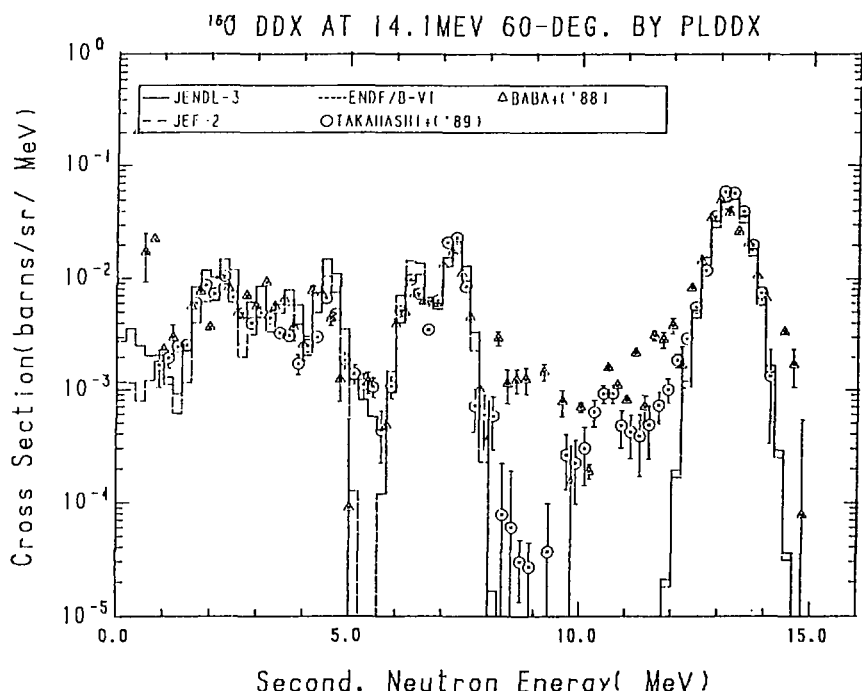


Fig. 15-2 The ^{160}O Double Differential Cross Section at 14.1 MeV,
Emitted Angle = 60° in Laboratory System

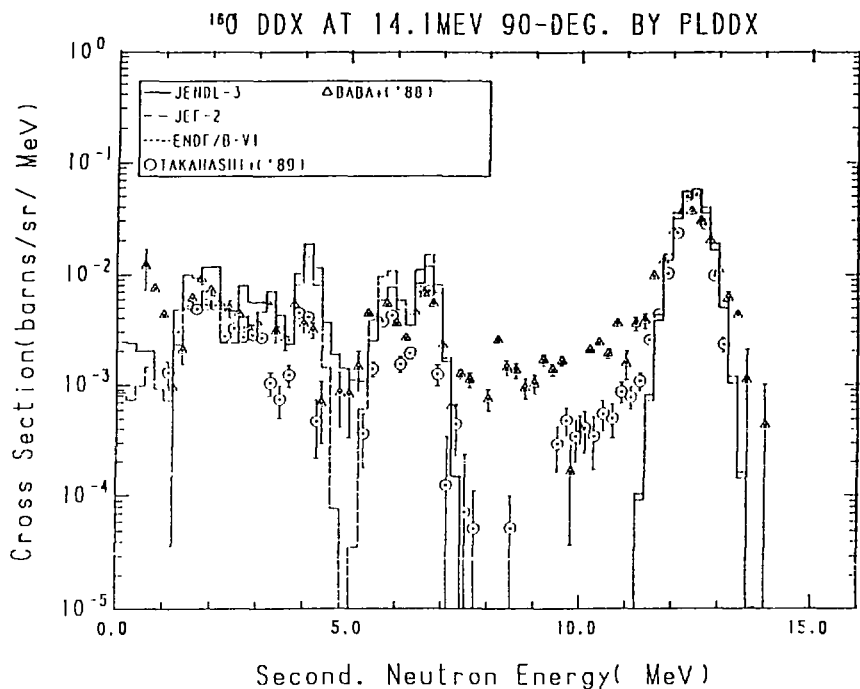


Fig. 15-3 The ^{160}O Double Differential Cross Section at 14.1 MeV,
Emitted Angle = 90° in Laboratory System

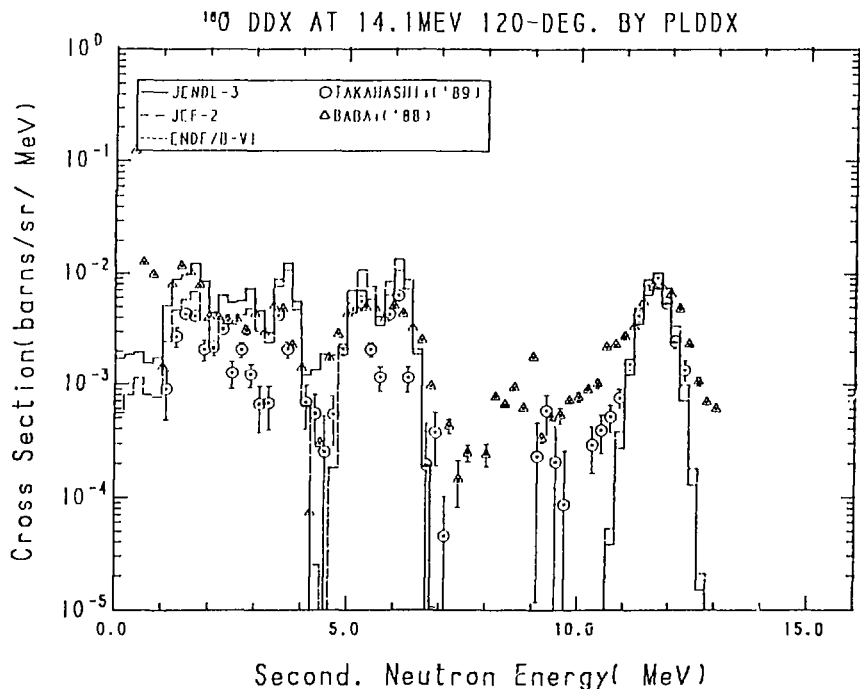


Fig. 15-4 The ^{160}O Double Differential Cross Section at 14.1 MeV,
Emitted Angle = 120° in Laboratory System

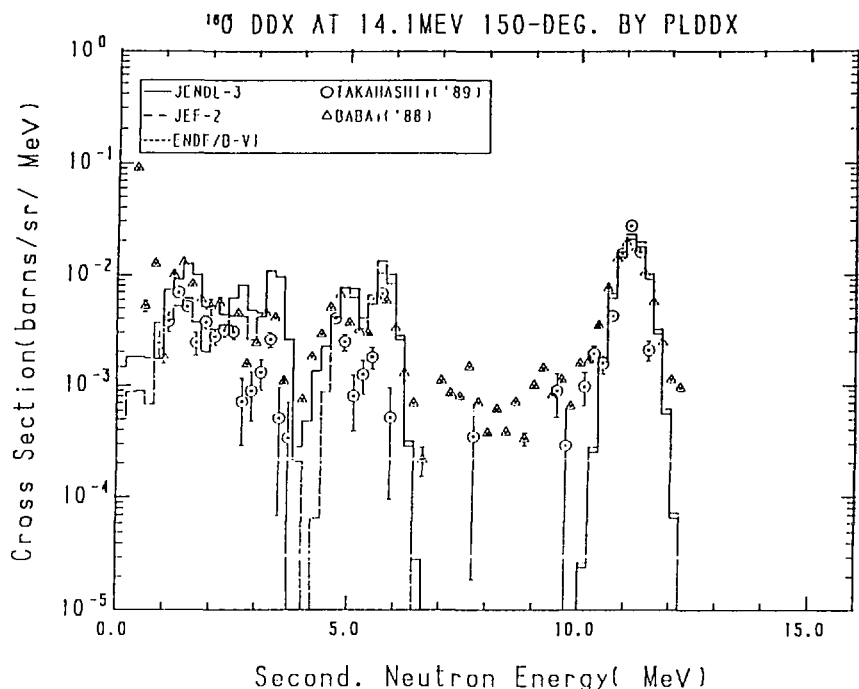


Fig. 15-5 The ¹⁶⁰O Double Differential Cross Section at 14.1 MeV,
Emitted Angle = 150° in Laboratory System

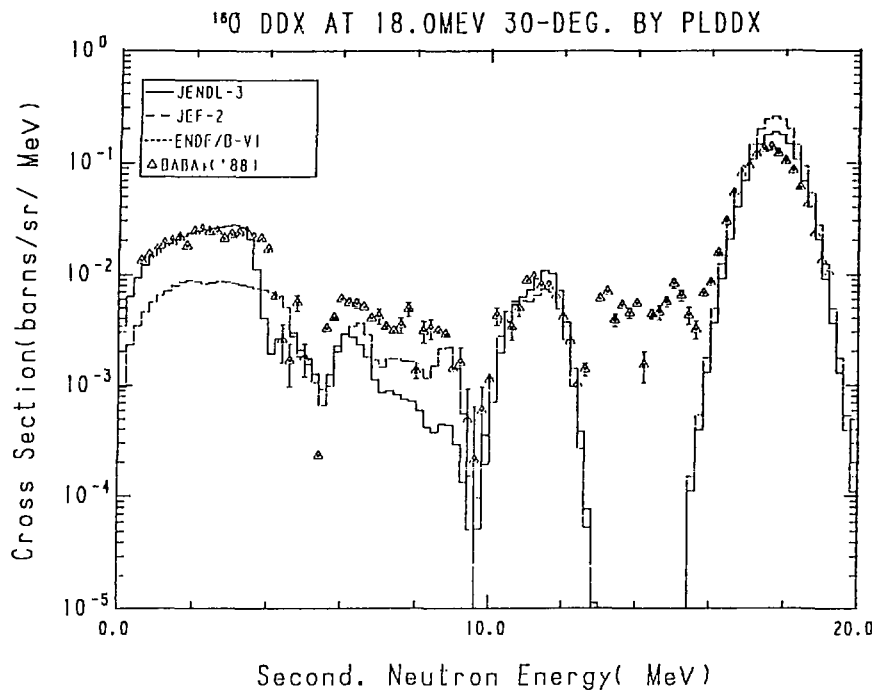


Fig. 16-1 The ^{160}O Double Differential Cross Section at 18.0 MeV,
Emitted Angle = 30° in Laboratory System

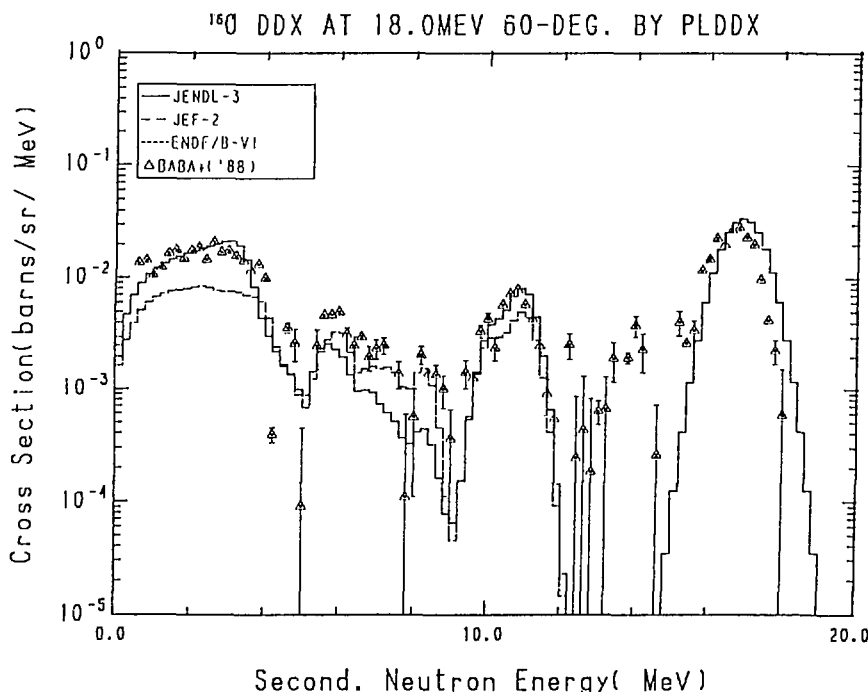


Fig. 16-2 The ^{160}O Double Differential Cross Section at 18.0 MeV,
Emitted Angle = 60° in Laboratory System

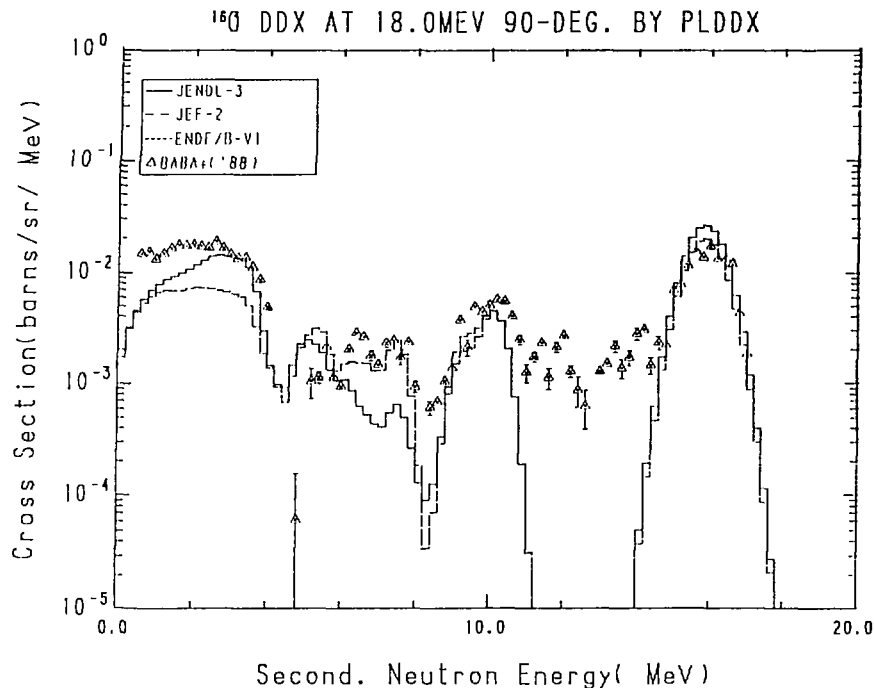


Fig. 16-3 The 160 Double Differential Cross Section at 18.0 MeV,
Emitted Angle = 90° in Laboratory System

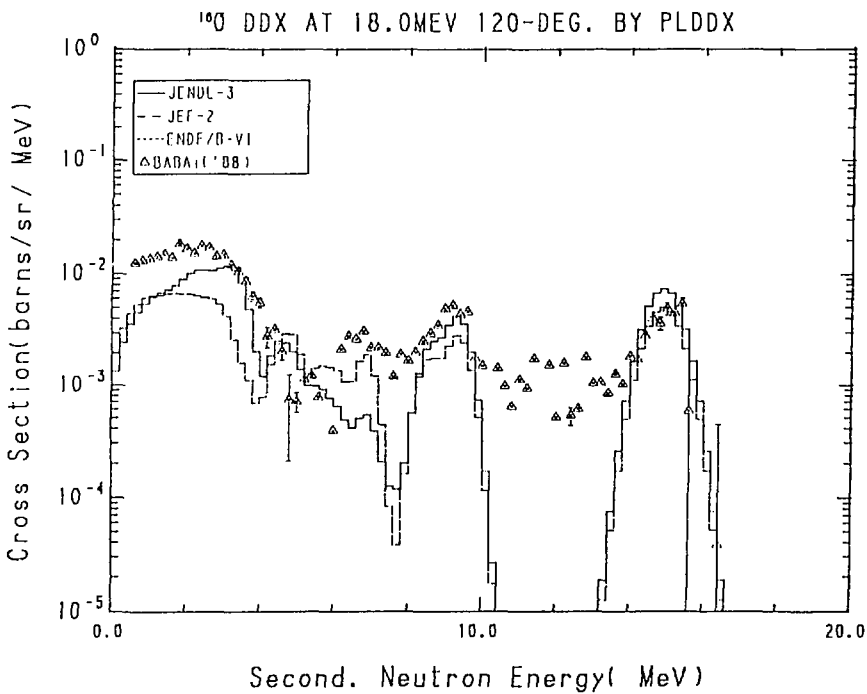


Fig. 16-4 The 160 Double Differential Cross Section at 18.0 MeV,
Emitted Angle = 120° in Laboratory System

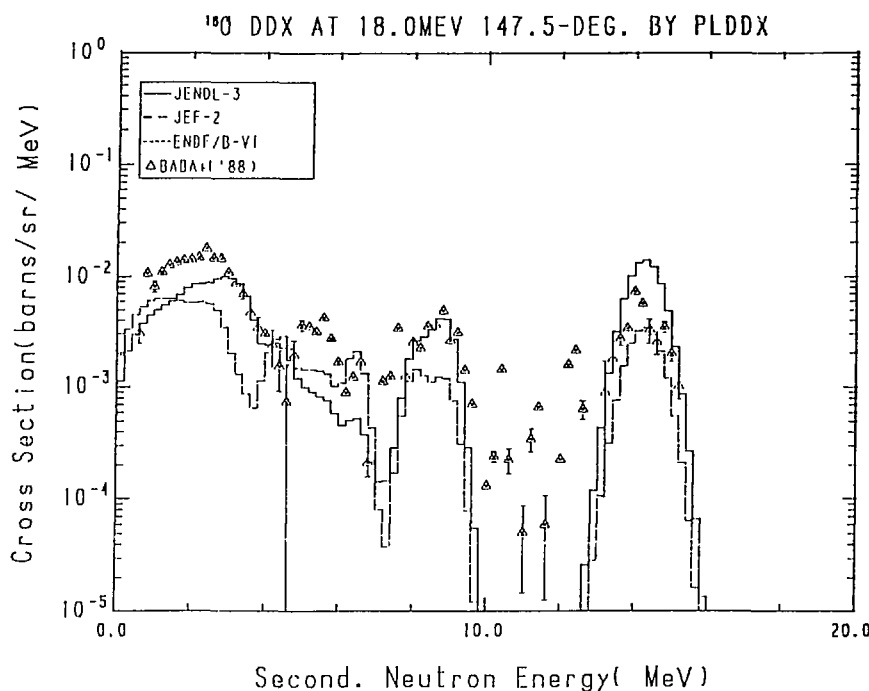


Fig. 16-5 The ¹⁶⁰ Double Differential Cross Section at 18.0 MeV,
Emitted Angle = 147.5° in Laboratory System

3.7 Fluorine

The DDXs calculated from the evaluated data of ^{19}F are compared with the experimental data/ONO('85),TAKAHASHI+('87)/ of 30° , 60° , 82° , 120° and 150° at the incident neutron energy of 14.1 MeV in Fig.17. In the discrete inelastic scattering region, the JENDL-3 data underestimate the DDX significantly, since the direct process is not considered in JENDL-3. The ENDF/B-VI and JEF-2 data reproduce the experimental data in that region. However, they have irregular bumps in the 5-8 MeV region at the forward angles. In the low energy region, the JENDL-3 and JEF-2 data have tendency of overestimation at the backward angles.

References for the Experimental Data in Figures

- ONO('85) : Baba M., Ono M., Yabuta N., Kikuchi T. and Hirakawa N., Proc. of Int. Conf. on Nucl. Data for Basic and Applied Sci. at Santa Fe in May 13-17, p.223 (1985).
- TAKAHASHI+('87): Takahashi A., Ichimura E., Sugimoto H. and Kato T., JAERI-M 86-080, 393 (1986).

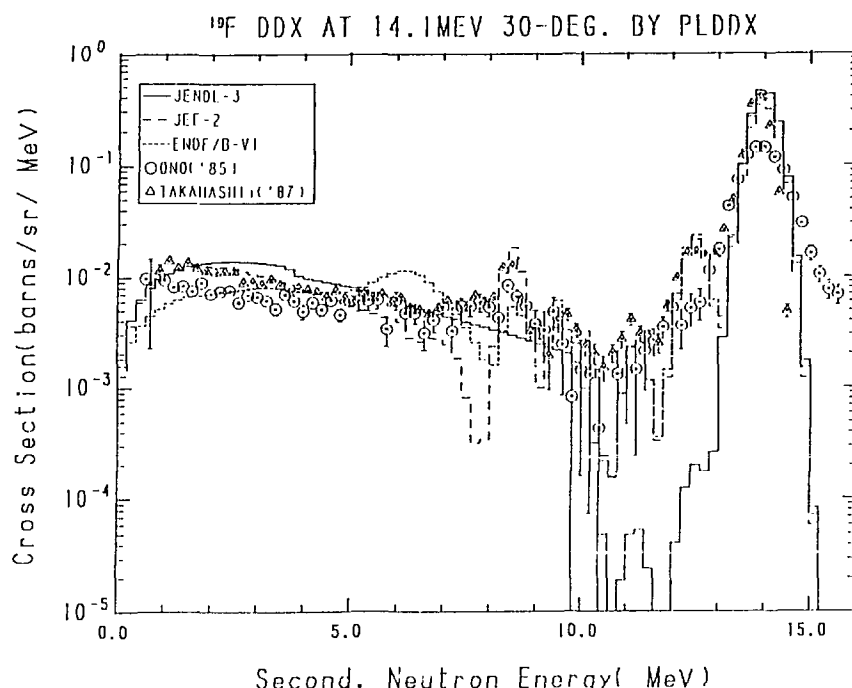


Fig. 17-1 The ^{19}F Double Differential Cross Section at 14.1 MeV,
Emitted Angle = 30° in Laboratory System

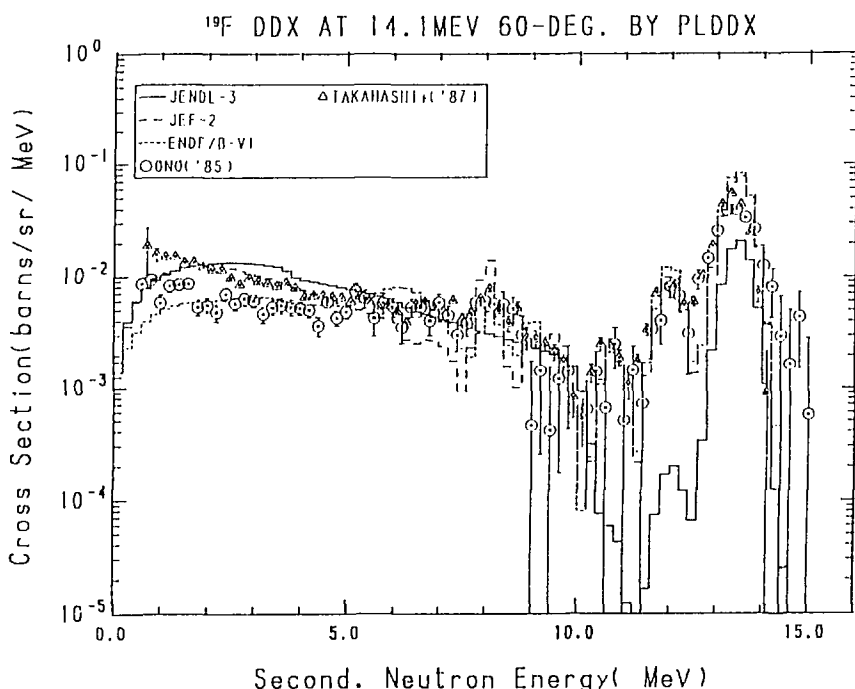


Fig. 17-2 The ^{19}F Double Differential Cross Section at 14.1 MeV,
Emitted Angle = 60° in Laboratory System

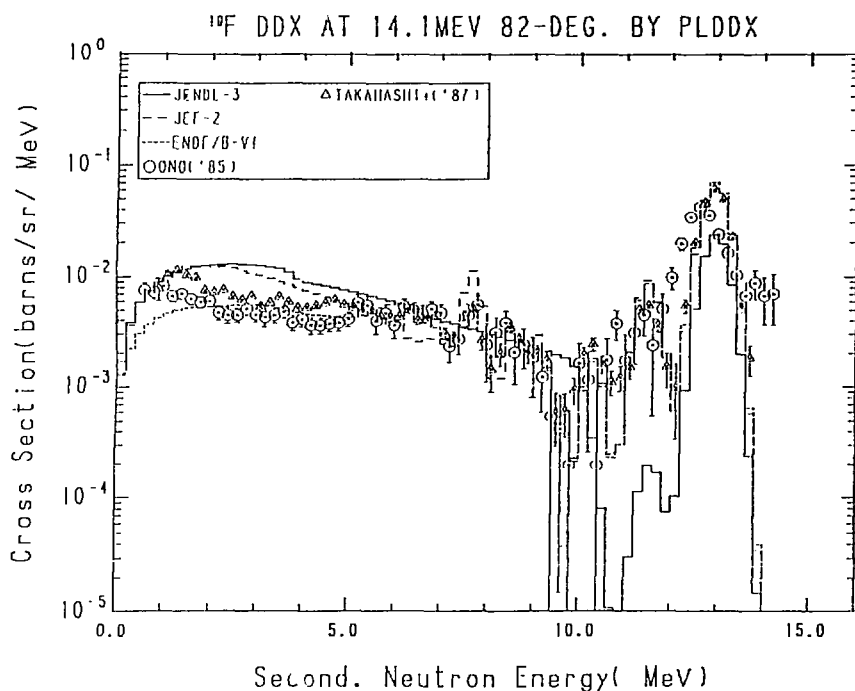


Fig. 17-3 The ¹⁹F Double Differential Cross Section at 14.1 MeV,
Emitted Angle = 82° in Laboratory System

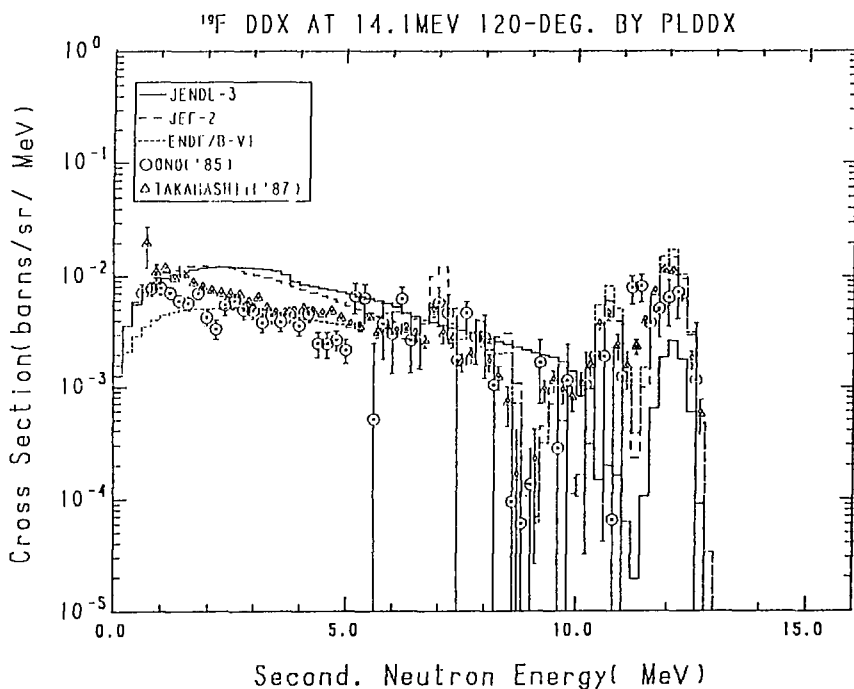


Fig. 17-4 The ¹⁹F Double Differential Cross Section at 14.1 MeV,
Emitted Angle = 120° in Laboratory System

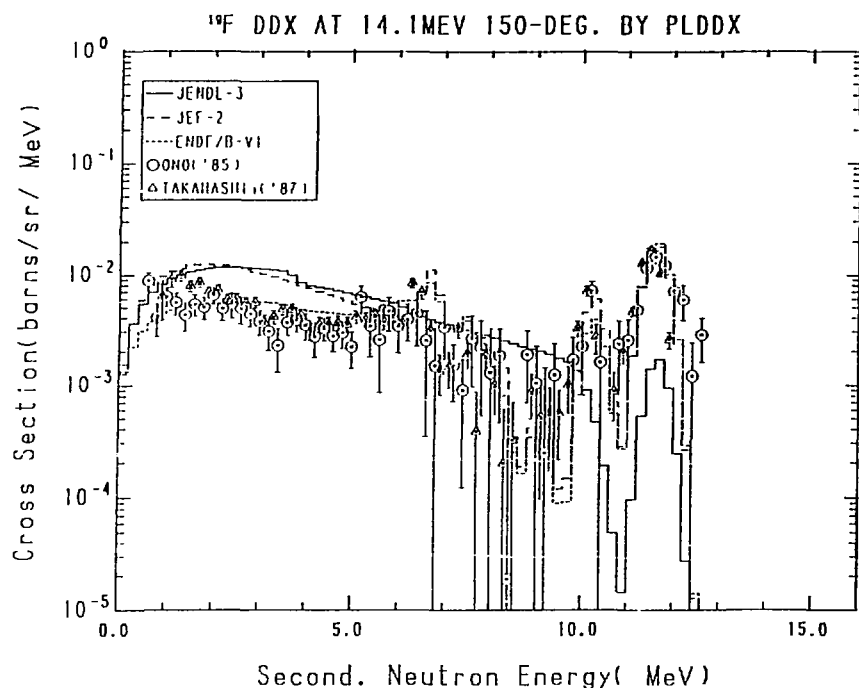


Fig. 17-5 The ¹⁹F Double Differential Cross Section at 14.1 MeV,
Emitted Angle = 150° in Laboratory System

3.8 Sodium

The DDXs calculated from the evaluated data of ^{23}Na are compared with the experimental data/TAKAHASHI+('86)/ of 45° , 60° , 80° , 110° and 135° , whose incident energies change according to scattered angles, in Fig.18. The JEF-2 data are equivalent to JENDL-3. The number of the experimental data points which can be compared with the evaluated data is insufficient. However, the evaluated data tend to overestimate the DDXs in the low energy region at the backward angles.

Reference for the Experimental Data in Figures

TAKAHASHI+('86): Takahashi A., JAERI-M 86-029, 99 (1986).

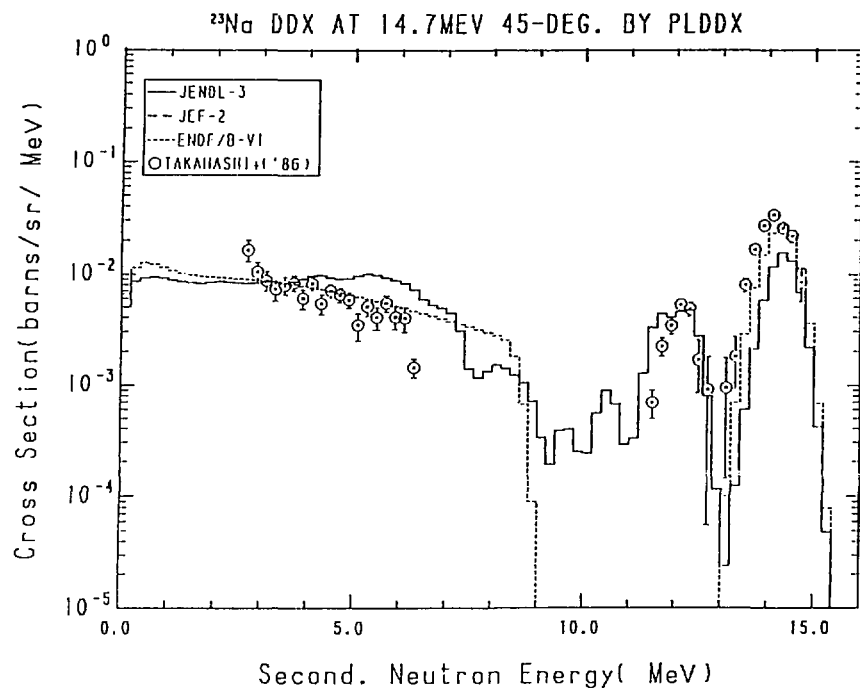


Fig. 18-1 The ^{23}Na Double Differential Cross Section,
Incident Energy = 14.7 MeV, Emitted Angle = 45°

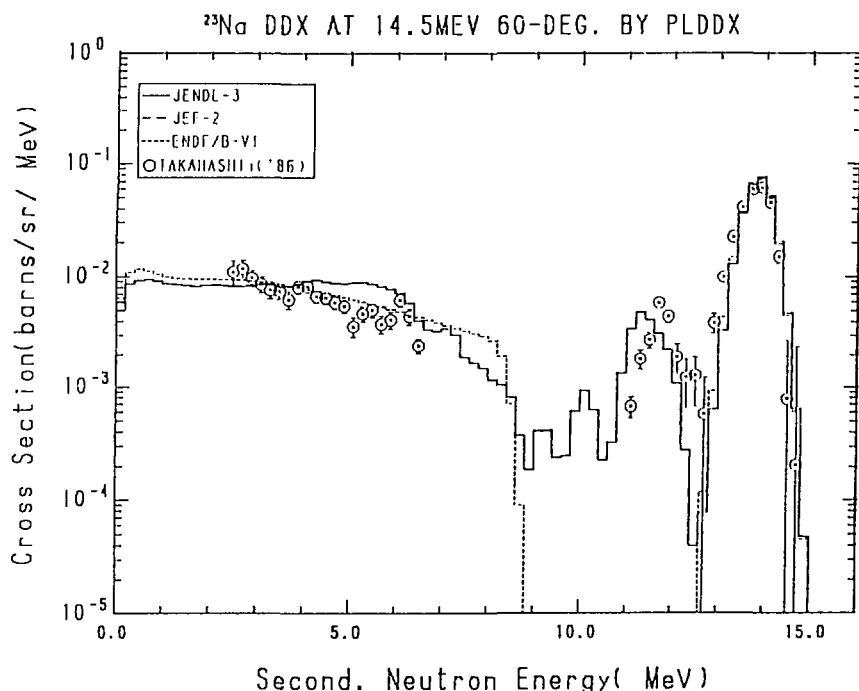


Fig. 18-2 The ^{23}Na Double Differential Cross Section,
Incident Energy = 14.5 MeV, Emitted Angle = 60°

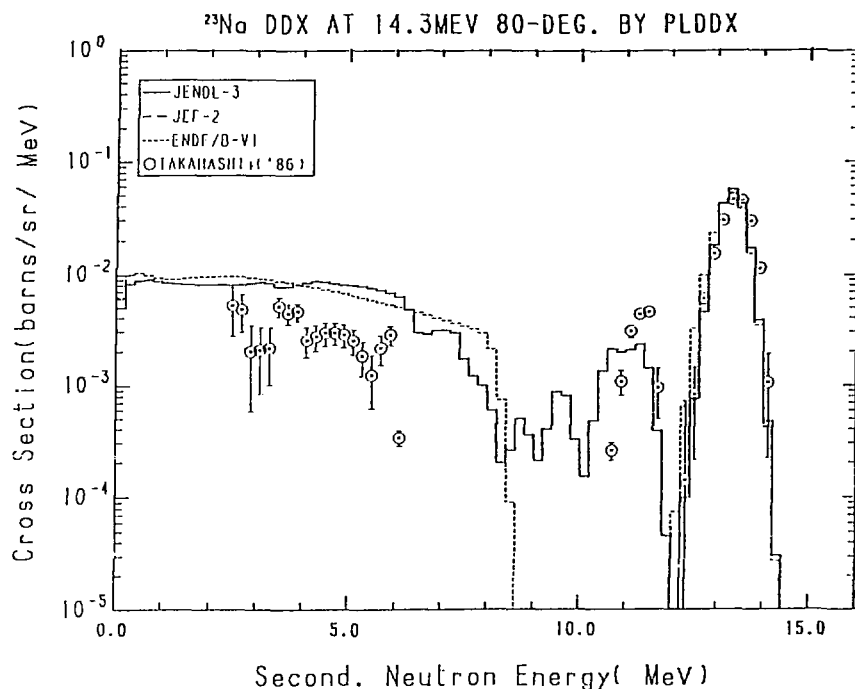


Fig. 18-3 The ^{23}Na Double Differential Cross Section,
Incident Energy = 14.3 MeV, Emitted Angle = 80°

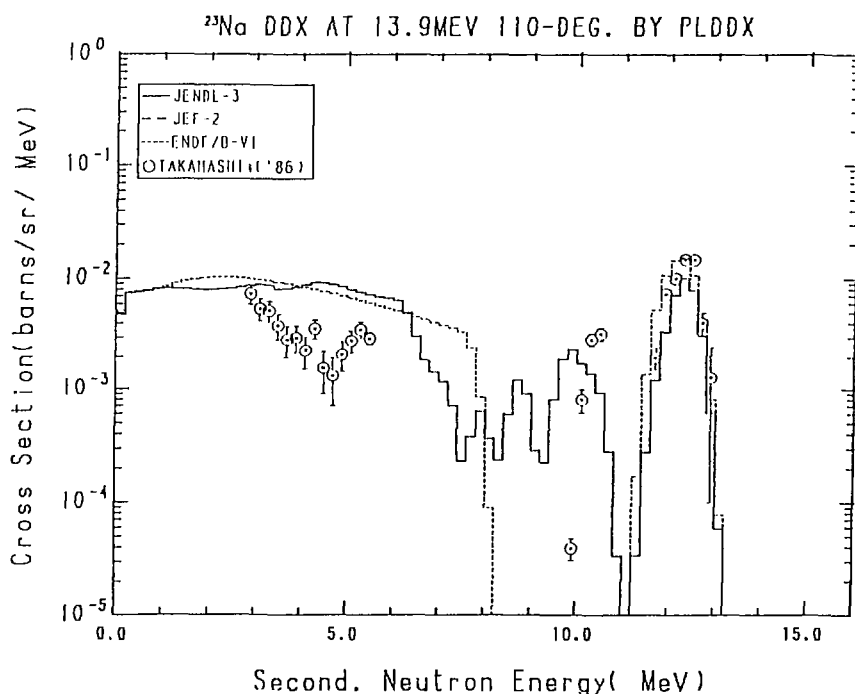


Fig. 18-4 The ^{23}Na Double Differential Cross Section,
Incident Energy = 13.9 MeV, Emitted Angle = 110°

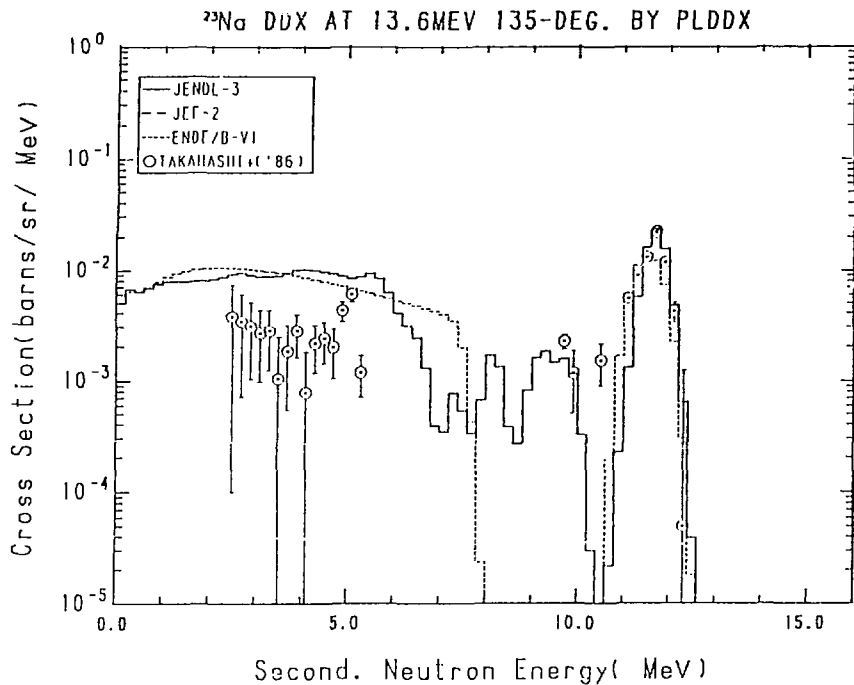


Fig. 18-5 The ^{23}Na Double Differential Cross Section,
Incident Energy = 13.6 MeV, Emitted Angle = 135°

3.9 Magnesium

The DDXs calculated from the evaluated data of magnesium are compared with the experimental data/TAKAHASHI+('87)/ of 30° , 60° , 90° , 120° and 150° at the incident neutron energy of 14.1 MeV in Fig.19. The JENDL-3 data well reproduce the experimental data in the high energy region of all the angles, while others give small values in the discrete inelastic scattering region. The JENDL-3 data, however, tend to give large values in the low energy region at the backward angles, and give a 'shoulder' above the elastic scattering peak due to the same reason mentioned at section 3.2.

Reference for the Experimental Data in Figures

TAKAHASHI+('87): Takahashi A., Ichimura E., Sugimoto H. and Kato T.,
JAERI-M 86-080, 393 (1986).

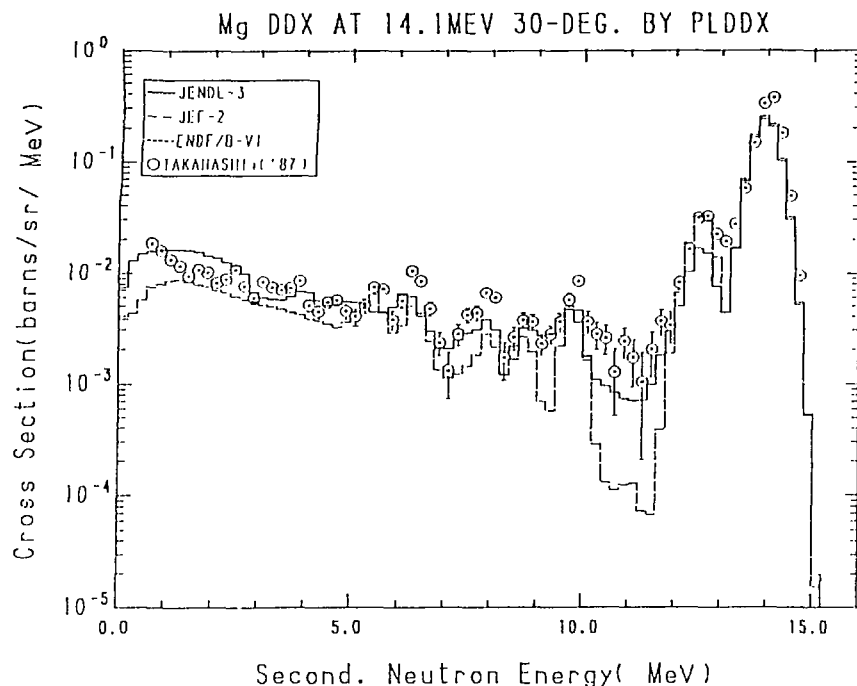


Fig. 19-1 The Magnesium Double Differential Cross Section at 14.1 MeV,
Emitted Angle = 30° in Laboratory System

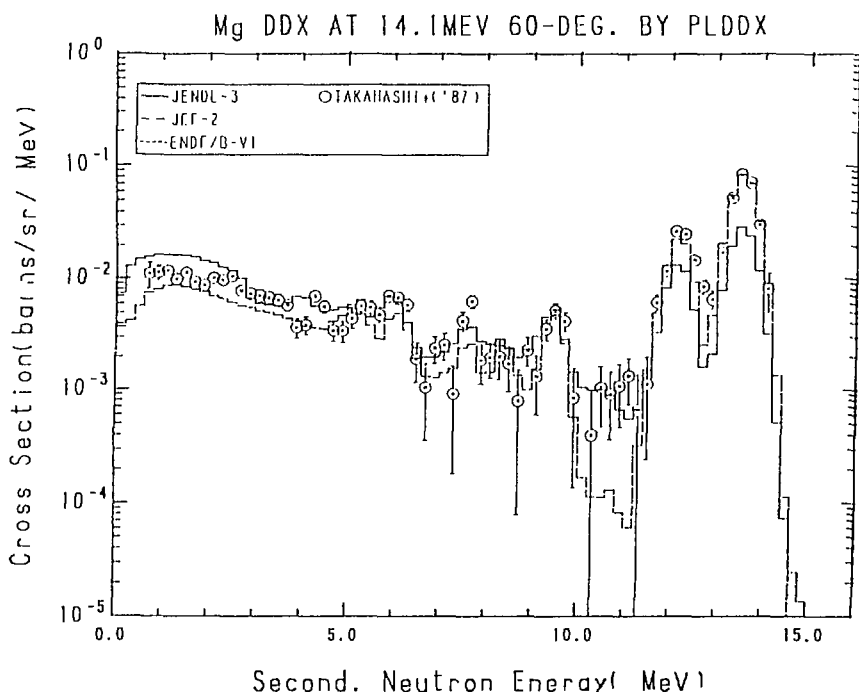


Fig. 19-2 The Magnesium Double Differential Cross Section at 14.1 MeV,
Emitted Angle = 60° in Laboratory System

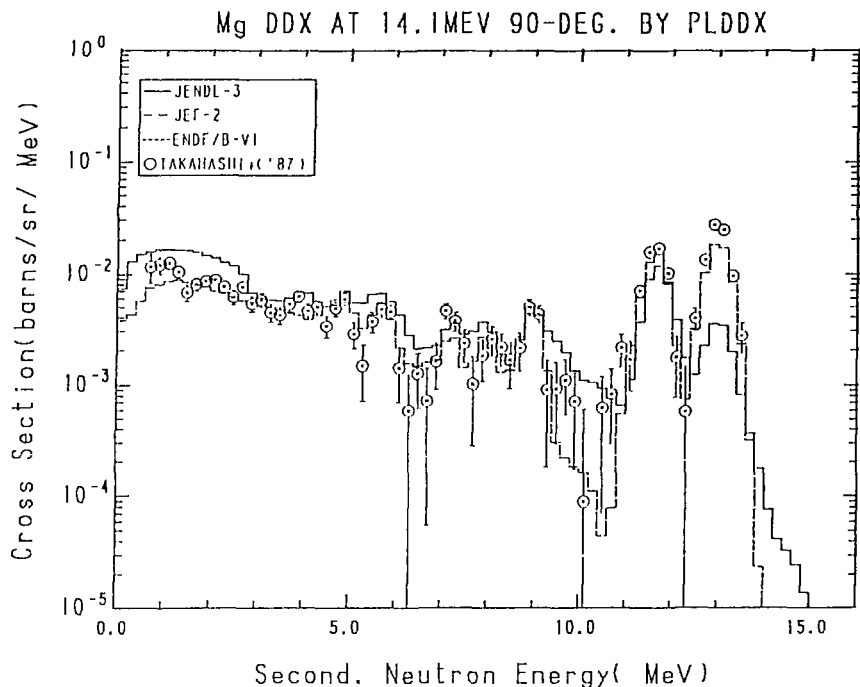


Fig. 19-3 The Magnesium Double Differential Cross Section at 14.1 MeV,
Emitted Angle = 90° in Laboratory System

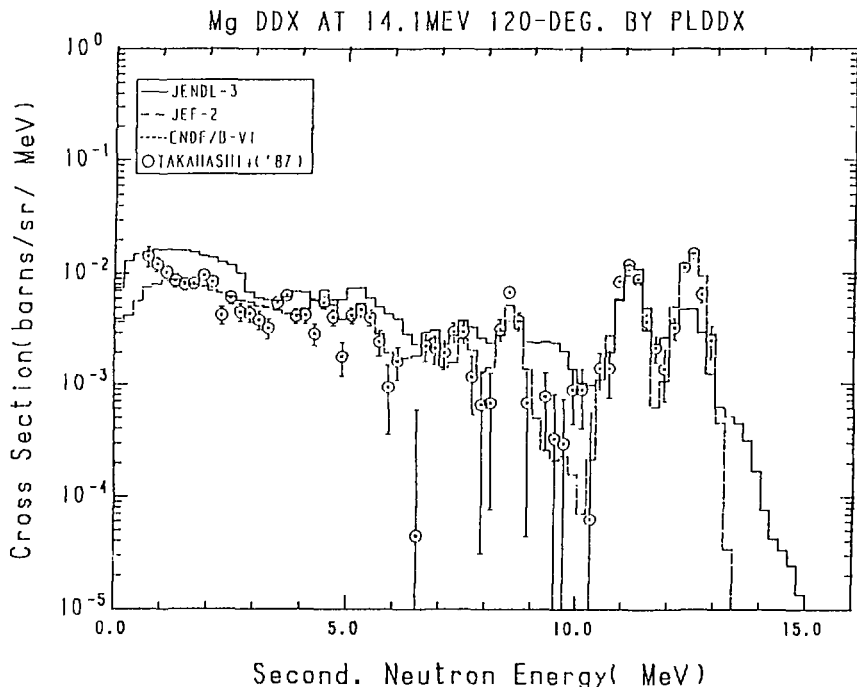


Fig. 19-4 The Magnesium Double Differential Cross Section at 14.1 MeV,
Emitted Angle = 120° in Laboratory System

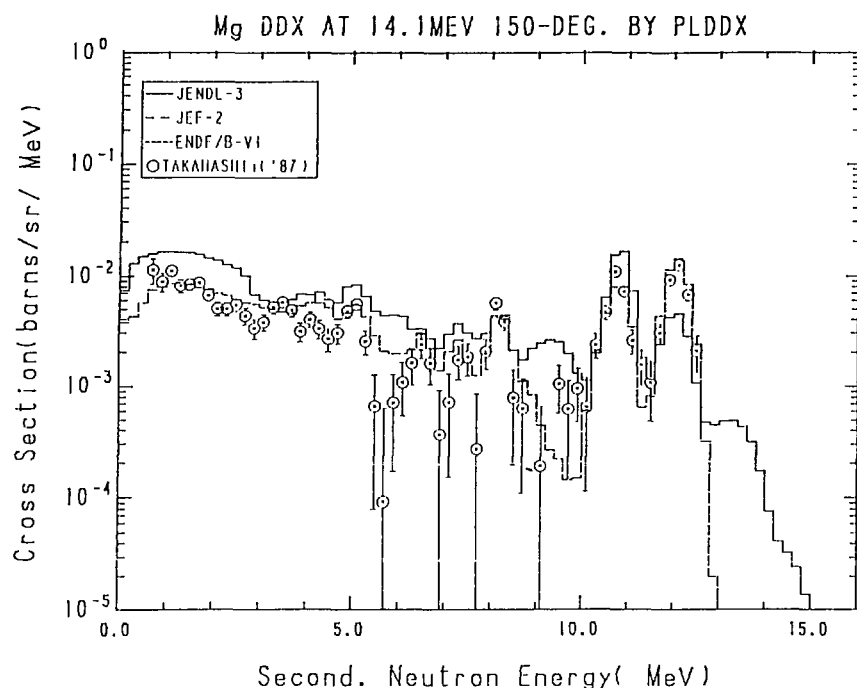


Fig. 19-5 The Magnesium Double Differential Cross Section at 14.1 MeV,
Emitted Angle = 150° in Laboratory System

3.10 Aluminum

The DDXs calculated from the evaluated data of ^{27}Al are compared with the experimental data/YABUTA+('86), TAKAHASHI+('87)/ of 36° , 60° , 80° , 120° and 150° at the incident neutron energy of 14.1 MeV in Fig.20, and those/BABA+('88)/ of 30° , 60° , 90° , 120° and 147° at 18.0 MeV in Fig.21. The evaluated data can almost reproduce the experimental data. However, the JENDL-3 data give smaller values in the middle energy region at the forward angles at 14.1 MeV and of all the angles at 18.0 MeV.

References for the Experimental Data in Figures

- BABA+('88) : Baba M., Ishikawa M., Yabuta N., Kikuchi T., Wakabayashi H. and Hirakawa H., Proc. of Int. Conf. on Nucl. Data for Sci. and Technol. at Mito in May 30- Jun. 3, p.291 (1988).
- TAKAHASHI+('87) : Takahashi A., Ichimura E., Sugimoto H. and Kato T., JAERI-M 86-080, 393 (1986).
- YABUTA('86) : Baba M., Ishikawa M., Yabuta N., Kikuchi T., Wakabayashi H. and Hirakawa H., Proc. of Int. Conf. on Nucl. Data for Sci. and Technol. at Mito in May 30- Jun. 3, p.291 (1988).

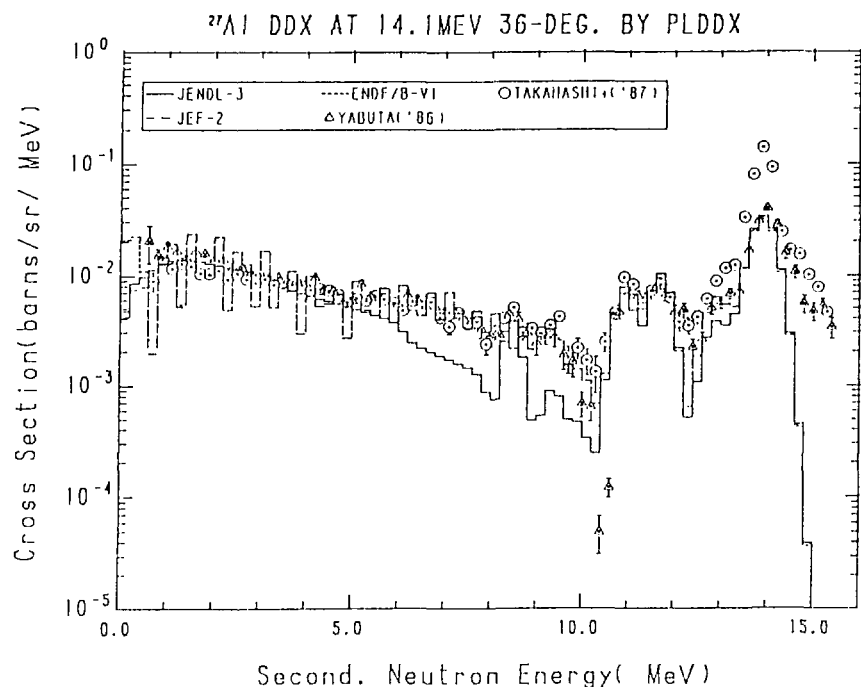


Fig. 20-1 The ^{27}Al Double Differential Cross Section at 14.1 MeV,
Emitted Angle = 36° in Laboratory System

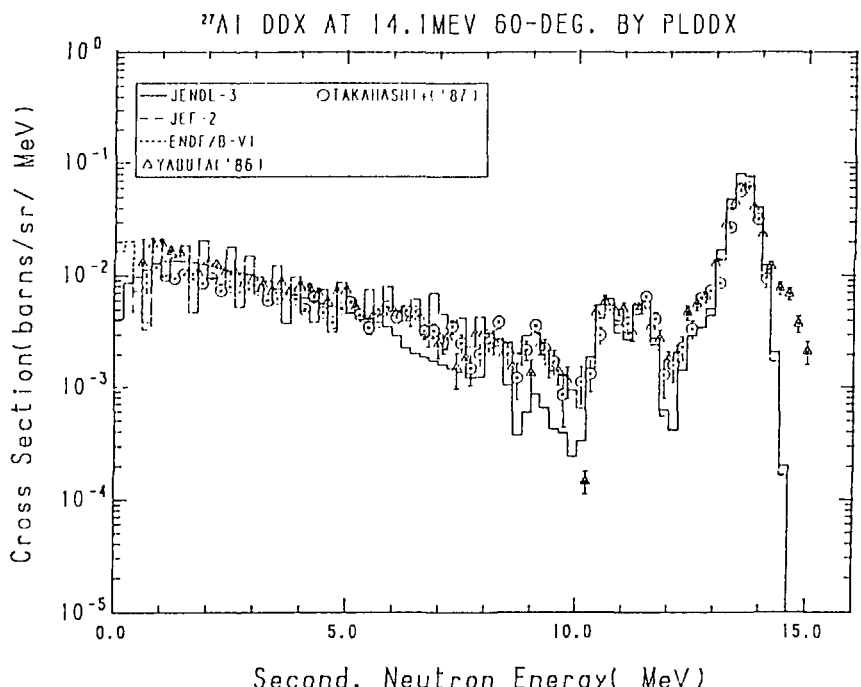


Fig. 20-2 The ^{27}Al Double Differential Cross Section at 14.1 MeV,
Emitted Angle = 60° in Laboratory System

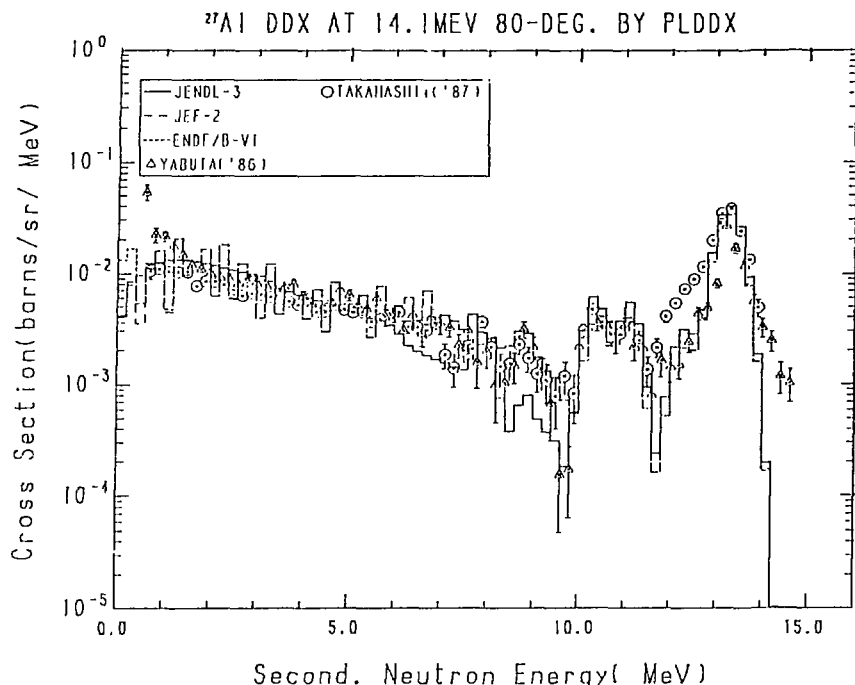


Fig. 20-3 The ^{27}Al Double Differential Cross Section at 14.1 MeV,
Emitted Angle = 80° in Laboratory System

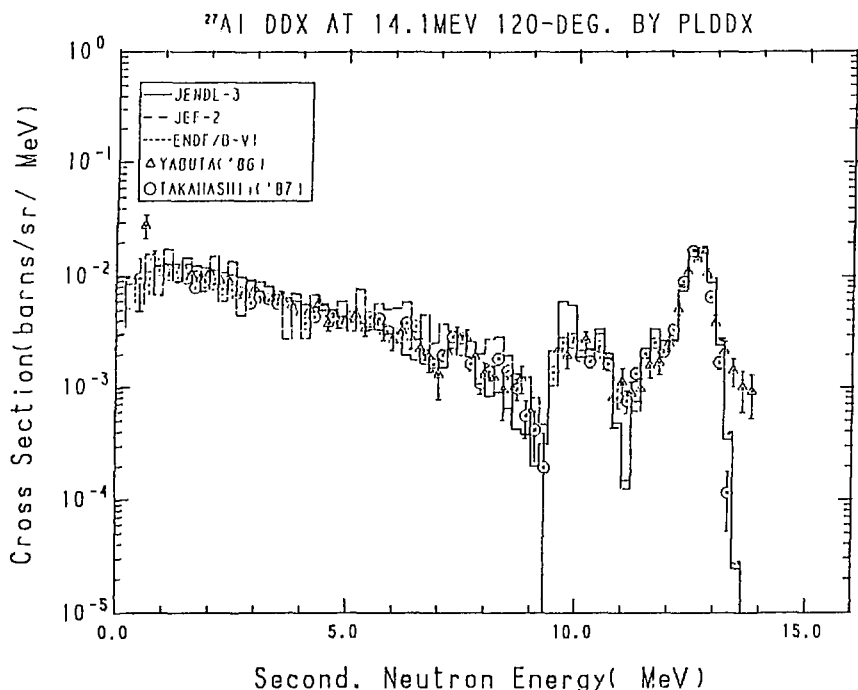


Fig. 20-4 The ^{27}Al Double Differential Cross Section at 14.1 MeV,
Emitted Angle = 120° in Laboratory System

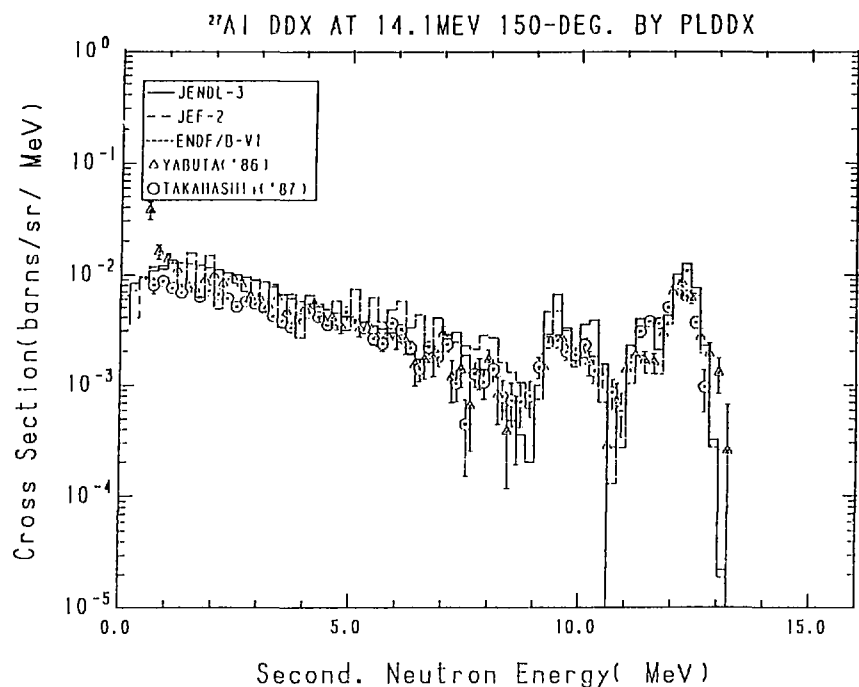


Fig. 20-5 The ^{27}Al Double Differential Cross Section at 14.1 Mev,
Emitted Angle = 150° in Laboratory System

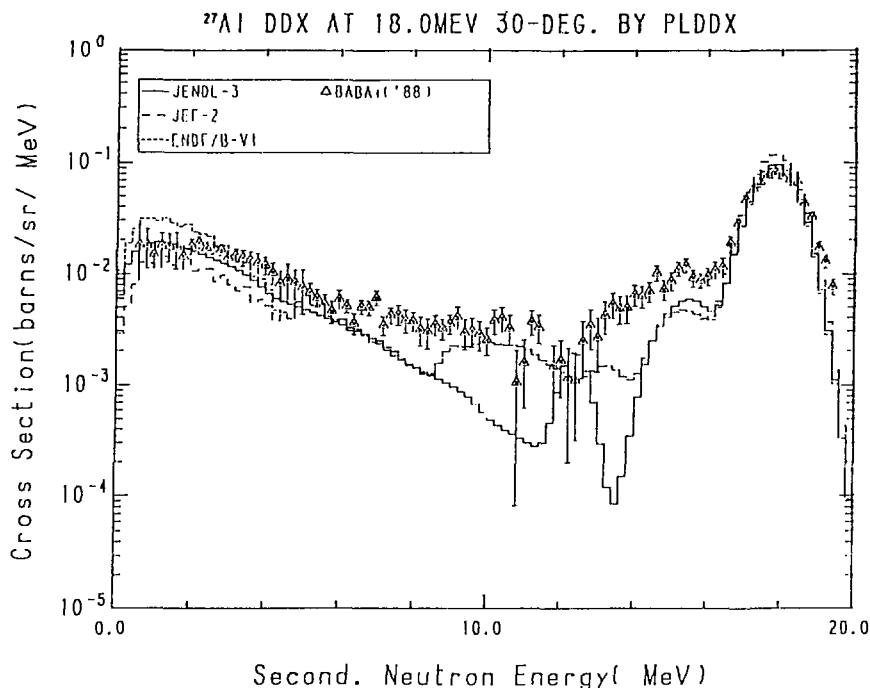


Fig. 21-1 The ^{27}Al Double Differential Cross Section at 18.0 MeV,
Emitted Angle = 30° in Laboratory System

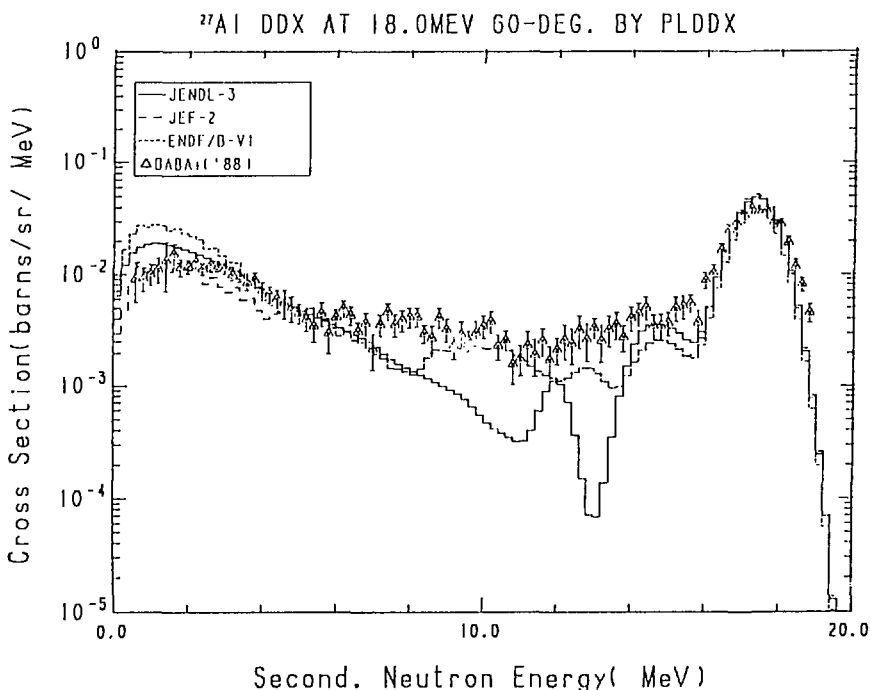


Fig. 21-2 The ^{27}Al Double Differential Cross Section at 18.0 MeV,
Emitted Angle = 60° in Laboratory System

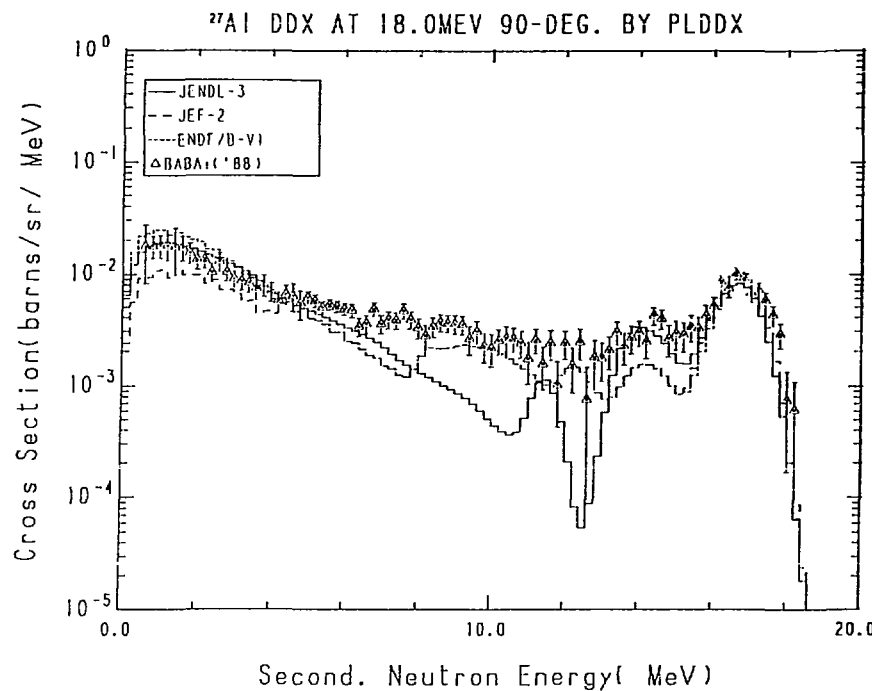


Fig. 21-3 The ^{27}Al Double Differential Cross Section at 18.0 MeV,
Emitted Angle = 90° in Laboratory System

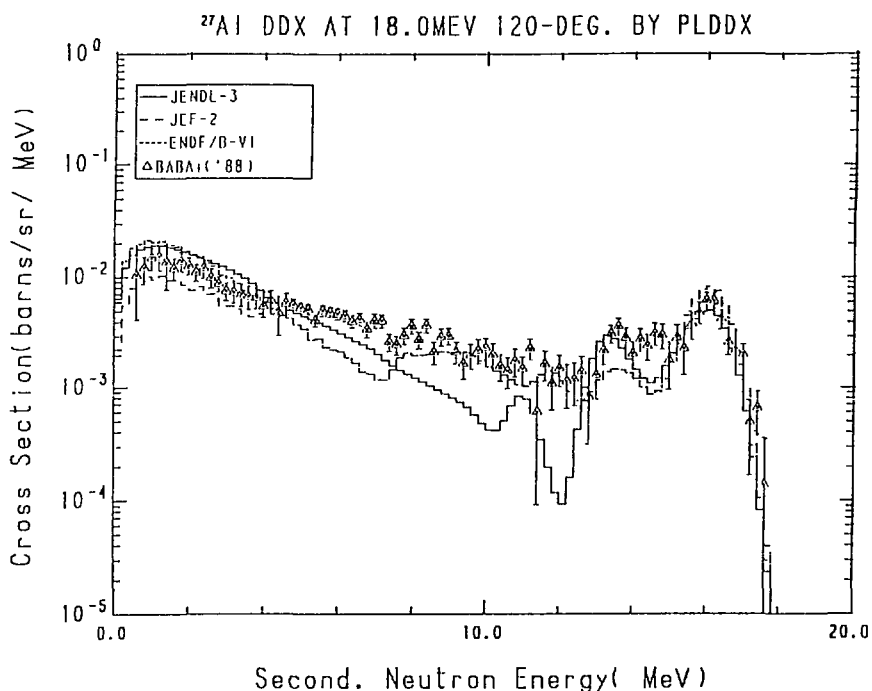


Fig. 21-4 The ^{27}Al Double Differential Cross Section at 18.0 MeV,
Emitted Angle = 120° in Laboratory System

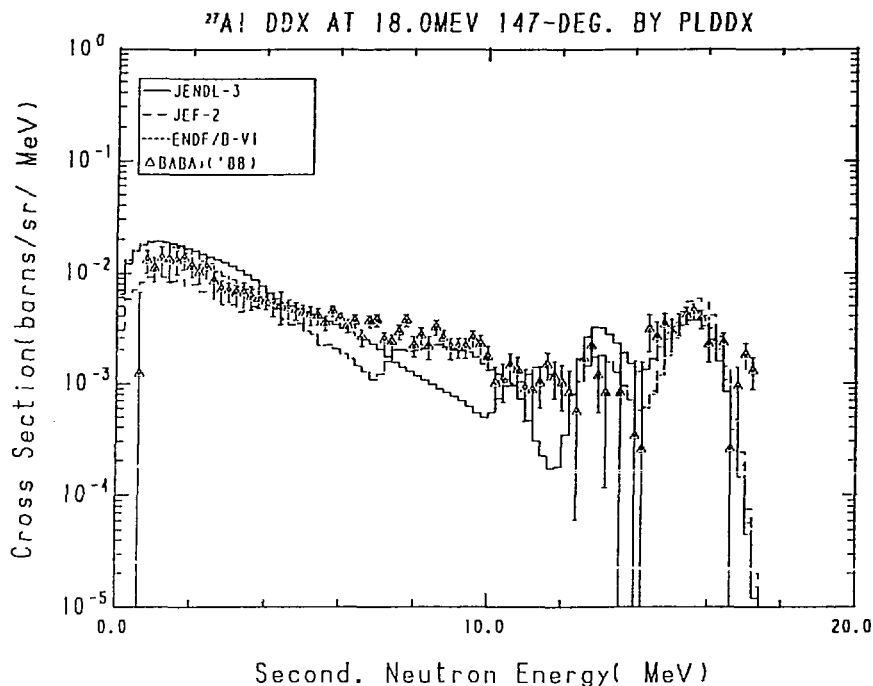


Fig. 21-5 The ^{27}Al Double Differential Cross Section at 18.0 MeV,
Emitted Angle = 147° in Laboratory System

3.11 Silicon

The DDXs calculated from the evaluated data of silicon are compared with the experimental data of 30° , 60° , 80° , 120° and 150° for $^{28}\text{Si}/\text{ONO('85)}/$ and $^{nat}\text{Si}/\text{TAKAHASHI+('86)}/$ at the incident neutron energy of 14.1 MeV in Fig.22. The evaluated data can reproduce the experimental data in the higher energy region. At 30° , they give small values in the lower energy region. At the other angles, the JENDL-3 data reproduce the data measured at Osaka university and the ENDF/B-VI and JEF-2 data reproduce the data measured at Tohoku university.

References for the Experimental Data in Figures

- ONO('85) : Baba M., Ono M., Yabuta N., Kikuchi T. and Hirakawa N.,
Proc. of Int. Conf. on Nucl. Data for Basic and Applied
Sci. at Santa Fe in May 13-17, p.223 (1985).
- TAKAHASHI+('86): Takahashi A., Ichimura E., Sugimoto H. and Kato T.,
JAERI-M 86-080, 393 (1986).

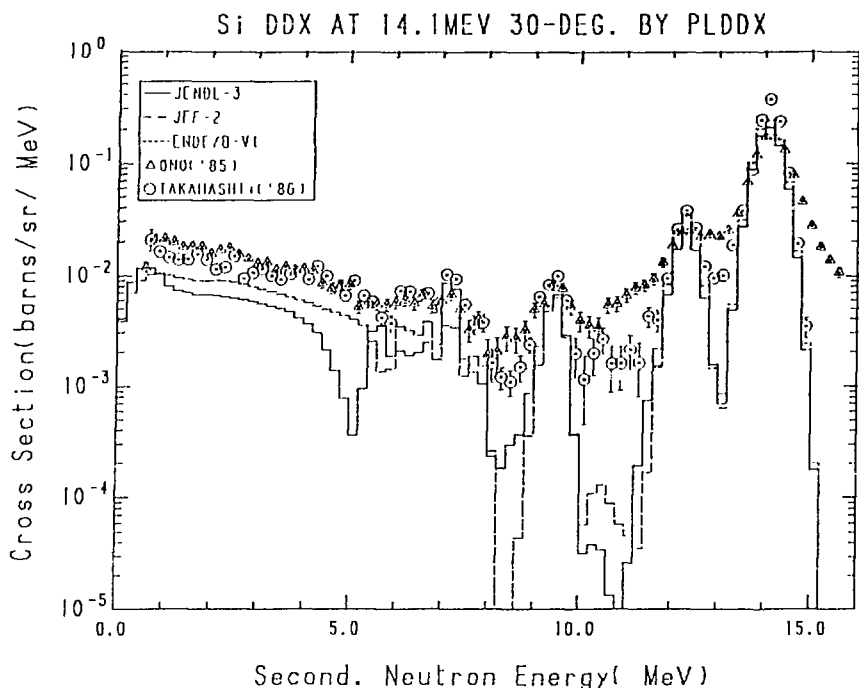


Fig. 22-1 The Silicon Double Differential Cross Section at 14.1 MeV,
Emitted Angle = 30° in Laboratory System

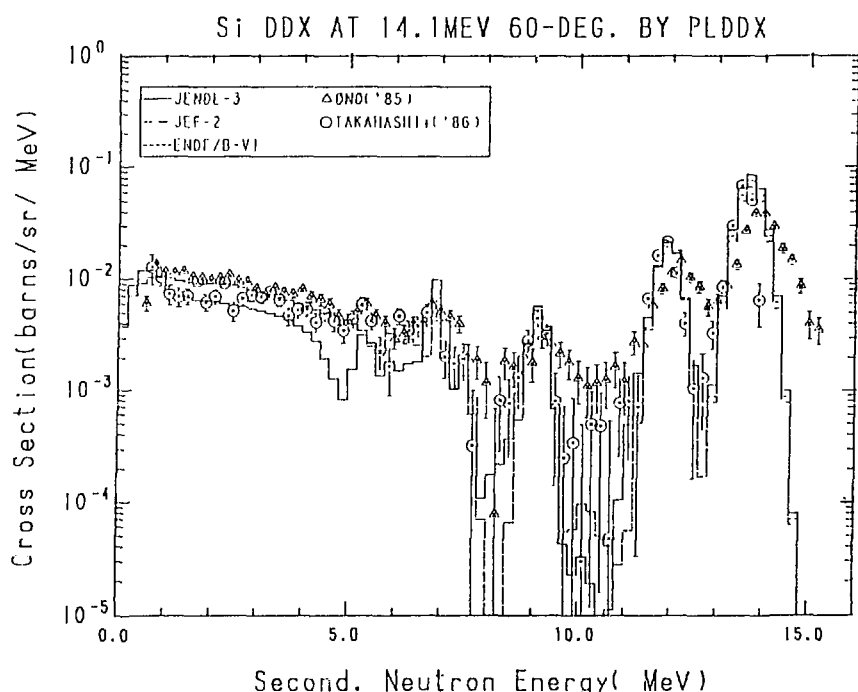


Fig. 22-2 The Silicon Double Differential Cross Section at 14.1 MeV,
Emitted Angle = 60° in Laboratory System

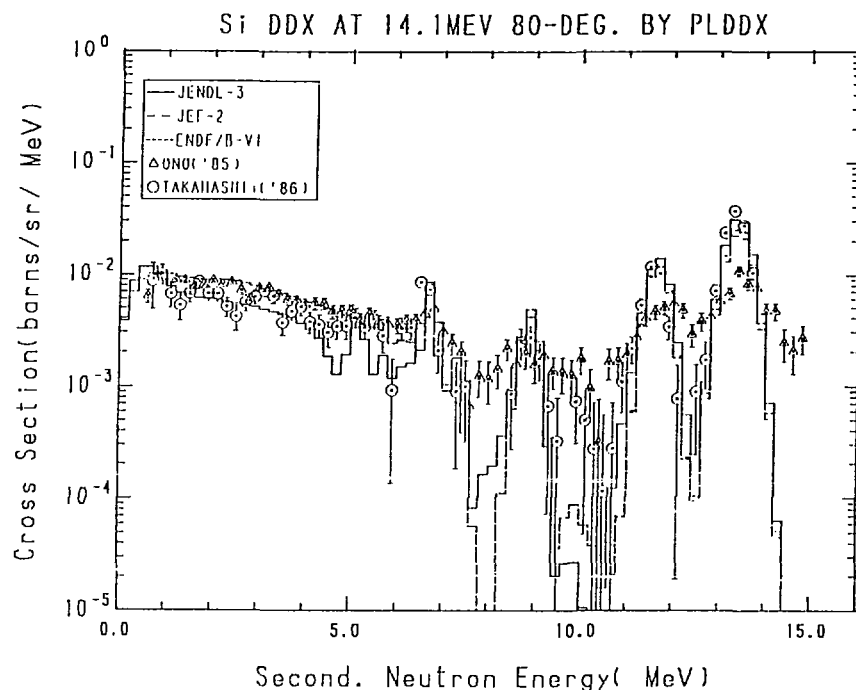


Fig. 22-3 The Silicon Double Differential Cross Section at 14.1 MeV,
Emitted Angle = 80° in Laboratory System

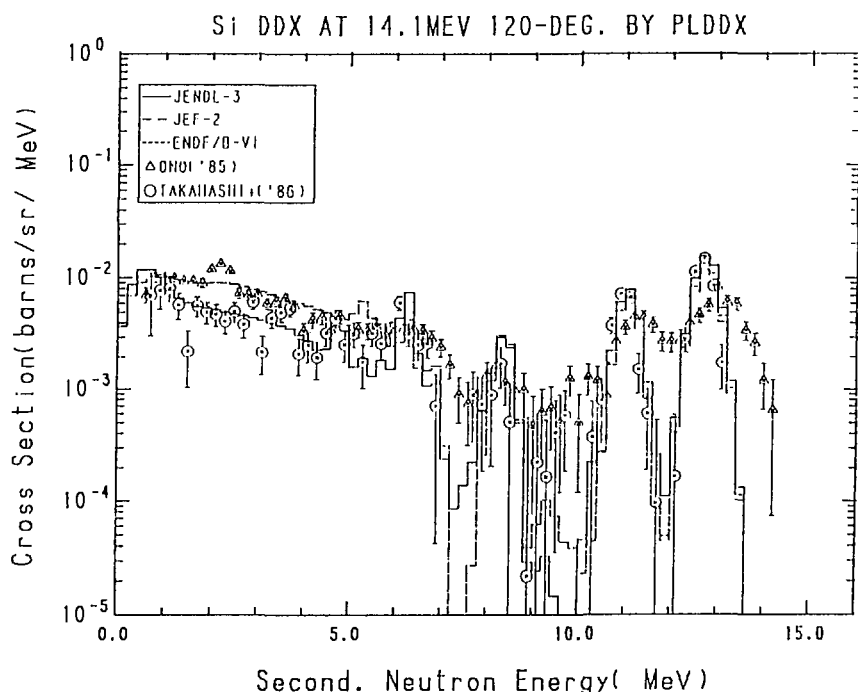


Fig. 22-4 The Silicon Double Differential Cross Section at 14.1 MeV,
Emitted Angle = 120° in Laboratory System

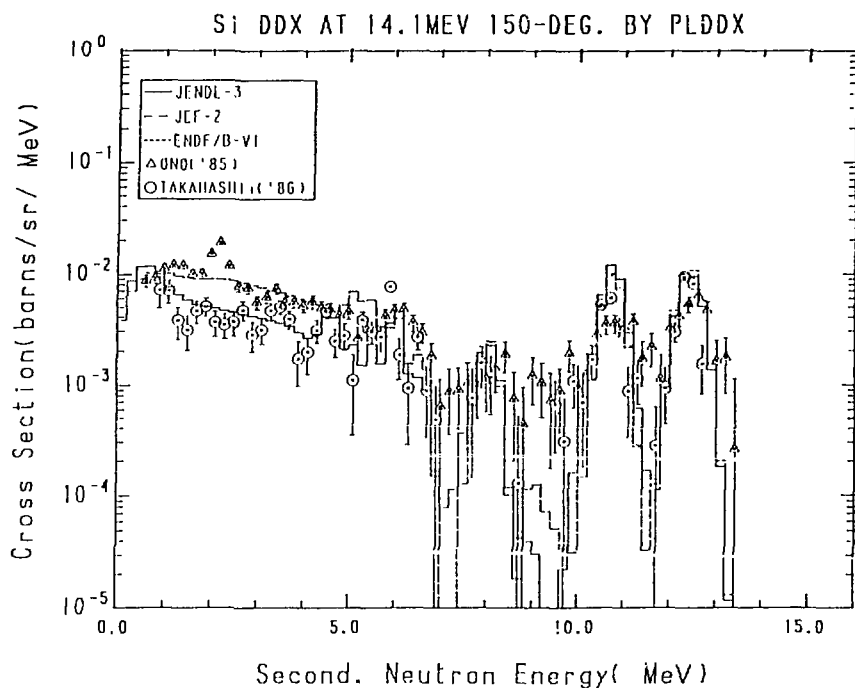


Fig. 22-5 The Silicon Double Differential Cross Section at 14.1 MeV,
Emitted Angle = 150° in Laboratory System

3.12 Sulphur

The DDXs calculated from the evaluated data of sulphur are compared with the experimental data/TAKAHASHI('86)/ of 45°, 60°, 80°, 110° and 135°, whose incident energies change according to scattered angles, in Fig.23. The comparison could not be made for JEF-2, since this library include no data for the natural elements and there exists no processing code which can create those data easily. In the discrete inelastic scattering region, the JENDL-3 data well reproduce the experimental data, while the ENDF/B-VI data give smaller values. In the lower energy region, the JENDL-3 data give small values below 4 MeV, and the ENDF/B-VI data lie lower than the experimental data in the 3-7 MeV region at 45°.

Reference for the Experimental Data in Figures

TAKAHASHI+('86): Takahashi A., JAERI-M 86-029, 99 (1986).

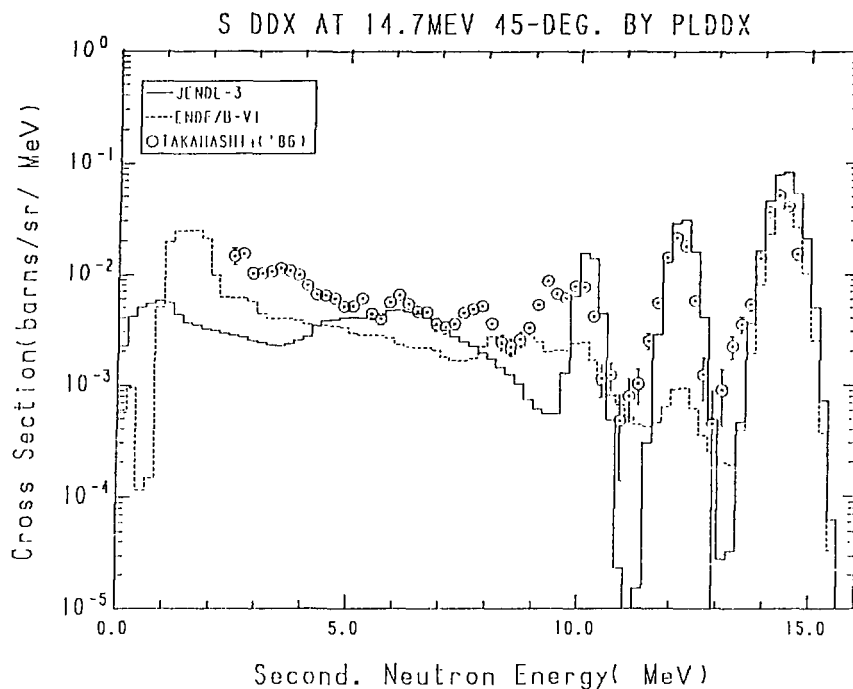


Fig. 23-1 The Sulphur Double Differential Cross Section,
Incident Energy = 14.7 MeV, Emitted Angle = 45°

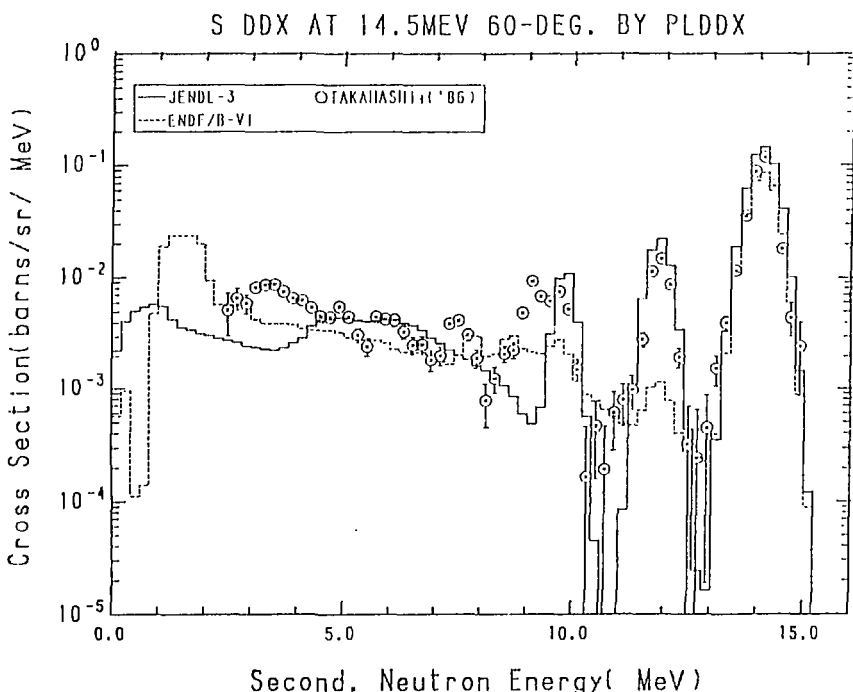


Fig. 23-2 The Sulphur Double Differential Cross Section,
Incident Energy = 14.5 MeV, Emitted Angle = 60°

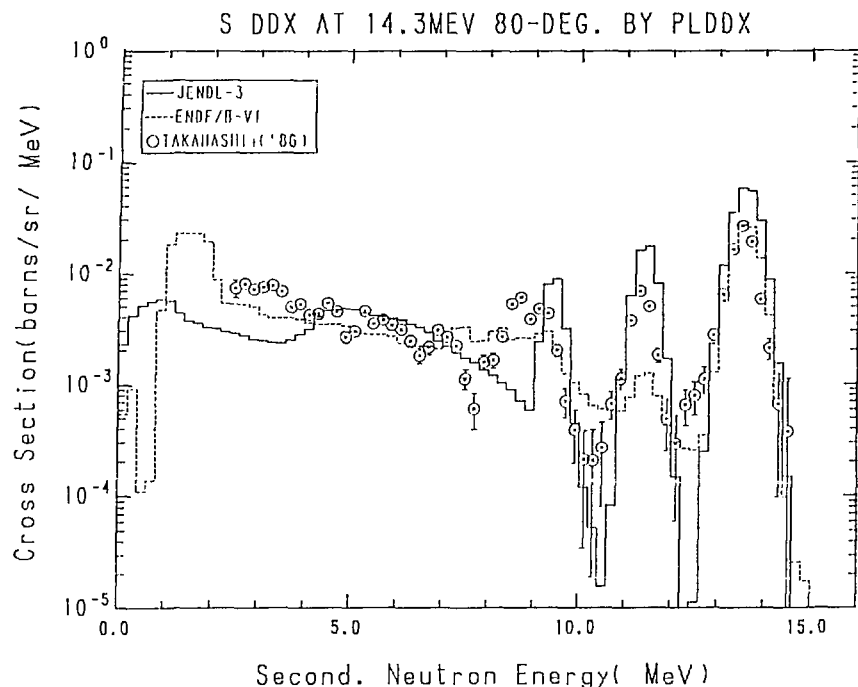


Fig. 23-3 The Sulphur Double Differential Cross Section,
Incident Energy = 14.3 MeV, Emitted Angle = 80°

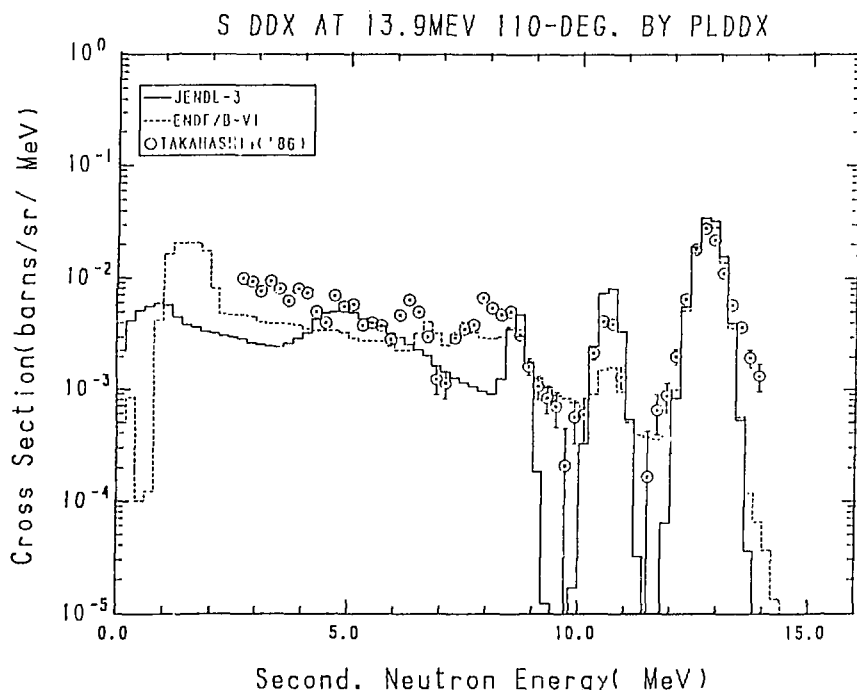


Fig. 23-4 The Sulphur Double Differential Cross Section,
Incident Energy = 13.9 MeV, Emitted Angle = 110°

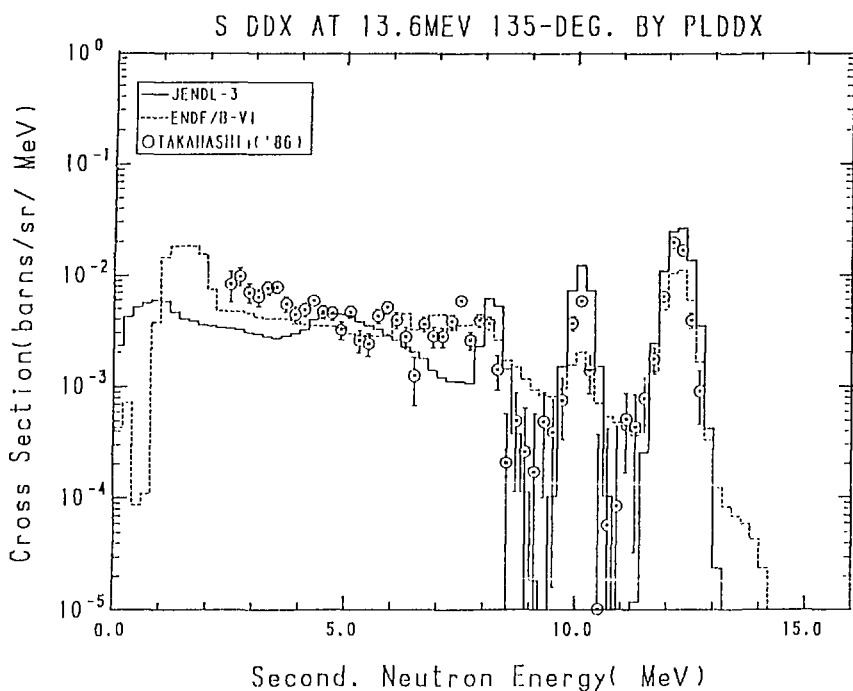


Fig. 23-5 The Sulphur Double Differential Cross Section,
Incident Energy = 13.6 MeV, Emitted Angle = 135°

3.13 Calcium

The DDXs calculated from the evaluated data of calcium are compared with the experimental data/TAKAHASHI+('86)/ of 30° , 60° , 90° , 120° and 150° at the incident neutron energy of 14.1 MeV in Fig.24. The evaluated data almost reproduce the experimental data. However, they, especially the JENDL-3 data, tend to overestimate the continuous spectra at the backward angles.

Reference for the Experimental Data in Figures

TAKAHASHI+('86): Takahashi A., private communication (1989).

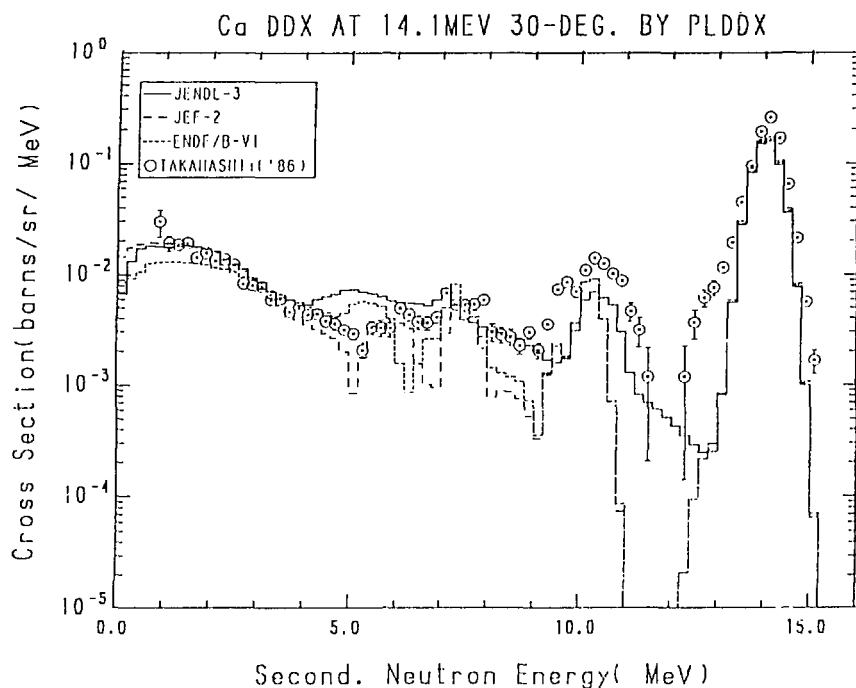


Fig. 24-1 The Calcium Double Differential Cross Section at 14.1 MeV,
Emitted Angle = 30° in Laboratory System

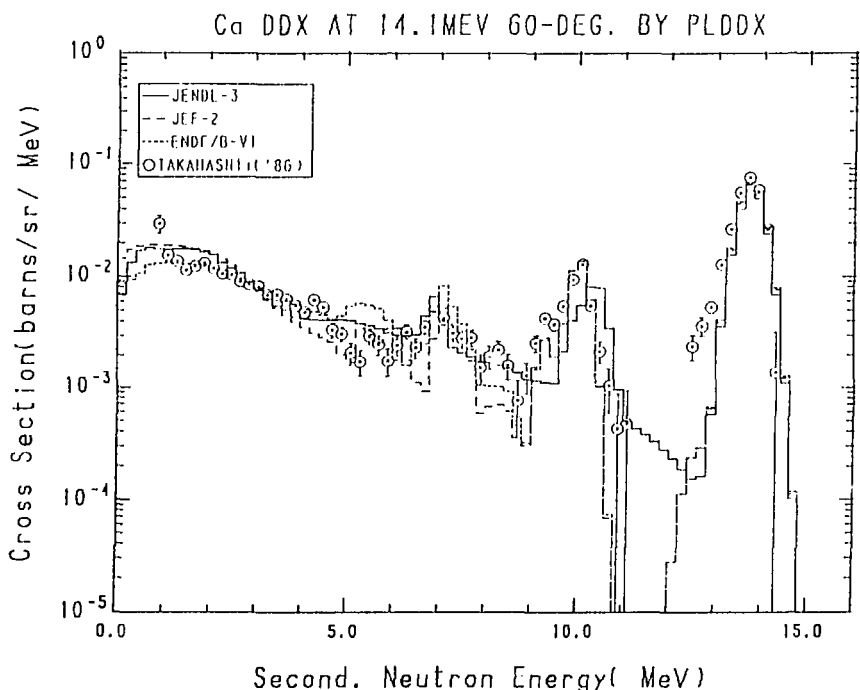


Fig. 24-2 The Calcium Double Differential Cross Section at 14.1 MeV,
Emitted Angle = 60° in Laboratory System

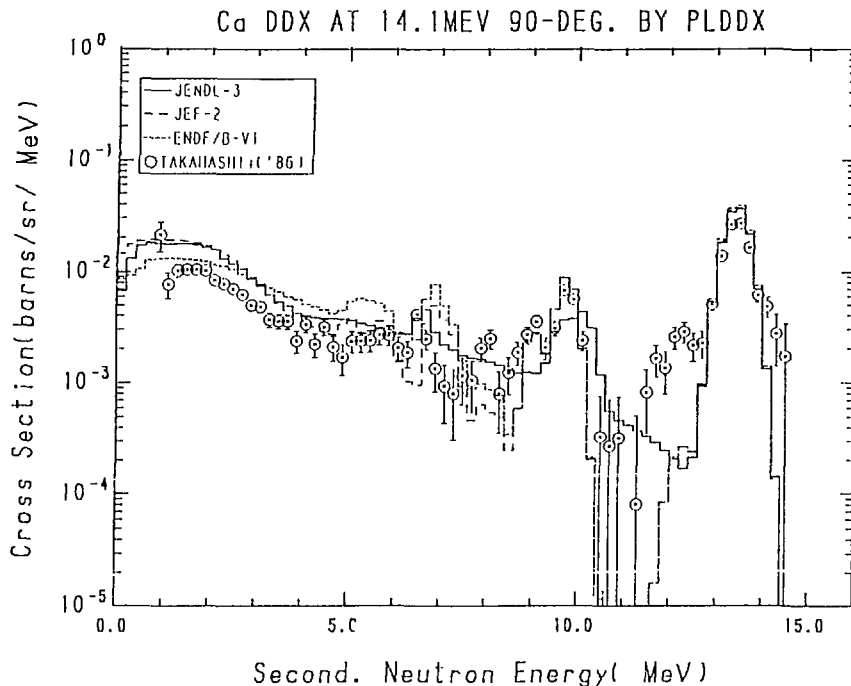


Fig. 24-3 The Calcium Double Differential Cross Section at 14.1 MeV,
Emitted Angle = 90° in Laboratory System

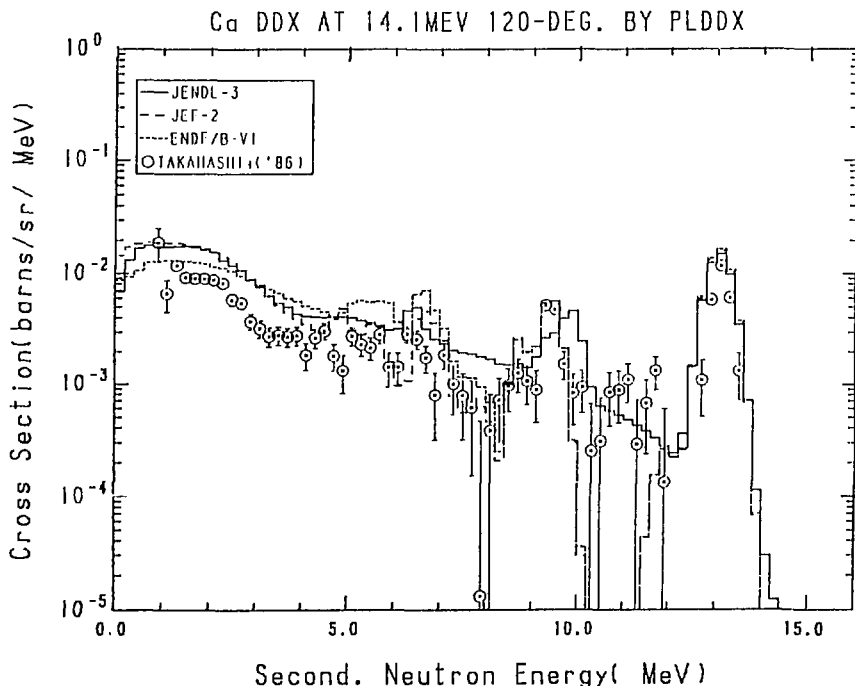


Fig. 24-4 The Calcium Double Differential Cross Section at 14.1 MeV,
Emitted Angle = 120° in Laboratory System

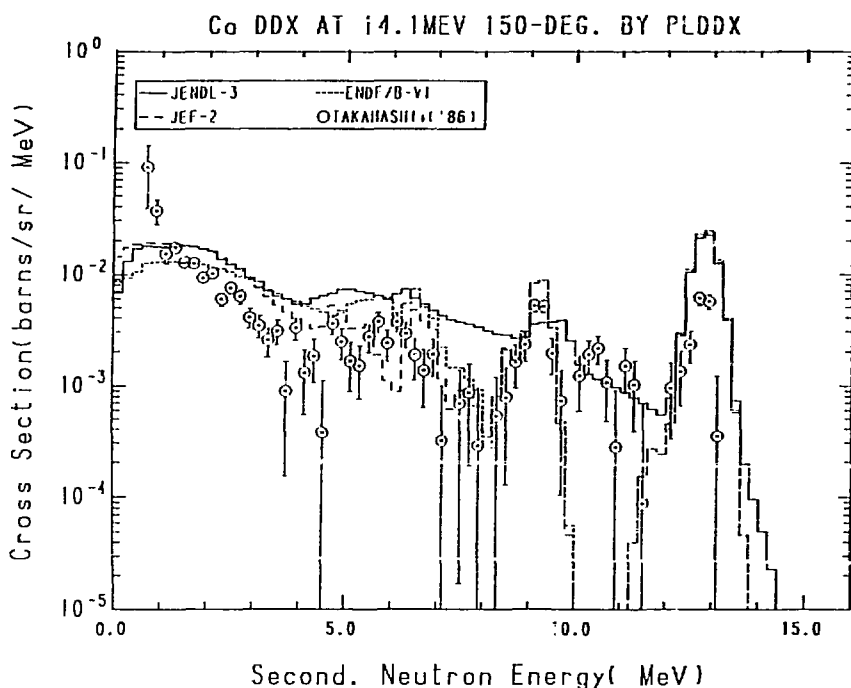


Fig. 24-5 The Calcium Double Differential Cross Section at 14.1 MeV,
Emitted Angle = 150° in Laboratory System

3.14 Titanium

The DDXs calculated from the evaluated data of titanium are compared with the experimental data/BABA+('88),TAKAHASHI+('86)/ of 30° , 50° , 80° , 120° and 150° at the incident neutron energy of 14.1 MeV in Fig.25. A discrepancy between two experimental data is observed just below the elastic scattering peak, and the JENDL-3 data reproduce the data measured at Tohoku university. In the low energy region, the JENDL-3 data give large values at 150° and the others give smaller values at the forward angles than the experimental data.

References for the Experimental Data in Figures

- BABA+('88) : Baba M., Ishikawa M., Yabuta N., Kikuchi T., Wakabayashi H. and Hirakawa H., Proc. of Int. Conf. on Nucl. Data for Sci. and Technol. at Mito in May 30- Jun. 3, p.291 (1988).
TAKAHASHI+('86): Takahashi A., private communication (1989).

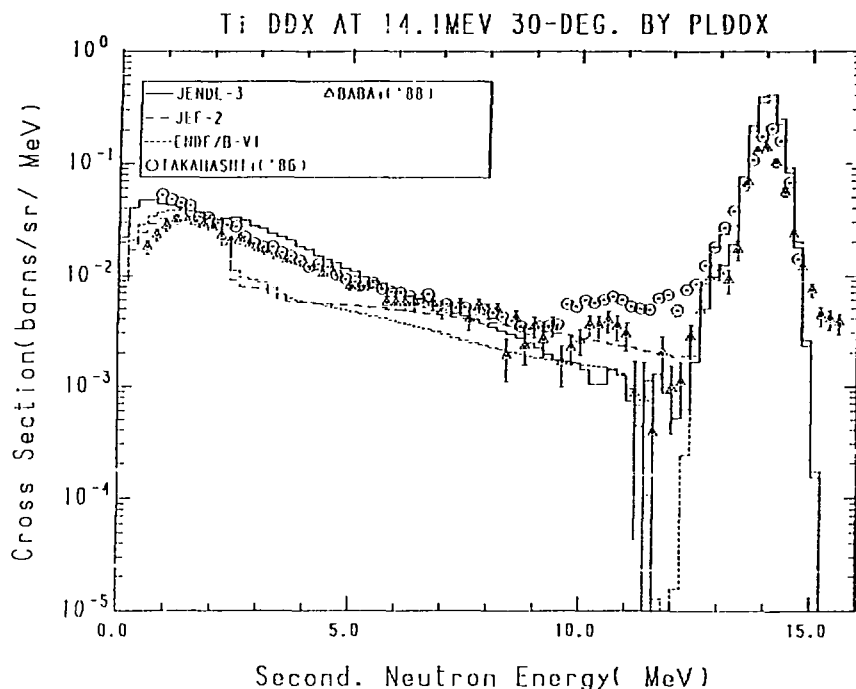


Fig. 25-1 The Titanium Double Differential Cross Section at 14.1 MeV,
Emitted Angle = 30° in Laboratory System

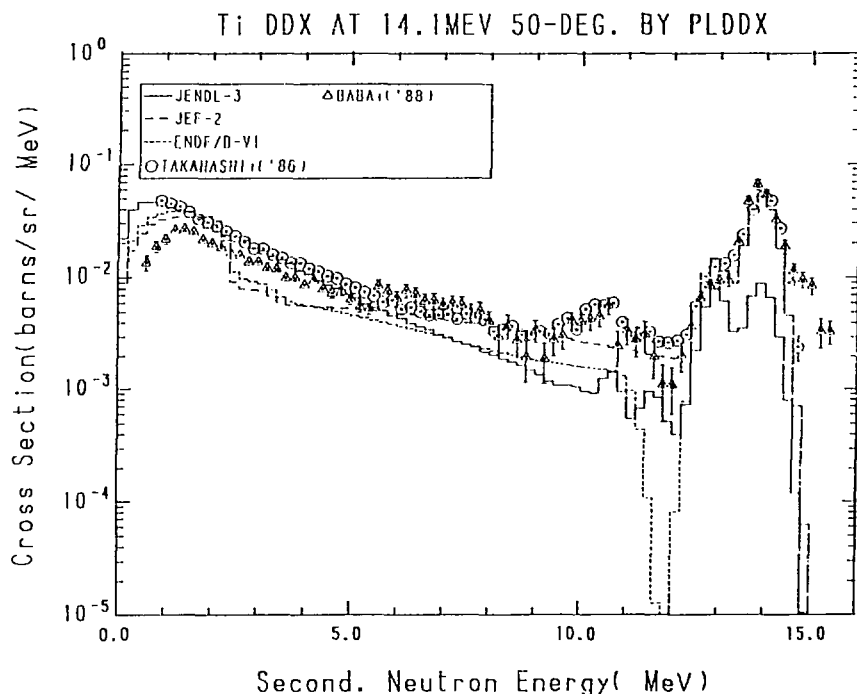


Fig. 25-2 The Titanium Double Differential Cross Section at 14.1 MeV,
Emitted Angle = 50° in Laboratory System

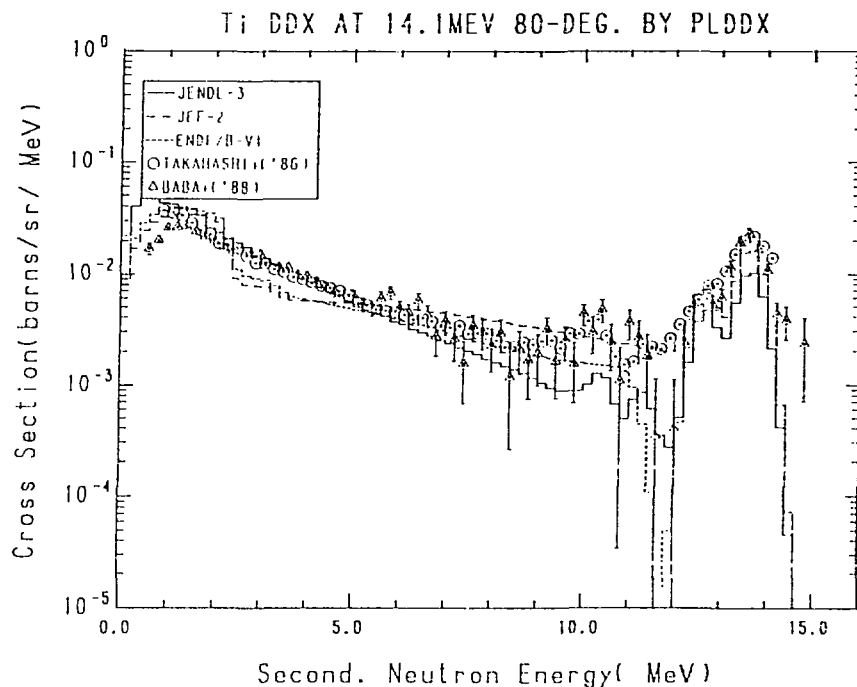


Fig. 25-3 The Titanium Double Differential Cross Section at 14.1 MeV,
Emitted Angle = 80° in Laboratory System

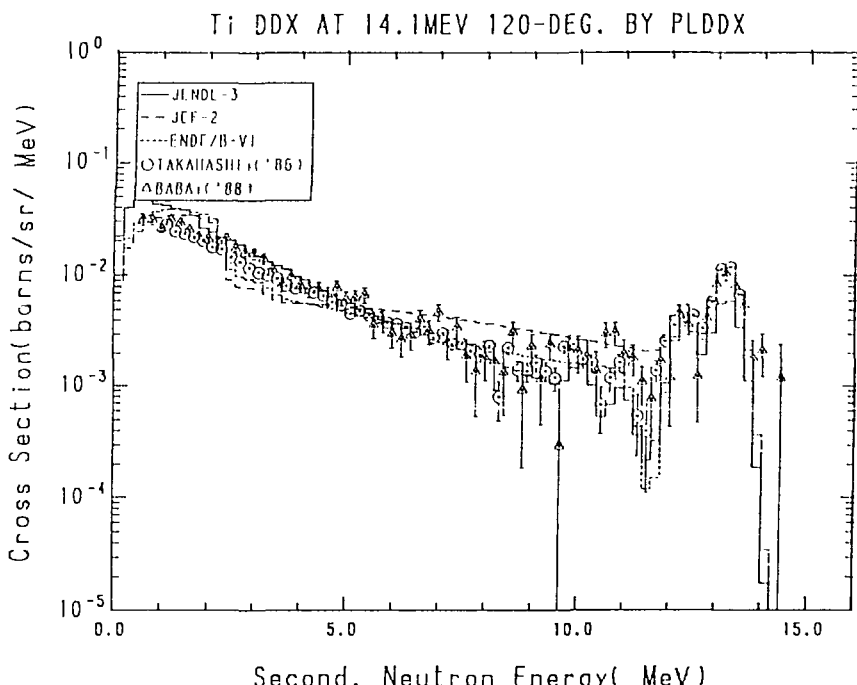


Fig. 25-4 The Titanium Double Differential Cross Section at 14.1 MeV,
Emitted Angle = 120° in Laboratory System

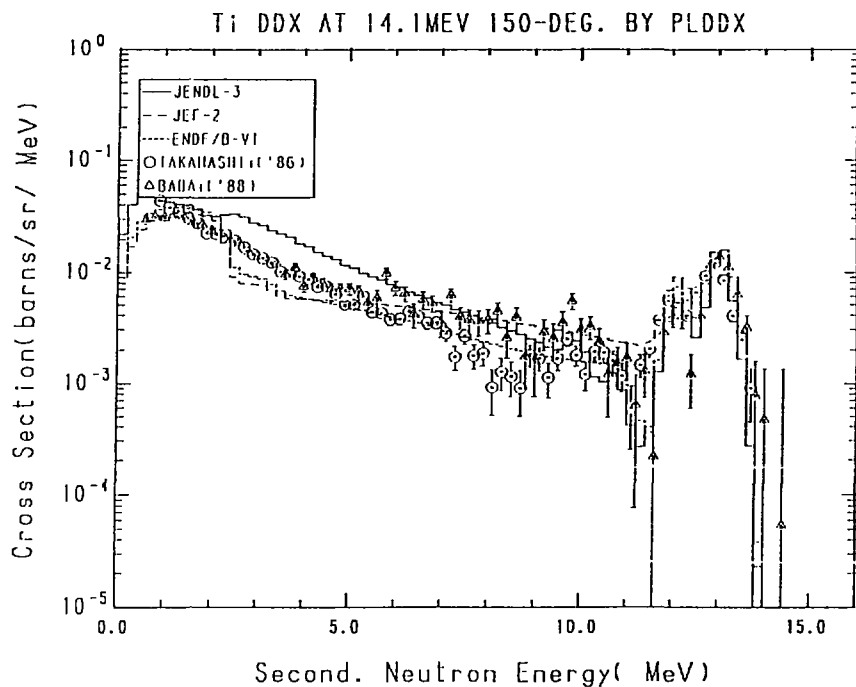


Fig. 25-5 The Titanium Double Differential Cross Section at 14.1 MeV,
Emitted Angle = 150° in Laboratory System

3.15 Vanadium

The DDXs calculated from the evaluated data of ^{51}V are compared with the experimental data/BABA+('88),TAKAHASHI+('87)/ of 30° , 60° , 90° , 120° and 150° at the incident neutron energy of 14.1 MeV in Fig.26. A large discrepancy between two experimental data is observed in the 6-9 MeV region, and the JENDL-3 and ENDF/B-VI data are close to the data measured at Tohoku university. The JEF-2 data underestimate but have the same trend of the data of the Osaka university. The JENDL-3 data give much higher values than the experimental data in the elastic and discrete inelastic scattering regions at the backward angles.

References for the Experimental Data in Figures

- BABA+('88) : Baba M., Ishikawa M., Yabuta N., Kikuchi T., Wakabayashi H. and Hirakawa H., Proc. of Int. Conf. on Nucl. Data for Sci. and Technol. at Mito in May 30- Jun. 3, p.291 (1988).
TAKAHASHI+('87): Takahashi A., Ichimura E., Sugimoto H. and Kato T., JAERI-M 86-080, 393 (1986).

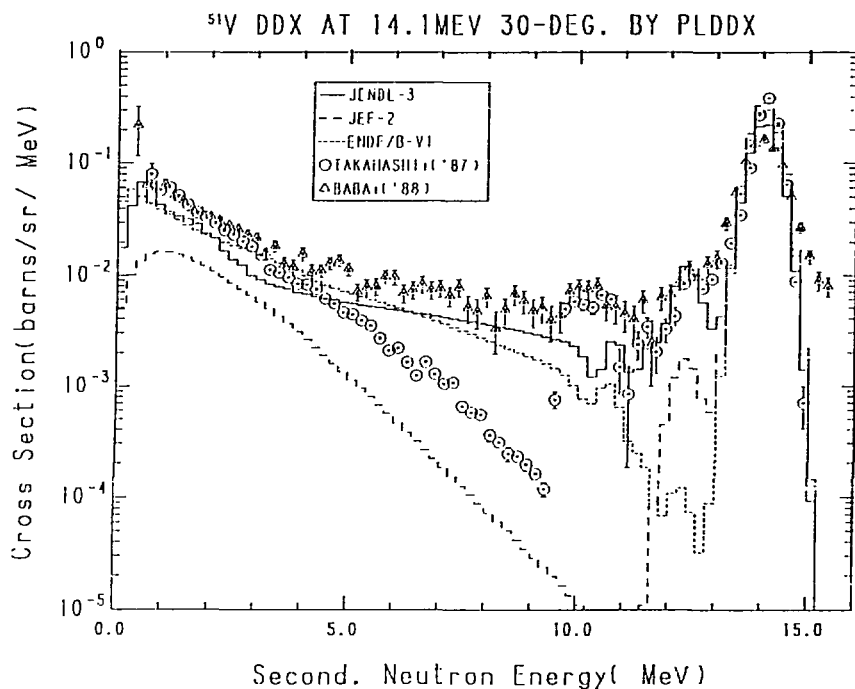


Fig. 26-1 The ^{51}V Double Differential Cross Section at 14.1 MeV,
Emitted Angle = 30° in Laboratory System

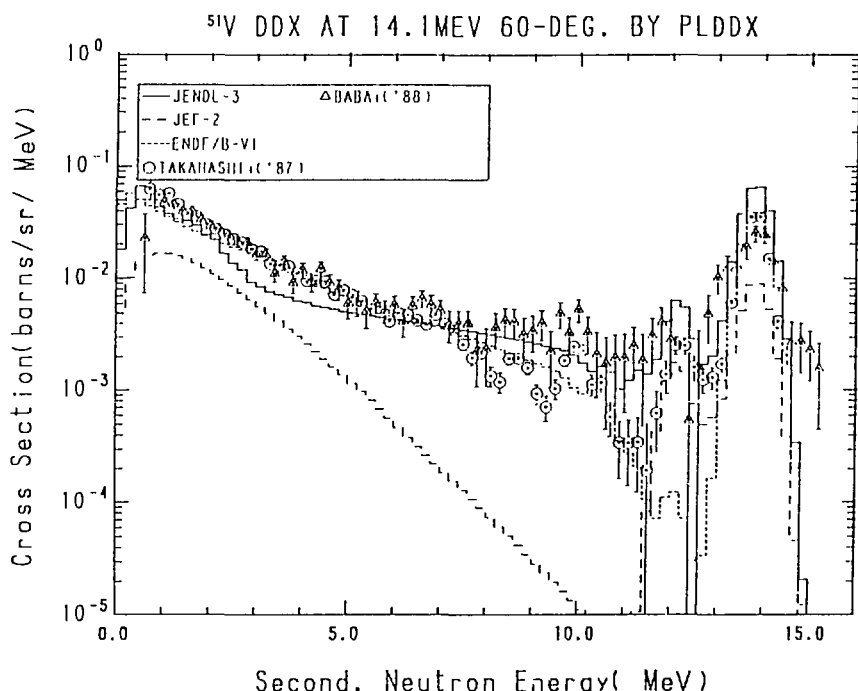


Fig. 26-2 The ^{51}V Double Differential Cross Section at 14.1 MeV,
Emitted Angle = 60° in Laboratory System

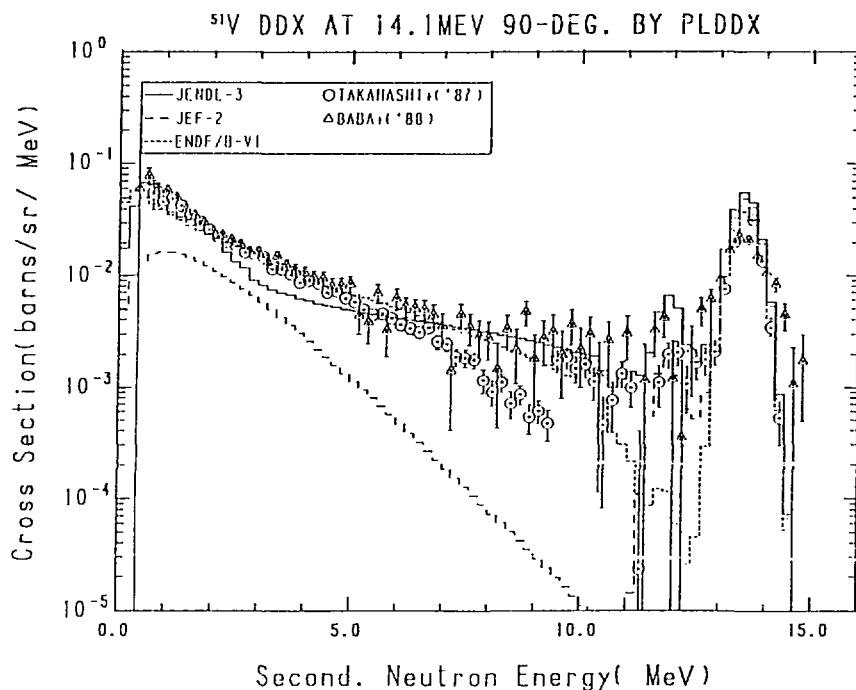


Fig. 26-3 The ^{51}V Double Differential Cross Section at 14.1 MeV,
Emitted Angle = 90° in Laboratory System

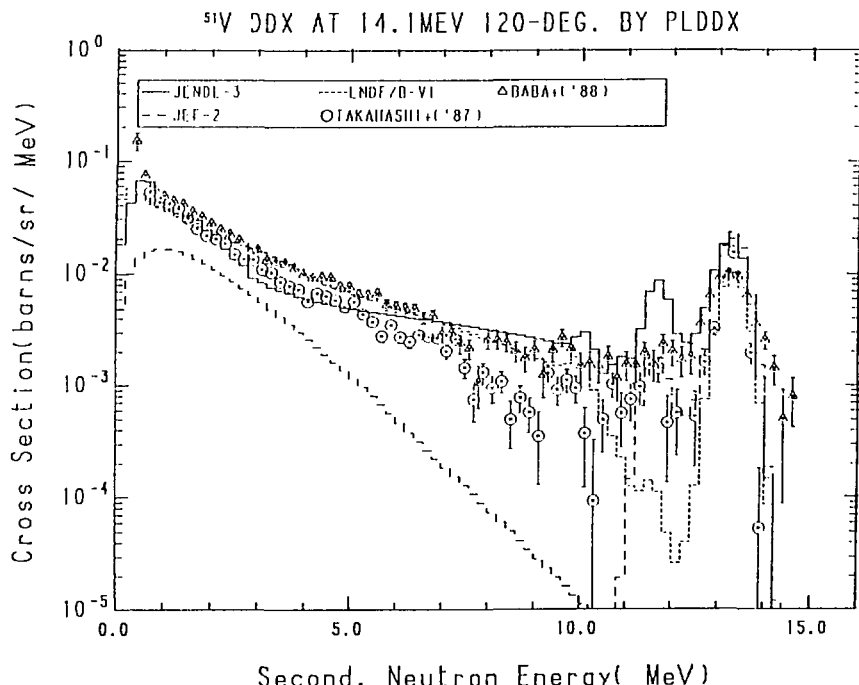


Fig. 26-4 The ^{51}V Double Differential Cross Section at 14.1 MeV,
Emitted Angle = 120° in Laboratory System

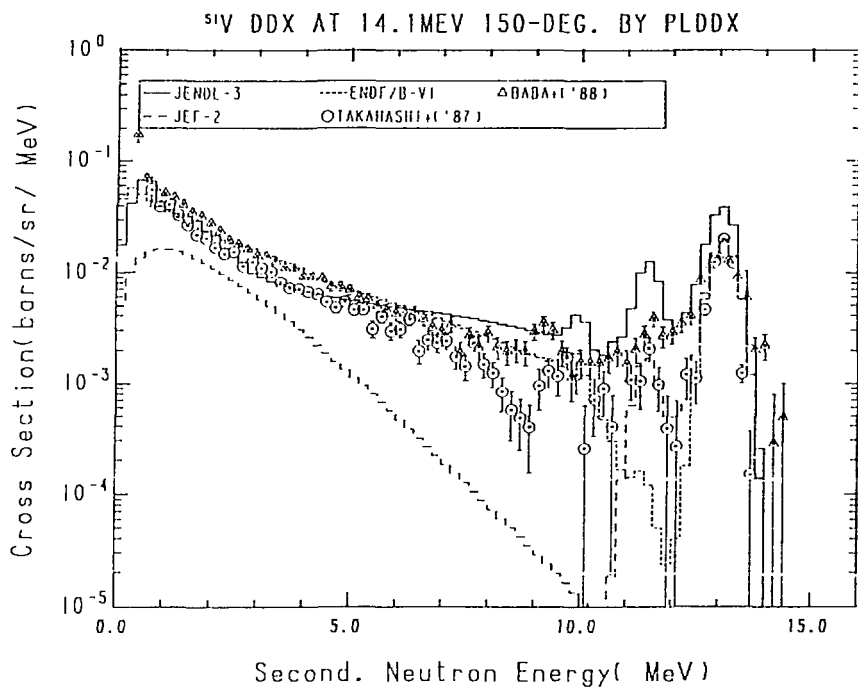


Fig. 26-5 The ^{51}V Double Differential Cross Section at 14.1 MeV,
Emitted Angle = 150° in Laboratory System

3.16 Chromium

Only the JENDL-3 DDX data of ^{nat}Cr are compared with the experimental data/BABA+('88),TAKAHASHI+('87)/ of 30°, 60°, 80°, 120° and 150° at the incident neutron energy of 14.1 MeV in Fig.27. The comparison could not be made for ENDF/B-VI and JEF-2, since these two libraries include no data for the natural elements and there exists no processing code which can create those data easily. The JENDL-3 data are almost in good agreement with the experimental data, except in the low energy region at 60° and 80° where they give smaller values, and in the 4-9 MeV region at 150° where they give larger values.

References for the Experimental Data in Figures

- BABA+('88) : Baba M., Ishikawa M., Yabuta N., Kikuchi T., Wakabayashi H. and Hirakawa H., Proc. of Int. Conf. on Nucl. Data for Sci. and Technol. at Mito in May 30- Jun. 3, p.291 (1988).
TAKAHASHI+('87): Takahashi A., private communication (1989).

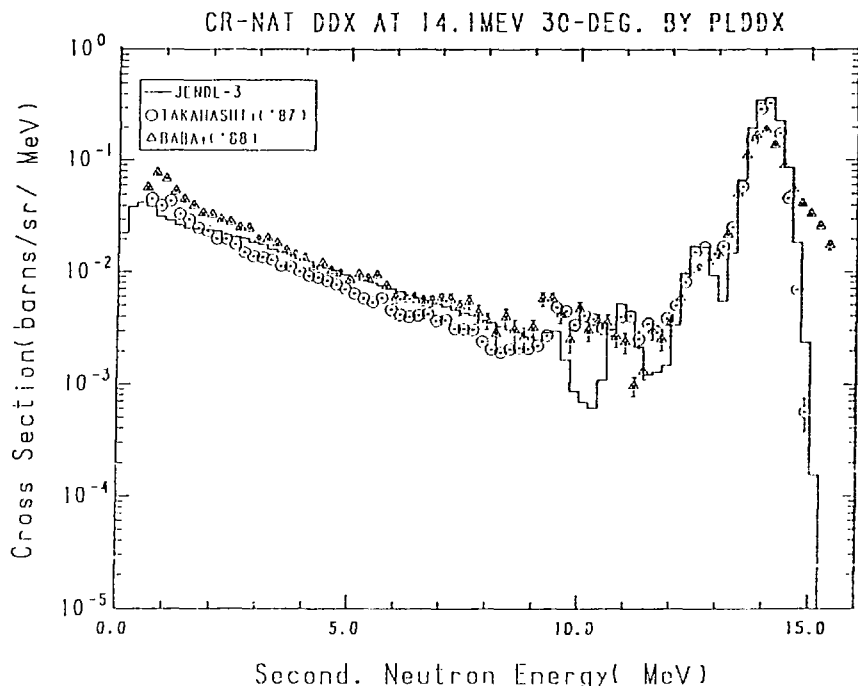


Fig. 27-1 The ^{nat}Cr Double Differential Cross Section at 14.1 MeV,
Emitted Angle = 30° in Laboratory System

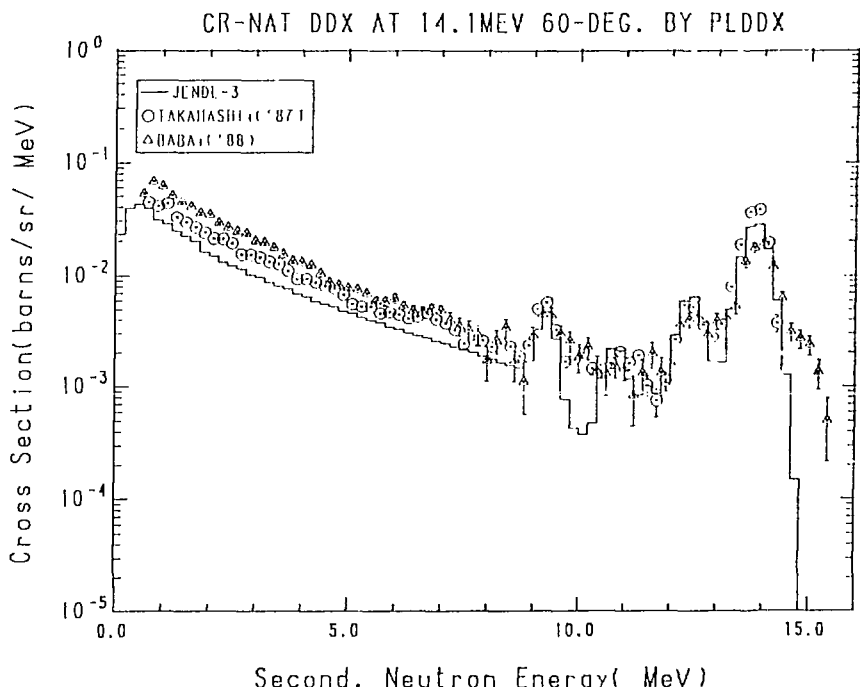


Fig. 27-2 The ^{nat}Cr Double Differential Cross Section at 14.1 MeV,
Emitted Angle = 60° in Laboratory System

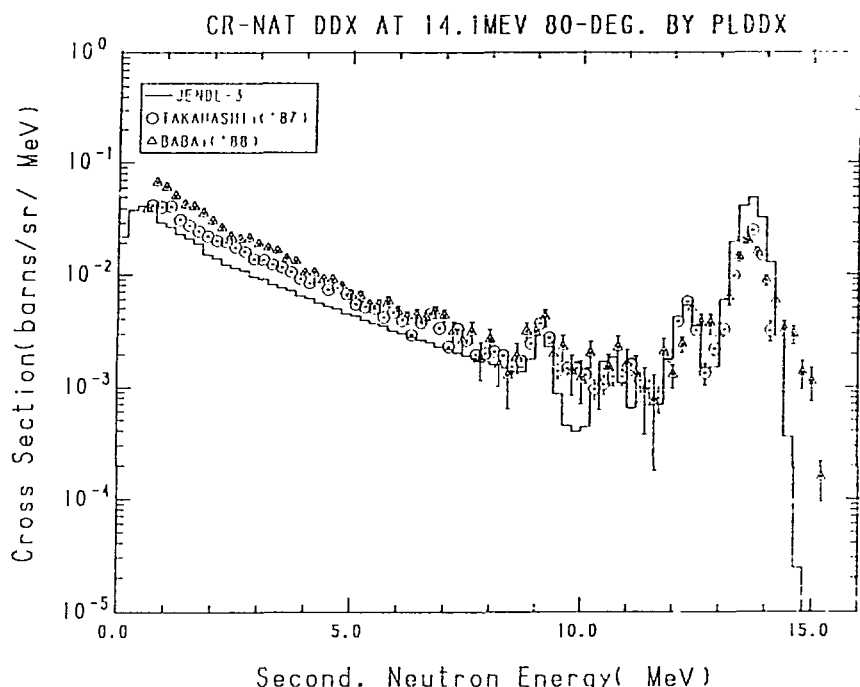


Fig. 27-3 The ^{nat}Cr Double Differential Cross Section at 14.1 MeV,
Emitted Angle = 80° in Laboratory System

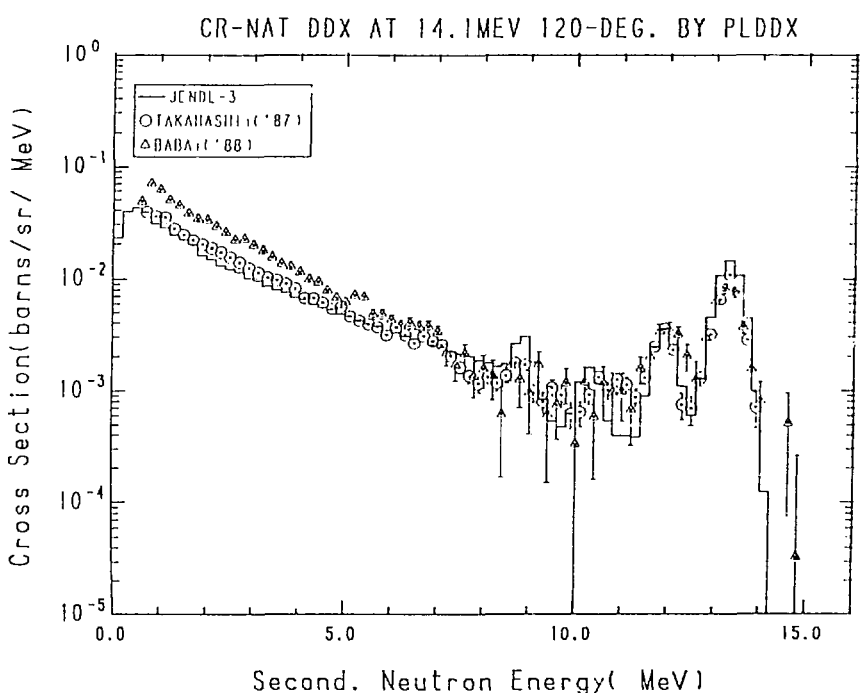


Fig. 27-4 The ^{nat}Cr Double Differential Cross Section at 14.1 MeV,
Emitted Angle = 120° in Laboratory System

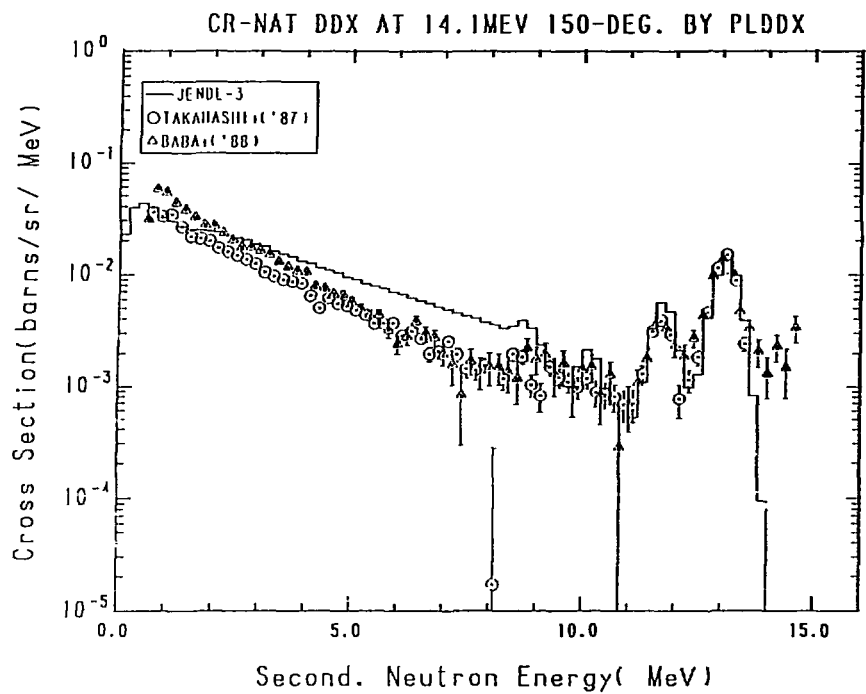


Fig. 27-5 The ^{nat}Cr Double Differential Cross Section at 14.1 MeV,
Emitted Angle = 150° in Laboratory System

3.17 Manganese

The DDXs calculated from the evaluated data of ^{55}Mn are compared with the experimental data/BABA+('88),TAKAHASHI+('88)/ of 30° , 60° , 90° , 120° and 150° at the incident neutron energy of 14.1 MeV in Fig.28. The JENDL-3 data are in good agreement with the experimental data, except that they underestimate the data in the energy region from 3 to 11 MeV at the forward angles. The ENDF/B-VI data have similar trends of the JENDL-3 data, but they give much smaller values in the discrete inelastic scattering region just below the elastic scattering peak. The JEF-2 data cannot reproduce the experimental data in the energy region from 4 to 12 MeV.

References for the Experimental Data in Figures

- BABA+('88) : Baba M., Ishikawa M., Yabuta N., Kikuchi T., Wakabayashi H. and Hirakawa H., Proc. of Int. Conf. on Nucl. Data for Sci. and Technol. at Mito in May 30- Jun. 3, p.291 (1988).
TAKAHASHI+('88): Takahashi A.. private communication (1989).

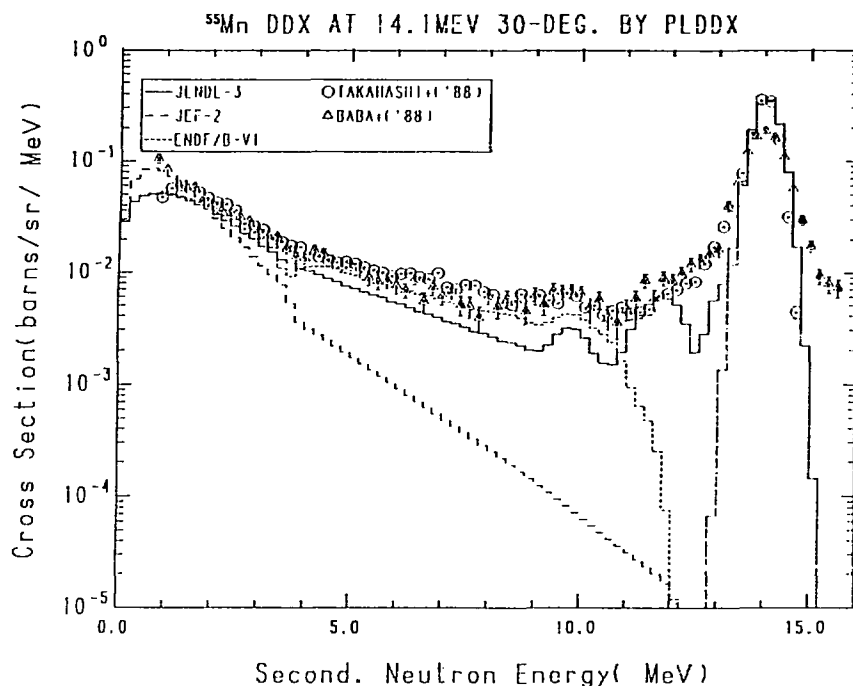


Fig. 28-1 The ^{55}Mn Double Differential Cross Section at 14.1 MeV,
Emitted Angle = 30° in Laboratory System

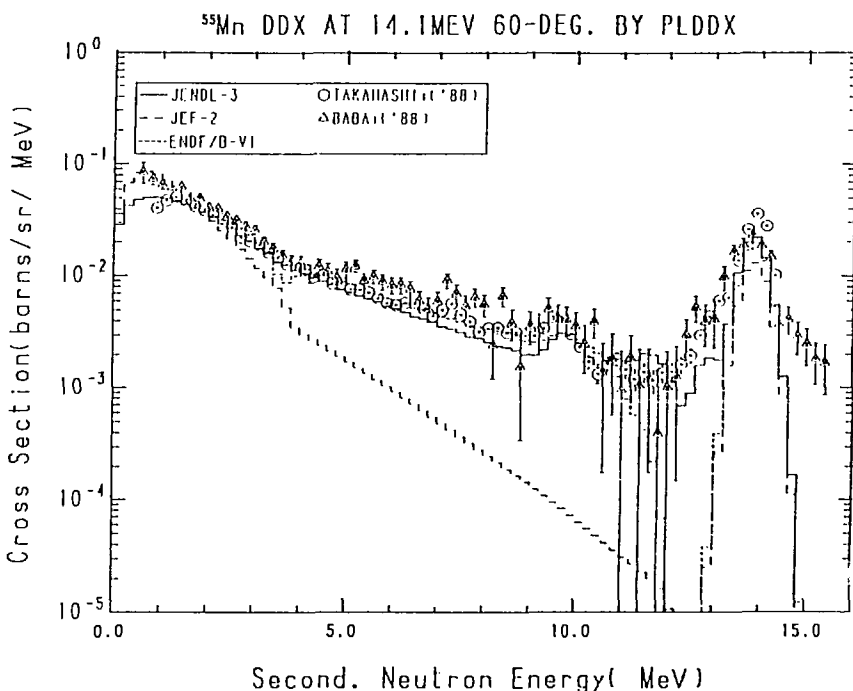


Fig. 28-2 The ^{55}Mn Double Differential Cross Section at 14.1 MeV,
Emitted Angle = 60° in Laboratory System

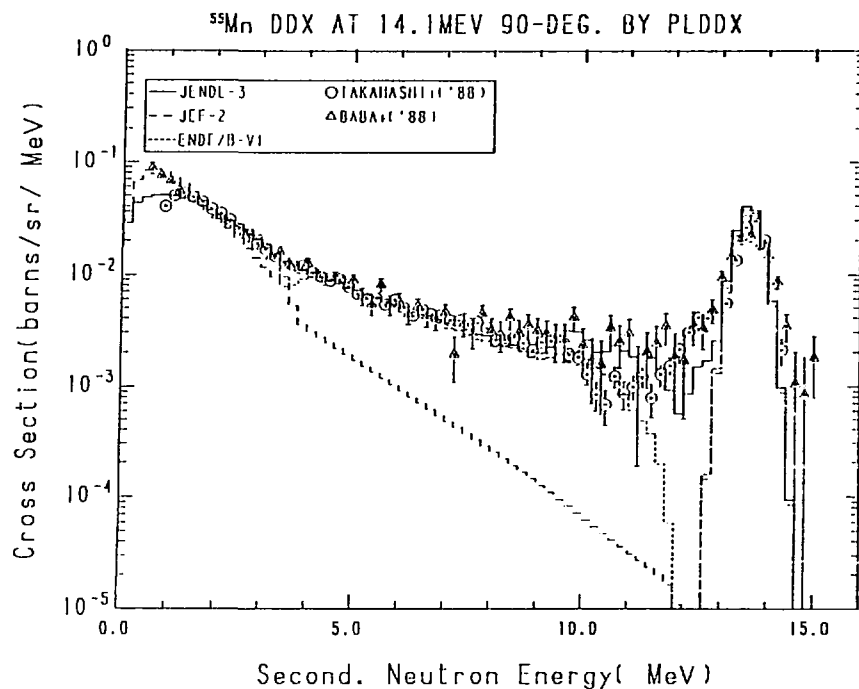


Fig. 28-3 The ^{55}Mn Double Differential Cross Section at 14.1 MeV,
Emitted Angle = 90° in Laboratory System

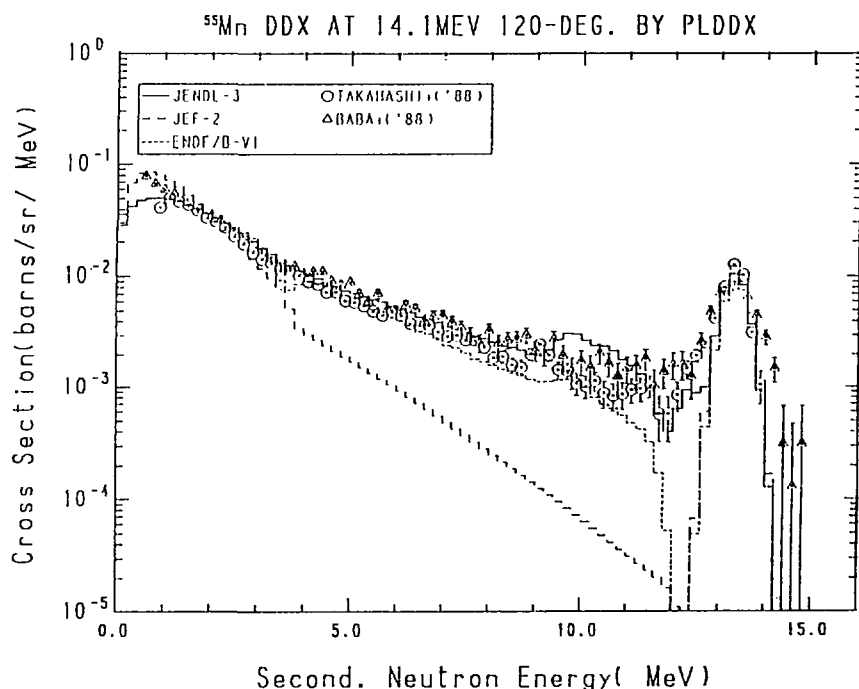


Fig. 28-4 The ^{55}Mn Double Differential Cross Section at 14.1 MeV,
Emitted Angle = 120° in Laboratory System

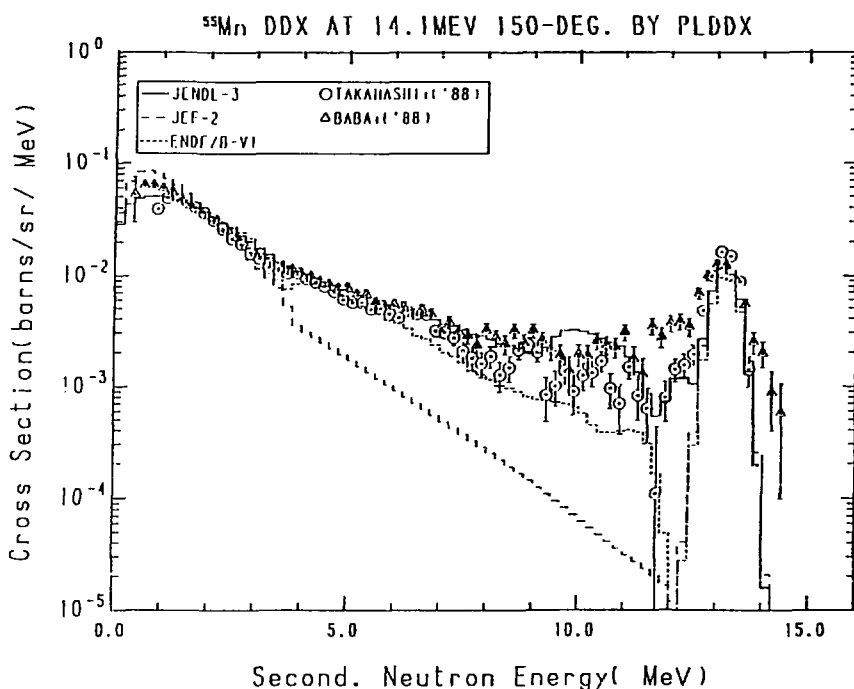


Fig. 28-5 The ⁵⁵Mn Double Differential Cross Section at 14.1 MeV,
Emitted Angle = 150° in Laboratory System

3.18 Iron

The DDXs calculated from the evaluated data of ^{nat}Fe are compared with the experimental data/BABA+('91),TAKAHASHI+('88)/ of 30° , 60° , $75^\circ/80^\circ$, 120° and 150° at the incident neutron energy of 14.1 MeV in Fig.29, and those/BABA+('88)/ of 30° , 60° , 90° , 120° and 150° at 18.0 MeV in Fig.30. The comparison could not be made for ENDF/B-VI, since this library include no data for the natural elements and there exists no processing code which can create those data easily. The JENDL-3 data of both incident energies tend to underestimate slightly at the forward angles and to overestimate at the backward angles in the middle energy region of secondary neutrons.

References for the Experimental Data in Figures

- BABA+('88) : Baba M., Ishikawa M., Yabuta N., Kikuchi T., Wakabayashi H. and Hirakawa H., Proc. of Int. Conf. on Nucl. Data for Sci. and Technol. at Mito in May 30- Jun. 3, p.291 (1988).
BABA+('91) : Baba M., private communication (1991).
TAKAHASHI+('88): Takahashi A., private communication (1989).

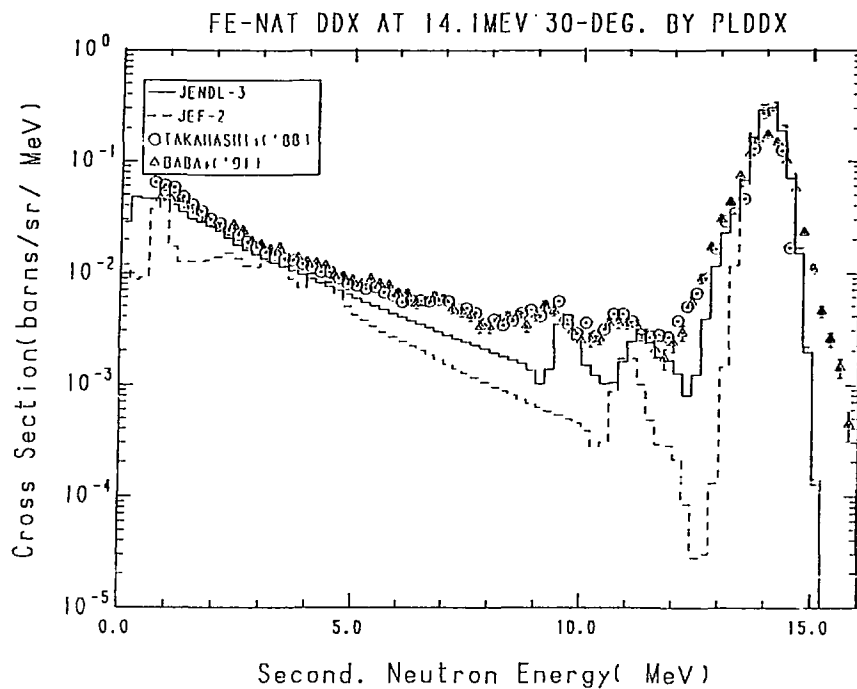


Fig. 29-1 The ^{nat}Fe Double Differential Cross Section at 14.1 MeV,
Emitted Angle = 30° in Laboratory System

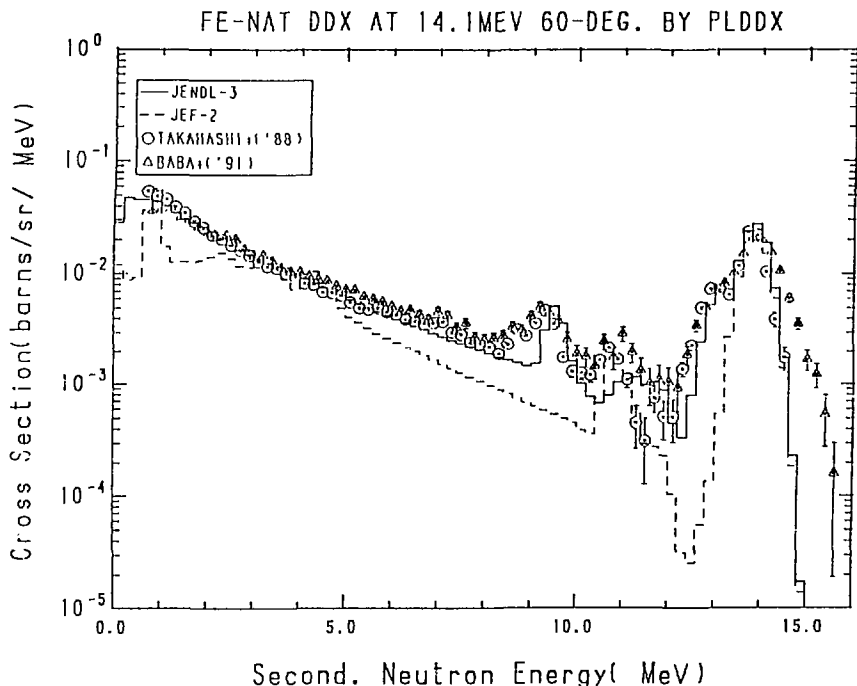


Fig. 29-2 The ^{nat}Fe Double Differential Cross Section at 14.1 MeV,
Emitted Angle = 60° in Laboratory System

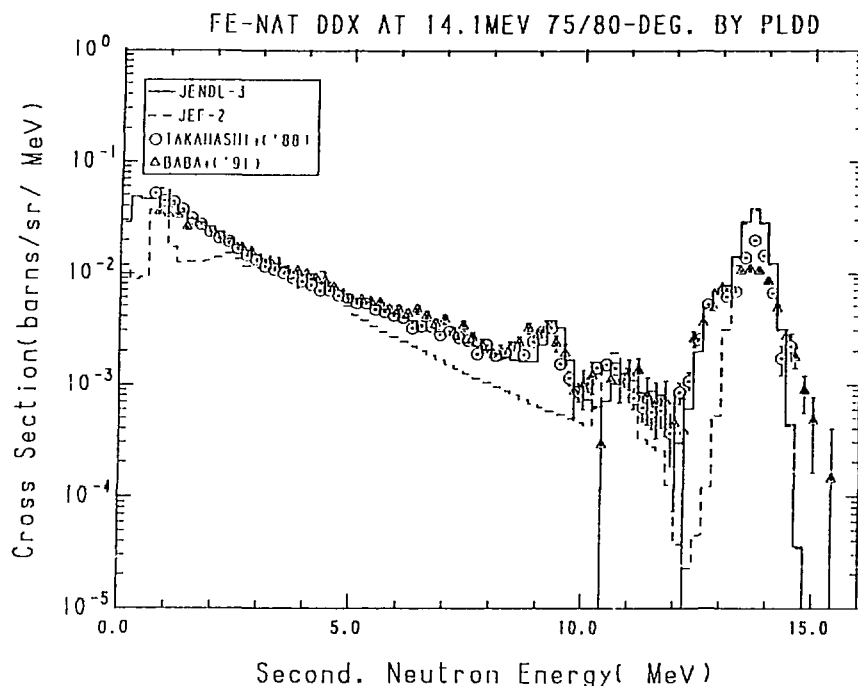


Fig. 29-3 The ^{nat}Fe Double Differential Cross Section at 14.1 MeV,
Emitted Angle = $75^\circ/80^\circ$ in Laboratory System

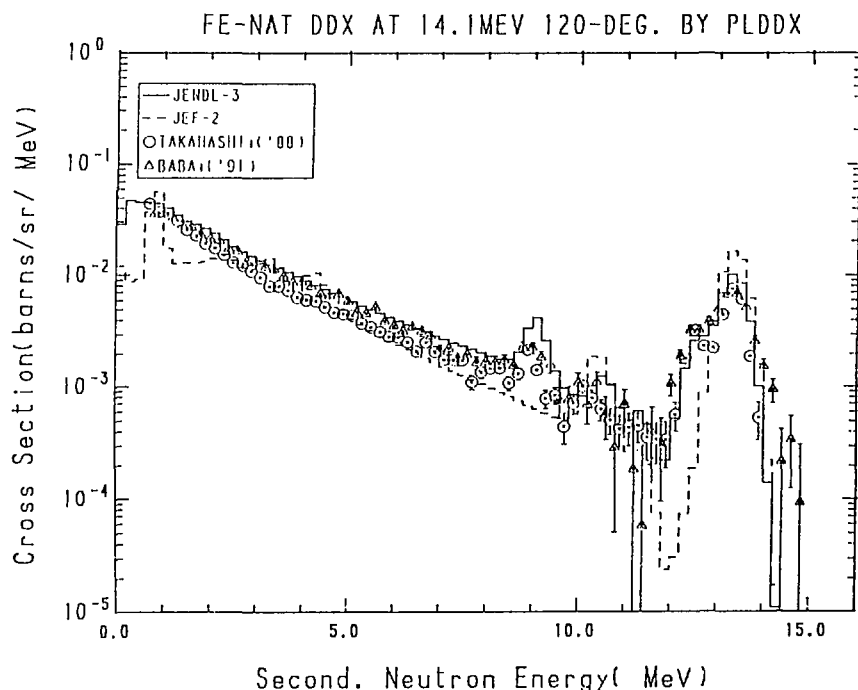


Fig. 29-4 The ^{nat}Fe Double Differential Cross Section at 14.1 MeV,
Emitted Angle = 120° in Laboratory System

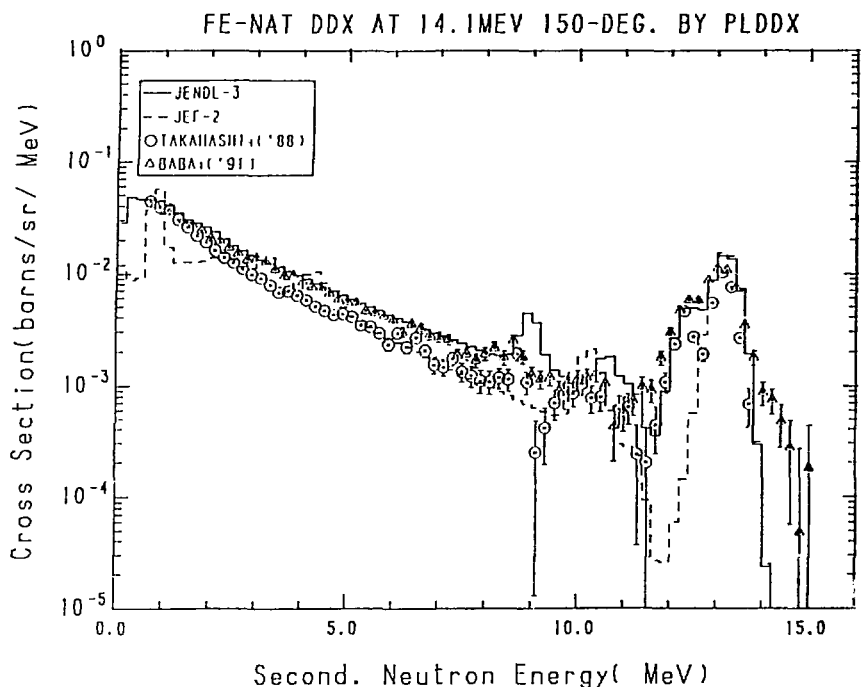


Fig. 29-5 The ^{nat}Fe Double Differential Cross Section at 14.1 MeV,
Emitted Angle = 150° in Laboratory System

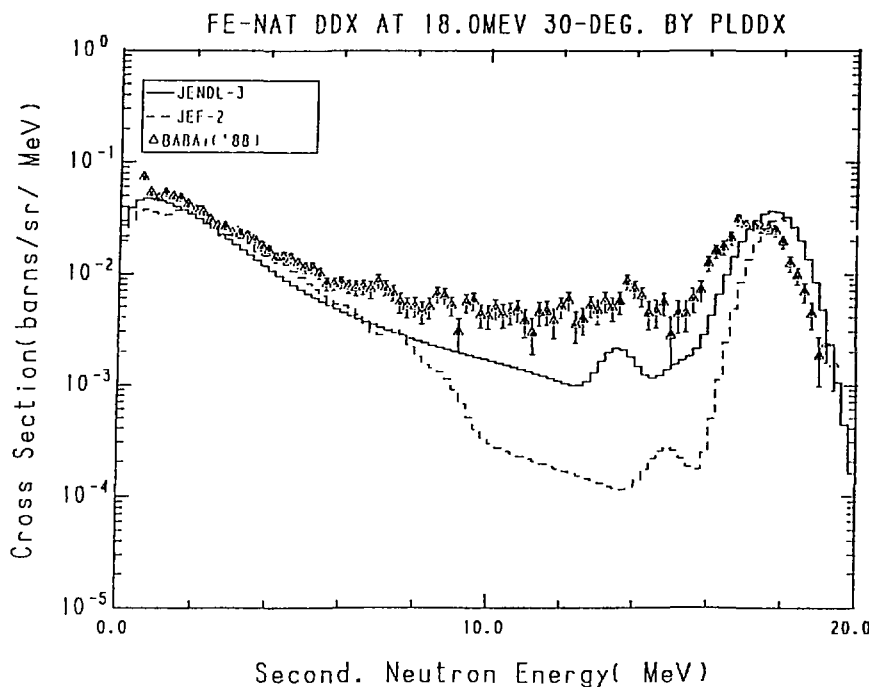


Fig. 30-1 The ^{nat}Fe Double Differential Cross Section at 18.0 MeV,
Emitted Angle = 30° in Laboratory System

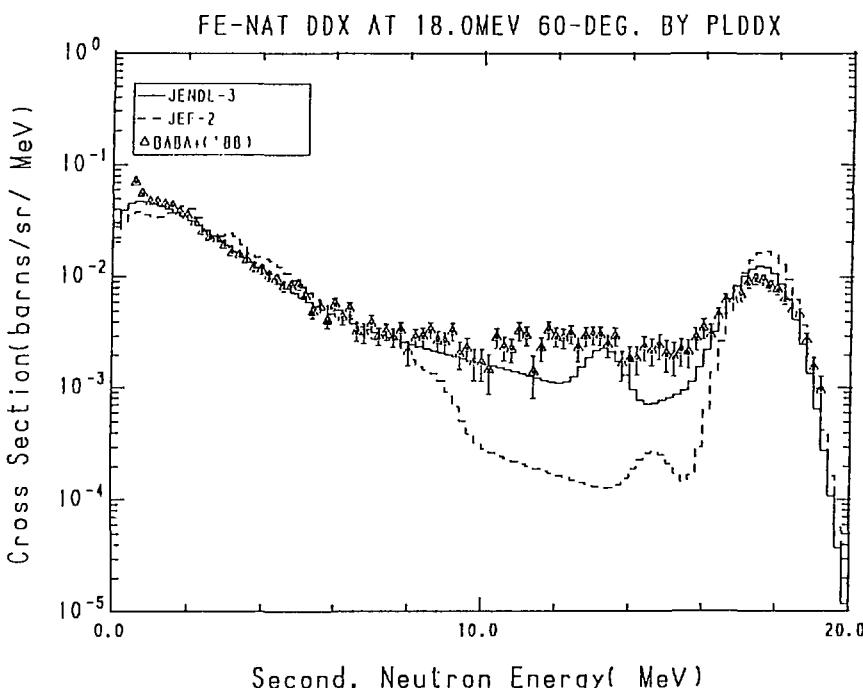


Fig. 30-2 The ^{nat}Fe Double Differential Cross Section at 18.0 MeV,
Emitted Angle = 60° in Laboratory System

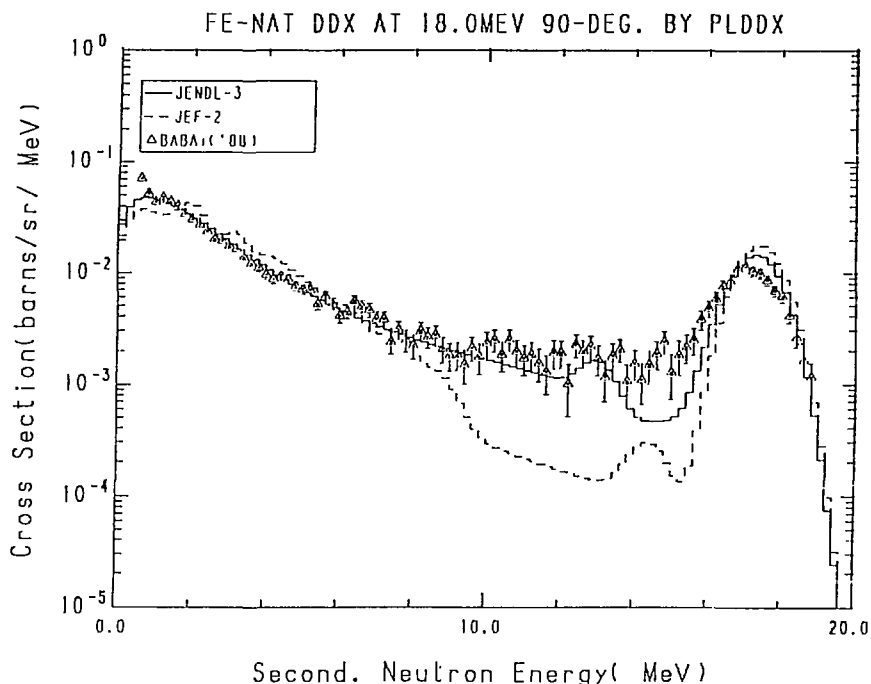


Fig. 30-3 The ^{nat}Fe Double Differential Cross Section at 18.0 MeV,
Emitted Angle = 90° in Laboratory System

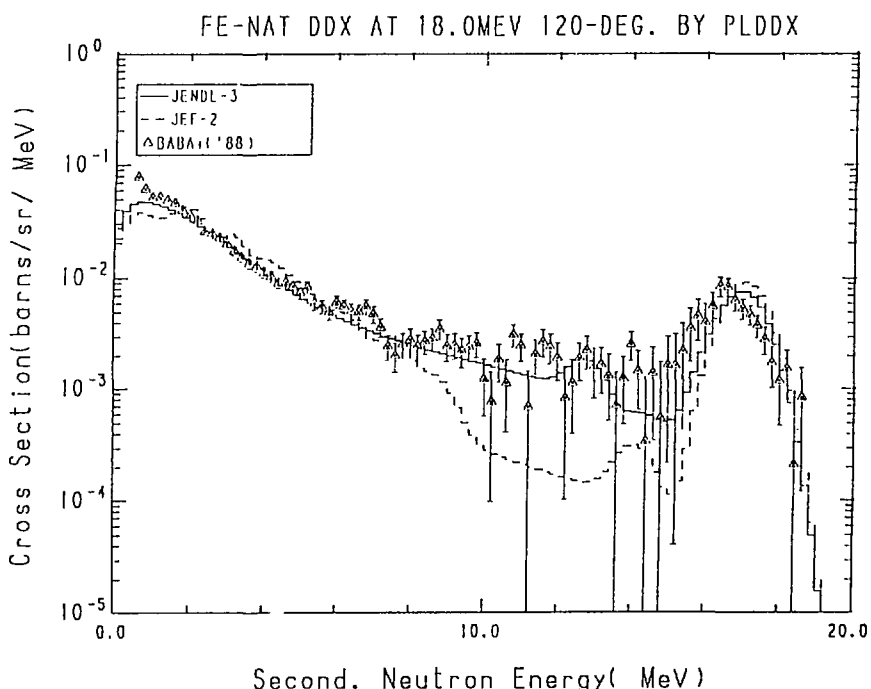


Fig. 30-4 The ^{nat}Fe Double Differential Cross Section at 18.0 MeV,
Emitted Angle = 120° in Laboratory System

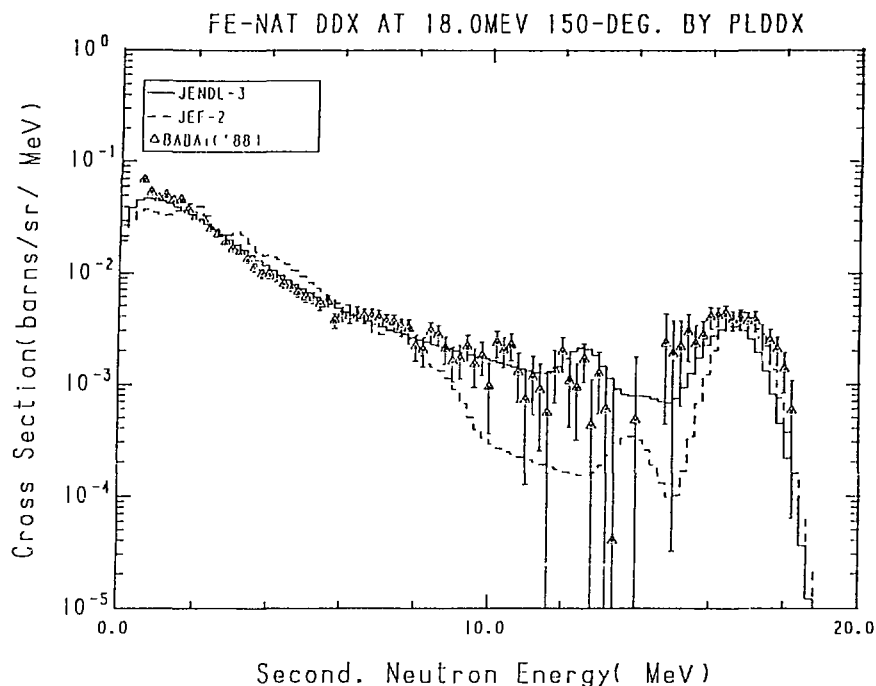


Fig. 30-5 The ^{nat}Fe Double Differential Cross Section at 18.0 MeV,
Emitted Angle = 150° in Laboratory System

3.19 Cobalt

The DDXs calculated from the evaluated data of ^{59}Co are compared with the experimental data/TAKAHASHI+('88)/ of 30° , 60° , 90° , 120° and 150° at the incident neutron energy of 14.1 MeV in Fig.31. The JENDL-3 data reproduce the experimental data in the low energy region, and overestimate them in the discrete inelastic scattering region of all the angles and in the middle energy region at the backward angles. The JEF-2 data are equivalent to the ENDF/B-VI data, and are almost in good agreement with the experimental data, except that they underestimate the experimental data in the middle energy region at the forward angles.

Reference for the Experimental Data in Figures

TAKAHASHI+('88): Takahashi A., private communication (1989).

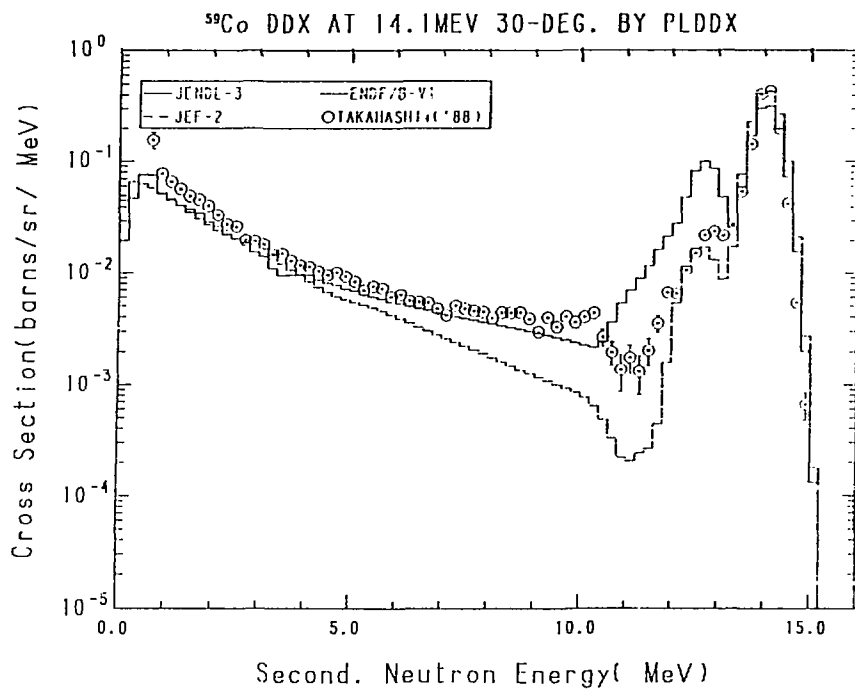


Fig. 31-1 The ^{59}Co Double Differential Cross Section at 14.1 MeV,
Emitted Angle = 30° in Laboratory System

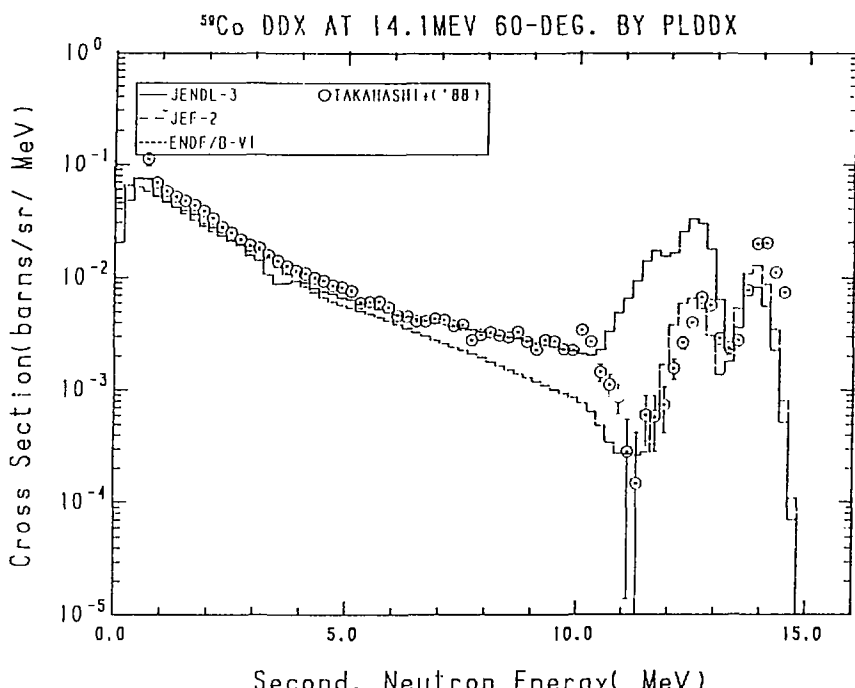


Fig. 31-2 The ^{59}Co Double Differential Cross Section at 14.1 MeV,
Emitted Angle = 60° in Laboratory System

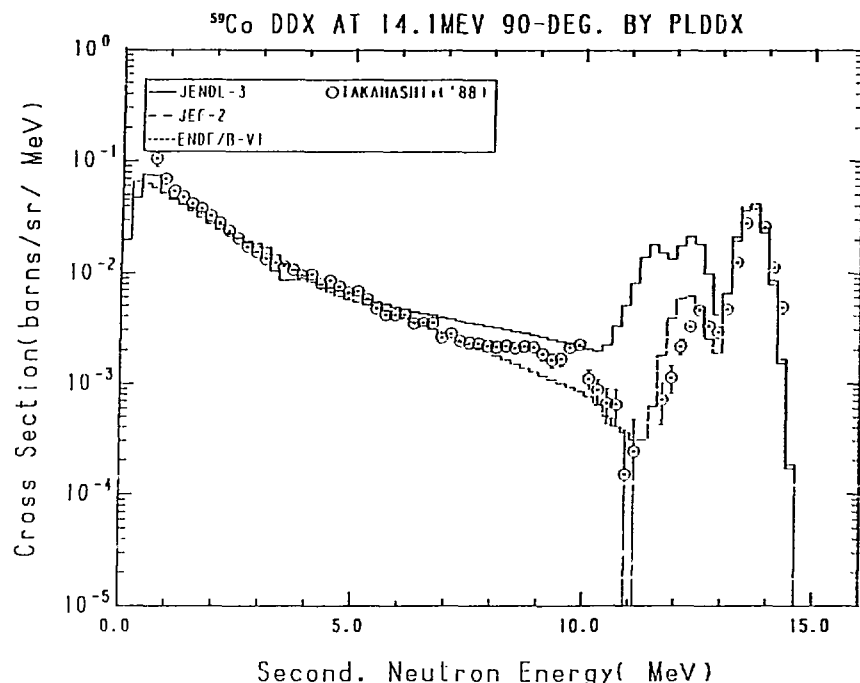


Fig. 31-3 The ^{59}Co Double Differential Cross Section at 14.1 MeV,
Emitted Angle = 90° in Laboratory System

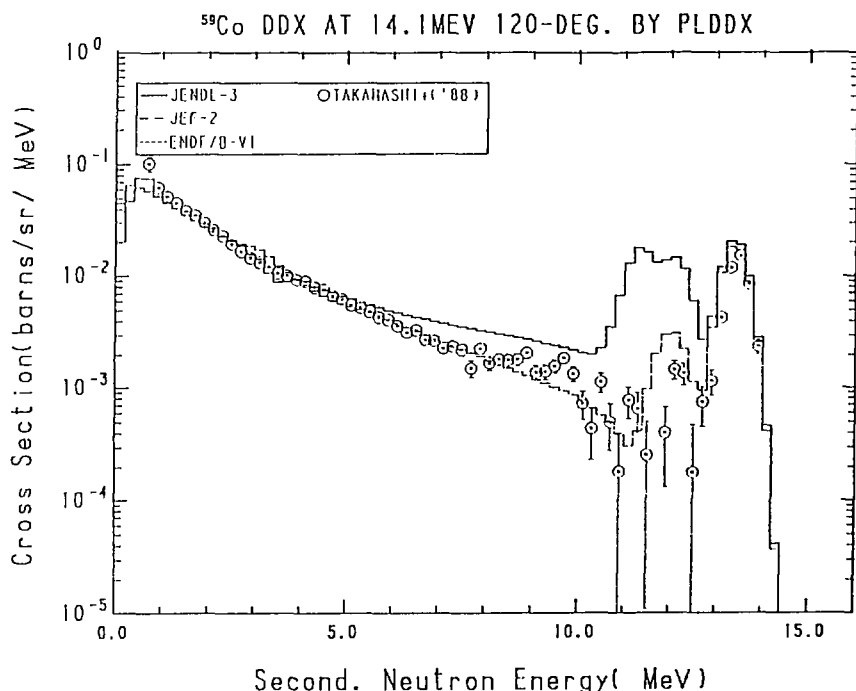


Fig. 31-4 The ^{59}Co Double Differential Cross Section at 14.1 MeV,
Emitted Angle = 120° in Laboratory System

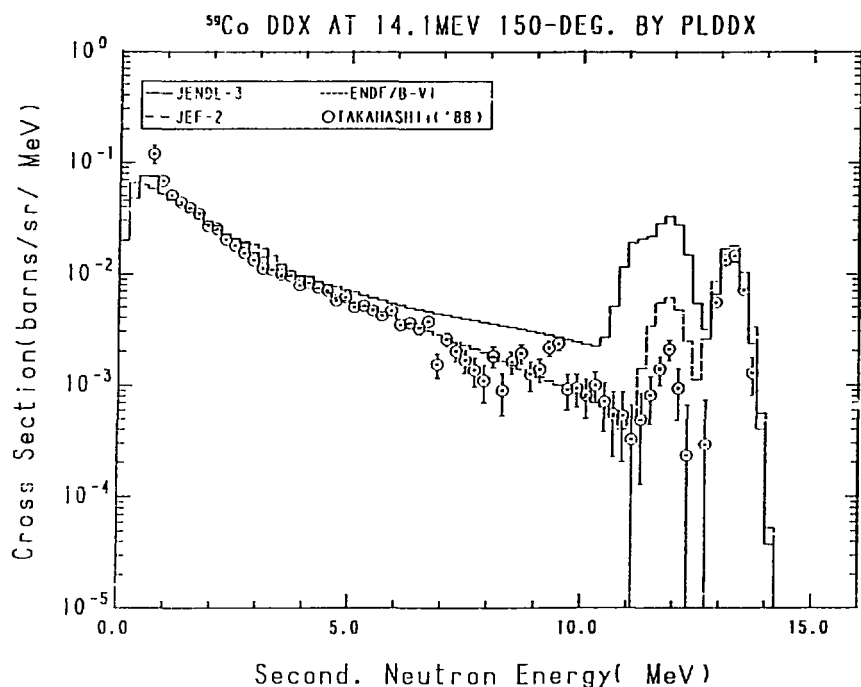


Fig. 31-5 The ⁵⁹Co Double Differential Cross Section at 14.1 MeV,
Emitted Angle = 150° in Laboratory System

3.20 Nickel

Only JENDL-3 is available for ^{nat}Ni . DDXs calculated from JENDL-3 at the emission angles of 30° , 60° , 80° , 120° and 150° at the incident neutron energy of 14.1 MeV in Fig.32. The data at the angles of 30° , 60° , 90° , 120° and 150° at 18.0 MeV are given in Fig.33. The comparison could not be made for ENDF/B-VI and JEF-2, since these two libraries include no data for the natural elements and there exists no processing code which can create those data easily. At 14.1 MeV, the JENDL-3 data reproduce the experimental data/BABA+('88),TAKAHASHI+('88)/, except for slightly overestimating in the 5-10 MeV region at the backward angles and underestimating below 5 MeV at the forward angles. At 18.0 MeV, the data calculated from JENDL-3 are in good agreement with the experimental data/BABA+('88)/, except at 30° where they are significantly lower than the experimental data.

References for the Experimental Data in Figures

- BABA+('88) : Baba M., Ishikawa M., Yabuta N., Kikuchi T., Wakabayashi H. and Hirakawa H., Proc. of Int. Conf. on Nucl. Data for Sci. and Technol. at Mito in May 30- Jun. 3, p.291 (1988).
 TAKAHASHI+('88): Takahashi A., private communication (1989).

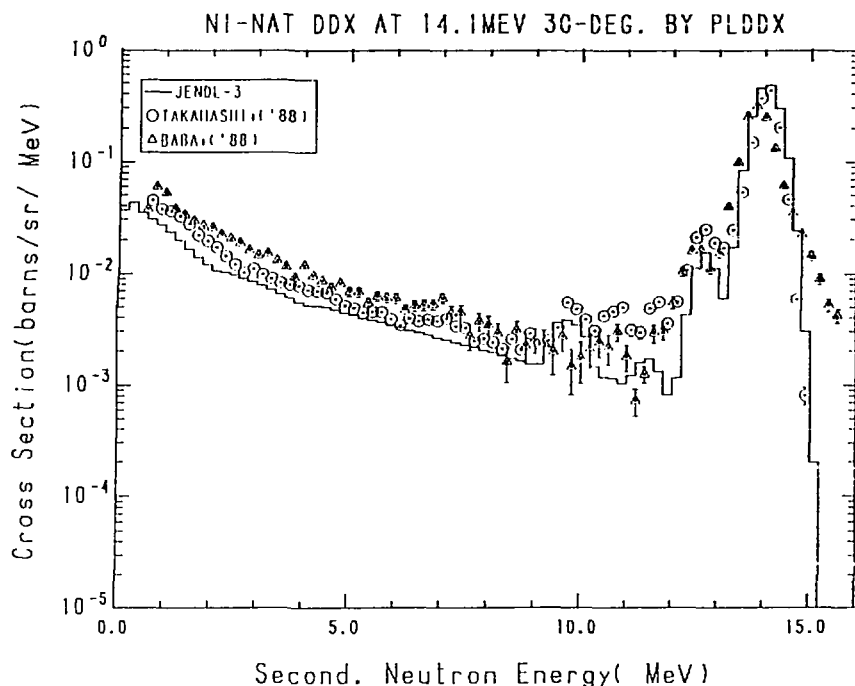


Fig. 32-1 The ^{nat}Ni Double Differential Cross Section at 14.1 MeV,
Emitted Angle = 30° in Laboratory System

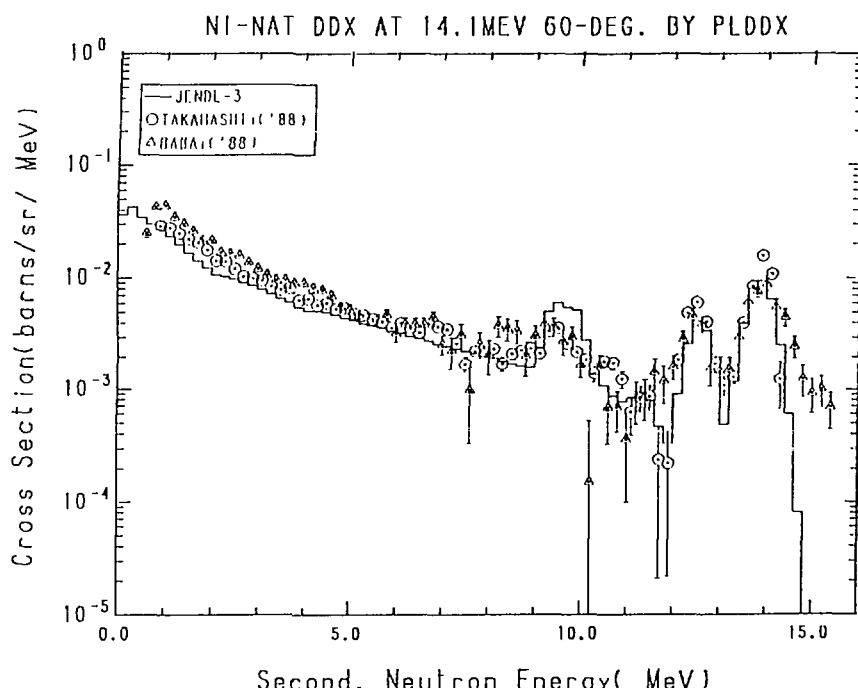


Fig. 32-2 The ^{nat}Ni Double Differential Cross Section at 14.1 MeV,
Emitted Angle = 60° in Laboratory System

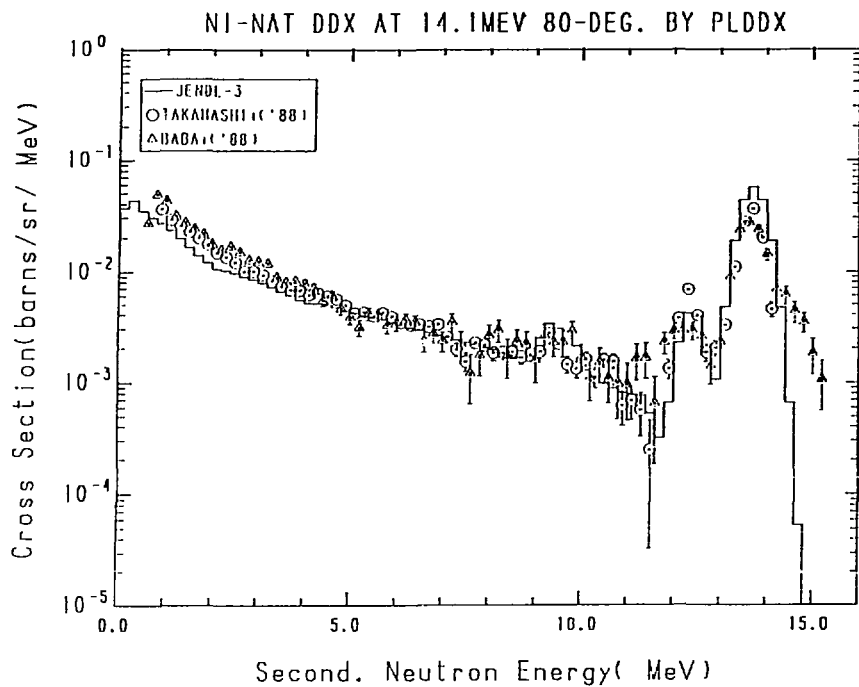


Fig. 32-3 The ^{nat}Ni Double Differential Cross Section at 14.1 MeV,
Emitted Angle = 80° in Laboratory System

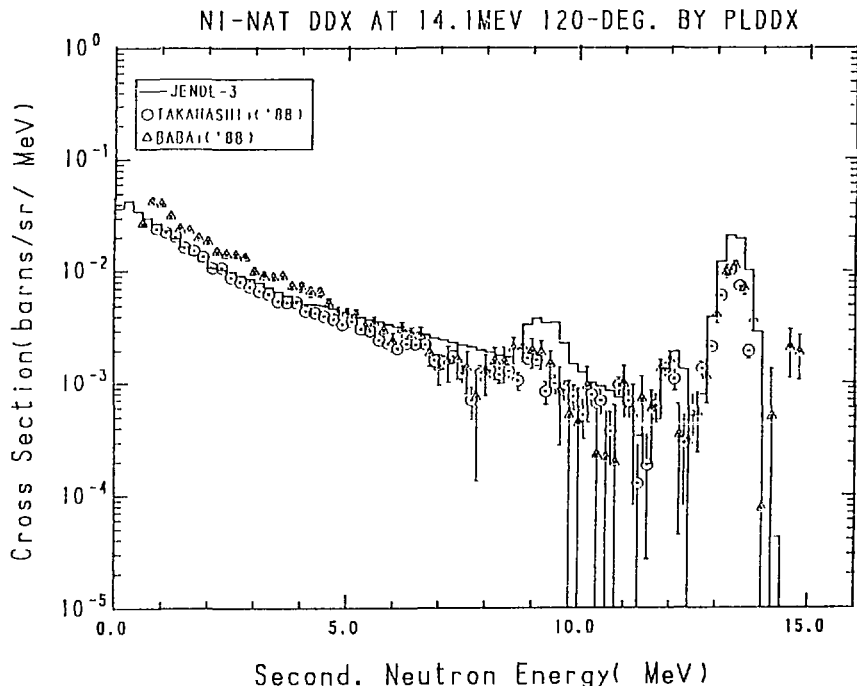


Fig. 32-4 The ^{nat}Ni Double Differential Cross Section at 14.1 MeV,
Emitted Angle = 120° in Laboratory System

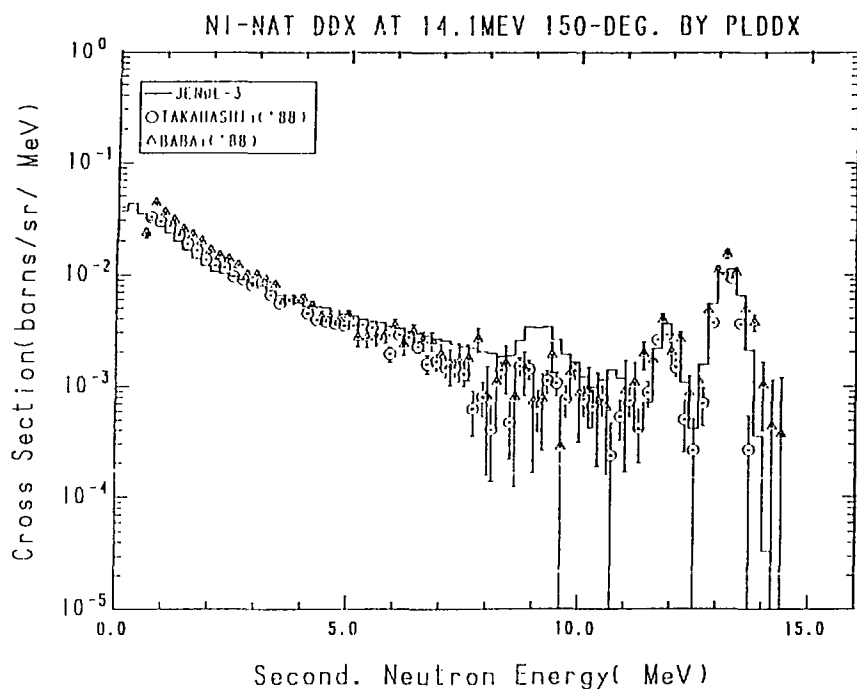


Fig. 32-5 The ^{nat}Ni Double Differential Cross Section at 14.1 MeV,
Emitted Angle = 150° in Laboratory System

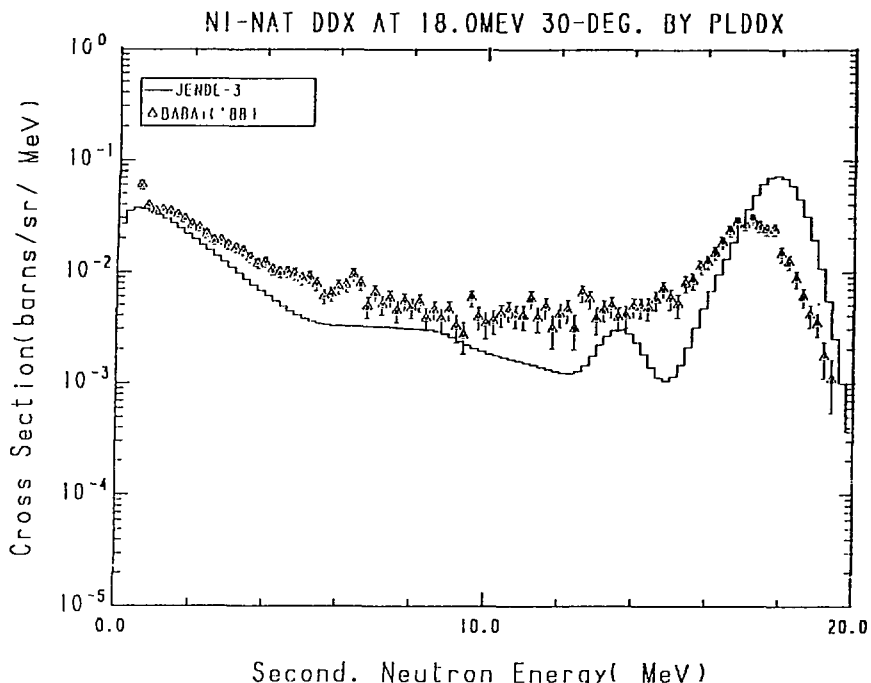


Fig. 33-1 The ^{nat}Ni Double Differential Cross Section at 18.0 MeV,
Emitted Angle = 30° in Laboratory System

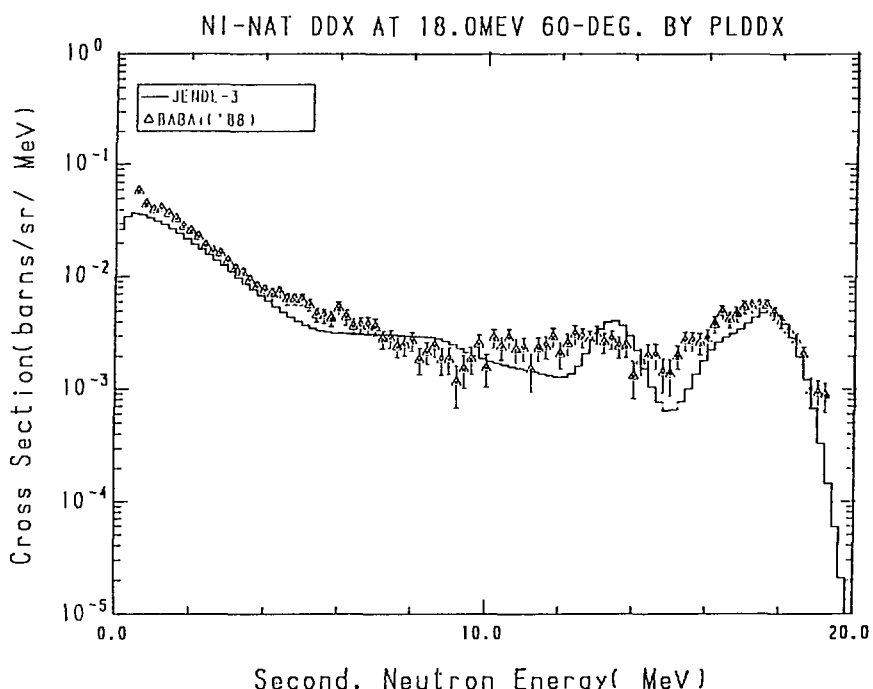


Fig. 33-2 The ^{nat}Ni Double Differential Cross Section at 18.0 MeV,
Emitted Angle = 60° in Laboratory System

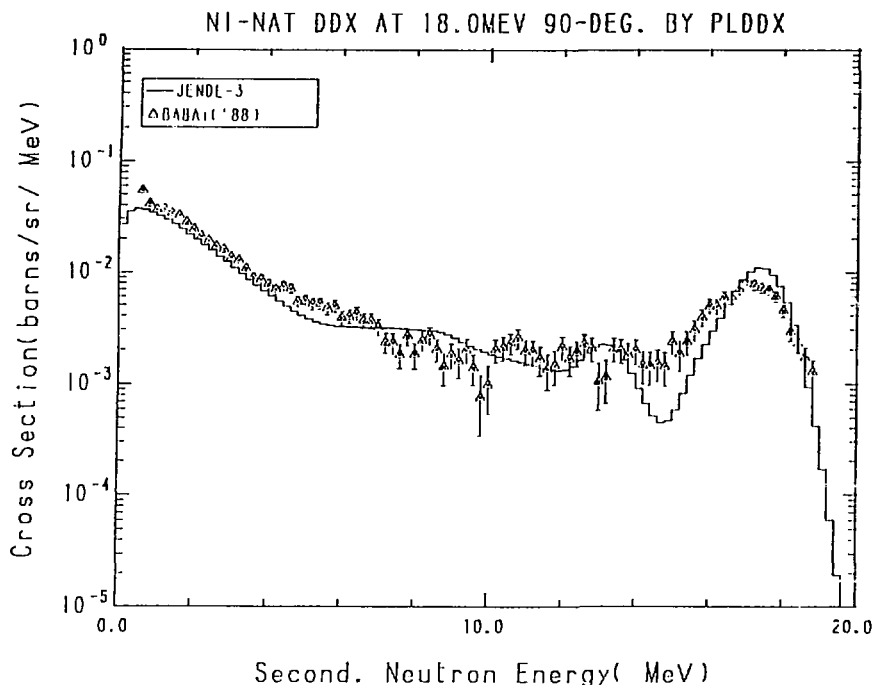


Fig. 33-3 The ^{nat}Ni Double Differential Cross Section at 18.0 MeV,
Emitted Angle = 90° in Laboratory System

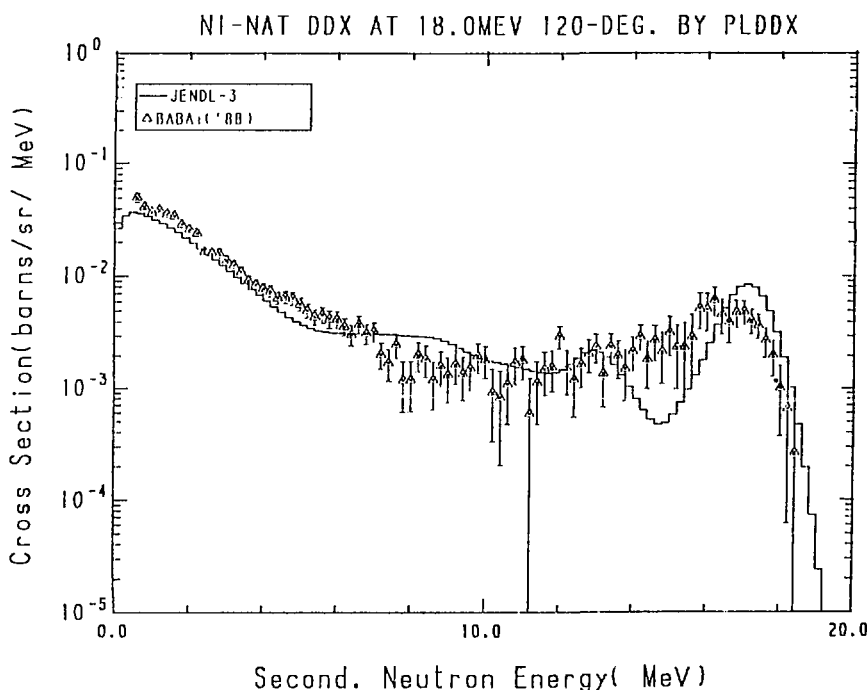


Fig. 33-4 The ^{nat}Ni Double Differential Cross Section at 18.0 MeV,
Emitted Angle = 120° in Laboratory System

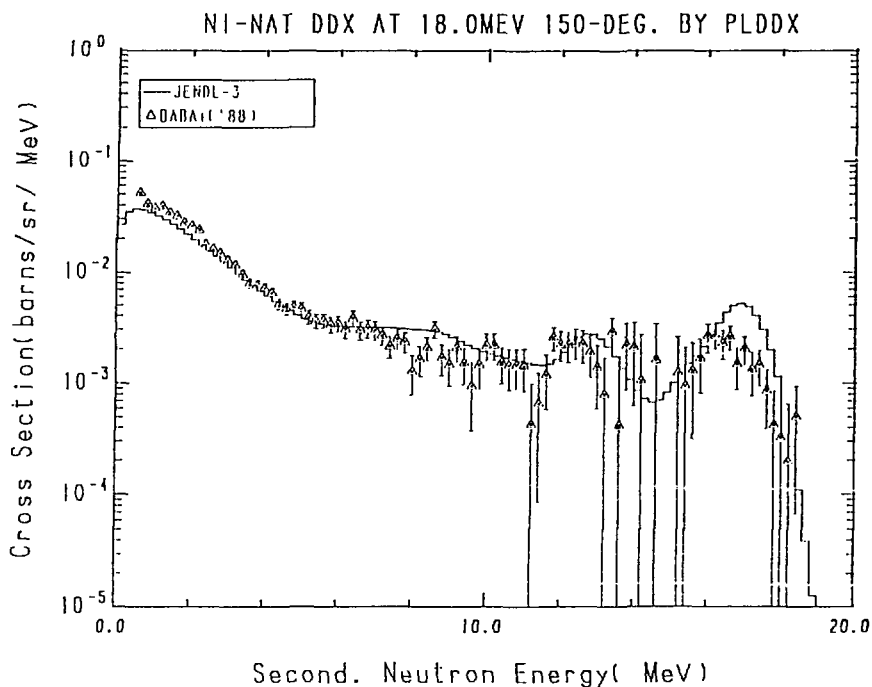


Fig. 33-5 The ^{nat}Ni Double Differential Cross Section at 18.0 MeV,
Emitted Angle = 150° in Laboratory System

3.21 Copper

The DDXs calculated from the evaluated data of ^{nat}Cu are compared with the experimental data/BABA+('88),TAKAHASHI+('86)/ of 30° , 60° , 80° , 120° and 150° at the incident neutron energy of 14.1 MeV in Fig.34, and those/BABA+('88)/ of 30° , 60° , 90° , 120° and 150° at 18.0 MeV in Fig.35. The comparison could not be made for ENDF/B-VI, since this library include no data for the natural elements and there exists no processing code which can create those data easily. The JENDL-3 data almost reproduce the experimental data at both incident energies, while the JEF-2 data are too small in the middle energy region.

References for the Experimental Data in Figures

- BABA+('88) : Baba M., Ishikawa M., Yabuta N., Kikuchi T., Wakabayashi H. and Hirakawa H., Proc. of Int. Conf. on Nucl. Data for Sci. and Technol. at Mito in May 30- Jun. 3, p.291 (1988).
TAKAHASHI+('86): Takahashi A., Ichimura E., Sugimoto H. and Kato T., JAERI-M 86-080, 393 (1986).

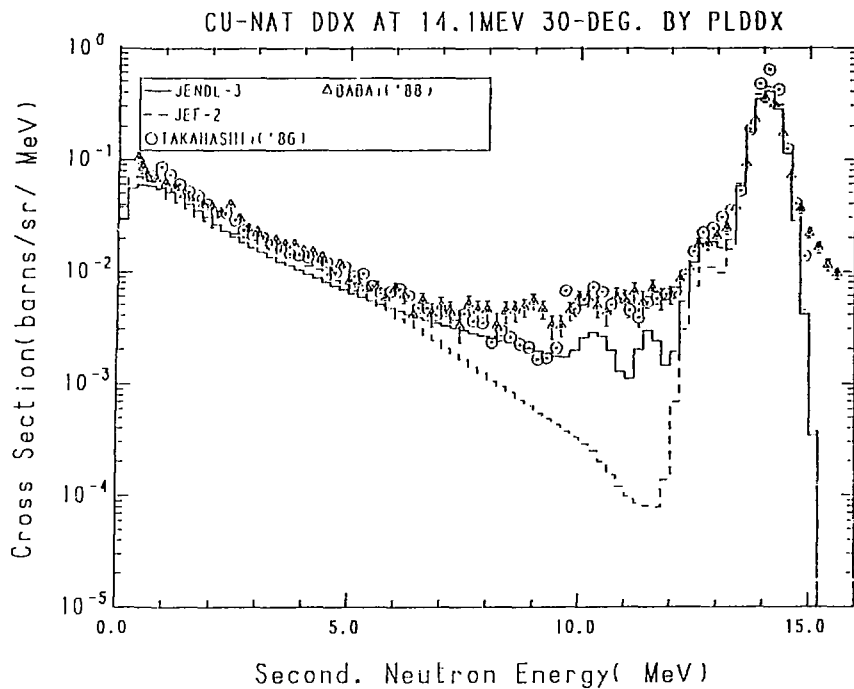


Fig. 34-1 The ^{nat}Cu Double Differential Cross Section at 14.1 MeV,
Emitted Angle = 30° in Laboratory System

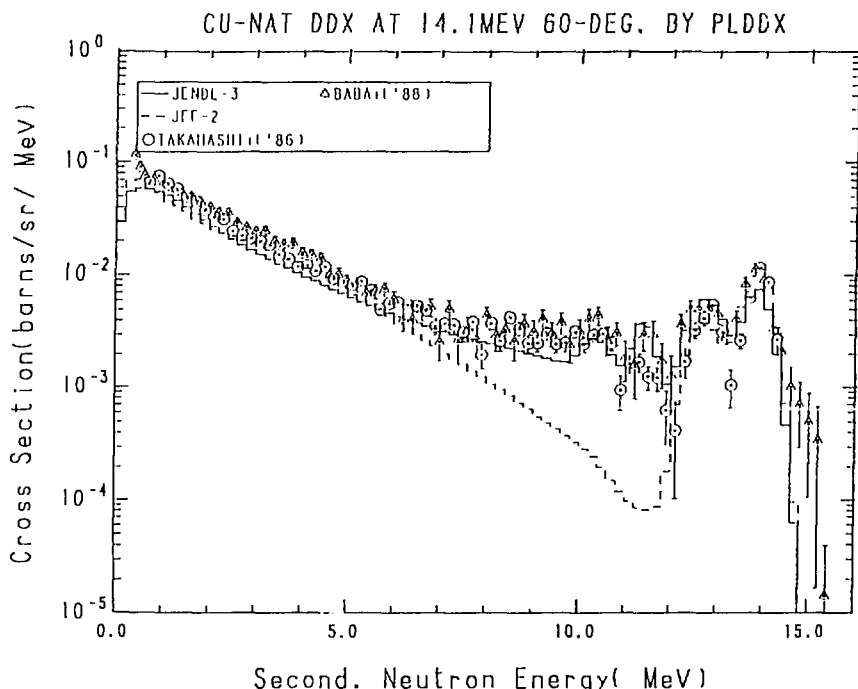


Fig. 34-2 The ^{nat}Cu Double Differential Cross Section at 14.1 MeV,
Emitted Angle = 60° in Laboratory System

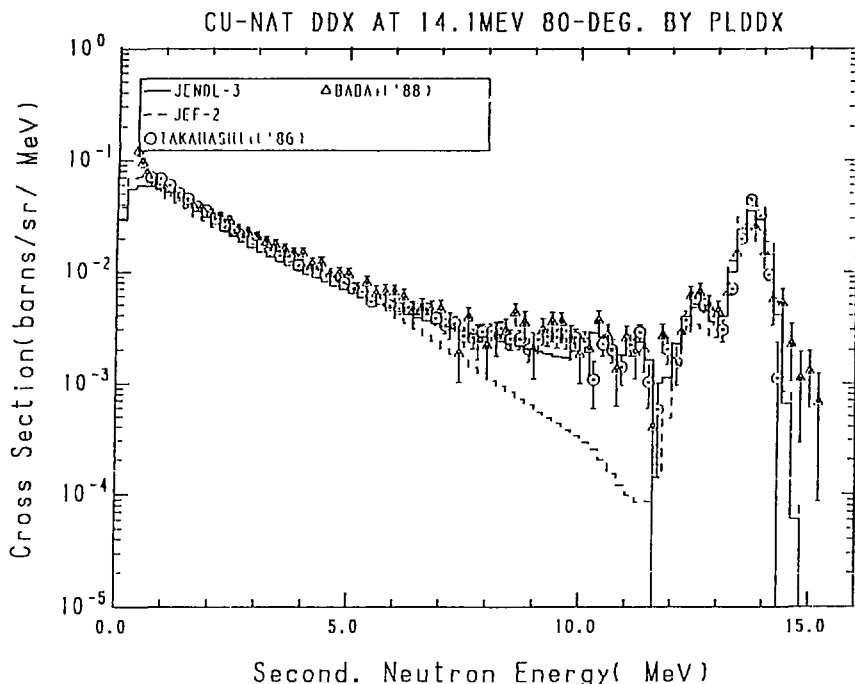


Fig. 34-3 The ^{nat}Cu Double Differential Cross Section at 14.1 MeV,
Emitted Angle = 80° in Laboratory System

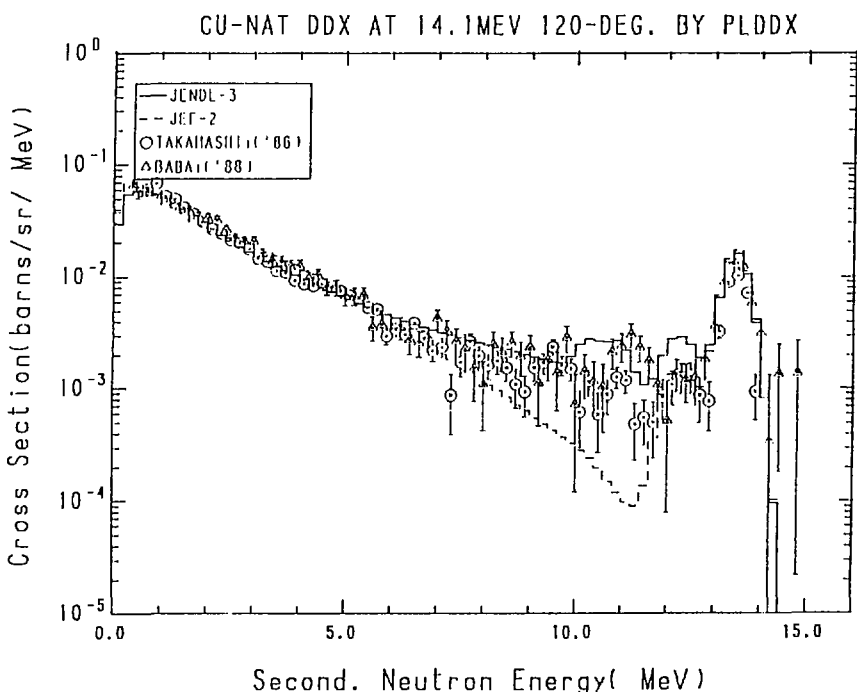


Fig. 34-4 The ^{nat}Cu Double Differential Cross Section at 14.1 MeV,
Emitted Angle = 120° in Laboratory System

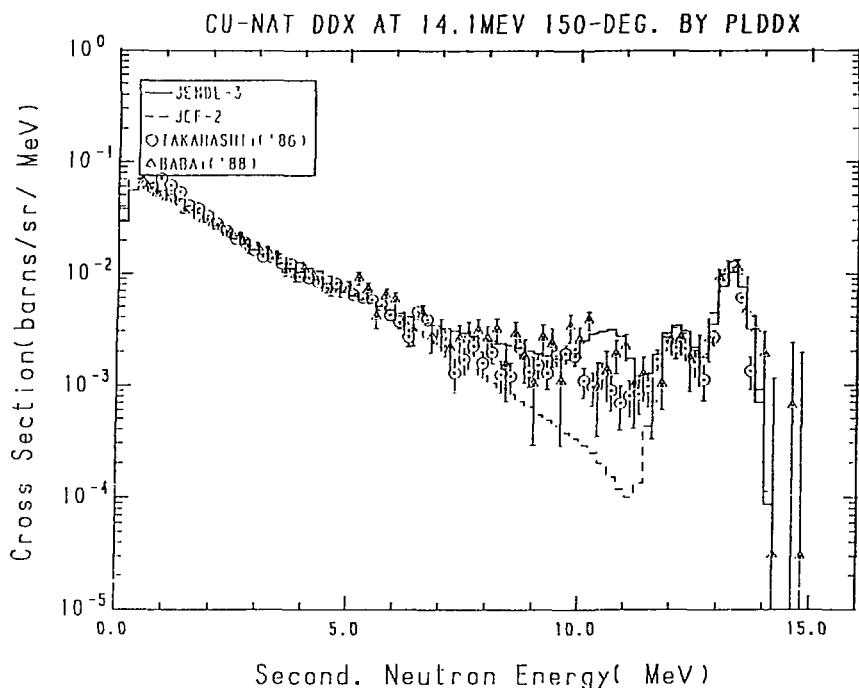


Fig. 34-5 The ^{nat}Cu Double Differential Cross Section at 14.1 MeV,
Emitted Angle = 150° in Laboratory System

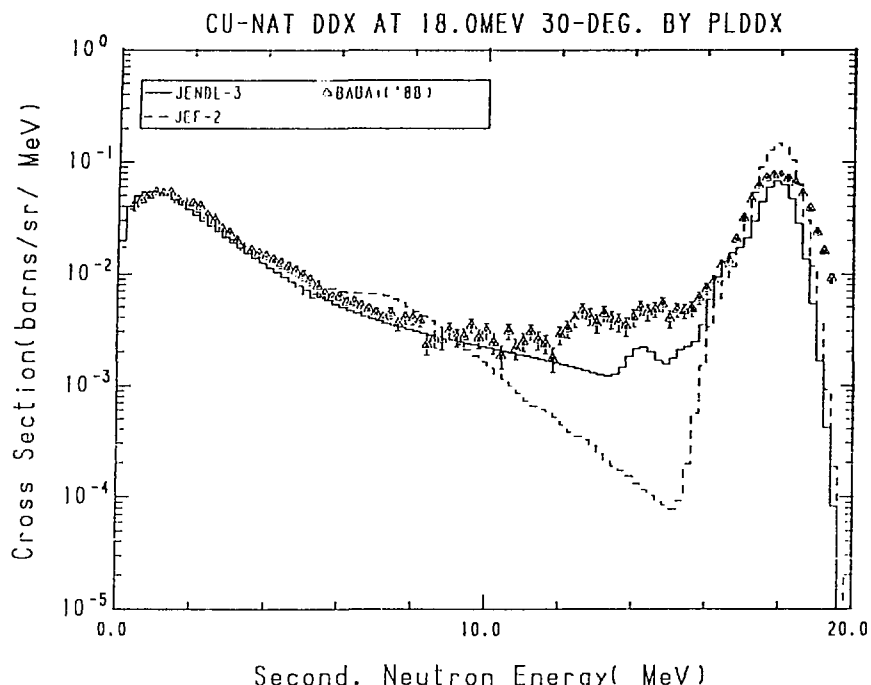


Fig. 35-1 The ^{nat}Cu Double Differential Cross Section at 18.0 MeV,
Emitted Angle = 30° in Laboratory System

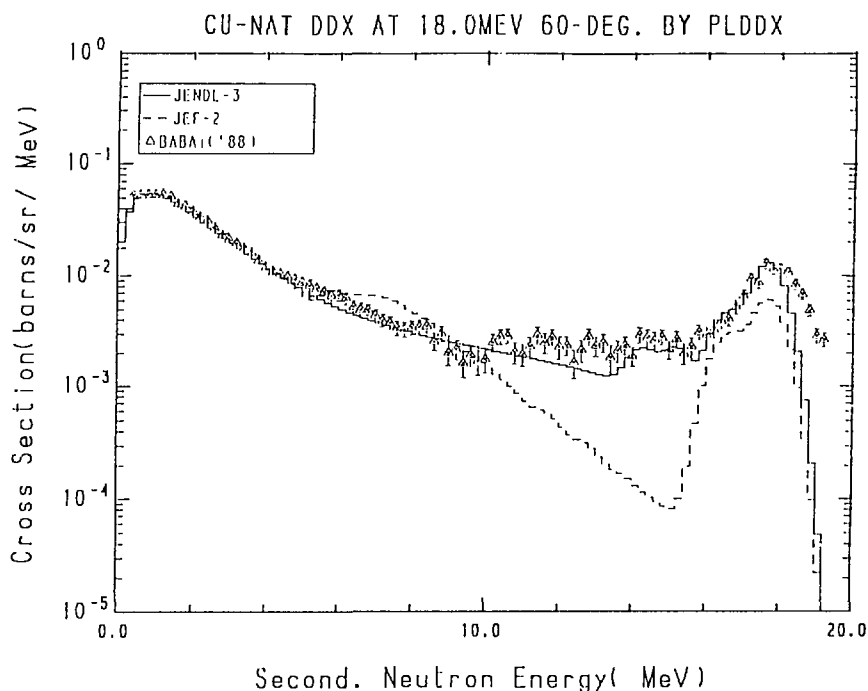


Fig. 35-2 The ^{nat}Cu Double Differential Cross Section at 18.0 MeV,
Emitted Angle = 60° in Laboratory System

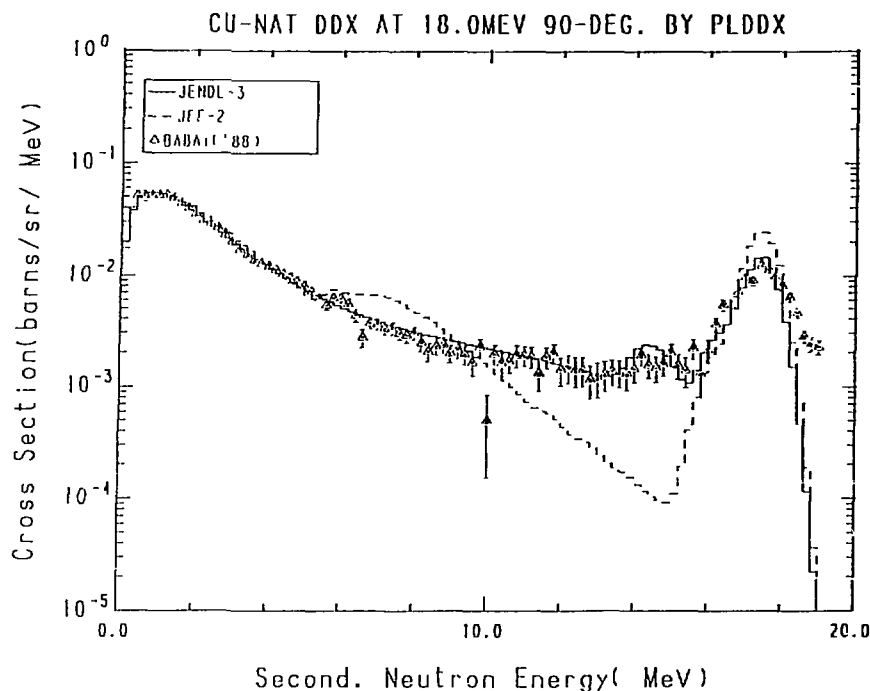


Fig. 35-3 The ^{nat}Cu Double Differential Cross Section at 18.0 MeV,
Emitted Angle = 90° in Laboratory System

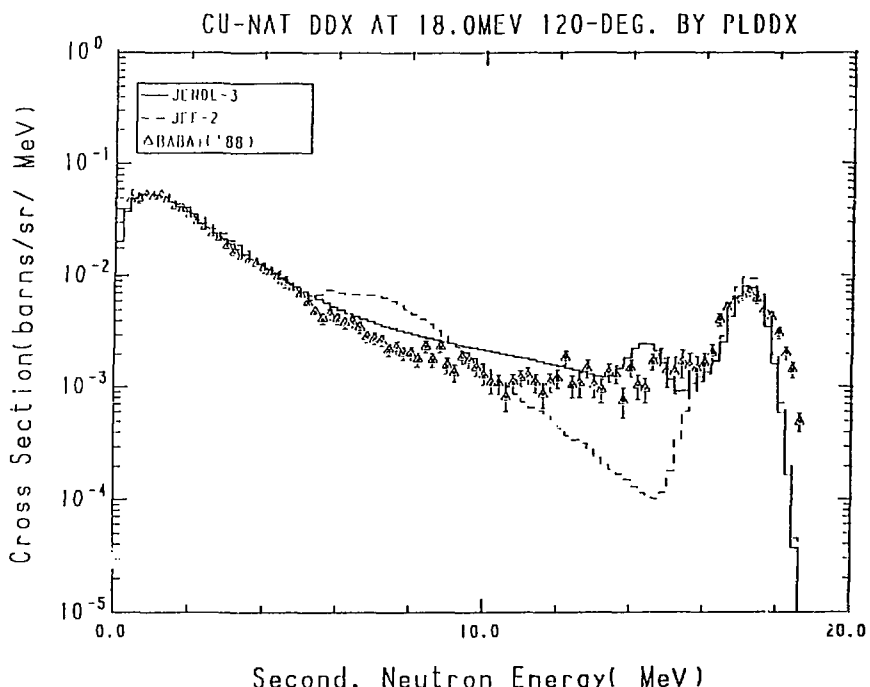


Fig. 35-4 The ^{nat}Cu Double Differential Cross Section at 18.0 MeV,
Emitted Angle = 120° in Laboratory System

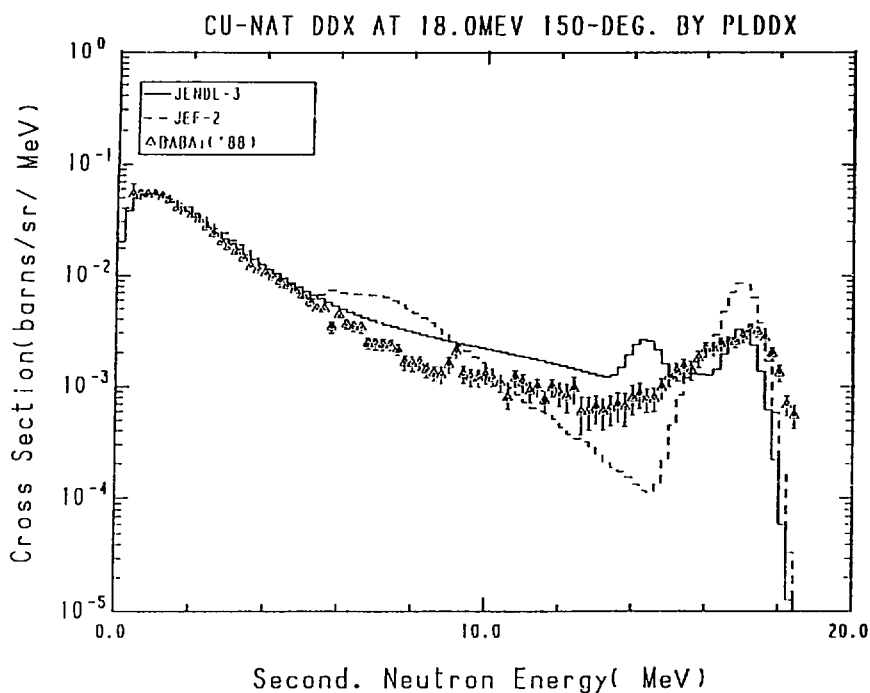


Fig. 35-5 The ^{nat}Cu Double Differential Cross Section at 18.0 MeV,
Emitted Angle = 150° in Laboratory System

3.22 Zirconium

The DDXs calculated from the evaluated data of ^{nat}Zr are compared with the experimental data/BABA+('88),TAKAHASHI+('88)/ of 30° , 60° , 80° , 120° and 150° at the incident neutron energy of 14.1 MeV in Fig.36, and those/BABA+('88)/ of 30° , 60° , 90° , 120° and 150° at 18.0 MeV in Fig.37. A discrepancy between two experimental data sets is observed around 9 MeV at the incident energy of 14.1 MeV, and the data calculated from JENDL-3 are close to the data measured at Tohoku university. Since the direct process of the inelastic scattering is not considered in JENDL-3, the DDXs calculated from JENDL-3 give small values in the energy region just below the peak of the elastic scattering. In the middle energy region, the JENDL-3 data reproduce the experimental data at the forward angles, but tend to be overestimated at the backward angles at the both incident energies.

References for the Experimental Data in Figures

- BABA+('88) : Baba M., Ishikawa M., Yabuta N., Kikuchi T., Wakabayashi H. and Hirakawa H., Proc. of Int. Conf. on Nucl. Data for Sci. and Technol. at Mito in May 30- Jun. 3, p.291 (1988).
TAKAHASHI+('88): Takahashi A., private communication (1989).

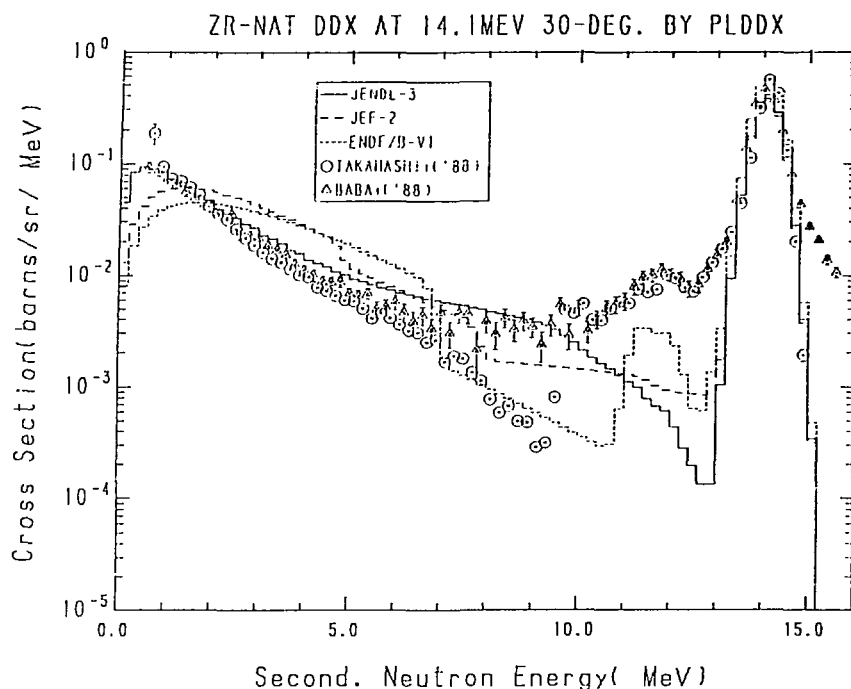


Fig. 36-1 The ^{nat}Zr Double Differential Cross Section at 14.1 MeV,
Emitted Angle = 30° in Laboratory System

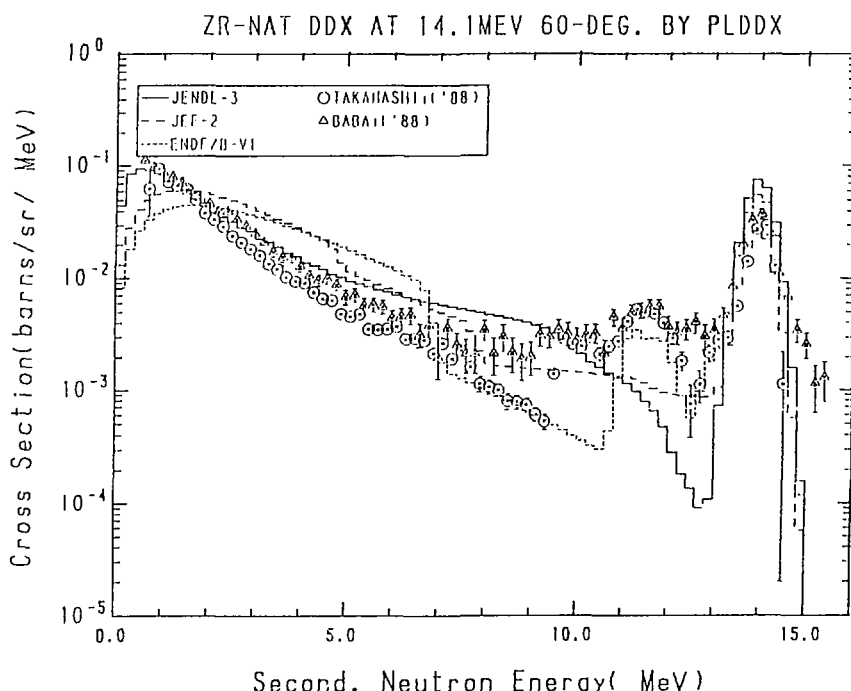


Fig. 36-2 The ^{nat}Zr Double Differential Cross Section at 14.1 MeV,
Emitted Angle = 60° in Laboratory System

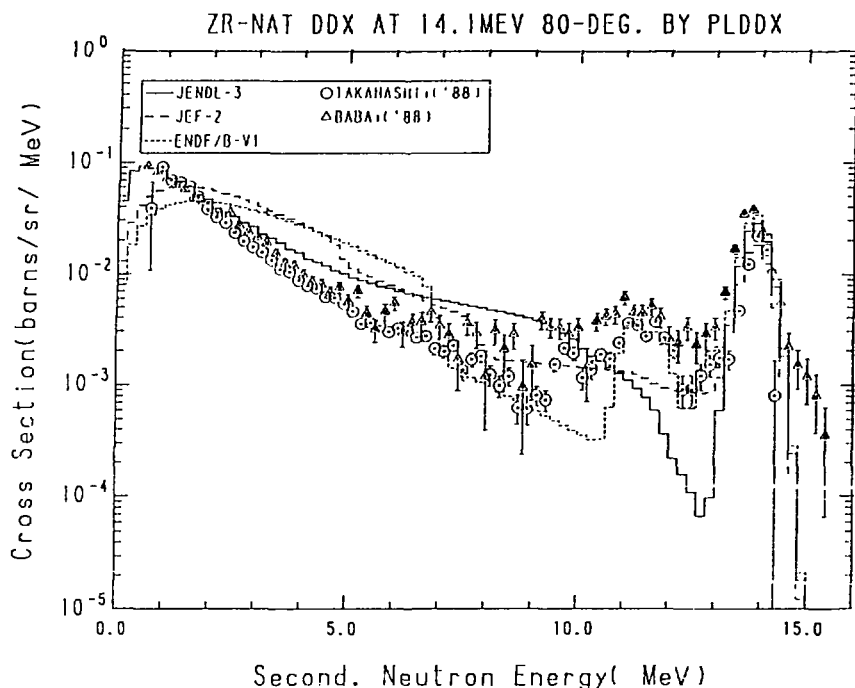


Fig. 36-3 The ^{nat}Zr Double Differential Cross Section at 14.1 MeV,
Emitted Angle = 80° in Laboratory System

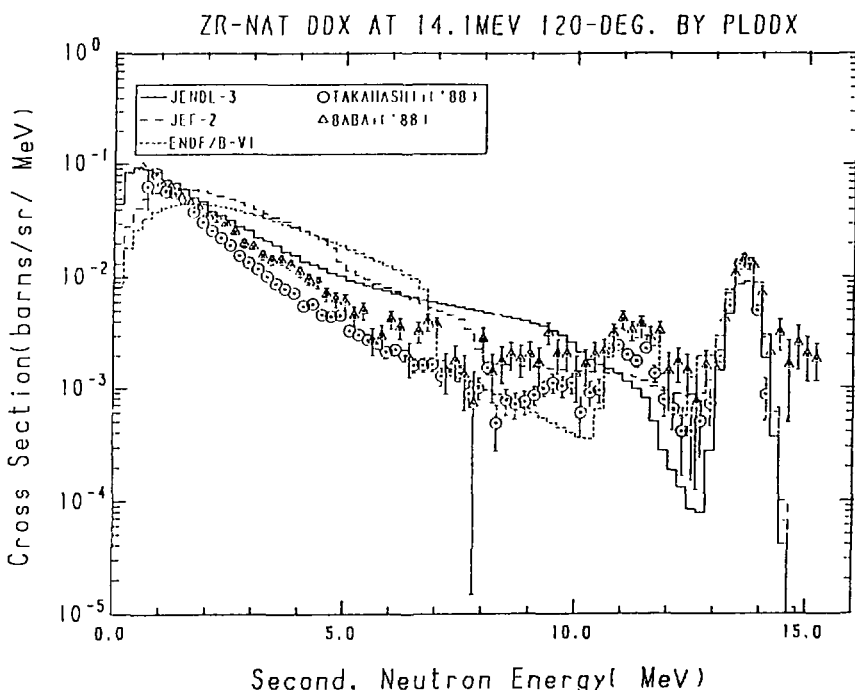


Fig. 36-4 The ^{nat}Zr Double Differential Cross Section at 14.1 MeV,
Emitted Angle = 120° in Laboratory System

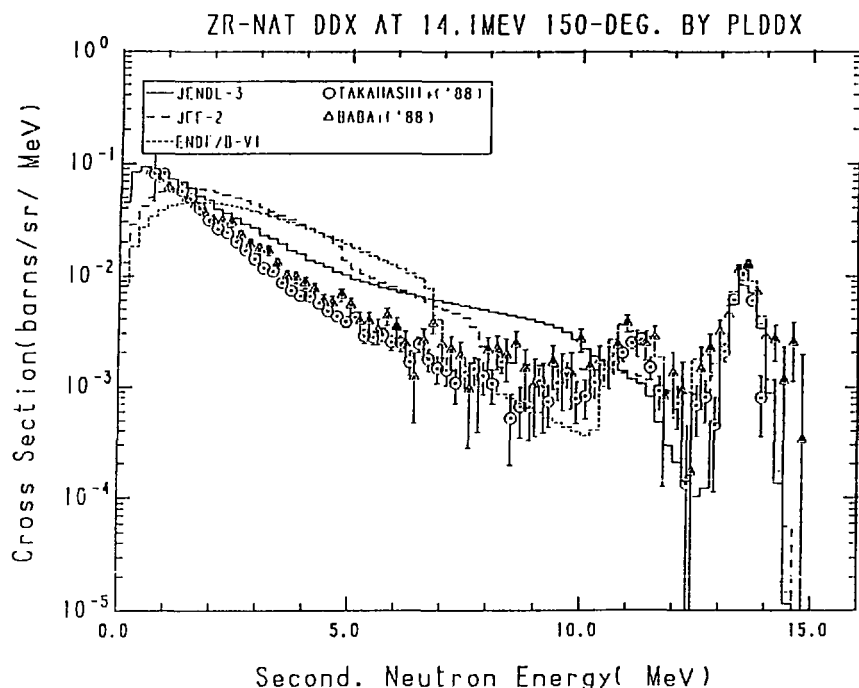


Fig. 36-5 The ^{nat}Zr Double Differential Cross Section at 14.1 MeV,
Emitted Angle = 150° in Laboratory System

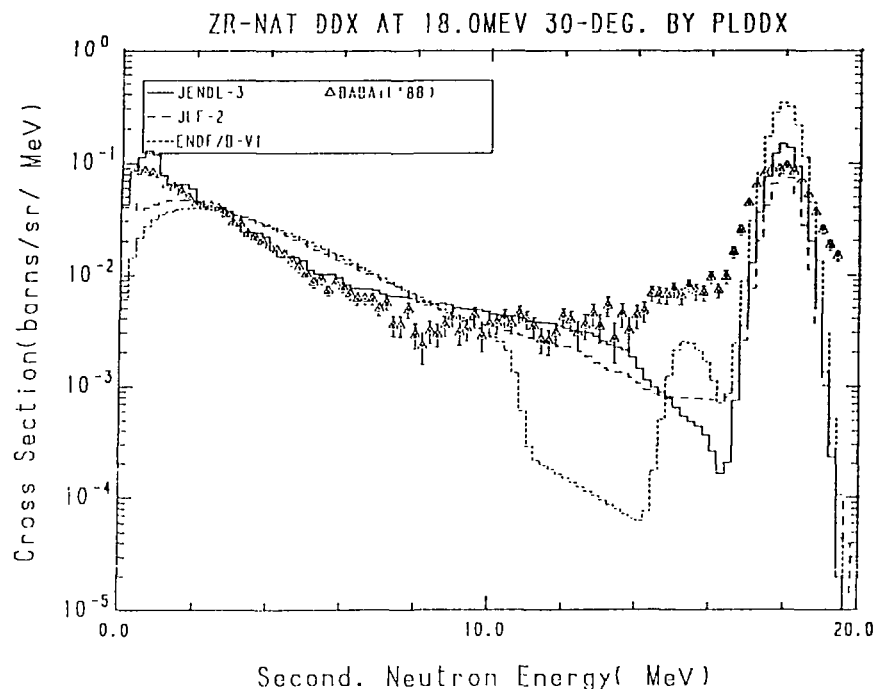


Fig. 37-1 The ^{nat}Zr Double Differential Cross Section at 18.0 MeV,
Emitted Angle = 30° in Laboratory System

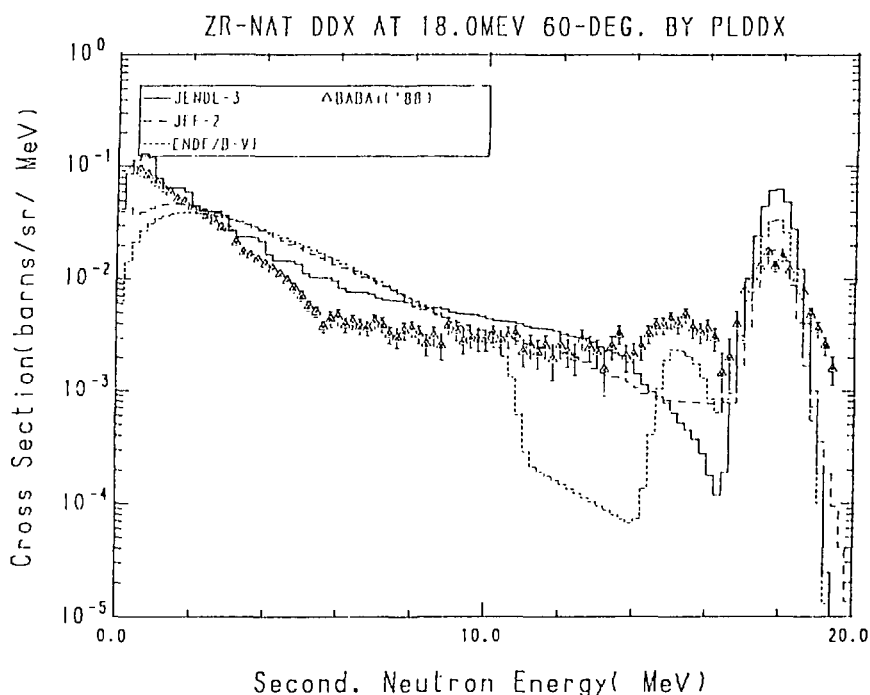


Fig. 37-2 The ^{nat}Zr Double Differential Cross Section at 18.0 MeV,
Emitted Angle = 60° in Laboratory System

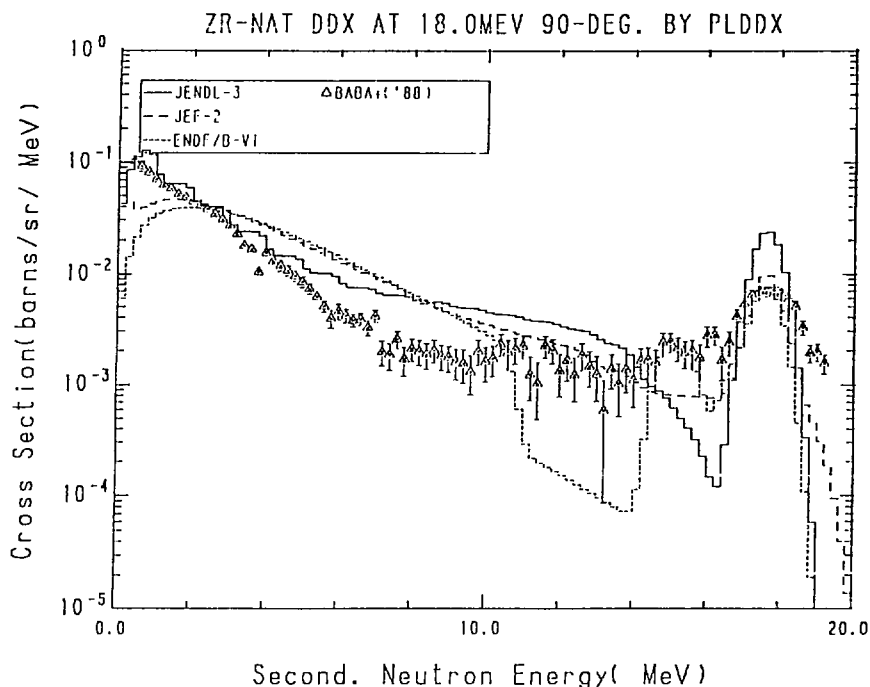


Fig. 37-3 The ^{nat}Zr Double Differential Cross Section at 18.0 MeV,
Emitted Angle = 90° in Laboratory System

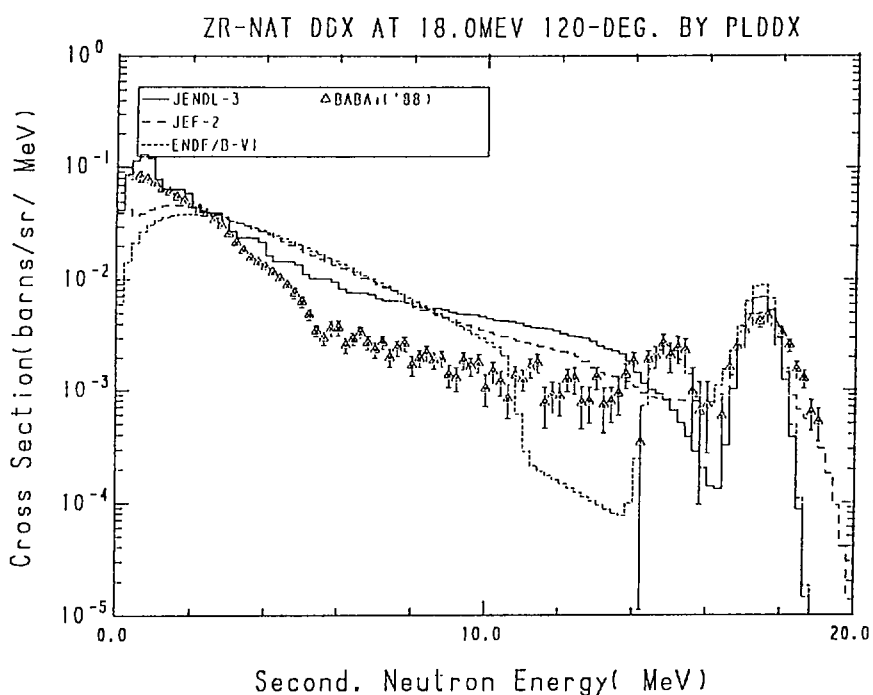


Fig. 37-4 The ^{nat}Zr Double Differential Cross Section at 18.0 MeV,
Emitted Angle = 120° in Laboratory System

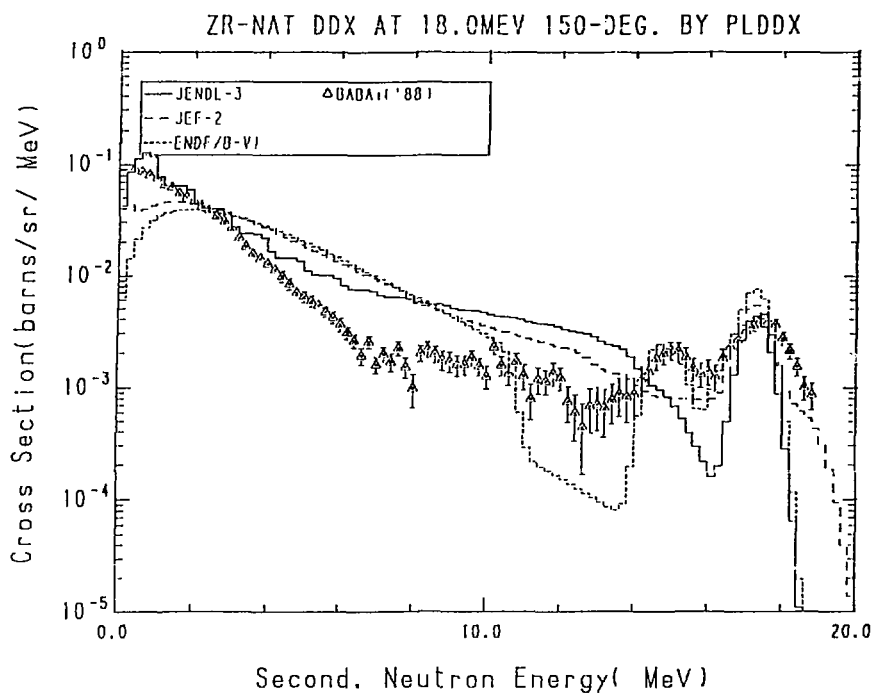


Fig. 37-5 The ^{nat}Zr Double Differential Cross Section at 18.0 MeV,
Emitted Angle = 150° in Laboratory System

3.23 Niobium

The DDXs calculated from the evaluated data of ^{93}Nb are compared with the experimental data/TAKAHASHI+('88)/ of 30° , 60° , 90° , 120° and 150° at the incident neutron energy of 14.1 MeV in Fig.38. The JENDL-3 data reproduce the experimental data excellently, while the others cannot reproduce them.

Reference for the Experimental Data in Figures

TAKAHASHI+('88): Takahashi A., private communication (1989).

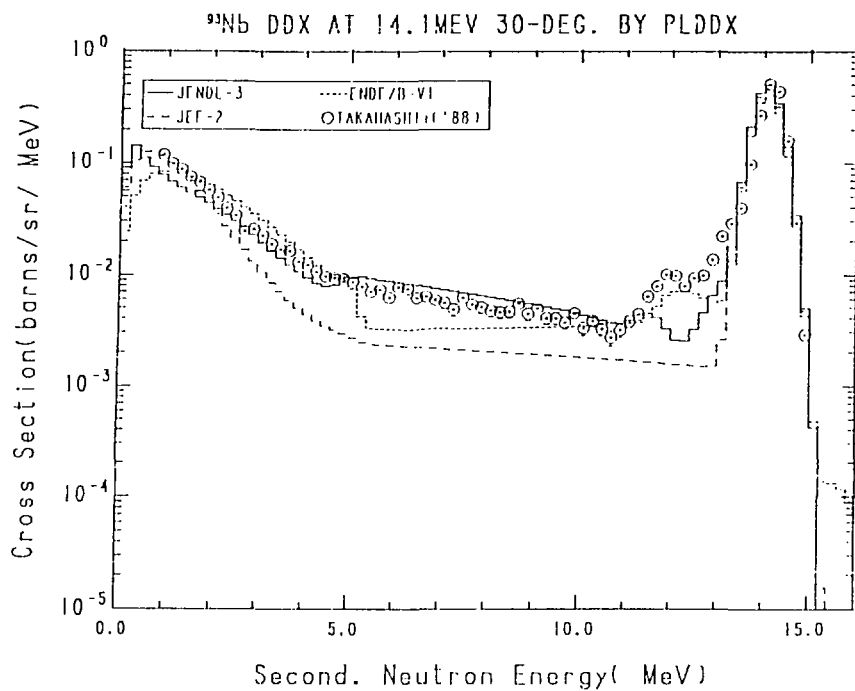


Fig. 38-1 The ^{93}Nb Double Differential Cross Section at 14.1 MeV,
Emitted Angle = 30° in Laboratory System

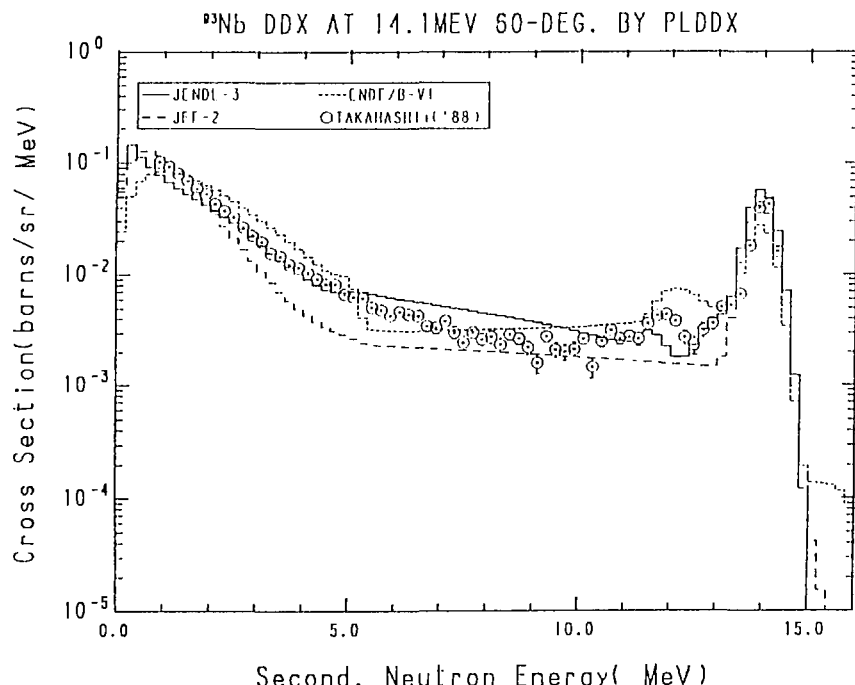


Fig. 38-2 The ^{93}Nb Double Differential Cross Section at 14.1 MeV,
Emitted Angle = 60° in Laboratory System

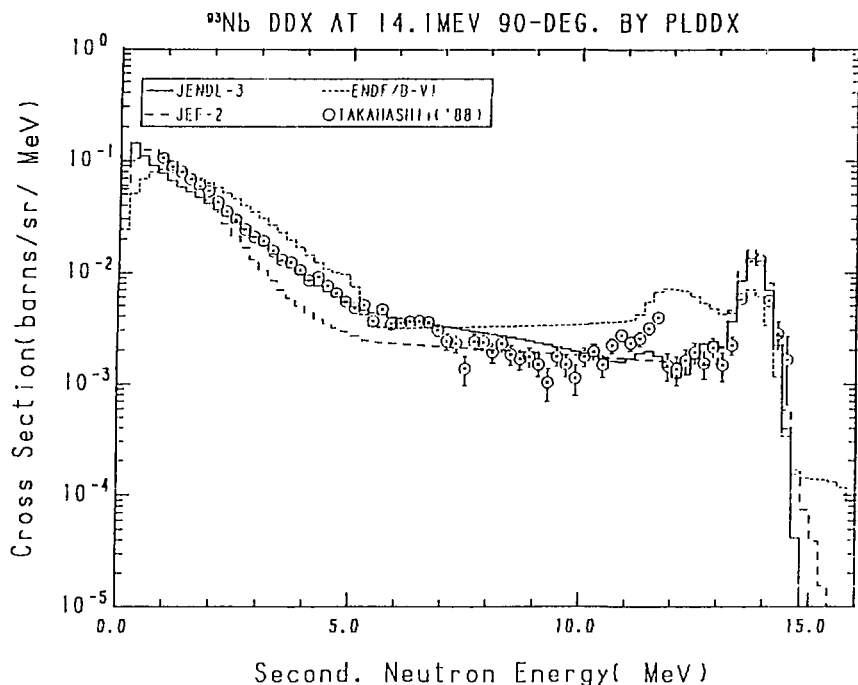


Fig. 38-3 The ^{93}Nb Double Differential Cross Section at 14.1 MeV,
Emitted Angle = 90° in Laboratory System

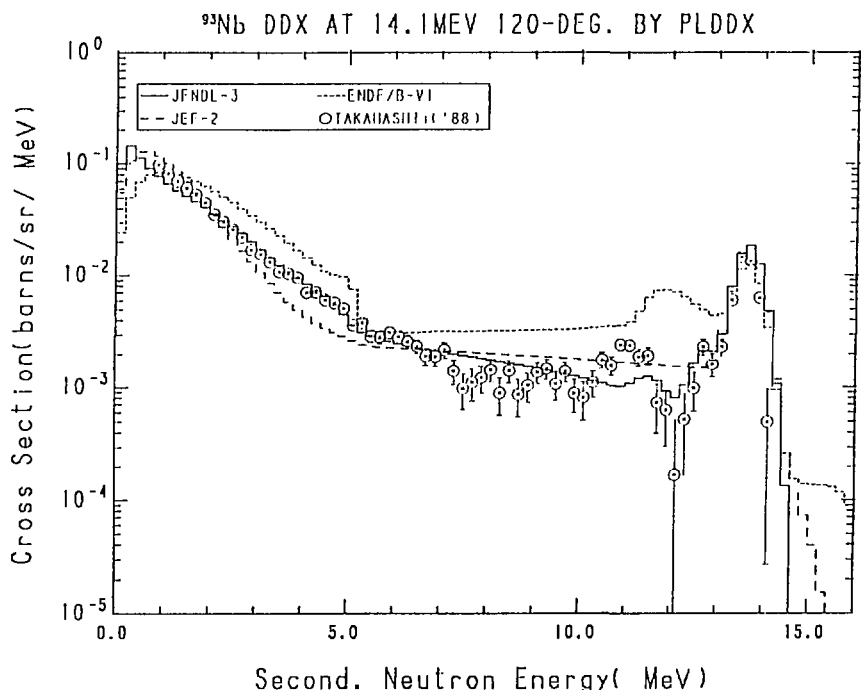


Fig. 38-4 The ^{93}Nb Double Differential Cross Section at 14.1 MeV,
Emitted Angle = 120° in Laboratory System

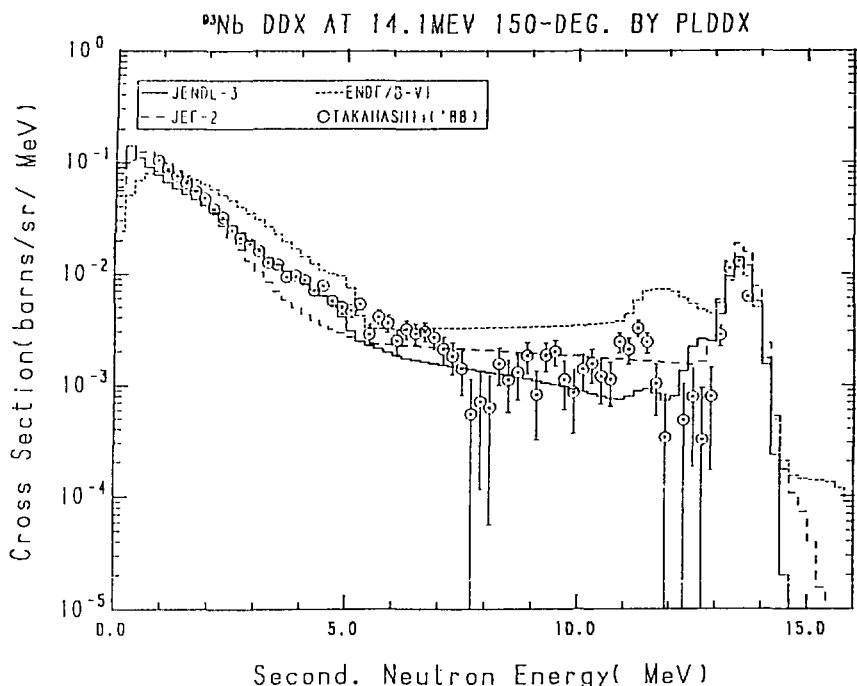


Fig. 38-5 The ^{93}Nb Double Differential Cross Section at 14.1 MeV,
Emitted Angle = 150° in Laboratory System

3.24 Molybdenum

The DDXs calculated from the evaluated data of ^{nat}Mo are compared with the experimental data/TAKAHASHI+('88)/ of 30° , 60° , 90° , 120° and 150° at the incident neutron energy of 14.1 MeV in Fig.39. In the energy region just below the elastic scattering peak, the three libraries cannot reproduce the experimental data, since the direct inelastic process is not considered. The JENDL-3 and ENDF/B-VI data are in good agreement with the experimental data in the energy region below about 10 MeV, except at the forward angles.

Reference for the Experimental Data in Figures

TAKAHASHI+('88): Takahashi A., private communication (1989).

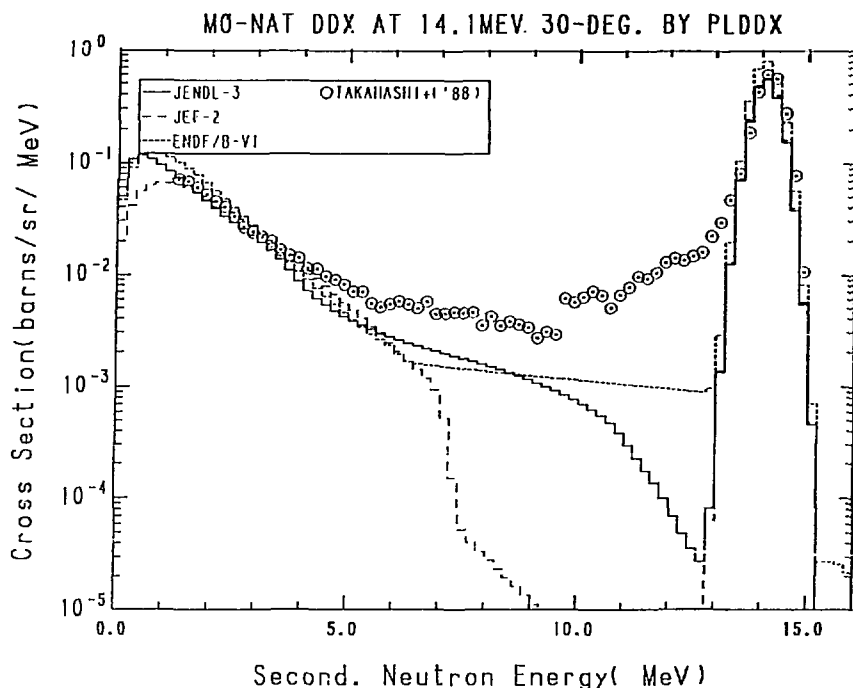


Fig. 39-1 The ^{nat}Mo Double Differential Cross Section at 14.1 MeV,
Emitted Angle = 30° in Laboratory System

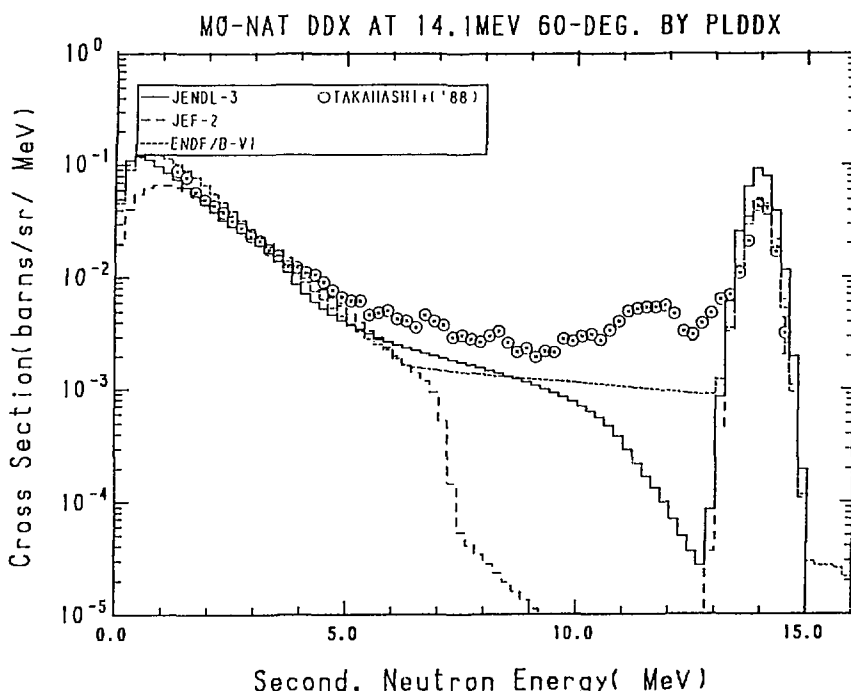


Fig. 39-2 The ^{nat}Mo Double Differential Cross Section at 14.1 MeV,
Emitted Angle = 60° in Laboratory System

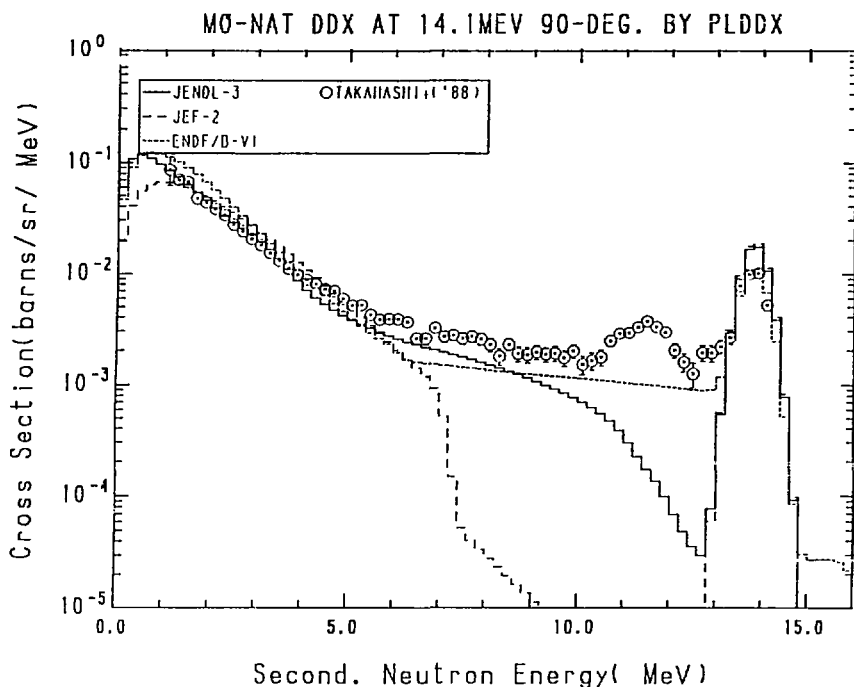


Fig. 39-3 The nat Mo Double Differential Cross Section at 14.1 MeV,
Emitted Angle = 90° in Laboratory System

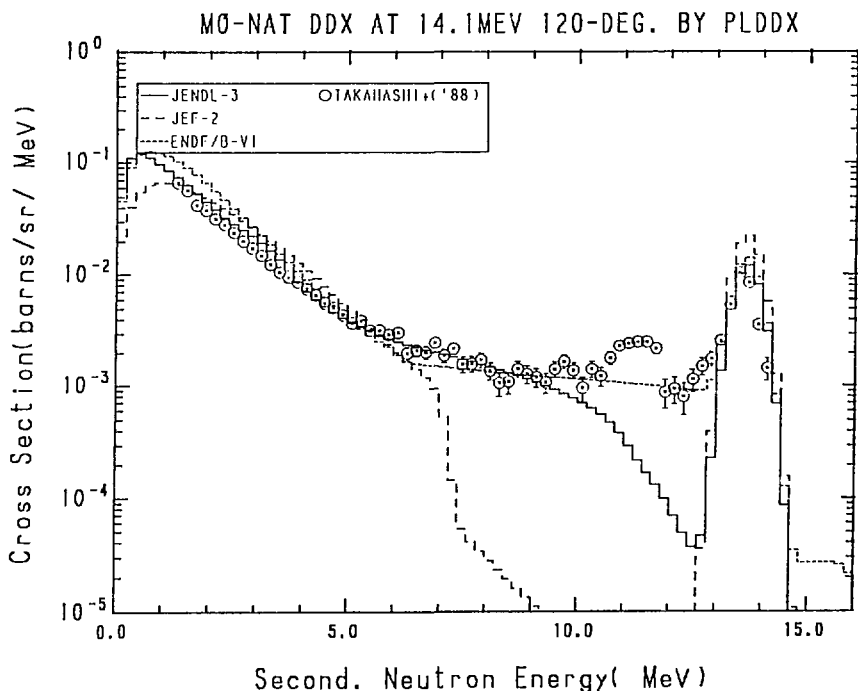


Fig. 39-4 The nat Mo Double Differential Cross Section at 14.1 MeV,
Emitted Angle = 120° in Laboratory System

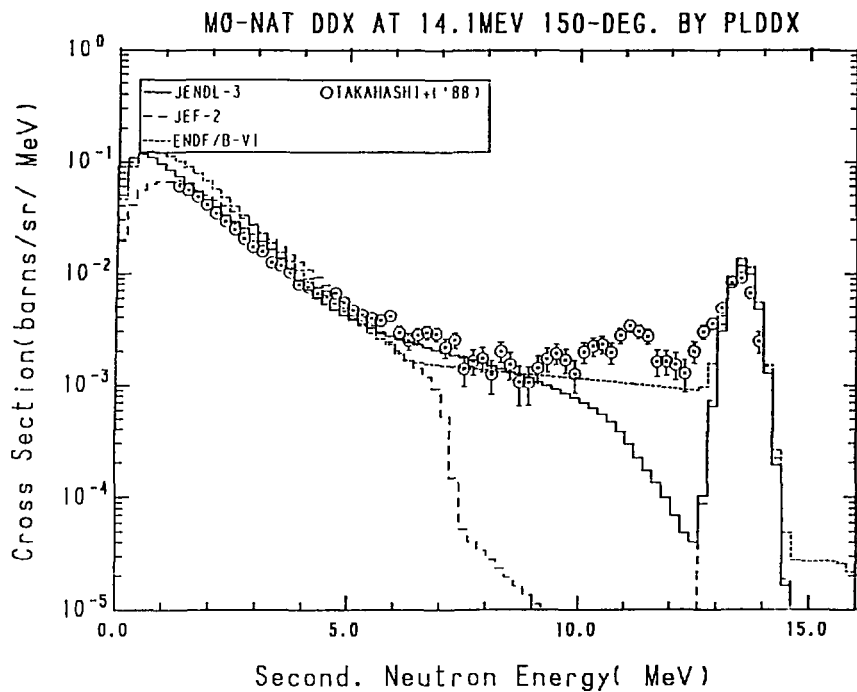


Fig. 39-5 The ^{nat}Mo Double Differential Cross Section at 14.1 MeV,
Emitted Angle = 150° in Laboratory System

3.25 Tin

The DDXs calculated from the evaluated data of ^{nat}Sn are compared with the experimental data/TAKAHASHI+('90)/ of 30°, 60°, 90°, 120° and 150° at the incident neutron energy of 14.1 MeV in Fig.40. The elemental tin is not included in the three evaluated libraries. The JENDL-3 data were constructed from the individual isotope data of JENDL-3 and angular distributions are assumed to be isotropic, except those of the elastic scattering. Since JENDL-3 did not consider the direct process to the discrete inelastic scattering, the JENDL-3 data are smaller than the experimental data in the discrete inelastic scattering energy region just below the elastic scattering peak. In the low energy region, the data calculated from JENDL-3 well reproduce the experimental data.

Reference for the Experimental Data in Figures

TAKAHASHI+('90): Takahashi A., private communication (1990).

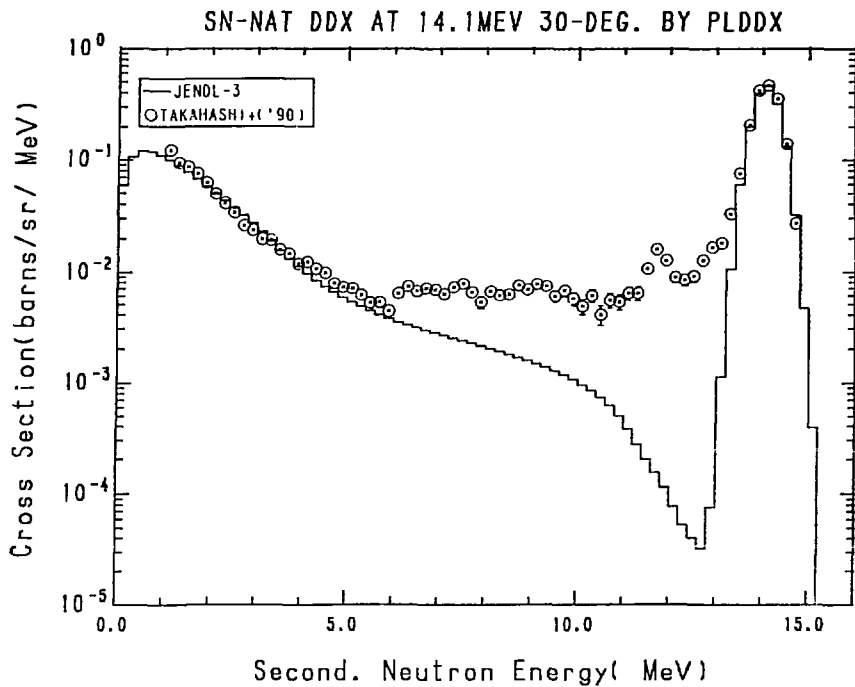


Fig. 40-1 The ^{nat}Sn Double Differential Cross Section at 14.1 MeV,
Emitted Angle = 30° in Laboratory System

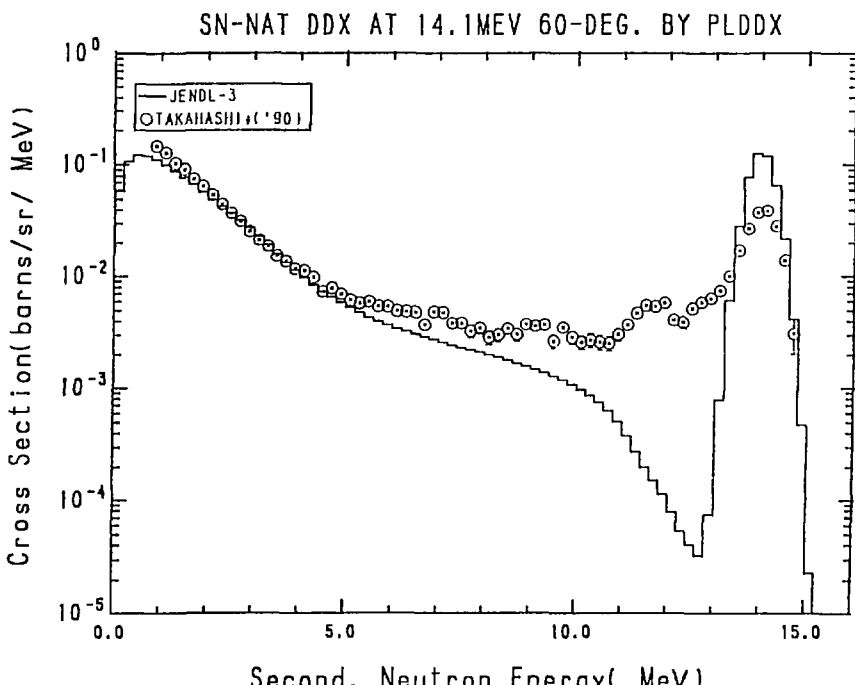


Fig. 40-2 The ^{nat}Sn Double Differential Cross Section at 14.1 MeV,
Emitted Angle = 60° in Laboratory System

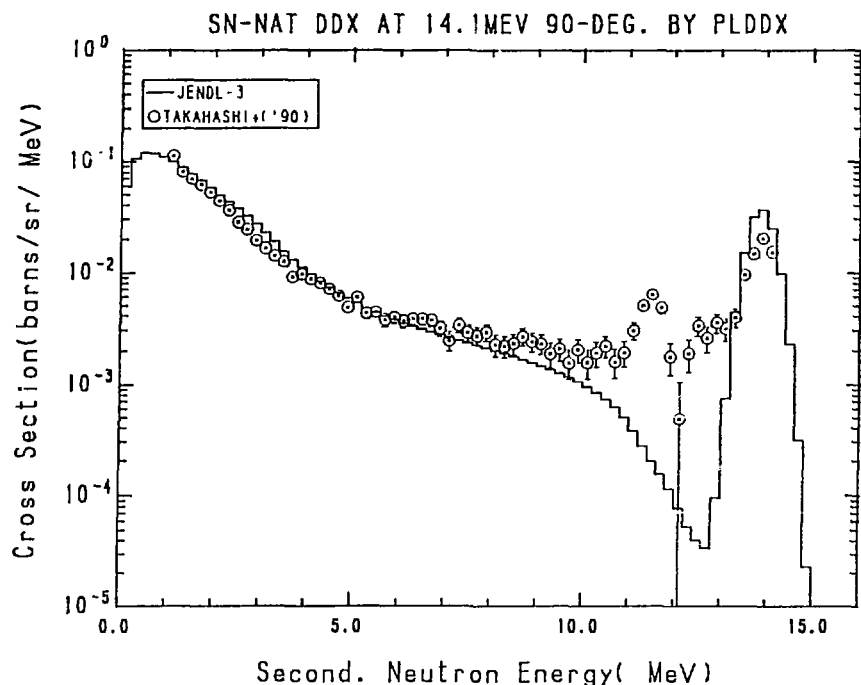


Fig. 40-3 The ^{nat}Sn Double Differential Cross Section at 14.1 MeV,
Emitted Angle = 90° in Laboratory System

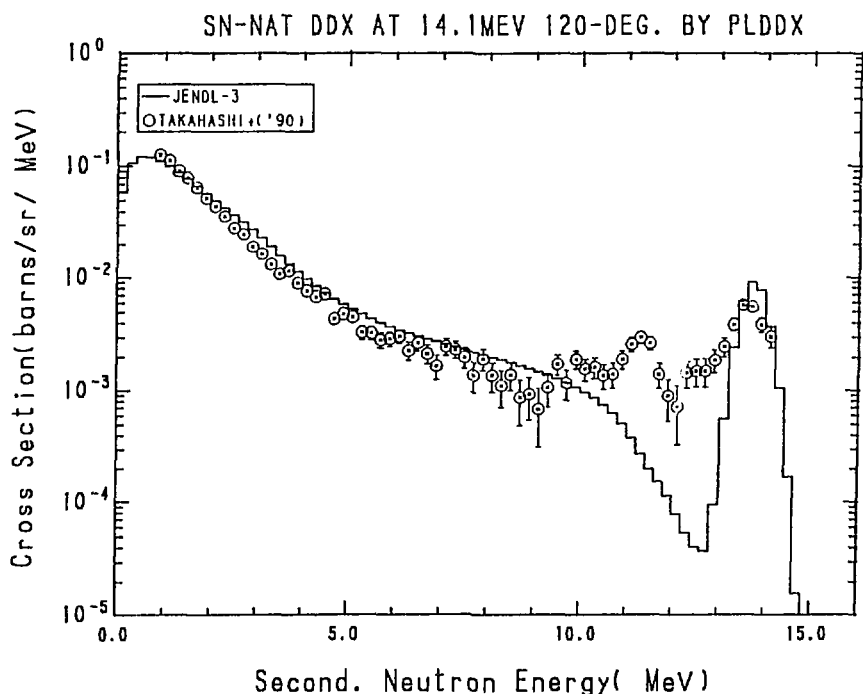


Fig. 40-4 The ^{nat}Sn Double Differential Cross Section at 14.1 MeV,
Emitted Angle = 120° in Laboratory System

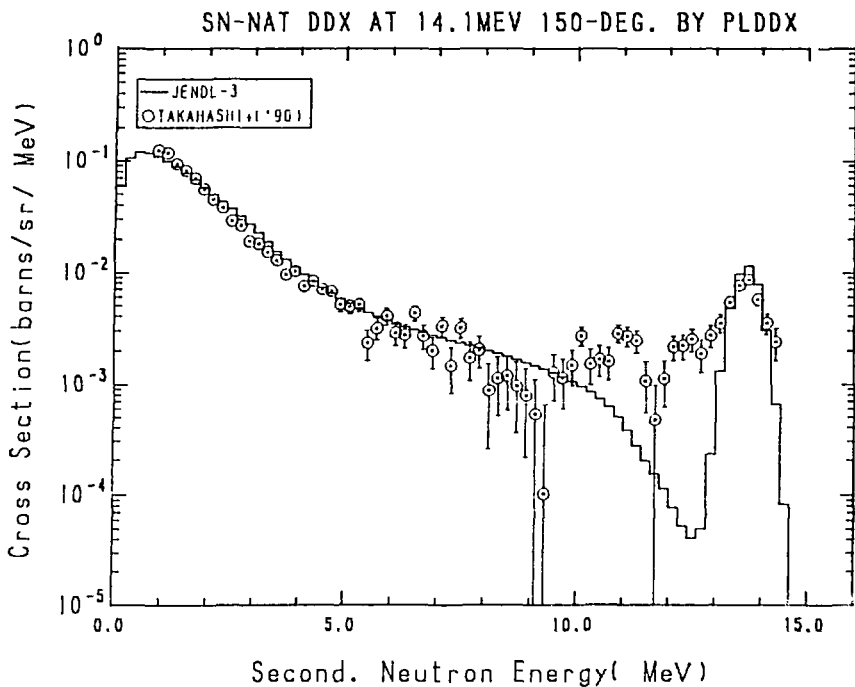


Fig. 40-5 The ^{nat}Sn Double Differential Cross Section at 14.1 MeV,
Emitted Angle = 150° in Laboratory System

3.26 Antimony

Only the DDXs calculated from JENDL-3 of ^{nat}Sb are compared with the experimental data /TAKAHASHI+('90)/ of 30° , 60° , 90° , 120° and 150° at the incident neutron energy of 14.1 MeV in Fig.41. The comparison could not be made for ENDF/B-VI and JEF-2, since these two libraries include no data for the natural elements and there exists no processing code which can create those data easily. The JENDL-3 data are in good agreement with the experimental data, except in the discrete inelastic scattering region, since the direct process of the inelastic scattering is not considered in JENDL-3.

Reference for the Experimental Data in Figures

TAKAHASHI+('90): Takahashi A., private communication (1990).

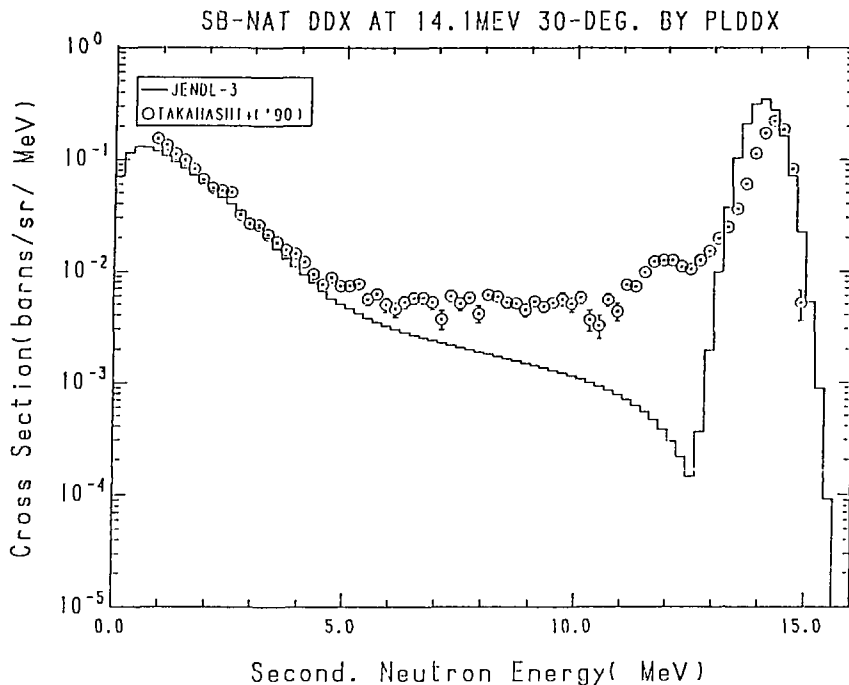


Fig. 41-1 The ^{nat}Sb Double Differential Cross Section at 14.1 MeV,
Emitted Angle = 30° in Laboratory System

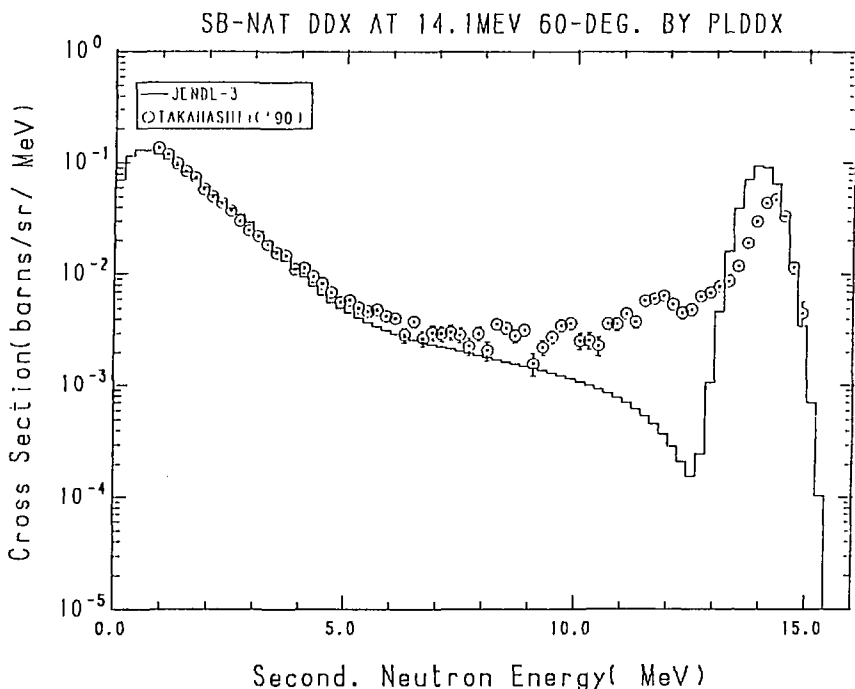


Fig. 41-2 The ^{nat}Sb Double Differential Cross Section at 14.1 MeV,
Emitted Angle = 60° in Laboratory System

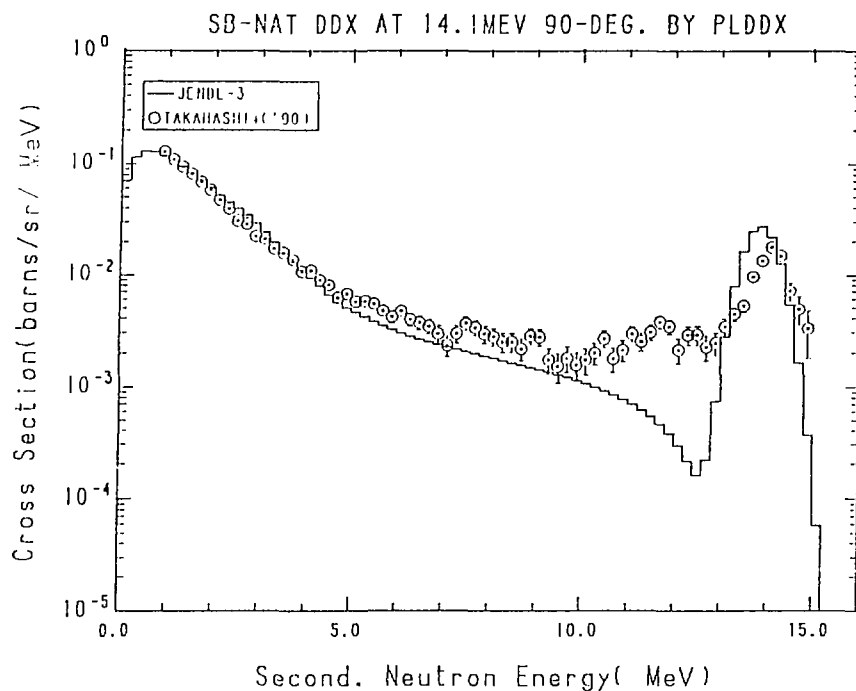


Fig. 41-3 The ^{nat}Sb Double Differential Cross Section at 14.1 MeV,
Emitted Angle = 90° in Laboratory System

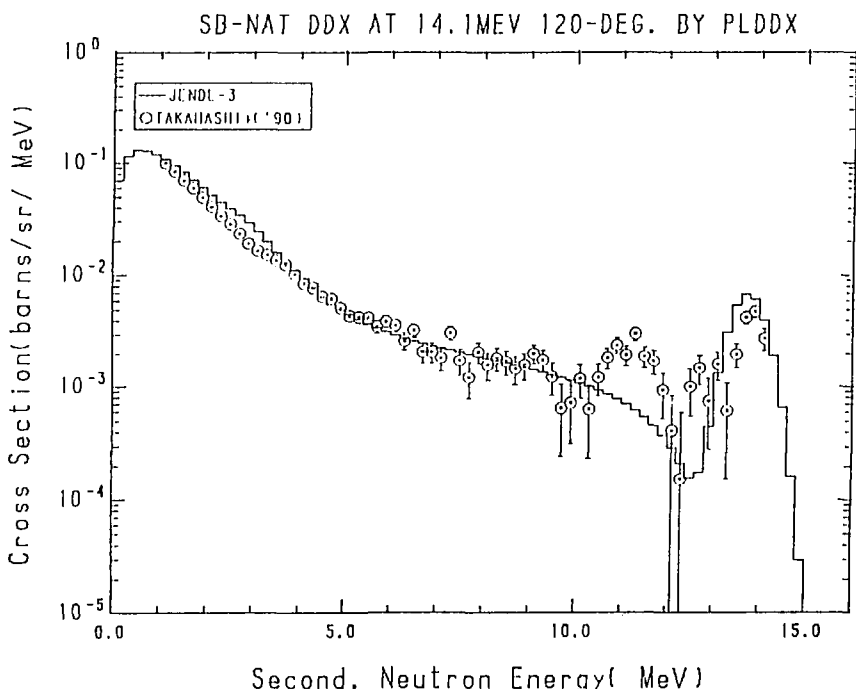


Fig. 41-4 The ^{nat}Sb Double Differential Cross Section at 14.1 MeV,
Emitted Angle = 120° in Laboratory System

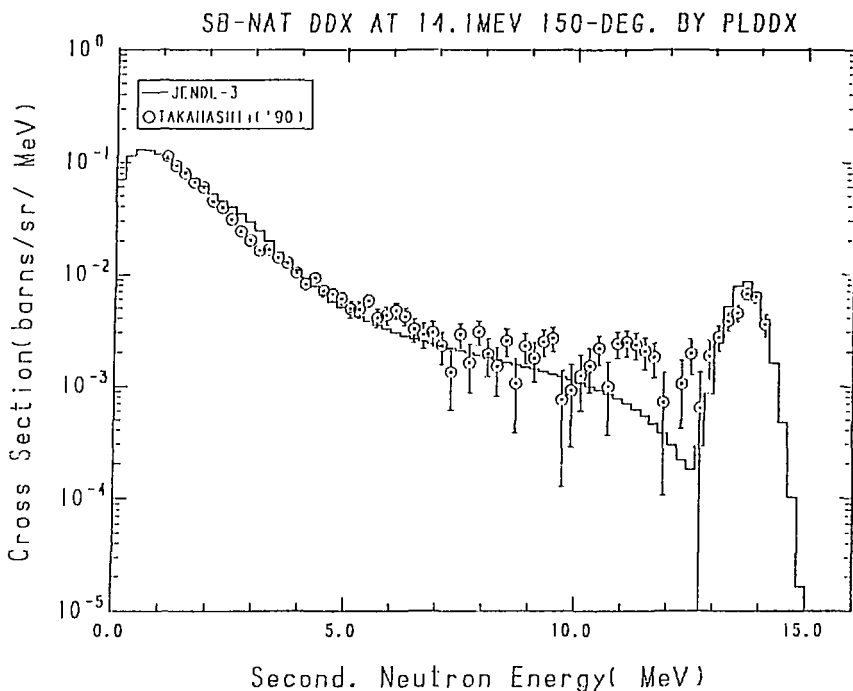


Fig. 41-5 The ^{nat}Sb Double Differential Cross Section at 14.1 MeV,
Emitted Angle = 150° in Laboratory System

3.27 Tantalum

The DDXs calculated from the evaluated data of ^{181}Ta are compared with the experimental data/BABA+('91)/ of 30° , 60° , 90° , 120° and 150° at the incident neutron energy of 14.1 MeV in Fig.42. The JENDL-3 data reproduce the experimental data, except in the energy region of the discrete inelastic scattering and of 5-10 MeV. The JEF-2 and ENDF/B-VI data are equivalent to each other, and they are almost in good agreement with the experimental data. However, they have strange valleys around 5 MeV.

Reference for the Experimental Data in Figures

BABA+('91): Baba M., private communication (1991).

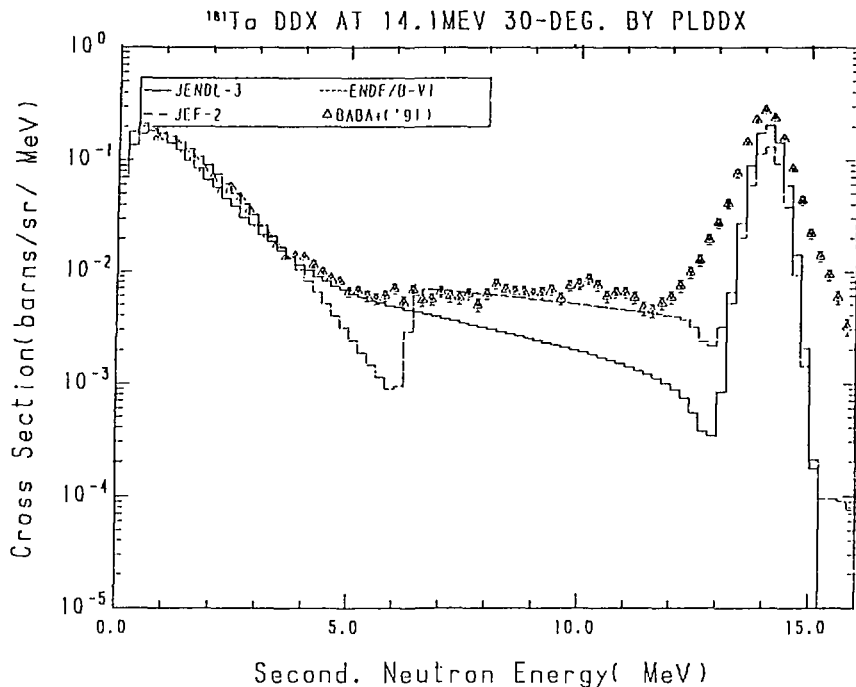


Fig. 42-1 The ^{181}Ta Double Differential Cross Section at 14.1 MeV,
Emitted Angle = 30° in Laboratory System

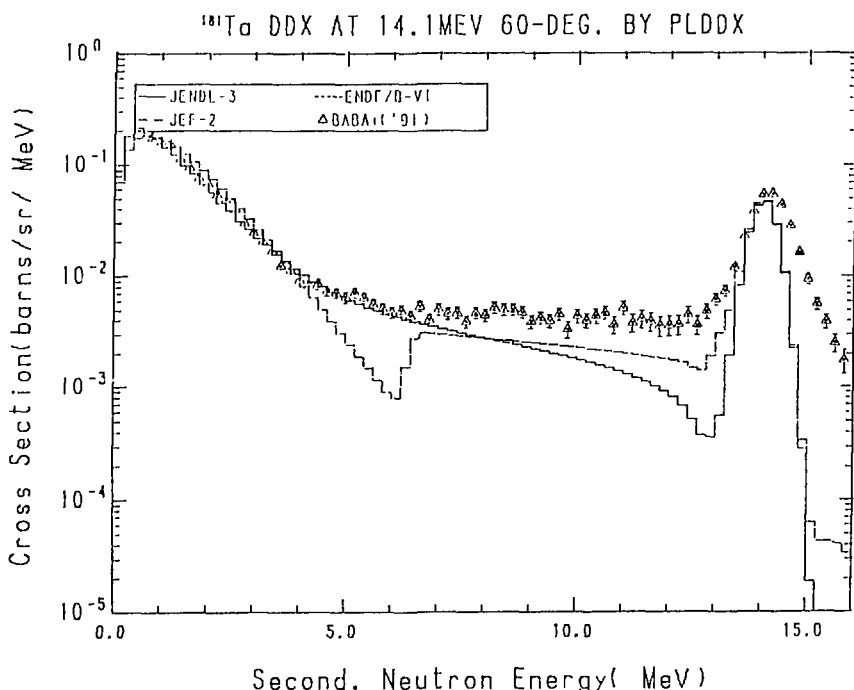


Fig. 42-2 The ^{181}Ta Double Differential Cross Section at 14.1 MeV,
Emitted Angle = 60° in Laboratory System

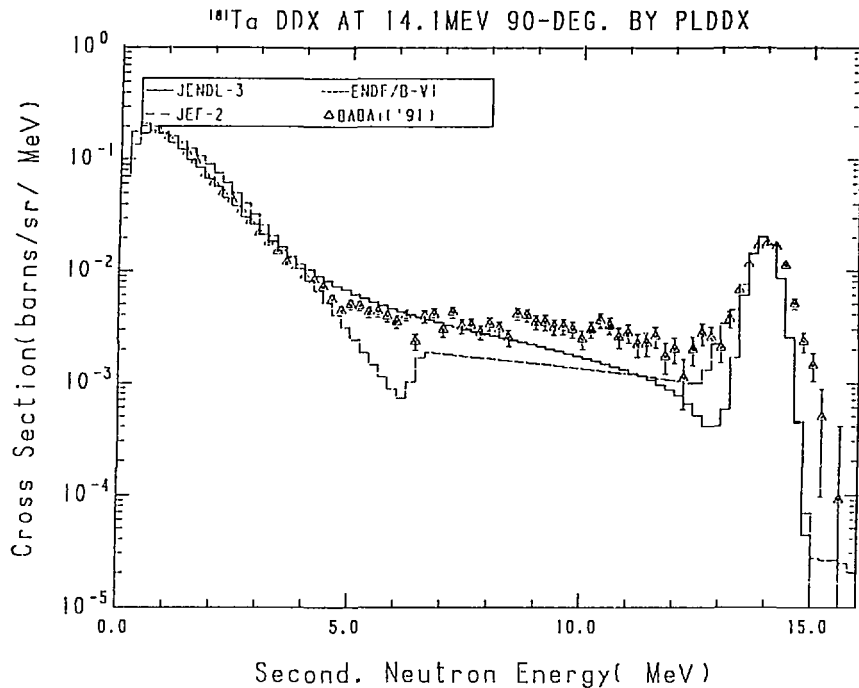


Fig. 42-3 The ^{181}Ta Double Differential Cross Section at 14.1 MeV,
Emitted Angle = 90° in Laboratory System

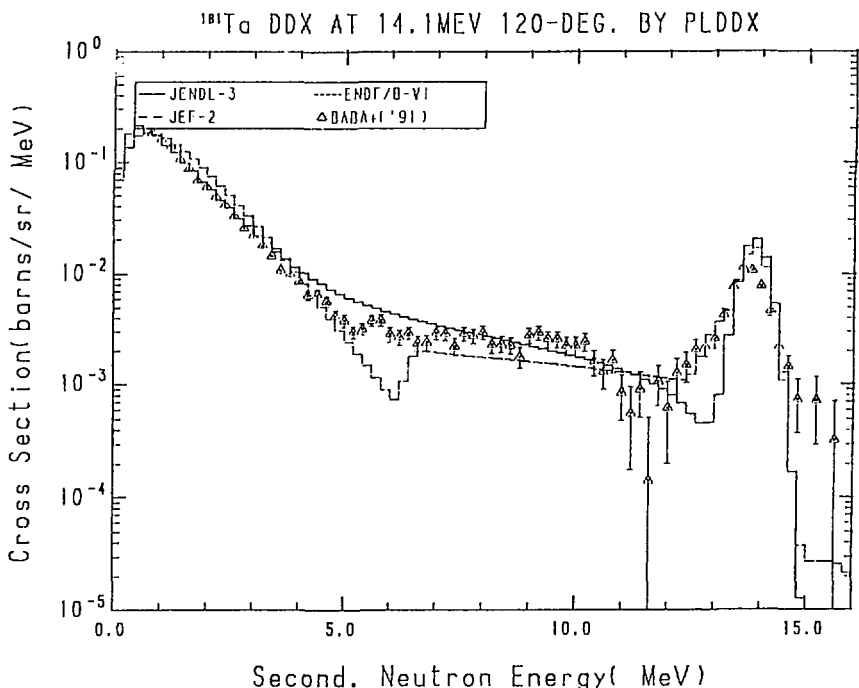


Fig. 42-4 The ^{181}Ta Double Differential Cross Section at 14.1 MeV,
Emitted Angle = 120° in Laboratory System

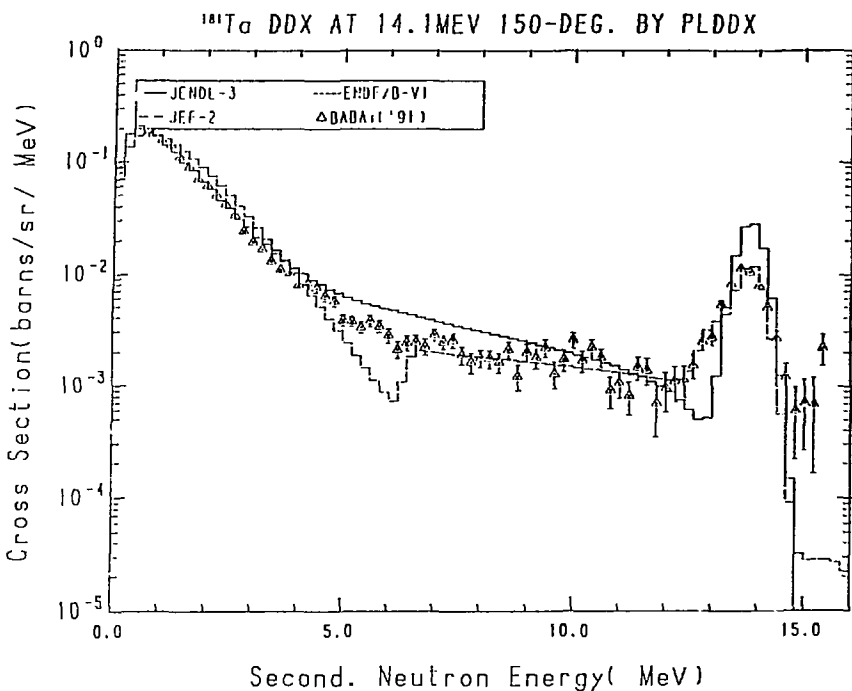


Fig. 42-5 The ^{181}Ta Double Differential Cross Section at 14.1 MeV,
Emitted Angle = 150° in Laboratory System

3.28 Tungsten

The DDXs calculated from the evaluated data of ^{nat}W are compared with the experimental data/TAKAHASHI+('88)/ of 30° , 60° , 90° , 120° and 150° at the incident neutron energy of 14.1 MeV in Fig.43. The comparison could not be made for JEF-2, since this library include no data for the natural elements and there exists no processing code which can create those data easily. The experimental data and the JENDL-3 data have a strange step around 9 and 5 MeV, respectively, while the ENDF/B-VI data have smooth shape. In the low energy region, both libraries reproduce the experimental data.

Reference for the Experimental Data in Figures

TAKAHASHI+('88): Takahashi A., private communication (1989).

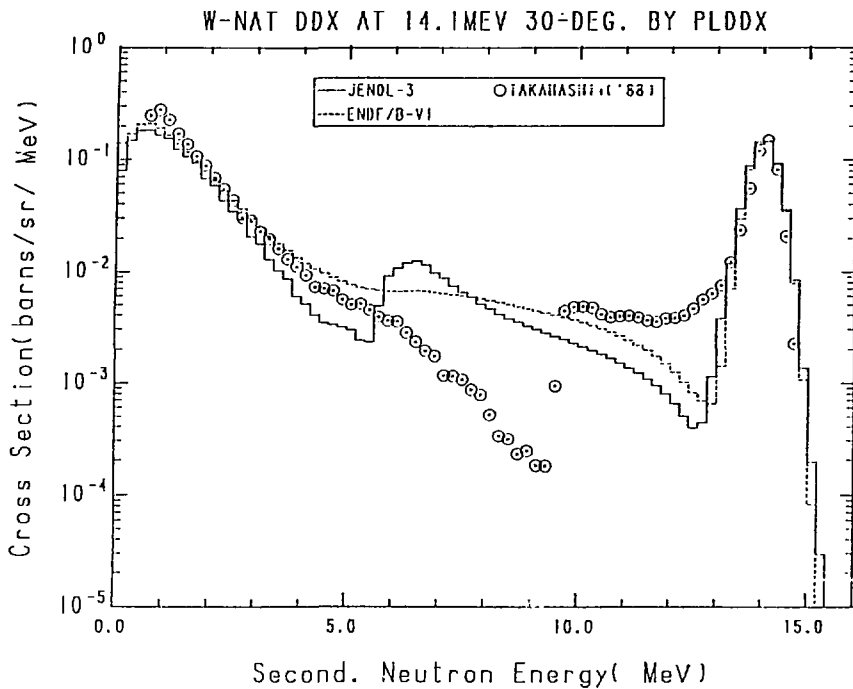


Fig. 43-1 The ^{nat}W Double Differential Cross Section at 14.1 MeV,
Emitted Angle = 30° in Laboratory System

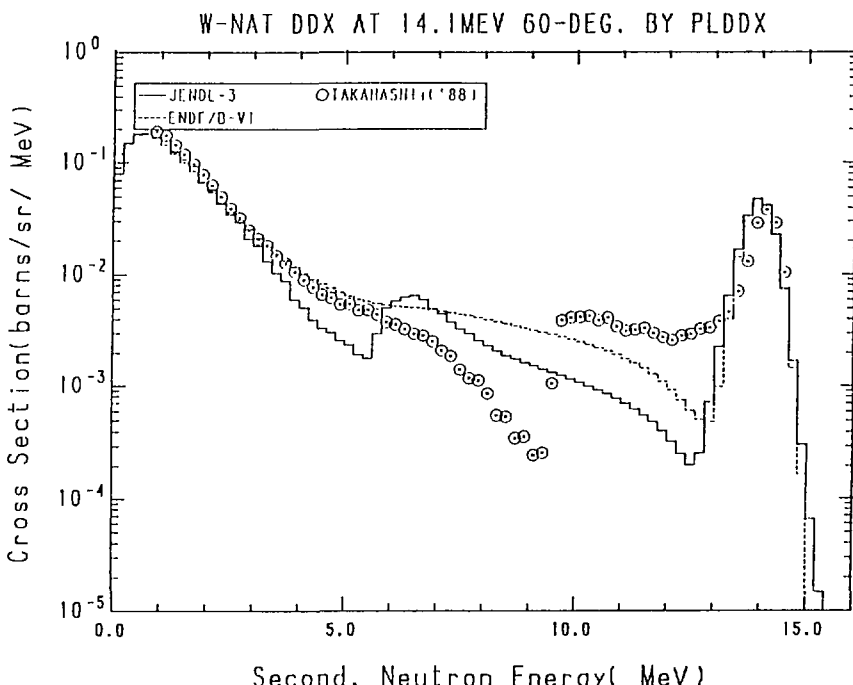


Fig. 43-2 The ^{nat}W Double Differential Cross Section at 14.1 MeV,
Emitted Angle = 60° in Laboratory System

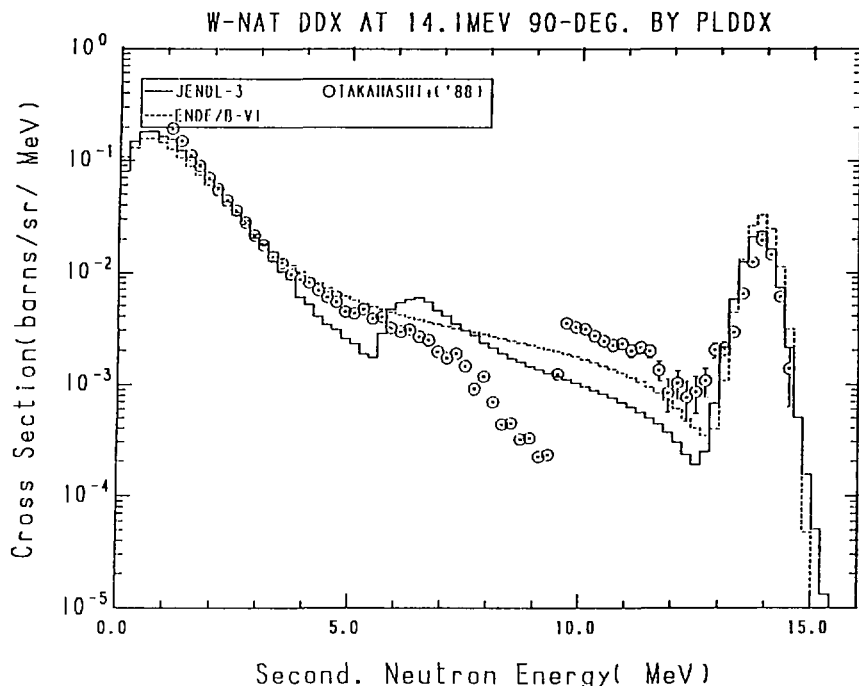


Fig. 43-3 The ^{nat}W Double Differential Cross Section at 14.1 MeV,
Emitted Angle = 90° in Laboratory System

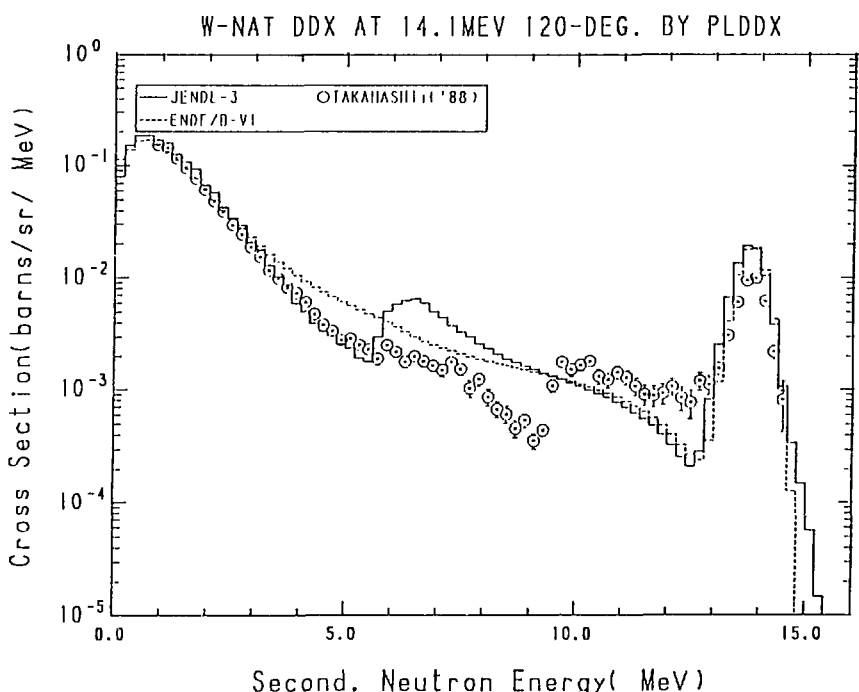


Fig. 43-4 The ^{nat}W Double Differential Cross Section at 14.1 MeV,
Emitted Angle = 120° in Laboratory System

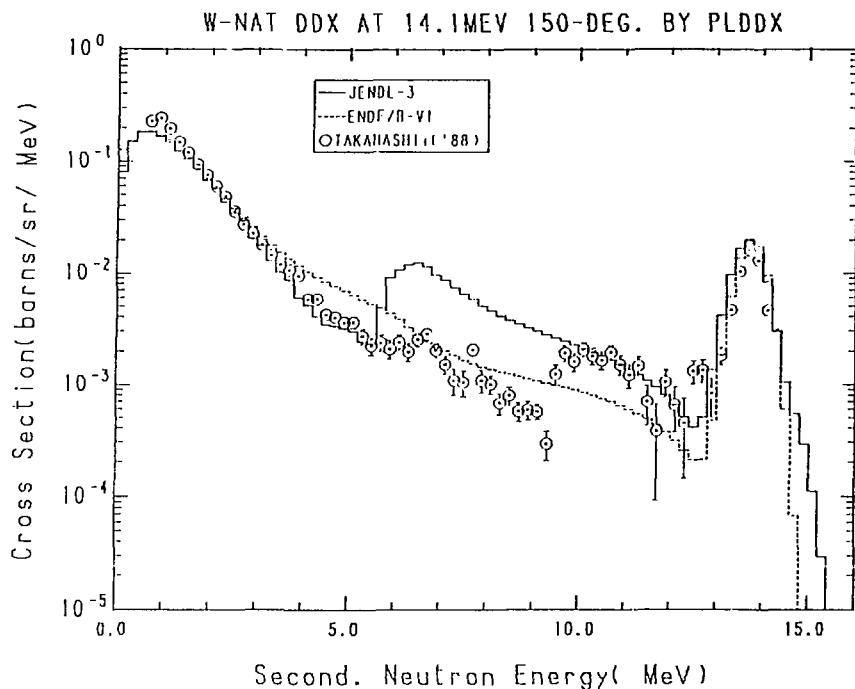


Fig. 43-5 The ^{nat}W Double Differential Cross Section at 14.1 MeV,
Emitted Angle = 150° in Laboratory System

3.29 Lead

The DDXs calculated from the evaluated data of ^{nat}Pb are compared with the experimental data /TAKAHASHI+('86)/ of 30° , 60° , 90° , 120° and 150° at the incident neutron energy of 14.1 MeV in Fig.44. The comparison could not be made for ENDF/B-VI, since this library include no data for the natural elements and there exists no processing code which can create those data easily. The JENDL-3 data reproduce the experimental data in the discrete inelastic scattering region at the forward angles and in the mid energy region at the backward angles. The experimental data in low energy region are reproduced well by JENDL-3. However, the JENDL-3 data overestimate the experimental data in the discrete inelastic scattering region just below the elastic scattering peak at the backward angles and underestimate in the middle energy region at the forward angles. The JEF-2 data cannot reproduce the experimental data in the discrete inelastic scattering region just below the elastic scattering peak.

Reference for the Experimental Data in Figures

TAKAHASHI+('86): Takahashi A., Ichimura E., Sugimoto H. and Kato T.,
JAERI-M 86-080, 393 (1986).

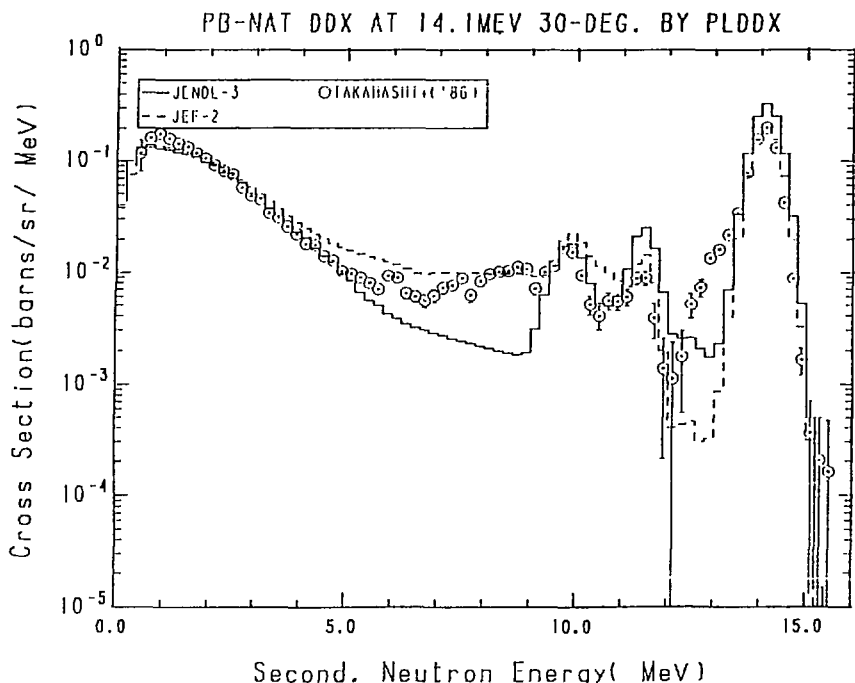


Fig. 44-1 The ^{nat}Pb Double Differential Cross Section at 14.1 MeV,
Emitted Angle = 30° in Laboratory System

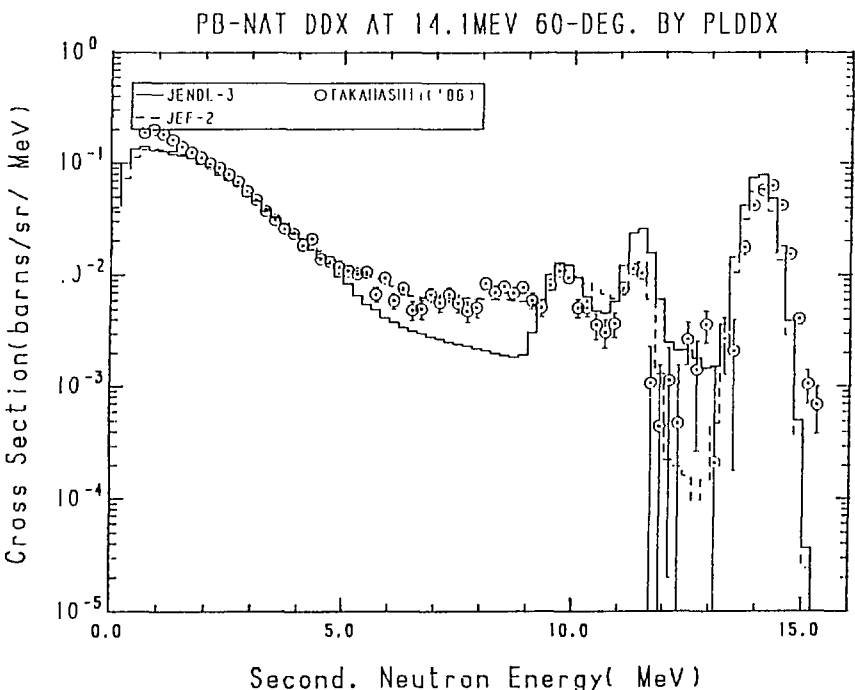


Fig. 44-2 The ^{nat}Pb Double Differential Cross Section at 14.1 MeV,
Emitted Angle = 60° in Laboratory System

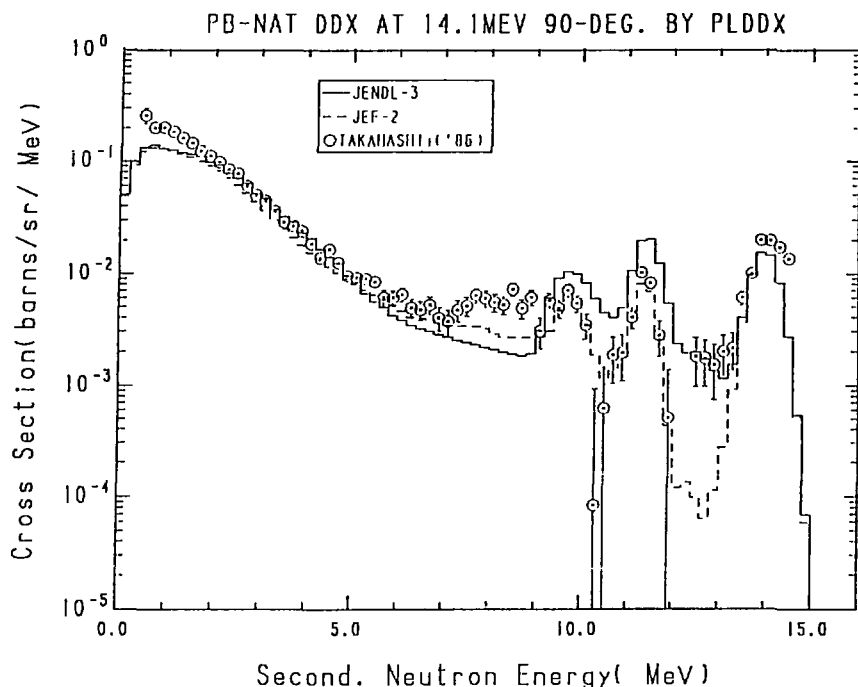


Fig. 44-3 The ^{nat}Pb Double Differential Cross Section at 14.1 MeV,
Emitted Angle = 90° in Laboratory System

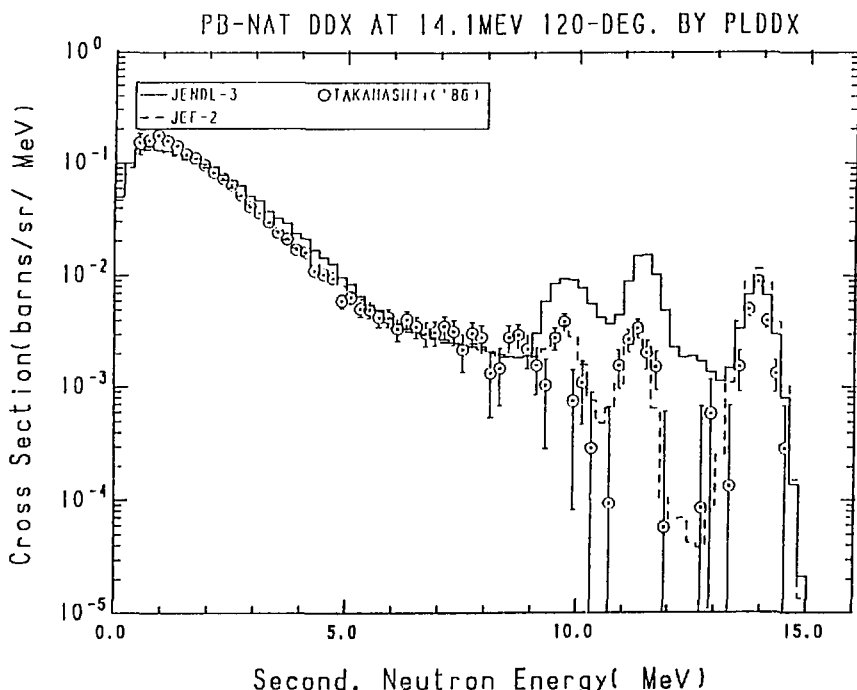


Fig. 44-4 The ^{nat}Pb Double Differential Cross Section at 14.1 MeV,
Emitted Angle = 120° in Laboratory System

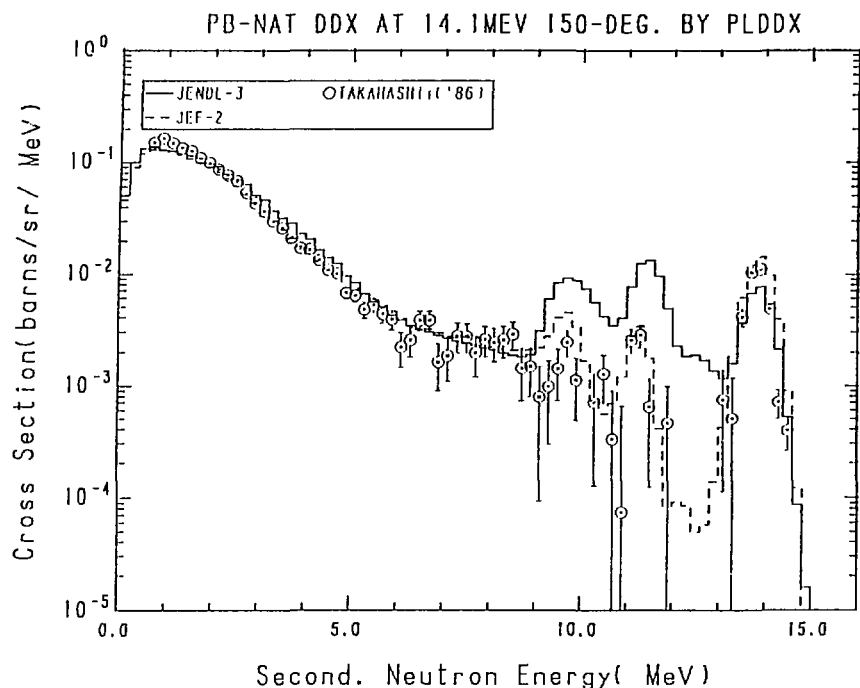


Fig. 44-5 The ^{nat}Pb Double Differential Cross Section at 14.1 MeV,
Emitted Angle = 150° in Laboratory System

3.30 Bismuth

The DDXs calculated from the evaluated data of ^{209}Bi are compared with the experimental data /TAKAHASHI+('88)/ of 30° , 60° , 90° , 120° and 150° at the incident neutron energy of 14.1 MeV in Fig.45. The JENDL-3 data well reproduce the experimental data of all the angles, except the third peak around 10 MeV appeared in the experimental data and below 1 MeV.

Reference for the Experimental Data in Figures

TAKAHASHI+('88): Takahashi A., private communication (1989).

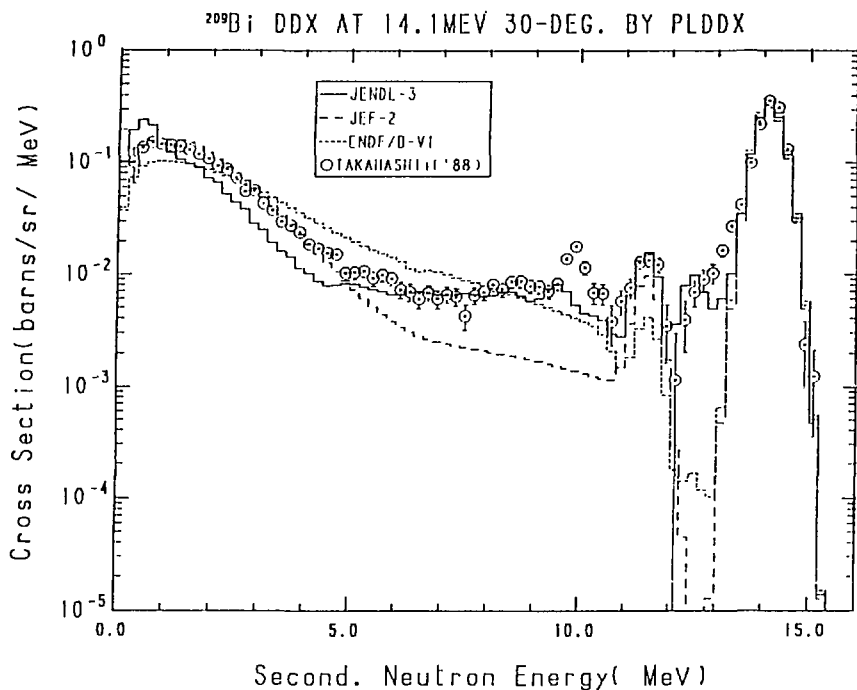


Fig. 45-1 The ^{209}Bi Double Differential Cross Section at 14.1 MeV,
Emitted Angle = 30° in Laboratory System

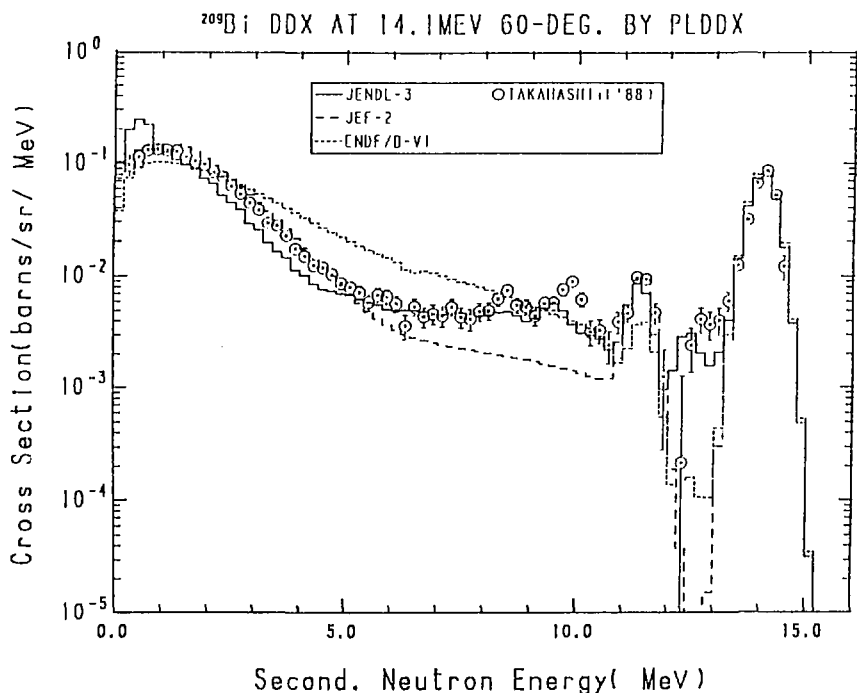


Fig. 45-2 The ^{209}Bi Double Differential Cross Section at 14.1 MeV,
Emitted Angle = 60° in Laboratory System

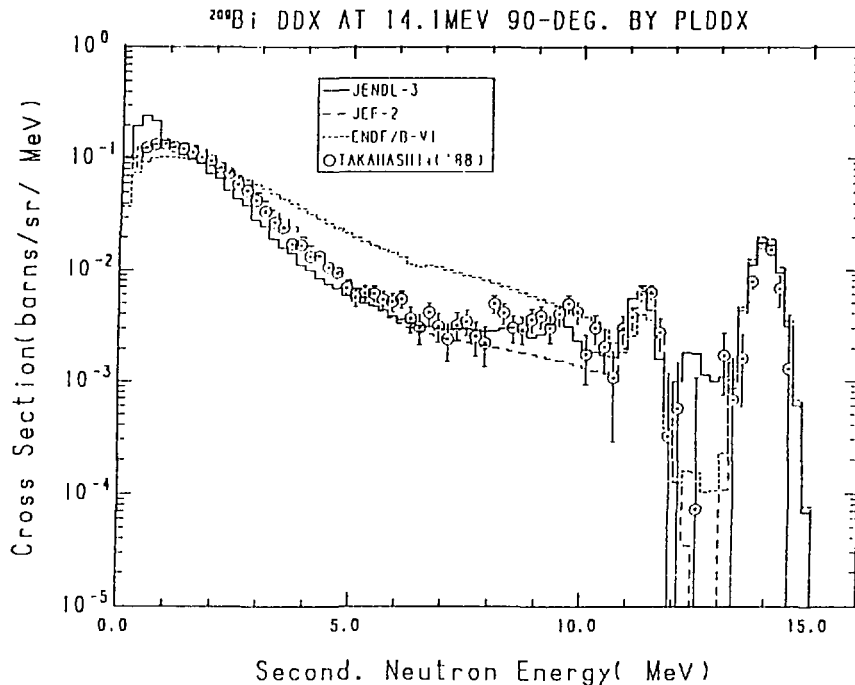


Fig. 45-3 The ^{209}Bi Double Differential Cross Section at 14.1 MeV,
Emitted Angle = 90° in Laboratory System

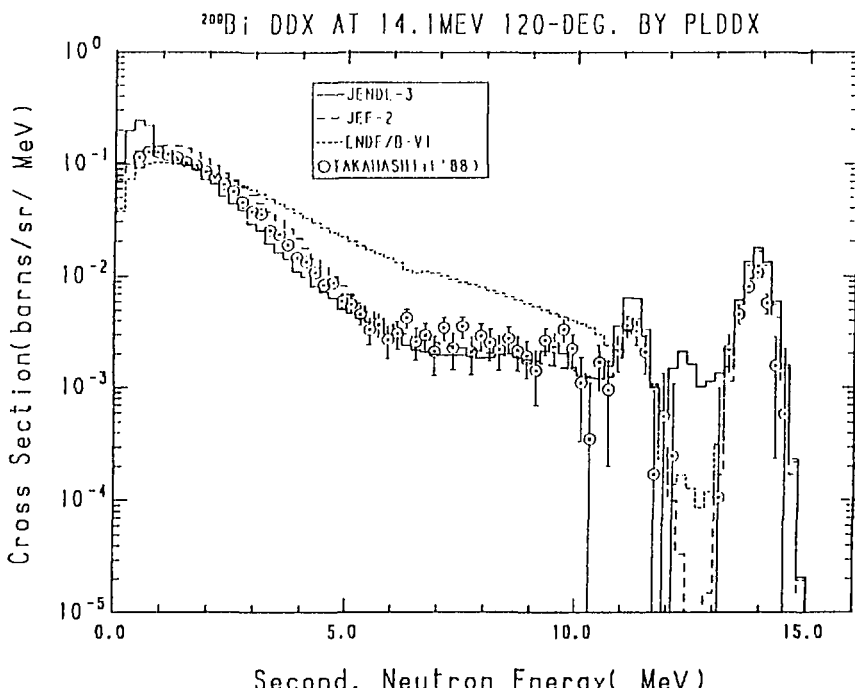


Fig. 45-4 The ^{209}Bi Double Differential Cross Section at 14.1 MeV,
Emitted Angle = 120° in Laboratory System

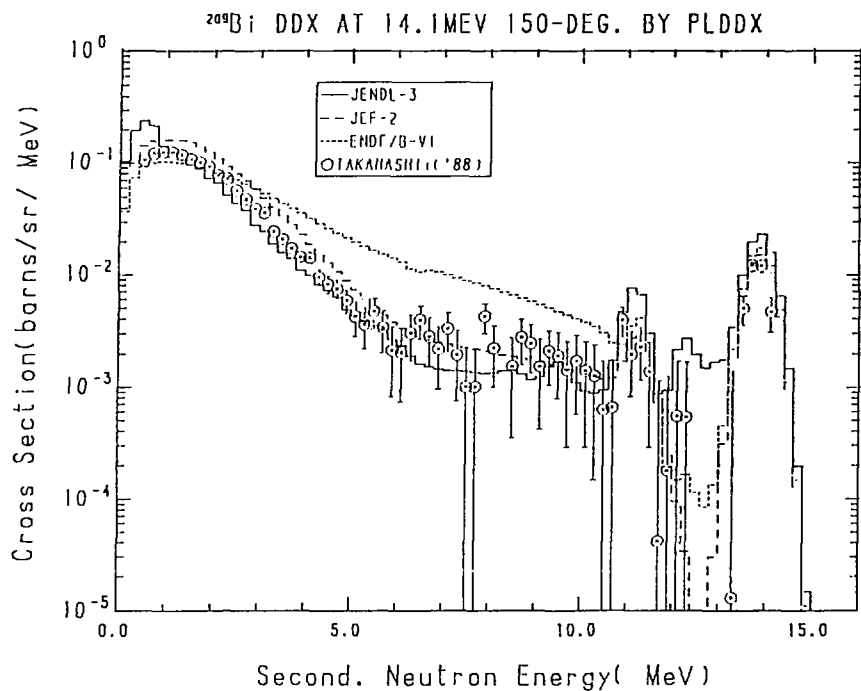


Fig. 45-5 The ^{209}Bi Double Differential Cross Section at 14.1 MeV,
Emitted Angle = 150° in Laboratory System

3.31 Thorium

The DDXs calculated from the evaluated data of ^{232}Th are compared with the experimental data /BABA+('90)/ of $^{\text{nat}}\text{Th}$ at the emitted angles of 30° , 60° , 90° , 120° and 150° at the incident neutron energy of 1.20 (60° and 120° only), 2.03, 4.25, 6.10, 14.1 MeV in Figs.46-50. The DDXs calculated from the evaluated data do not include contributions of fission neutrons for a technical reason. The JENDL-3 data almost reproduce the experimental data, except the second peak continuing the elastic scattering peak at the backward angles.

Reference for the Experimental Data in Figures

BABA+('90): Baba M., Wakabayashi H., Itoh N., Maeda K. and Hirakawa N., JAERI-M 89-143 (1986) in Japanese.

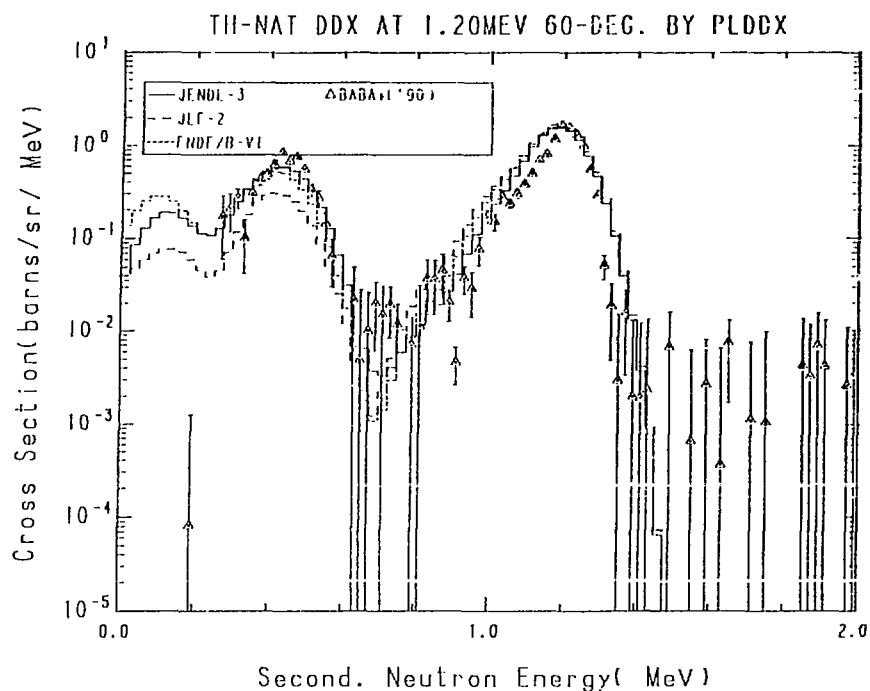


Fig. 46-1 The ^{nat}Th Double Differential Cross Section at 1.20 MeV,
Emitted Angle = 60° in Laboratory System

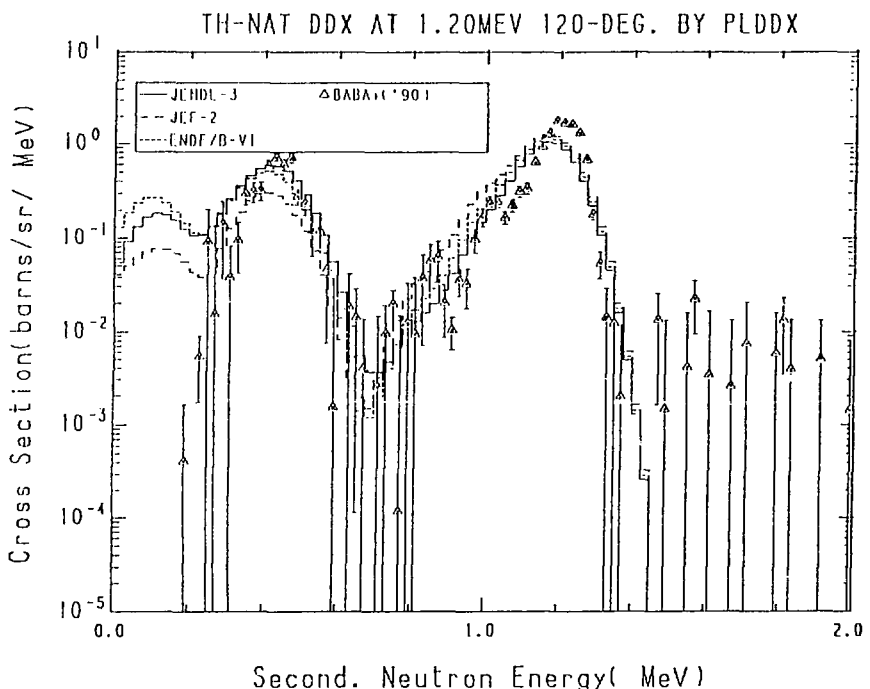


Fig. 46-2 The ^{nat}Th Double Differential Cross Section at 1.20 MeV,
Emitted Angle = 120° in Laboratory System

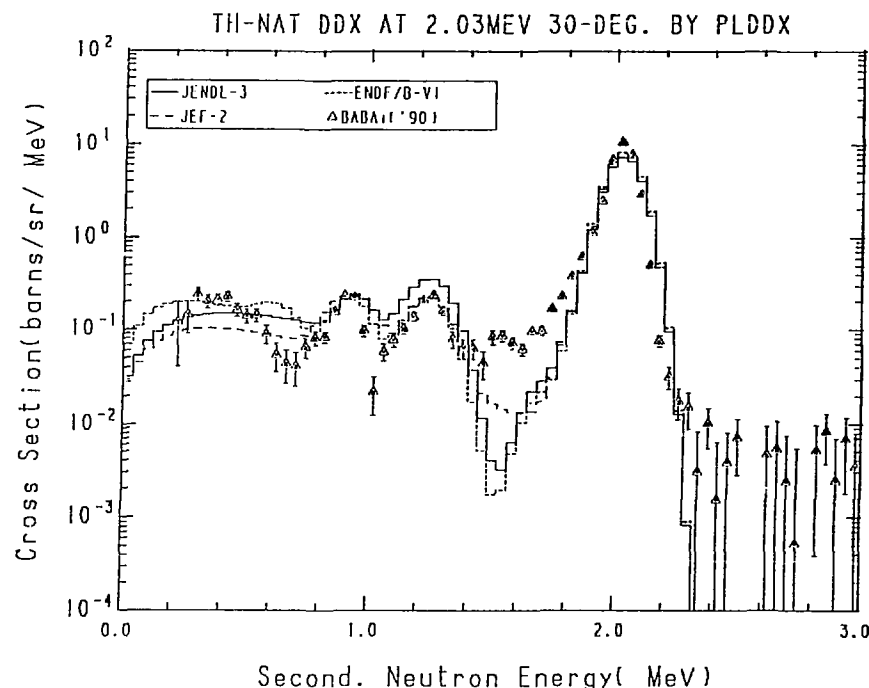


Fig. 47-1 The ^{nat}Th Double Differential Cross Section at 2.03 MeV,
Emitted Angle = 30° in Laboratory System

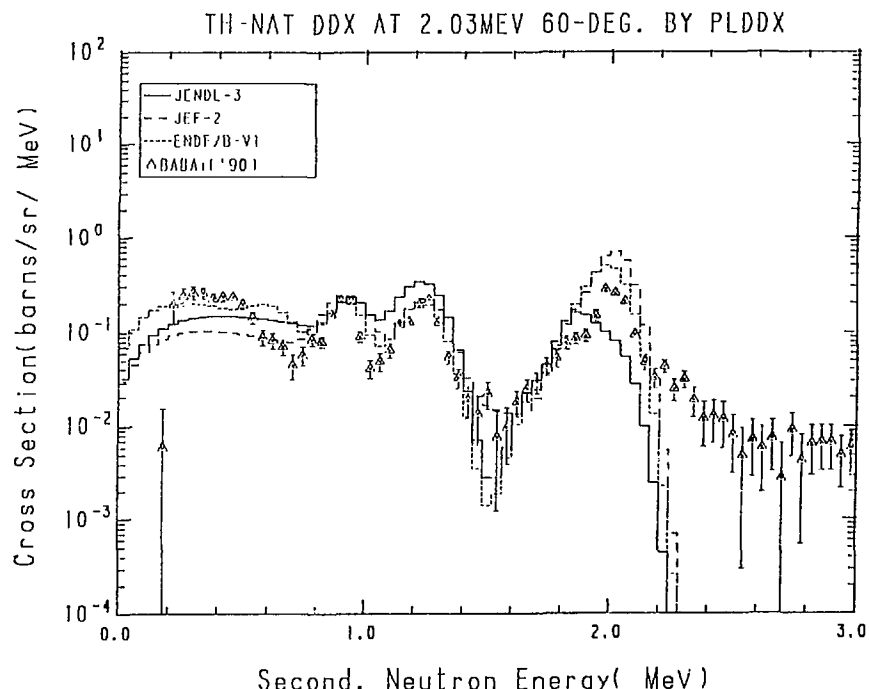


Fig. 47-2 The ^{nat}Th Double Differential Cross Section at 2.03 MeV,
Emitted Angle = 60° in Laboratory System

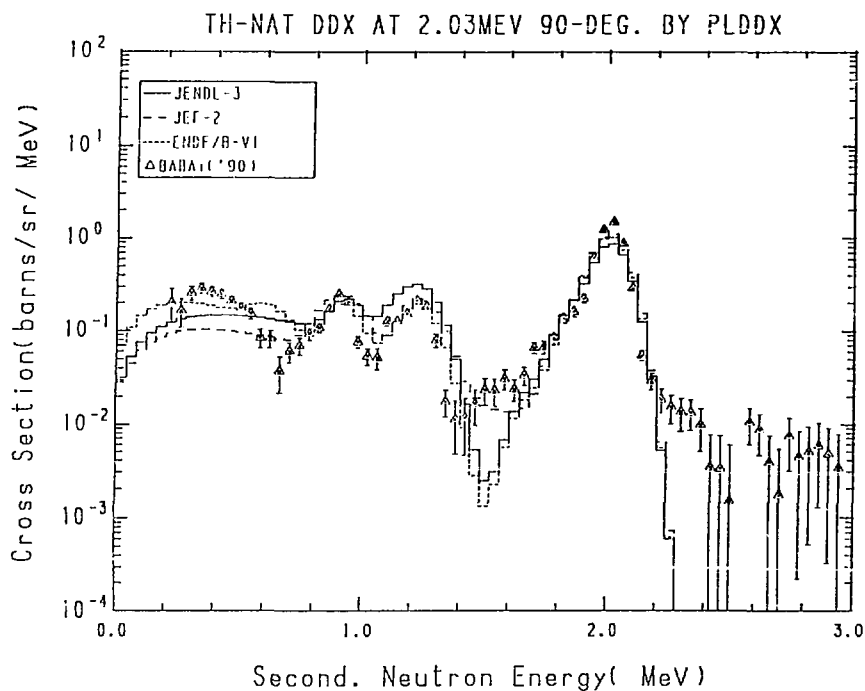


Fig. 47-3 The ^{nat}Th Double Differential Cross Section at 2.03 MeV,
Emitted Angle = 90° in Laboratory System

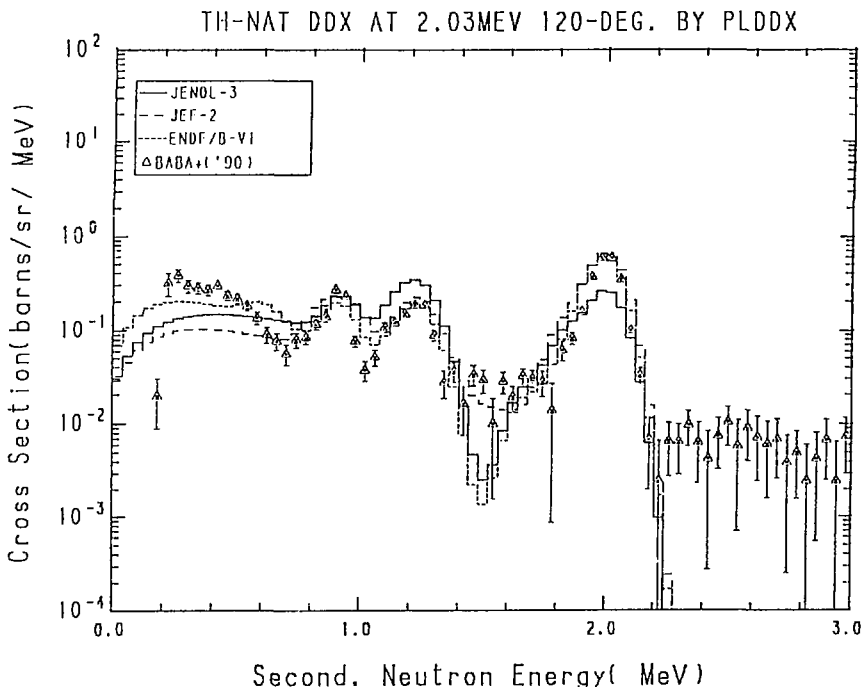


Fig. 47-4 The ^{nat}Th Double Differential Cross Section at 2.03 MeV,
Emitted Angle = 120° in Laboratory System

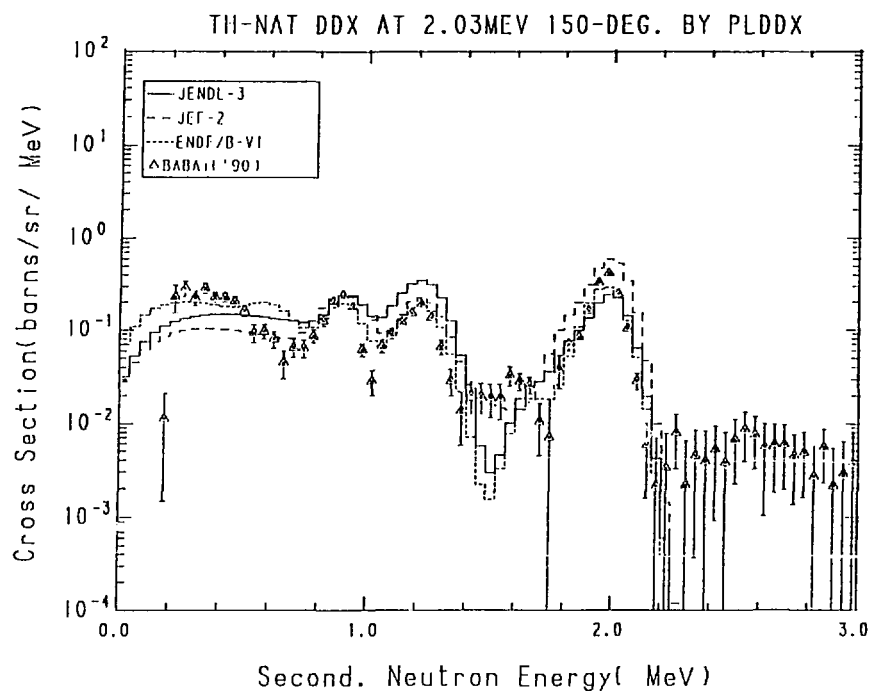


Fig. 47-5 The ^{nat}Th Double Differential Cross Section at 2.03 MeV,
Emitted Angle = 150° in Laboratory System

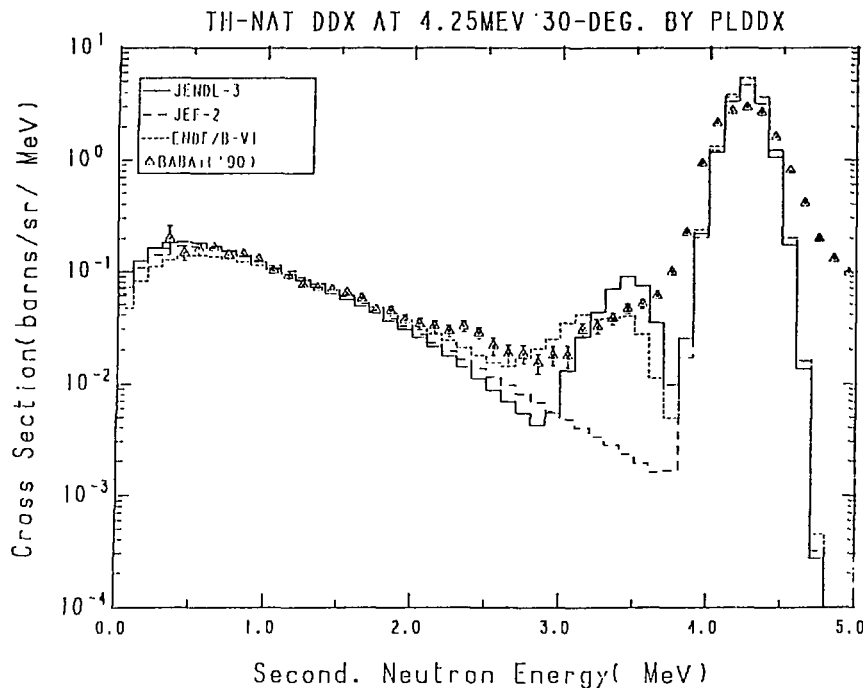


Fig. 48-1 The ^{nat}Th Double Differential Cross Section at 4.25 MeV,
Emitted Angle = 30° in Laboratory System

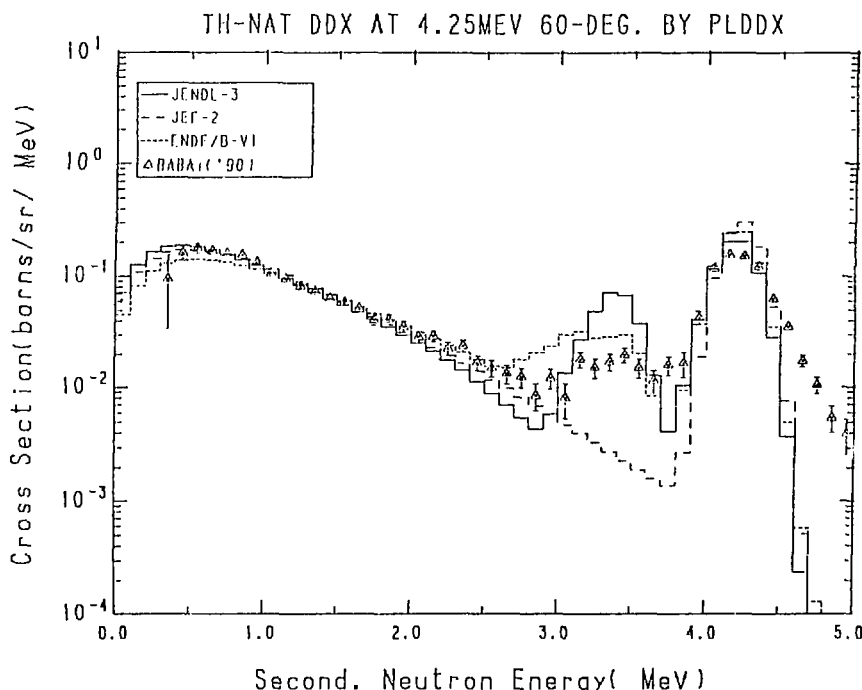


Fig. 48-2 The ^{nat}Th Double Differential Cross Section at 4.25 MeV,
Emitted Angle = 60° in Laboratory System

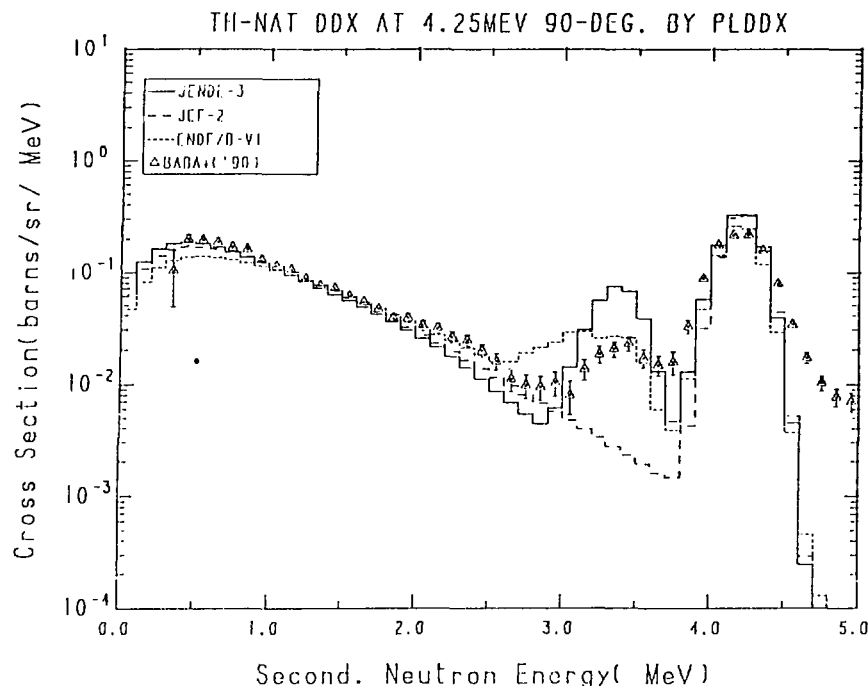


Fig. 48-3 The ^{nat}Th Double Differential Cross Section at 4.25 MeV,
Emitted Angle = 90° in Laboratory System

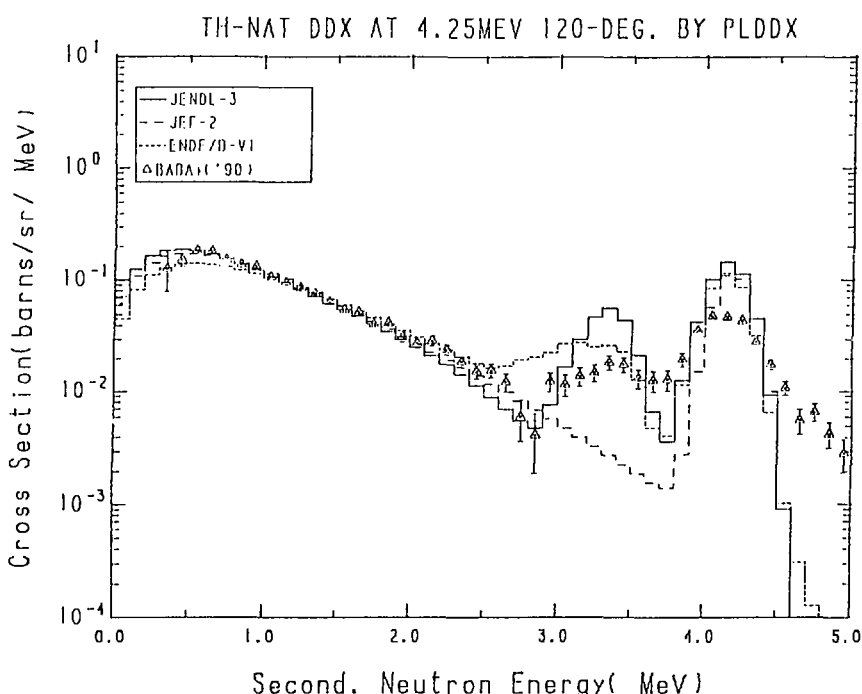


Fig. 48-4 The ^{nat}Th Double Differential Cross Section at 4.25 MeV,
Emitted Angle = 120° in Laboratory System

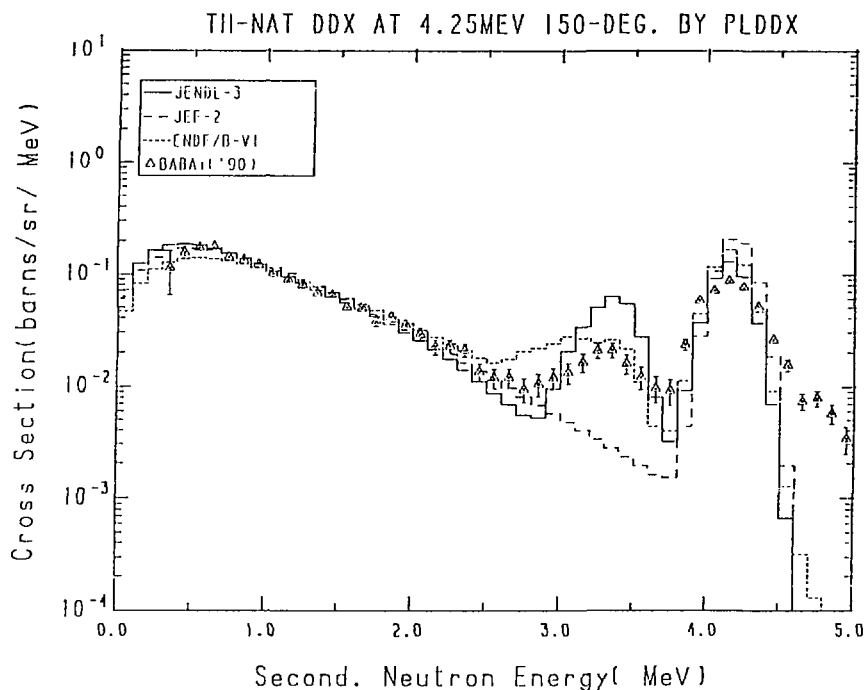


Fig. 48-5 The $n_{\text{nat}}\text{Th}$ Double Differential Cross Section at 4.25 MeV,
Emitted Angle = 150° in Laboratory System

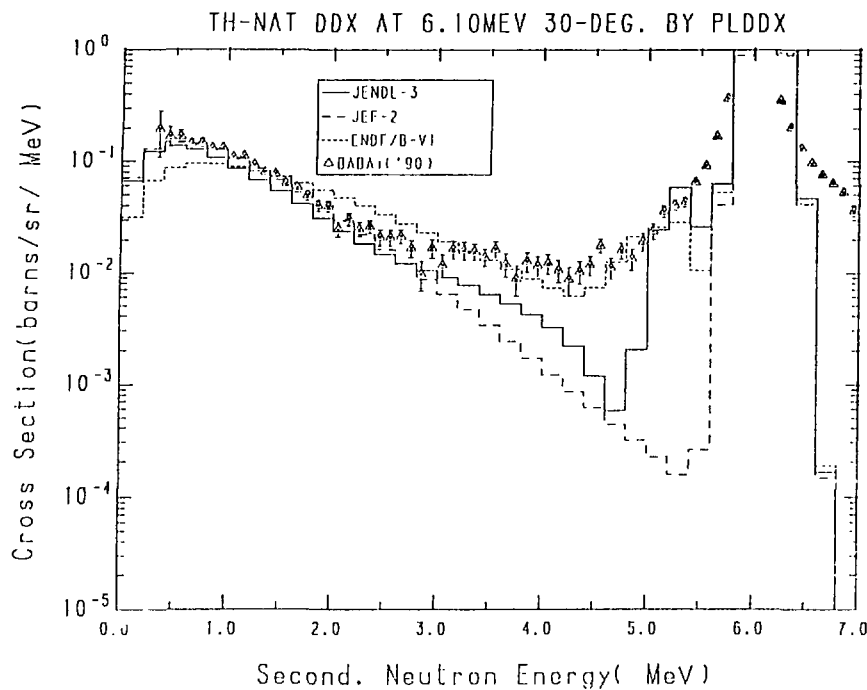


Fig. 49-1 The ^{nat}Th Double Differential Cross Section at 6.10 MeV,
Emitted Angle = 30° in Laboratory System

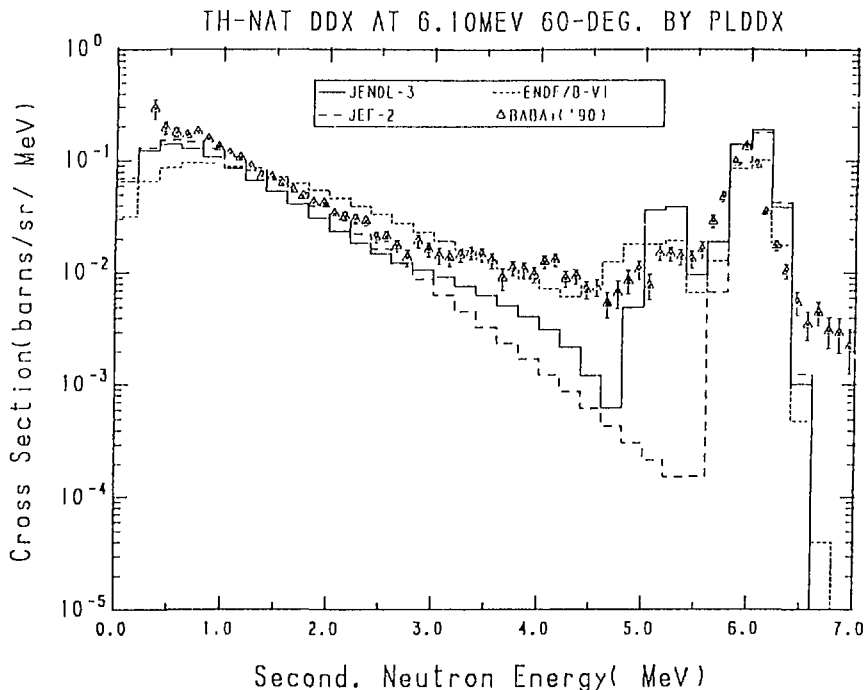


Fig. 49-2 The ^{nat}Th Double Differential Cross Section at 6.10 MeV,
Emitted Angle = 60° in Laboratory System

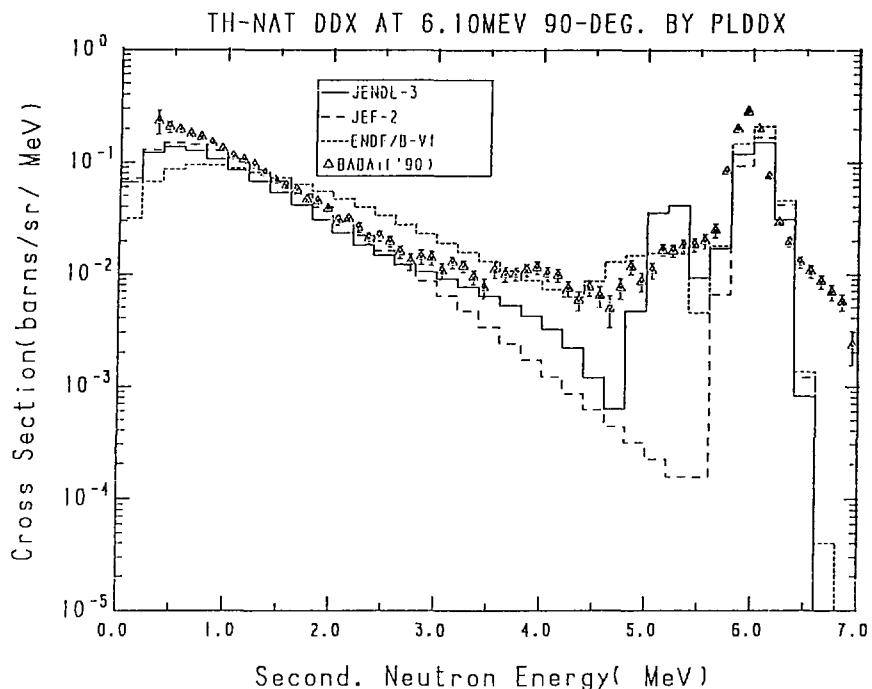


Fig. 49-3 The ^{nat}Th Double Differential Cross Section at 6.10 MeV,
Emitted Angle = 90° in Laboratory System

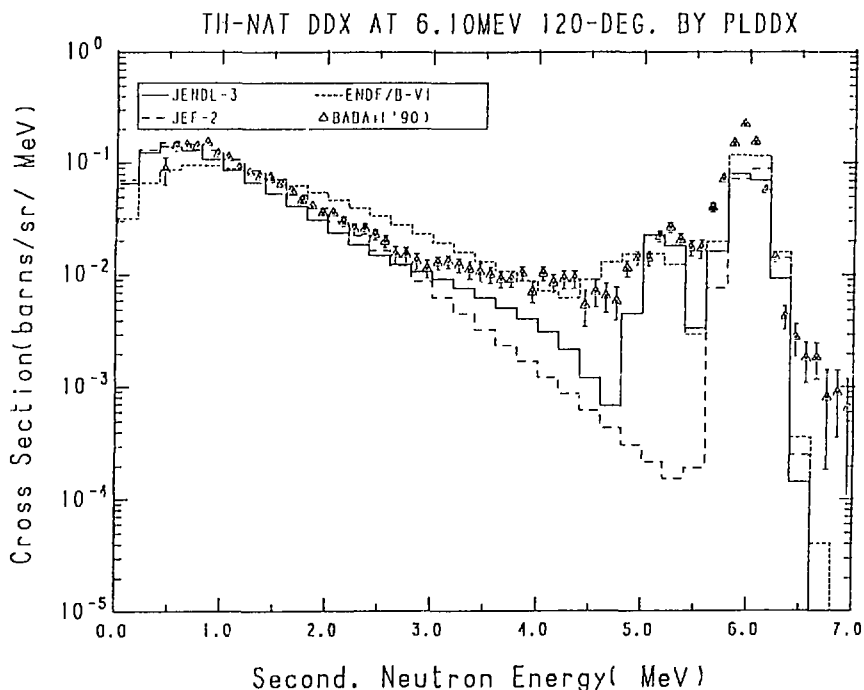


Fig. 49-4 The ^{nat}Th Double Differential Cross Section at 6.10 MeV,
Emitted Angle = 120° in Laboratory System

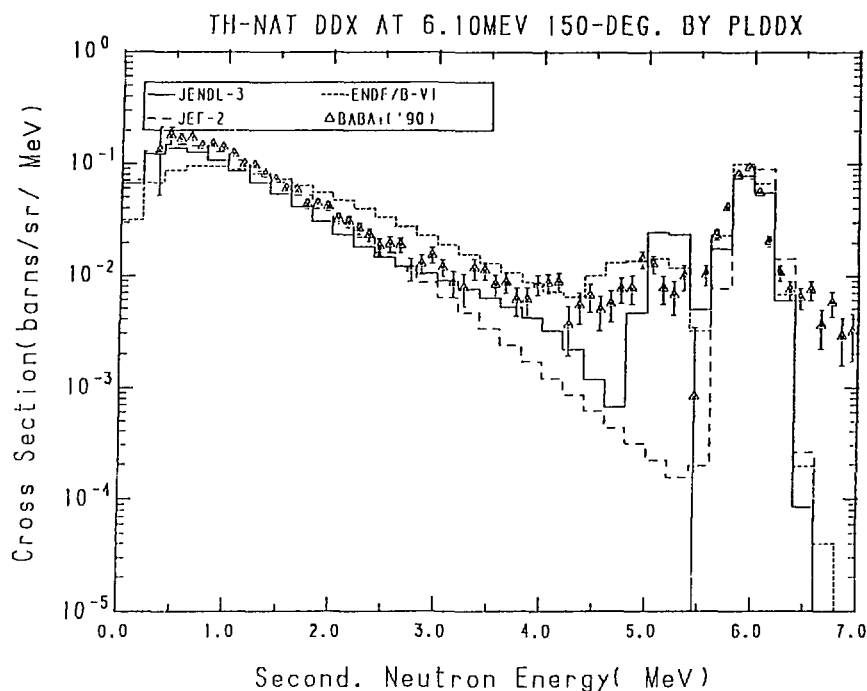


Fig. 49-5 The ^{nat}Th Double Differential Cross Section at 6.10 MeV,
Emitted Angle = 150° in Laboratory System

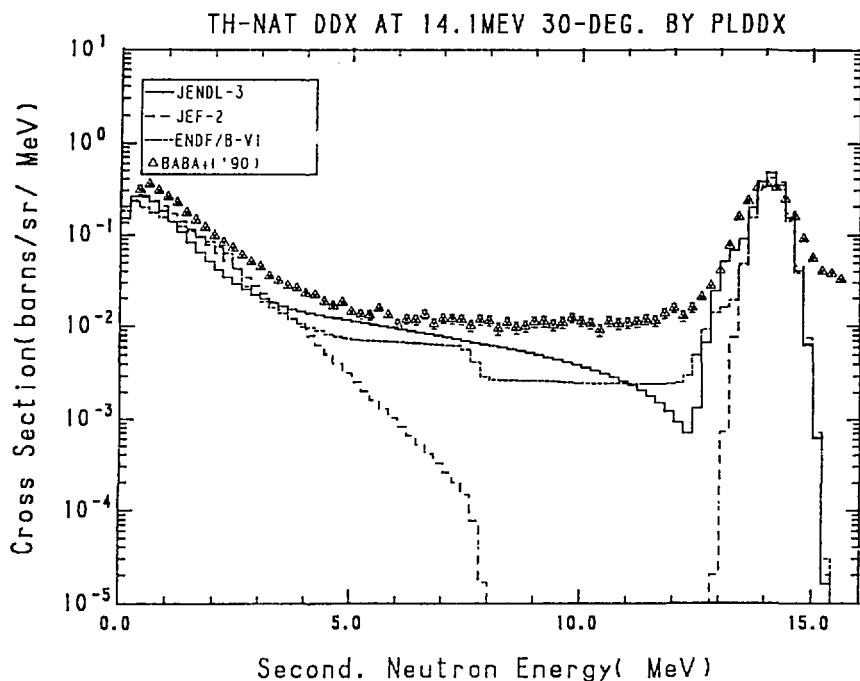


Fig. 50-1 The ^{nat}Th Double Differential Cross Section at 14.1 MeV,
Emitted Angle = 30° in Laboratory System

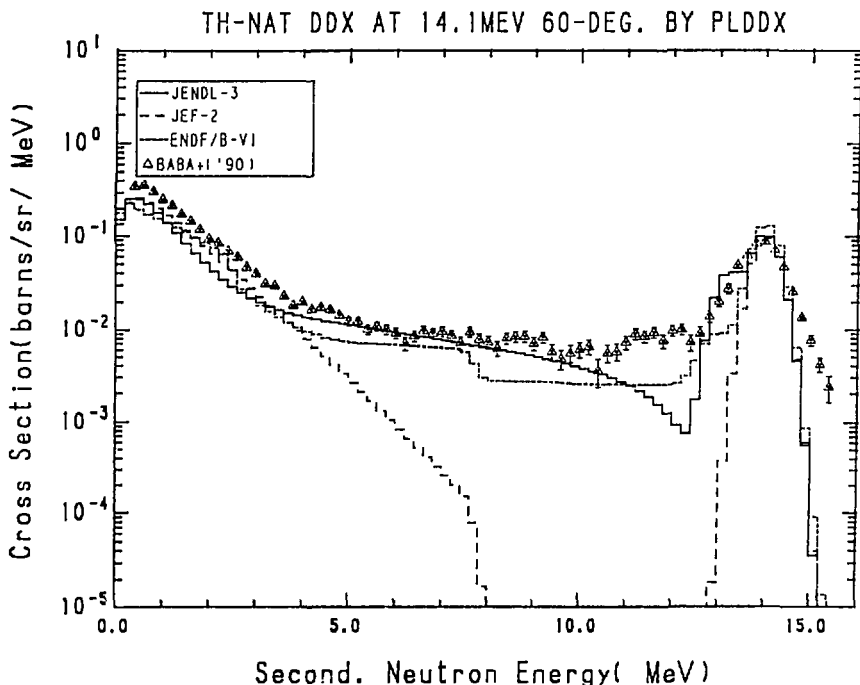


Fig. 50-2 The ^{nat}Th Double Differential Cross Section at 14.1 MeV,
Emitted Angle = 60° in Laboratory System

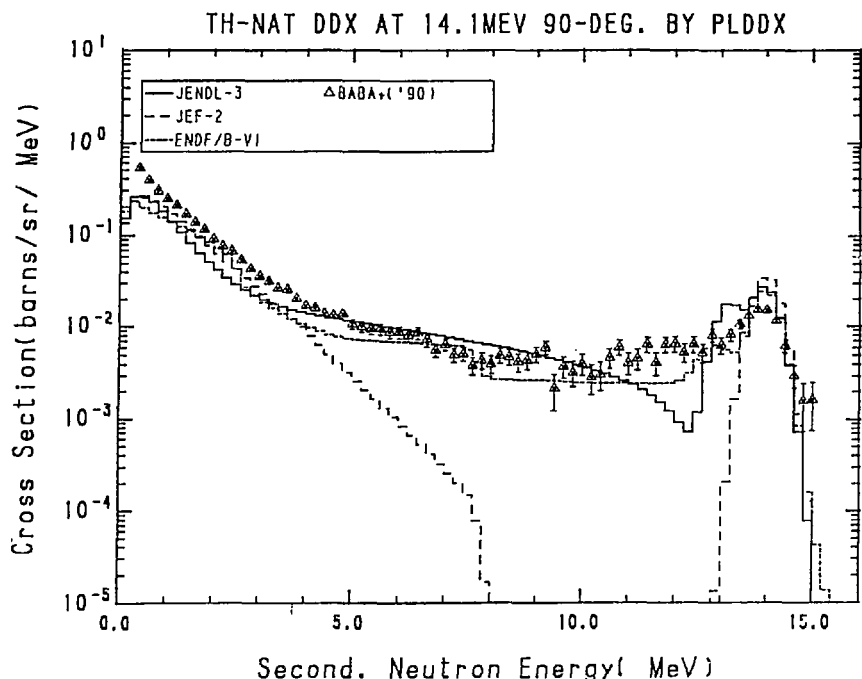


Fig. 50-3 The ^{nat}Th Double Differential Cross Section at 14.1 MeV,
Emitted Angle = 90° in Laboratory System

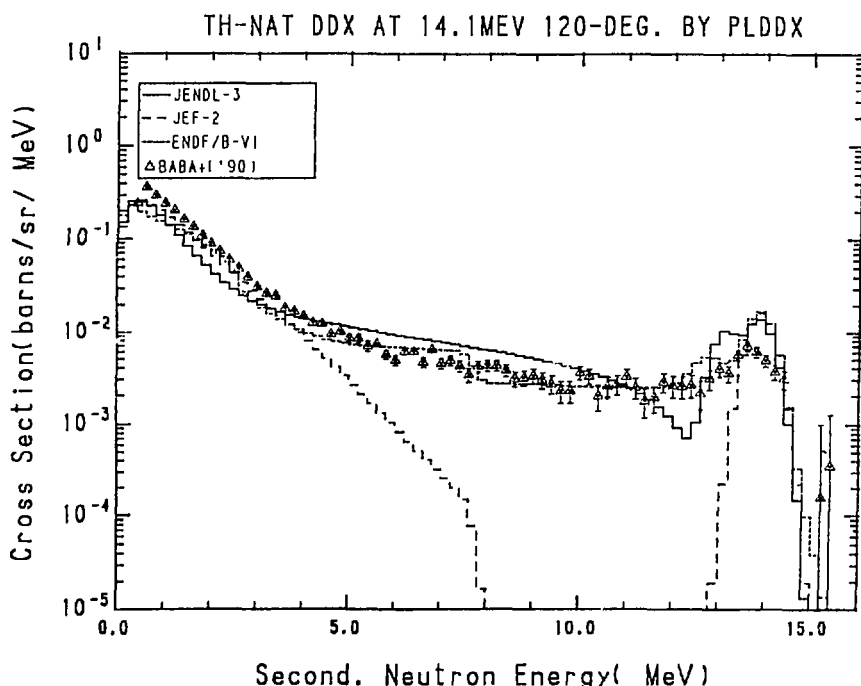


Fig. 50-4 The ^{nat}Th Double Differential Cross Section at 14.1 MeV,
Emitted Angle = 120° in Laboratory System

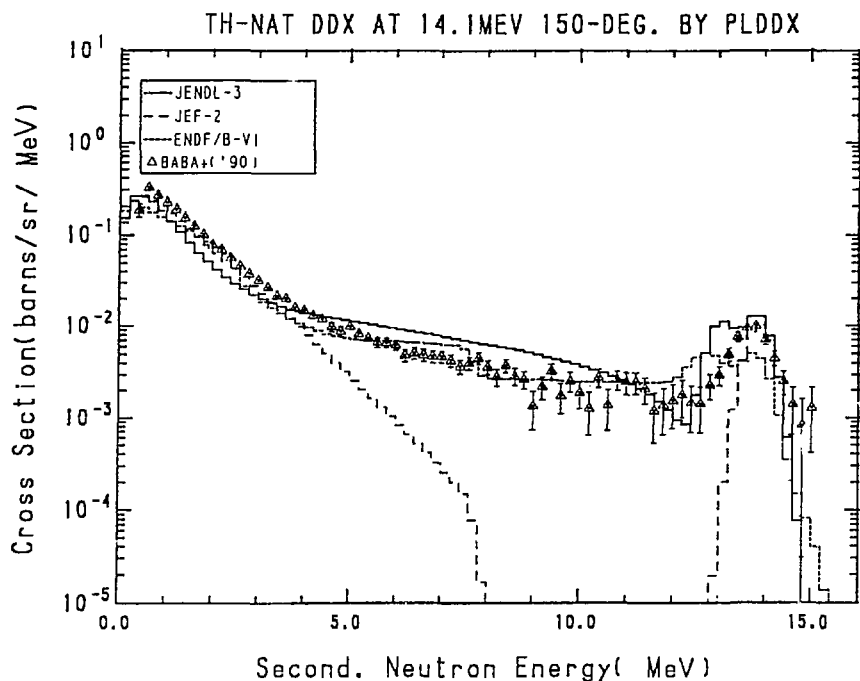


Fig. 50-5 The ^{nat}Th Double Differential Cross Section at 14.1 MeV,
Emitted Angle = 150° in Laboratory System

3.32 Uranium

The DDXs calculated from the evaluated data of ^{238}U are compared with the experimental data /BABA+('90)/ of ^{nat}U at the emitted angles of 30° , 60° , 90° , 120° and 150° at the incident neutron energy of 1.20 (60° and 120° only), 2.03, 4.25, 6.10, 14.1 MeV in Figs.51-55. The DDXs calculated from JENDL-3 include contributions of fission neutrons, except for the 1.20 MeV incident energy data. For the other evaluated libraries, however, fission neutrons could not be added to DDXs calculations for a technical reason. For the other quantities, the JEF-2 data are equivalent to the JENDL-3 data. The JENDL-3 data almost reproduce the experimental data at 1.20 and 4.25 MeV. At the incident neutron energy of 14.1 MeV, the JENDL-3 data give small values in the energy region of 5 to 12 MeV, since the energy spectrum of the continuum inelastic scattering in JENDL-3 is adopted only the evaporation spectrum. In the discrete inelastic scattering energy region, JENDL-3 gives much higher values than the experimental data. The fission tail lying in the higher energy region above the elastic scattering peak is in good agreement with the experimental data.

Reference for the Experimental Data in Figures

BABA+('90): Baba M., Wakabayashi H., Itoh N., Maeda K. and Hirakawa N., JAERI-M 89-143 (1986) in Japanese.

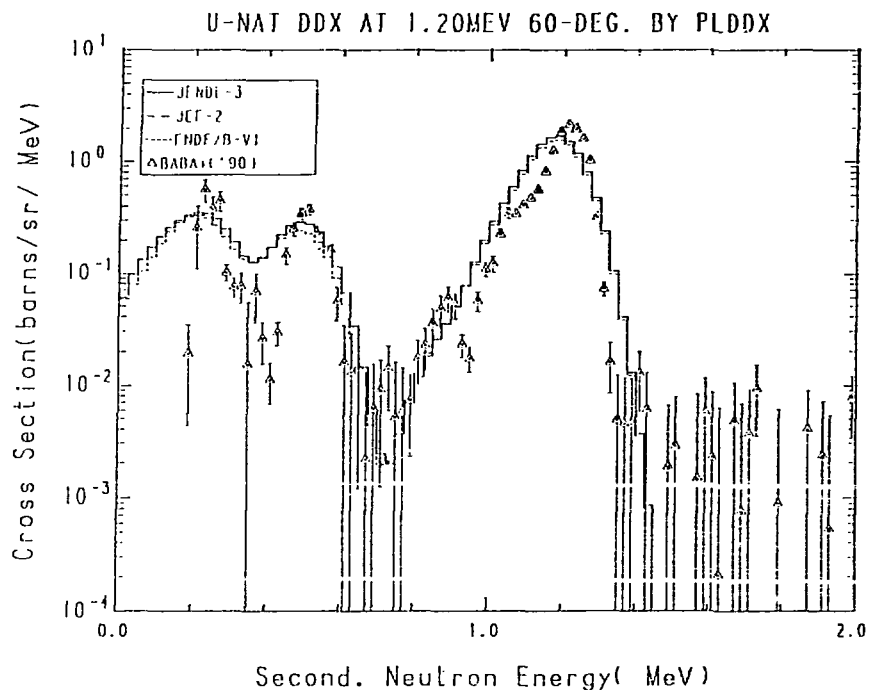


Fig. 51-1 The ^{nat}U Double Differential Cross Section at 1.20 MeV,
Emitted Angle = 60° in Laboratory System

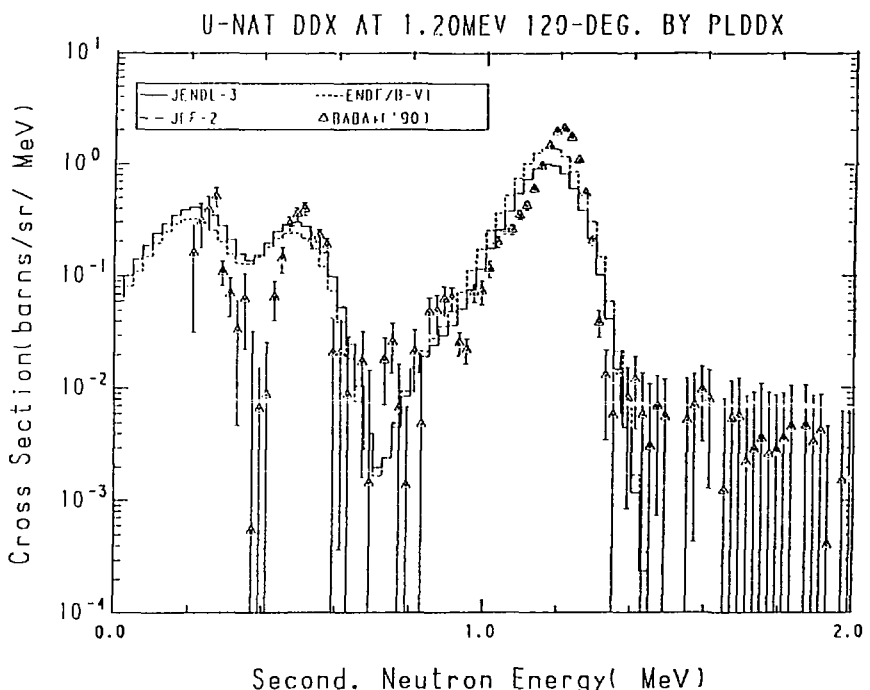


Fig. 51-2 The ^{nat}U Double Differential Cross Section at 1.20 MeV,
Emitted Angle = 120° in Laboratory System

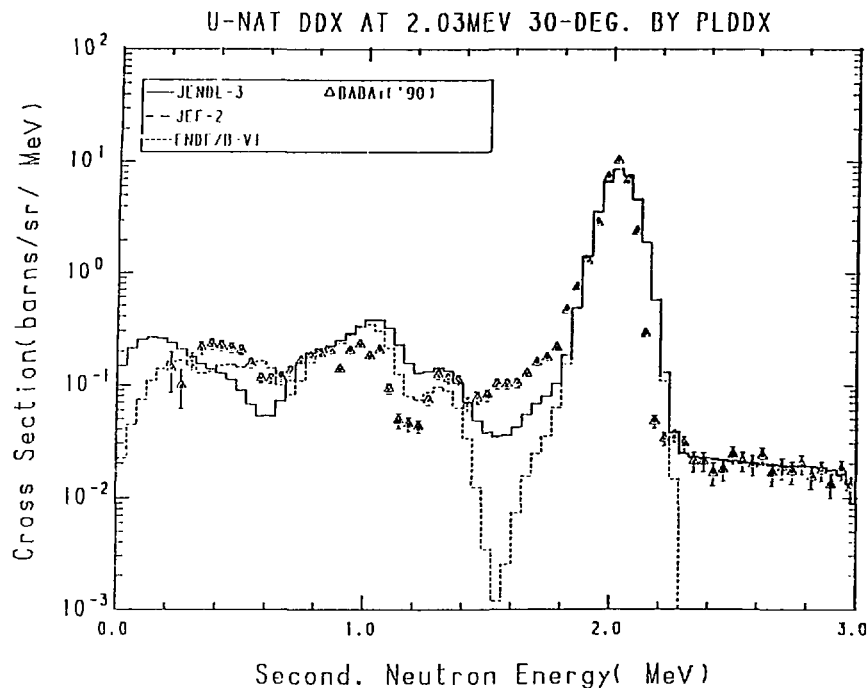


Fig. 52-1 The ^{nat}U Double Differential Cross Section at 2.03 MeV,
Emitted Angle = 30° in Laboratory System

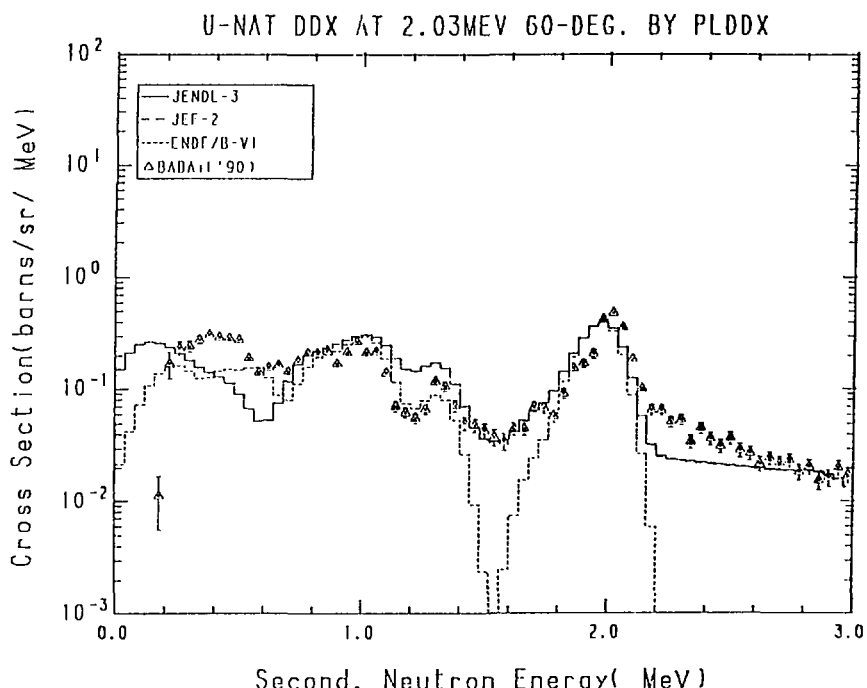


Fig. 52-2 The ^{nat}U Double Differential Cross Section at 2.03 MeV,
Emitted Angle = 60° in Laboratory System

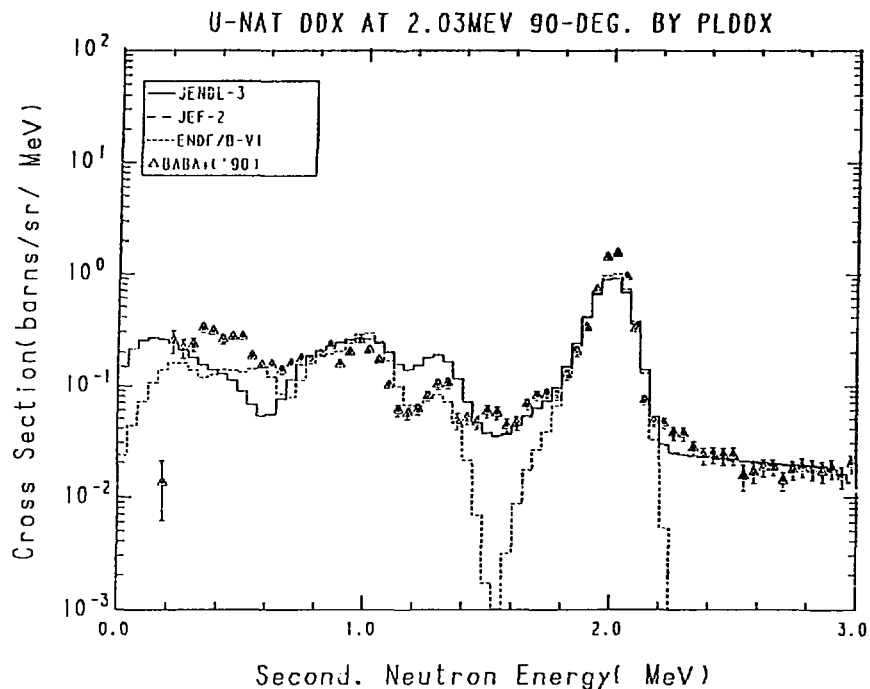


Fig. 52-3 The ^{nat}U Double Differential Cross Section at 2.03 MeV,
Emitted Angle = 90° in Laboratory System

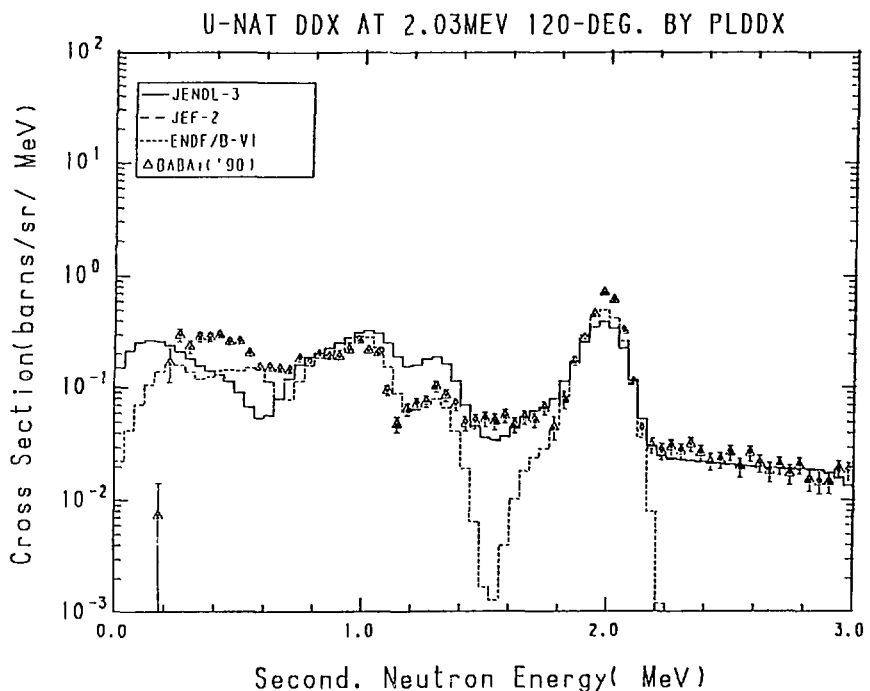


Fig. 52-4 The ^{nat}U Double Differential Cross Section at 2.03 MeV,
Emitted Angle = 120° in Laboratory System

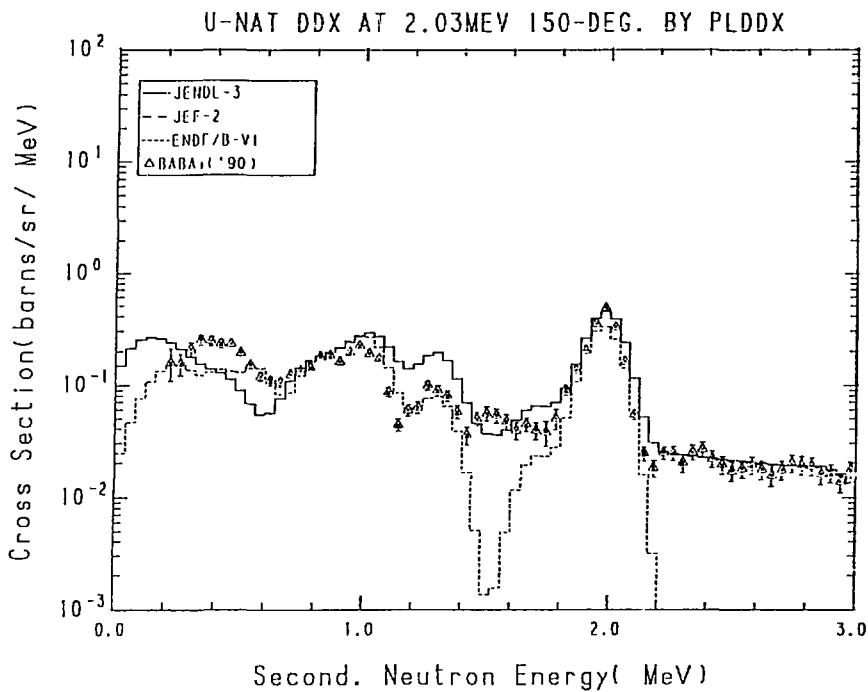


Fig. 52-5 The ^{nat}U Double Differential Cross Section at 2.03 MeV,
Emitted Angle = 150° in Laboratory System

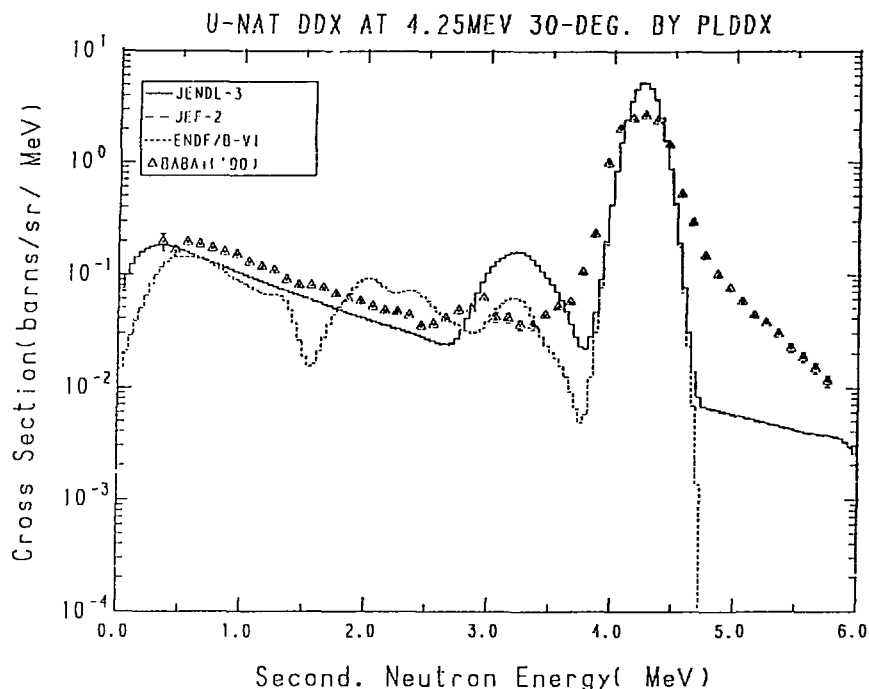


Fig. 53-1 The ^{nat}U Double Differential Cross Section at 4.25 MeV,
Emitted Angle = 30° in Laboratory System

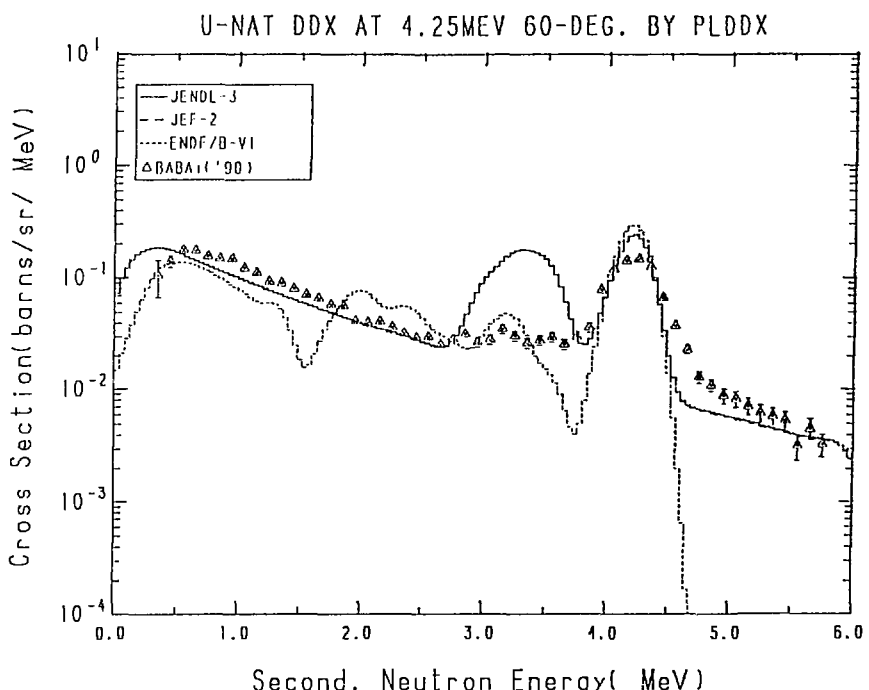


Fig. 53-2 The ^{nat}U Double Differential Cross Section at 4.25 MeV,
Emitted Angle = 60° in Laboratory System

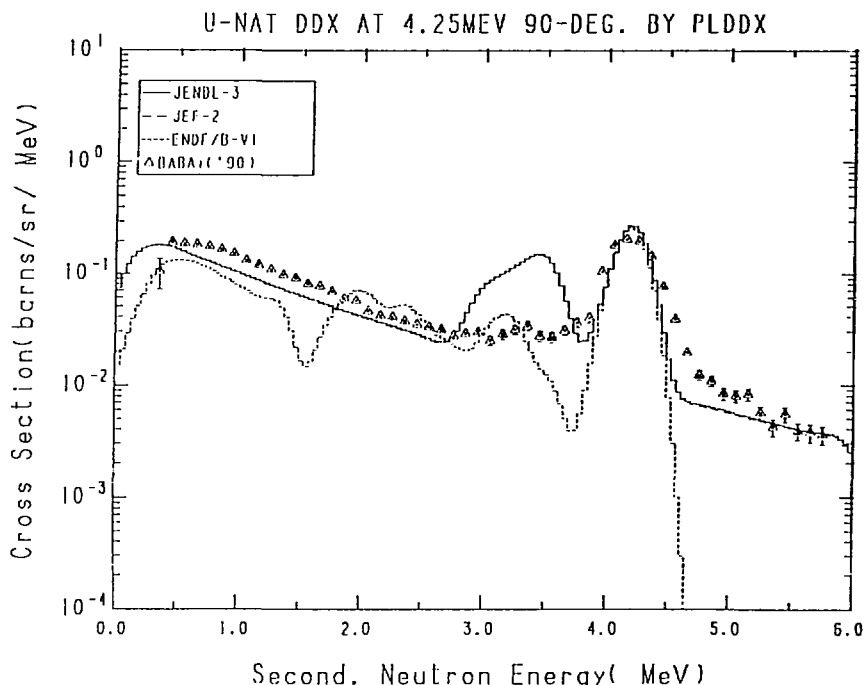


Fig. 53-3 The ^{nat}U Double Differential Cross Section at 4.25 MeV,
Emitted Angle = 90° in Laboratory System

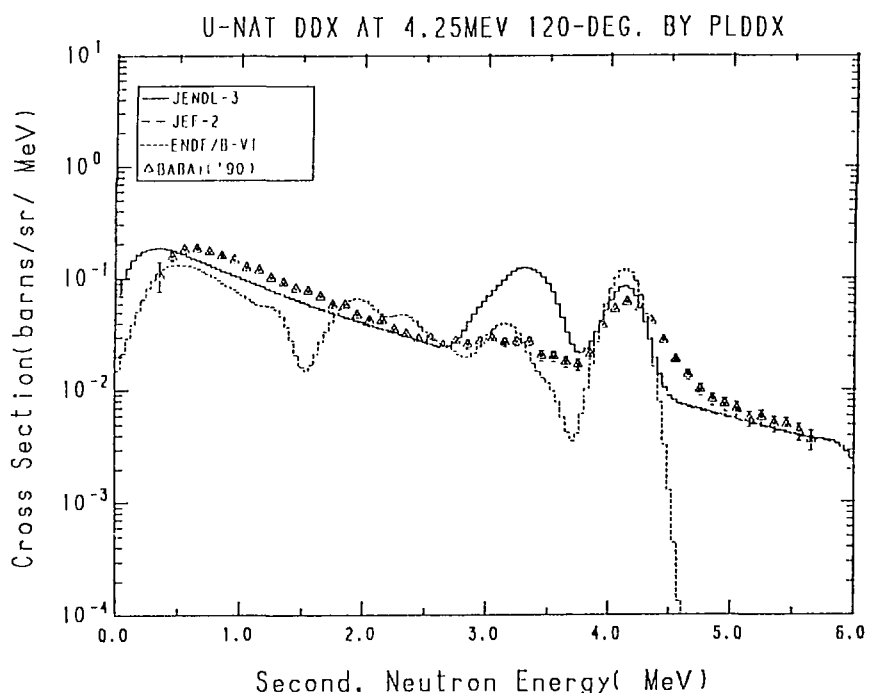


Fig. 53-4 The ^{nat}U Double Differential Cross Section at 4.25 MeV,
Emitted Angle = 120° in Laboratory System

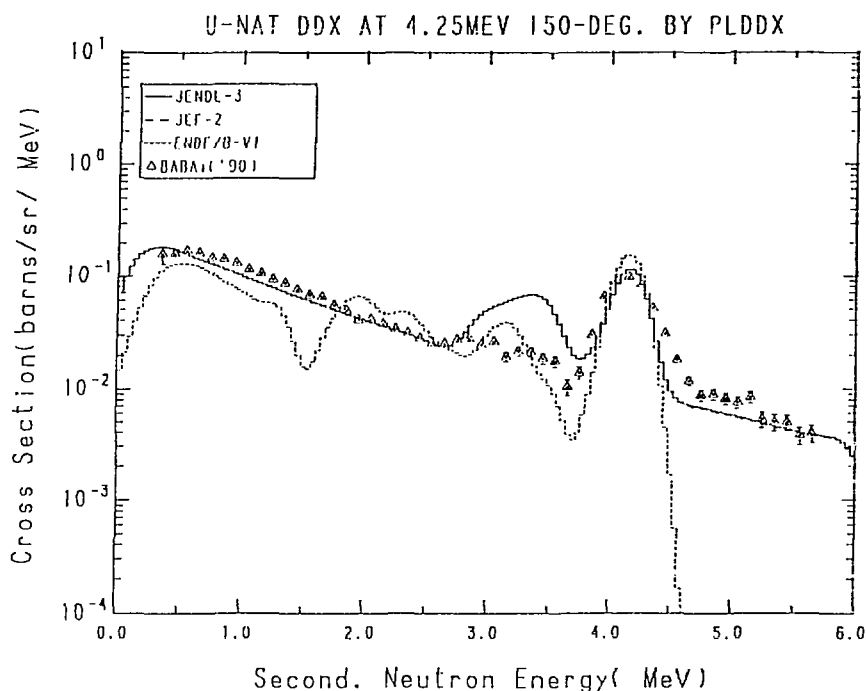


Fig. 53-5 The *nau* Double Differential Cross Section at 4.25 Mev,
Emitted Angle = 150° in Laboratory System

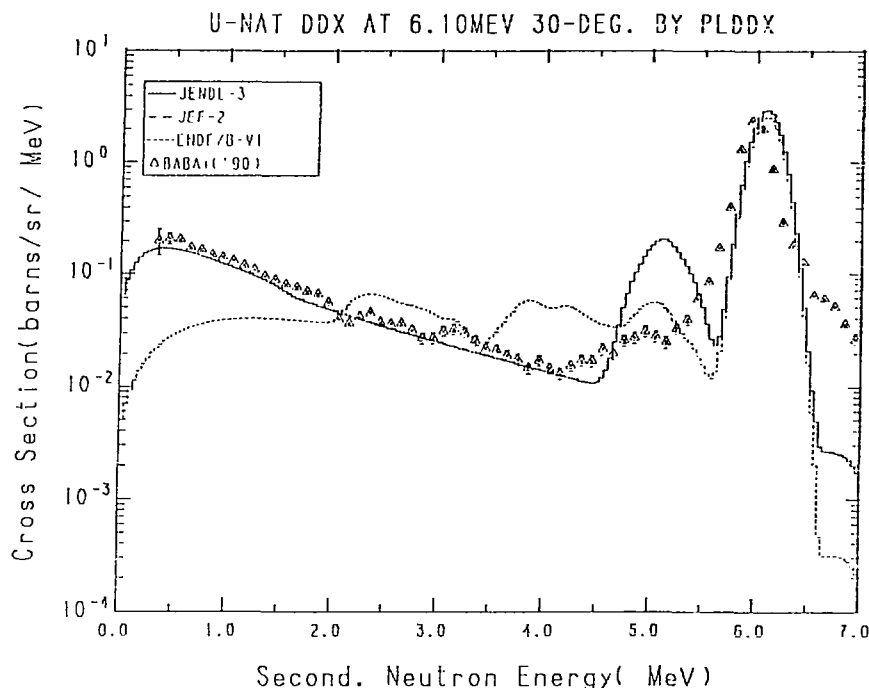


Fig. 54-1 The ^{nat}U Double Differential Cross Section at 6.10 MeV,
Emitted Angle = 30° in Laboratory System

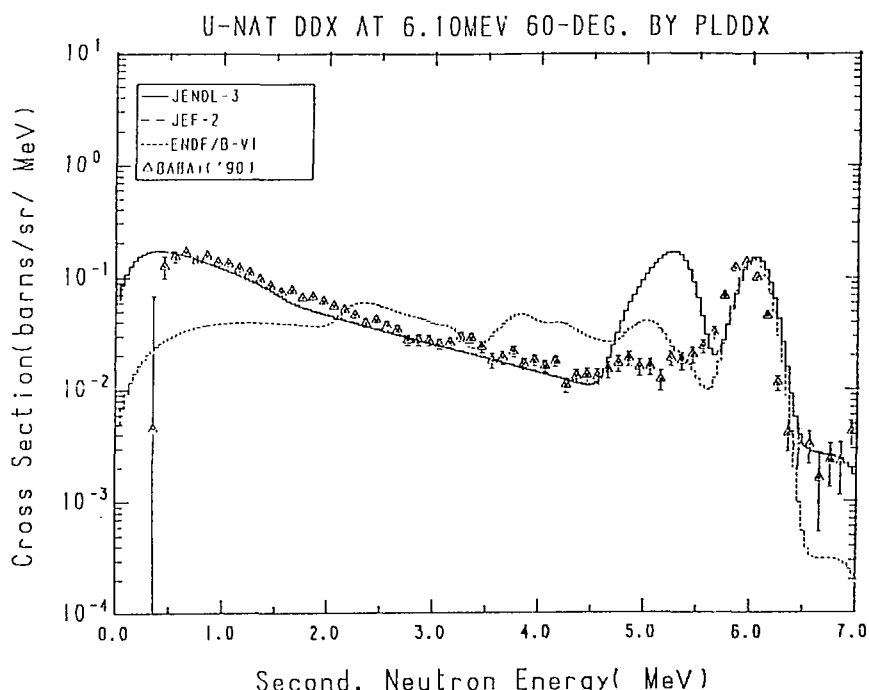


Fig. 54-2 The ^{nat}U Double Differential Cross Section at 6.10 MeV,
Emitted Angle = 60° in Laboratory System

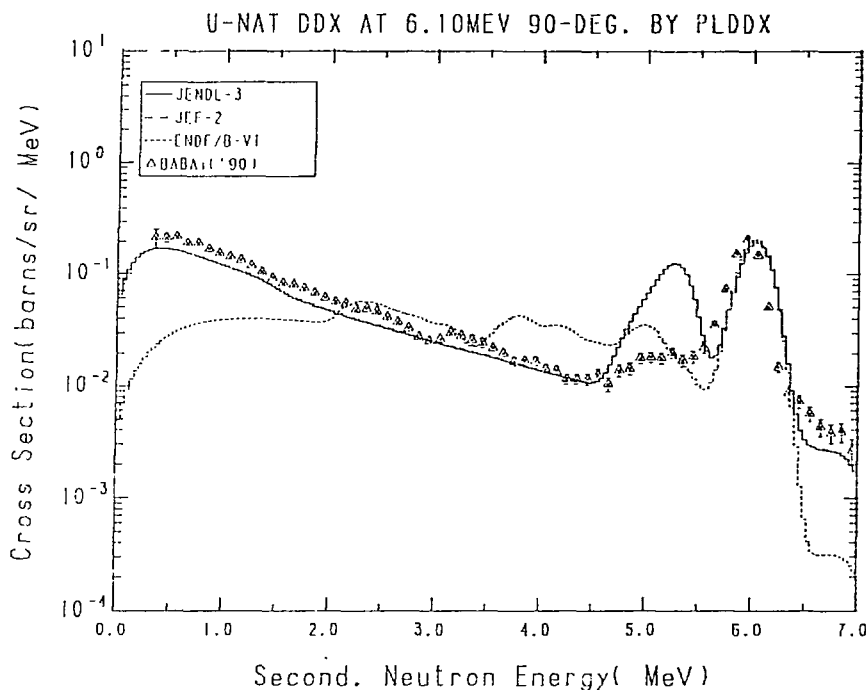


Fig. 54-3 The ^{nat}U Double Differential Cross Section at 6.10 MeV,
Emitted Angle = 90° in Laboratory System

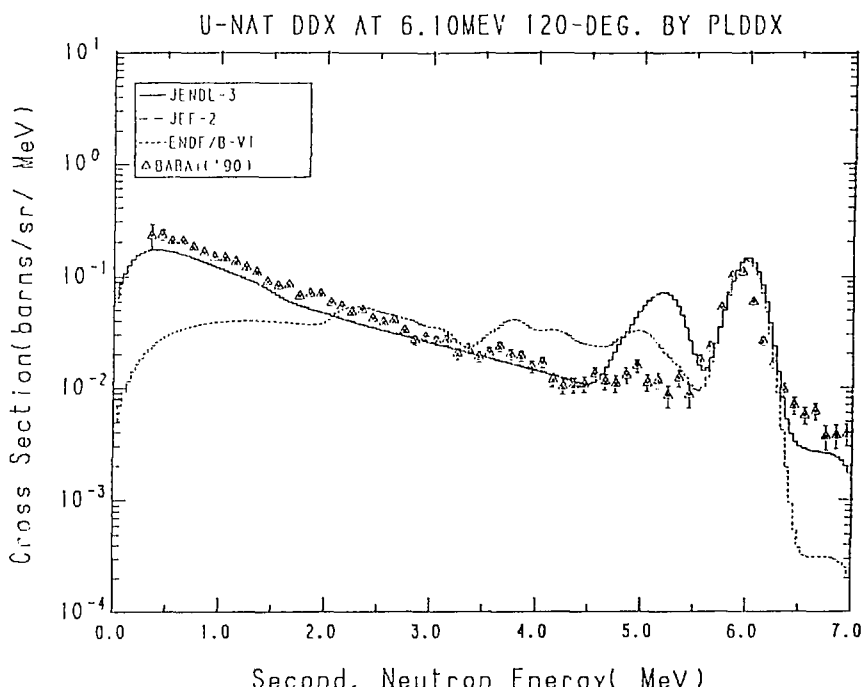


Fig. 54-4 The ^{nat}U Double Differential Cross Section at 6.10 MeV,
Emitted Angle = 120° in Laboratory System

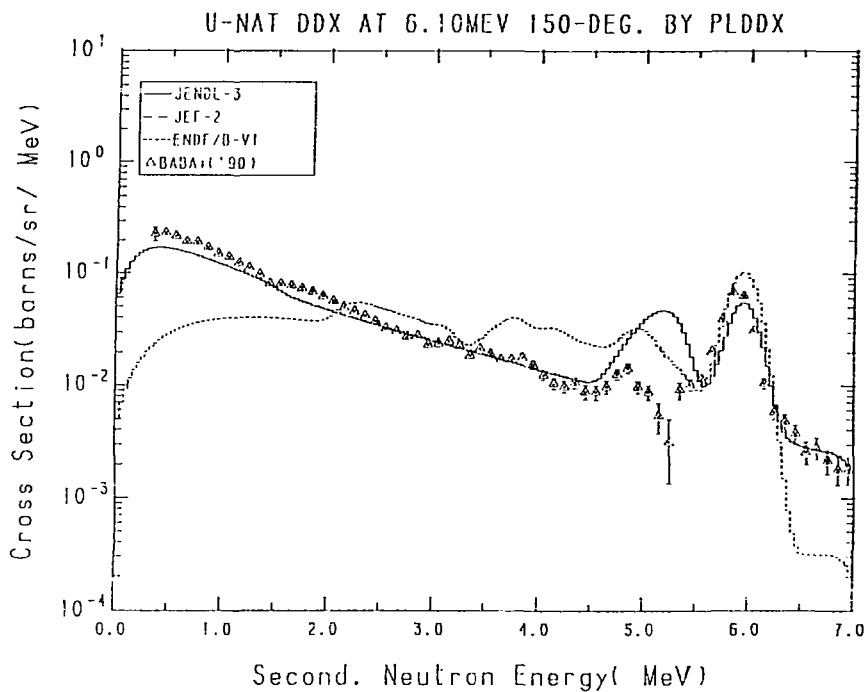


Fig. 54-5 The ^{nat}U Double Differential Cross Section at 6.10 MeV,
Emitted Angle = 150° in Laboratory System

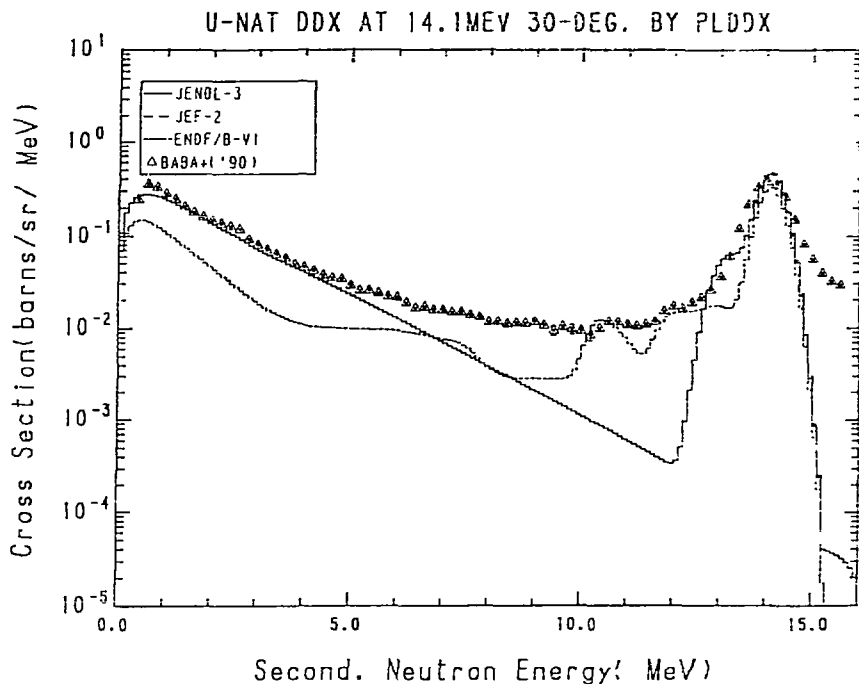


Fig. 55-1 The ^{nat}U Double Differential Cross Section at 14.1 MeV,
Emitted Angle = 30° in Laboratory System

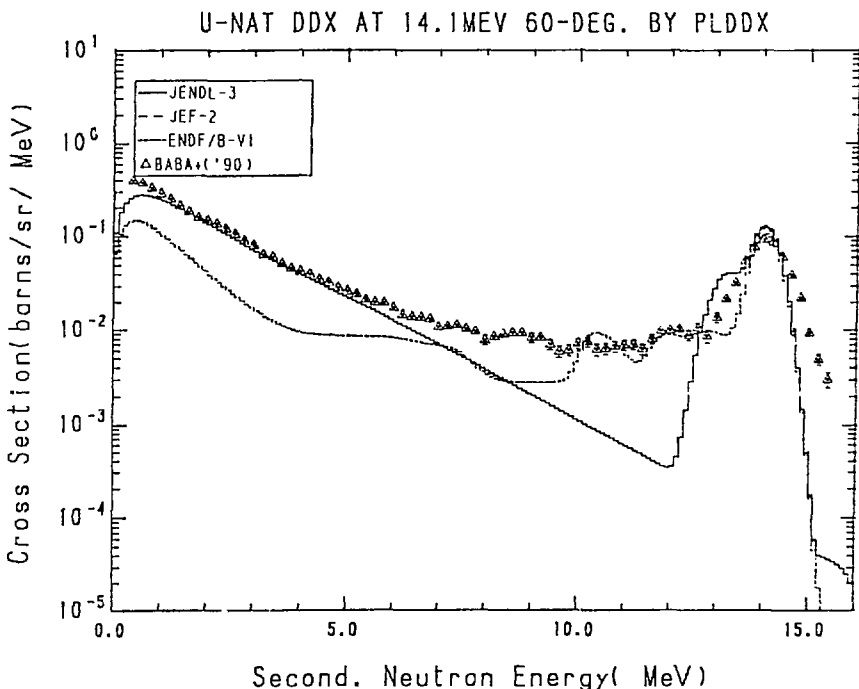


Fig. 55-2 The ^{nat}U Double Differential Cross Section at 14.1 MeV,
Emitted Angle = 60° in Laboratory System

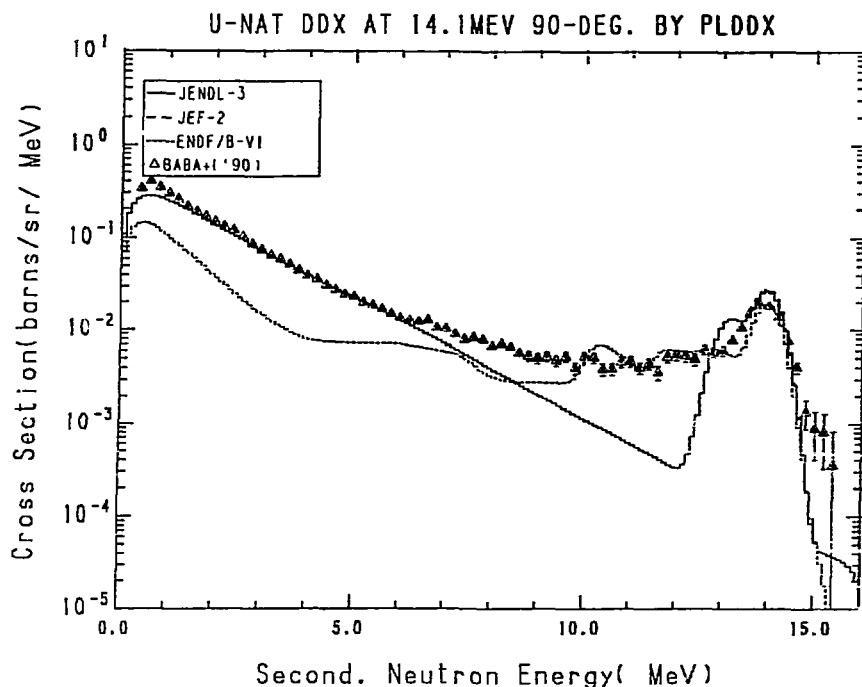


Fig. 55-3 The ^{nat}U Double Differential Cross Section at 14.1 MeV,
Emitted Angle = 90° in Laboratory System

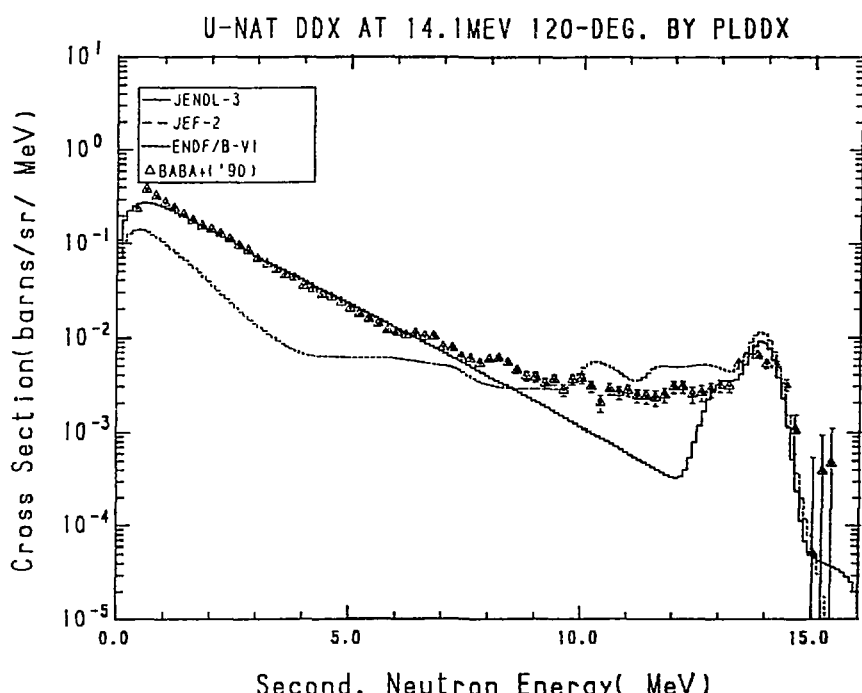


Fig. 55-4 The ^{nat}U Double Differential Cross Section at 14.1 MeV,
Emitted Angle = 120° in Laboratory System

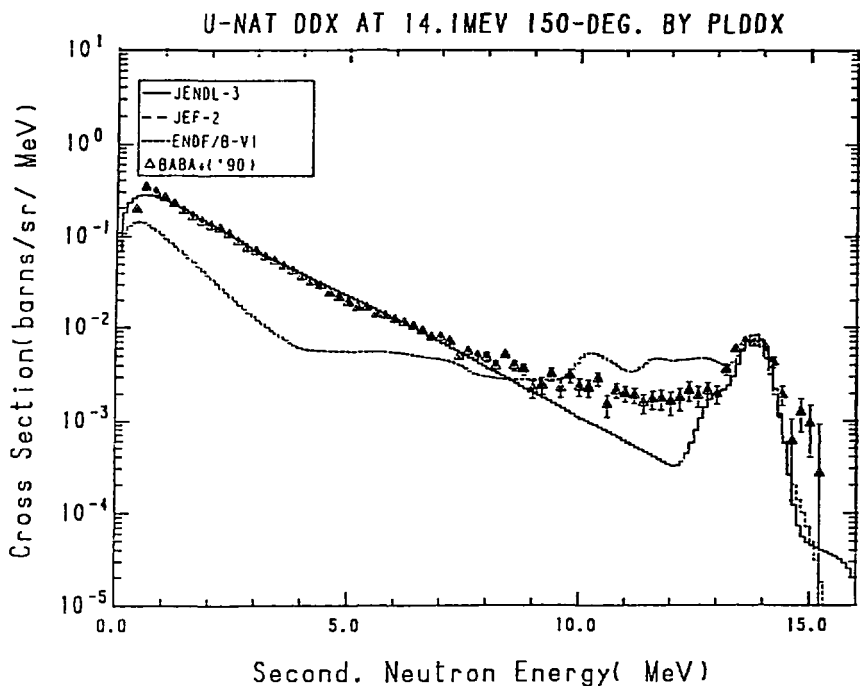


Fig. 55-5 The ^{nat}U Double Differential Cross Section at 14.1 MeV,
Emitted Angle = 150° in Laboratory System

4. Concluding Remarks

The comparisons of DDXs calculated from the evaluated data libraries with the experimental data were performed by using the PLDDX code. The considered elements and isotopes were $^{6,7}\text{Li}$, ^9Be , $^{10,11}\text{B}$, C , N , ^{16}O , ^{19}F , ^{23}Na , Mg , ^{27}Al , Si , S , Ca , Ti , V , Cr , ^{55}Mn , Fe , Co , Ni , Cu , Zr , ^{93}Nb , Mo , Sn , Sb , W , ^{181}Ta , Pb , ^{209}Bi , Th and U . The comparison could not be made for the elements of Cr , Fe , Ni , Cu , Sn , Sb , and Pb of ENDF/B-VI, and S , Cr , Ni , Sn , Sb , and W of JEF-2, since these two libraries include no data for the natural elements and there exists no processing code which can create those data easily. The fission spectra are included in only the DDXs for uranium of JENDL-3, since the PLDDX code can convert only the probability distribution and Watt-type formula of the fission spectrum. Further improvement is necessary to solve the above problems.

The comparisons gave important information on the evaluated data of JENDL-3. The discrepancies between the experimental data and the JENDL-3 data are summarized as following:

- 1) ^9Be : At the backward angles, a 'shoulder' appears above the elastic scattering peak in the DDXs calculated from JENDL-3. In JENDL-3, the continuum ($n, 2n$) neutron spectrum is given in MF=5, which cannot take account of the energy-angle correlation. Although it is shown that the data given in JENDL-3 can reproduce the overall trend of DDX for ^9Be , drawbacks of not employing MF=6 become clear.
- 2) ^{11}B : The JENDL-3 data give lower values than the experimental data in the energy region below 2 MeV.
- 3) ^{16}O : In the case of 18.0 MeV, the JENDL-3 data give smaller values below 4 MeV at the backward angles, and are significantly lower than the experimental data just below the second peak.
- 4) ^{19}F : In the discrete inelastic scattering region, the JENDL-3 data underestimate the DDX significantly, since the direct process is not considered in JENDL-3. In the low energy region, the JENDL-3 data have tendency of overestimation at the backward angles.
- 5) ^{23}Na : The JENDL-3 data tend to overestimate the DDXs in the low energy region at the backward angles.
- 6) ^{nat}Mg : The JENDL-3 data tend to give large values in the low energy region at the backward angles, and give a 'shoulder' above the elastic scattering peak due to the same reason of ^9Be .

- 7) ^{27}Al : The JENDL-3 data give smaller values in the middle energy region at the forward angles at 14.1 MeV and of all the angles at 18.0 MeV.
- 8) ^{nat}Si : The JENDL-3 data give small values at 30° in the lower energy region.
- 9) ^{nat}S : In the lower energy region, the JENDL-3 data give small values below 4 MeV.
- 10) ^{nat}Ca : The JENDL-3 data tend to overestimate the continuous spectra at the backward angles.
- 11) ^{nat}Ti : In the low energy region, the JENDL-3 data give large values at 150° .
- 12) ^{51}V : The JENDL-3 data give much higher values than the experimental data in the elastic and discrete inelastic scattering regions at the backward angles.
- 13) ^{nat}Cr : The JENDL-3 data give smaller values in the low energy region at 60° and 80° , and larger values in the 4-9 MeV region at 150° .
- 14) ^{55}Mn : The JENDL-3 data underestimate the experimental data in the energy region from 3 to 11 MeV at the forward angles.
- 15) ^{nat}Fe : The JENDL-3 data tend to underestimate the experimental data slightly at the forward angles and to overestimate them at the backward angles in the middle energy region of secondary neutrons.
- 16) ^{59}Co : The JENDL-3 data overestimate the experimental data in the discrete inelastic scattering region of all the angles and in the middle energy region at the backward angles.
- 17) ^{nat}Ni : At 14.1 MeV, the JENDL-3 data slightly overestimate the experimental data in the 5-10 MeV region at the backward angles, and underestimate them below 5 MeV at the forward angles. At 18.0 MeV, the JENDL-3 data are significantly lower than the experimental data at 30° .
- 18) ^{nat}Zr : Since the direct process of the inelastic scattering is not considered in JENDL-3, the DDXs calculated from JENDL-3 give small values in the energy region just below the peak of the elastic scattering. In the middle energy region, the JENDL-3 data tend to be overestimated at the backward angles.
- 19) ^{nat}Mo : In the energy region just below the elastic scattering peak, the JENDL-3 data cannot reproduce the experimental data, since the direct inelastic process is not considered. The JENDL-3 data are smaller than the experimental data in the energy region from 5 to 10 MeV at the forward angles.

- 20) ^{nat}Sn : Since JENDL-3 did not consider the direct process to the discrete inelastic scattering, the JENDL-3 data are smaller than the experimental data in the discrete inelastic scattering energy region just below the elastic scattering peak.
- 21) ^{nat}Sb : The JENDL-3 data give small values in the discrete inelastic scattering region, since the direct process of the inelastic scattering is not considered in JENDL-3.
- 22) ^{181}Ta : The JENDL-3 data underestimate the experimental data in the energy region of the discrete inelastic scattering and of 5-10 MeV.
- 23) ^{nat}W : The JENDL-3 data have a strange step around 6 MeV.
- 24) ^{nat}Pb : The JENDL-3 data overestimate the experimental data in the discrete inelastic scattering region just below the elastic scattering peak at the backward angles and underestimate in the middle energy region at the forward angles.
- 25) ^{209}Bi : The JENDL-3 data cannot reproduce the third peak around 10 MeV appeared in the experimental data and below 1 MeV.
- 26) ^{232}Th : The JENDL-3 data cannot reproduce the second peak of the experimental data continuing the elastic scattering peak at the backward angles.
- 27) ^{238}U : At the incident neutron energy of 14.1 MeV, the JENDL-3 data give small values in the energy region of 5 to 12 MeV, since the energy spectrum of the continuum inelastic scattering in JENDL-3 is adopted only the evaporation spectrum. In the discrete inelastic scattering energy region, the JENDL-3 data give much higher values than the experimental data.

The discrepancies between the experimental data and the JENDL-3 data described above are mainly caused by two reasons: 1) The direct process of the discrete inelastic scattering is not considered. 2) The energy-angle correlation cannot be included in JENDL-3, since the ENDF-5 format is adopted. They will be improved in the JENDL Fusion File which is one of the JENDL special purpose files, and the file will be adopted to the 'JENDL-3.2'. The authors wish they are useful to many evaluators and users of the evaluated data.

Acknowledgements

The authors would like to thank to Dr. A. Takahashi of Osaka university, Dr. M. Baba of Tohoku university, and the members of these groups to support collecting their experimental data.

References

- 1) Shibata K., Nakagawa T., Asami T., Fukahori T., Narita T., Chiba S., Mizumoto M., Hasegawa A., Kikuchi Y., Nakajima Y. and Igarasi S., JAERI-1319, (1990).
- 2) BNL/NNDC, ENDF/B-VI (1990).
- 3) NEA/Data Bank, JEF-2 (1991).
- 4) Nakagawa T., JAERI-M 9499 (1981) (in Japanese).

Appendix: Brief Manual of Code 'PLDDX'

I. Functions of PLDDX

The code PLDDX has two main functions. One is to read evaluated data in an ENDF-4, -5 or -6 format file, to calculate an energy differential (EDX) or double differential cross section (DDX) at an incident energy and an outgoing angle, and write it onto a disk file in the same format as MF=3 of the ENDF-5 format. The interpolation is fixed to 'histogram-type' (INT=1). The resolution broadening is considered in the secondary neutron energy, and finite timing resolution of the time-of-flight experiments is also taken into account. The latter is expressed by a resolution function of a Gaussian form with a width which varies with the secondary neutron energy. The other function of this code is to read in experimental EDX or DDX data stored in the EXFOR-type format, and write them onto a disk file in a special format called 'transmission format'. In order to compare several kinds of data in the same graph, a common factor can be multiplied to the calculated and experimental data. Within a job, this code can be used repeatedly to produce EDX or DDX of several incident energies and outgoing angles, or to retrieve several sets of experimental data.

At present, this code has two limitations. First, it cannot take account of the finite incident energy spread. Secondly, it cannot deal with some of the fission spectra expressed by simple functions. The former drawback can be covered up approximately by using this code at several incident energies inside the incident energy resolution, and sum up those results by CRECTJ5 code taking a proper weighting function. In the same manner, effects of the finite angular resolution can be dealt with if it is necessary.

II. Input and Output Files

Unit 1 : The ENDF-4, -5 or -6 format file for input, required if N and MAT in card n+3 are given.

Unit 2 : The EXFOR-type EDX or DDX data file for input, required if SUBE in card n+2 is given.

Unit 11 : The ENDF-5 format file for output of calculated EDX or DDX.

Unit 12 : A transmission format file for output of experimental EDX or DDX.

III. Description of the Input Data

Card 1 to n-1 : Comment cards (80A1)

The number of comment cards is not restricted. A blank card indicates the end of comment cards.

Card n : E_{in} , Angle, Factor (3F10.3)

E_{in} : Incident energy in MeV. If this is 0, the job finishes.

Angle : Laboratory scattering angle in degrees. If this is greater than 180.0, an EDX is created. Otherwise, a DDX at angle 'Angle' is created.

Factor : A factor which is multiplied to the calculated and the retrieved experimental data. A default value is 1.0.

Card n+1 : E_{min} , E_{max} , dE, ES, ET (5F10.3)

E_{min} : The minimum secondary energy (MeV) of EDX or DDX to be calculated.

E_{max} : The maximum secondary energy (MeV) of EDX or DDX to be calculated.

dE : The energy interval (MeV) of calculation of EDX or DDX.

ES : Resolution of the secondary particle energy (MeV) applied to the calculated EDX or DDX. If ES = 0.0, the resolution broadening is not applied.

ET : Timing resolution of the time-of-flight experiments (ns/m) to be applied to the calculated EDX or DDX.

Note : Contributions to the calculated EDX or DDX from the energy region outside (E_{min}, E_{max}) are neglected in PLDDX, even if they do in actual experiments due to finite resolutions. So the user must take (E_{min}, E_{max}) wide enough to cover the secondary energy region which can contribute to the domain where he is interested in.

Note : ES and ET denote the standard deviation. However, user must determine these values by comparing the width of the calculated elastic scattering peak with that of the experimental data.

Card n+2 : SUBE, IZA (A8, 2X, I6)

SUBE : Subentry number of the EXFOR-type data to be retrieved from unit 2. If SUBE is left blank, the experimental data are not retrieved. In that case, the input file on unit 2 and output file on unit 12 do not have to be assigned.

IZA : 1000Z+A of the retrieved data which will be written on unit 12, where Z denotes atomic number, A the mass number.

Note : In retrieving the experimental data, PLDDX recognizes only the subentry number. The entry number has no meanings.

Note : The subentry number is recognized as a character data, so symbols of ' ' and '0' are considered to be different.

Note : The retrieved data are identified only by the IZA.

Note : The 'Q1' flag of the retrieved data is fixed to 'TOT'. Therefore, if the user retrieves several experimental data in a job, he has to change IZA subsequently to identify different data even if the data corresponds to the same Z and A.

Card n+3 : N, MAT (*)

N : The number of MT's from which the EDX or DDX is constructed. If N is greater than or equal to 100, PLDDX takes a combination of MT=2, 16, 17, 22, 24, 28, 32, 51 to 90, and 91 as a default. If N is less than 100, the user must specify the combination of MT's in the following card.

MAT : The material number given in the ENDF-type data set.

Note : If MAT is left blank, the EDX or DDX is not calculated. In that case, the input file on unit 1 and output file on unit 11 do not have to be assigned.

Card n+4 to m : (MT(i), i=1,N) (10I5)

MT(i) : The MT number of i-th reaction to be included in the calculation of EDX or DDX. For example, if the user want to make a DDX of only the (n,2n) reaction, N must be 1, and MT given on this card must be 16.

Note : This card is required only if N is less than 100.

Card m+1 to up : For the next calculation, repeat inputs from Card n. The job is terminated if $E_{in} = 0.0$ on Card n.

IV. Output Format

The calculated EDX or DDX is written onto a file assigned as the logical unit 11. It is written in the same format as the usual smooth cross section in MF=3 of the ENDF-5 format, i.e., as pairs of (energy, EDX) or (energy, DDX). Here, the energy is interpreted as the secondary particle energy in eV, and EDX is given in (barns/Sr), and DDX in (barns/Sr/MeV). The MT number of calculated DDX at an angle of θ (degrees) is determined by the following rule:

$$MT(\theta) = \text{Integer}(\frac{\theta}{2.0}) \times 10.0 + i \quad (A-1)$$

where $i = 1$ for the first calculation, 2 for the next calculation, and so forth until E_{in} becomes 0.0. In the example shown in next chapter, the DDXs are calculated at 40 and 120 deg. at 14.1 MeV in a single job. The MT number of the calculated DDX at 40 deg. is therefore $MT = \text{Integer}(40.0/2.0) \times 10 + 1 = 201$, while that of 120 deg. becomes $MT = \text{Integer}(120.0/2.0) \times 10 + 2 = 602$. If you have the third set, the MT will be $MT = \text{Integer}(0/2.0) \times 10 + 3 \dots$. The MT number of reproduced EDX is calculated by setting $\theta=0.0$ in eq. (A-1).

V. Sample JCL and Input

In the following example of JCL and input data, DDXs of ^{93}Nb are calculated at 40 and 120 deg., at an incident energy of 14.1 MeV (Fig.A-1). At the same time, two sets of experimental data at 40 and 120 deg. are retrieved. The calculated and experimental data at 120 deg. are multiplied by 0.1 in order to plot the DDXs of these two angles in a same figure. The IZA of the first experimental data set is set to 41093. On the other hand, that of the second data is artificially set to 41094 in order to be distinguished from the 40 deg. data.

In the second step of the JCL, SPLINT executes plotting of the calculated and experimental DDXs.

```

//JOBPROC DD DSN=J2608.PROCLIB.CNTL
// EXEC LMGO,LM='J4013.LOADM',PNM=PLDDX
// EXPAND DISKTO,DDN=FT01F001,DSN='J1615.JENDL303',MODE=IN
// EXPAND DISKTO,DDN=FT02F001,DSN='J4013.DDXEXPO2',
//      Q=''.DATA(OKNBDD90)',MODE=IN
// EXPAND TPDISK,DDN=FT11F001,DSN=CAL
// EXPAND TPDISK,DDN=FT12F001,DSN=EXP,RSIZE=160
//SYSIN DD *

DDX OF 93-NB AT 14.1-MEV, 40- AND 120-DEG.

    14.1      40.0      1.0
    0.0       16.0      0.2      0.5      0.5
00018005  41093
    100      3411
    14.1     120.0      0.1
    0.0       16.0      0.2      0.5      0.5
00018013  41094
    100      3411
    0.0

// EXEC SPLINT89
// EXPAND TPDISK,DDN=FT01F001,DSN=CAL,DISP=OLD
// EXPAND TPDISK,DDN=FT02F001,DSN=EXP,DISP=OLD,RSIZE=160
//SYSIN DD *

TITLE=DDX OF 93-NB AT 14.2MEV. 40- AND 120-DEG.
XTITLE=SECONDARY NEUTRON ENERGY ( MEV )
YTITLE=CROSS SECTION (B/ SR/ MEV)
XMIN=0.0,XMAX=16.0E6,XLEN=18.0
YMIN=0.0,YMAX=1.0,YLEN=12.0
DATA1,ENDF(3411,3,201),INP=1,LINE=2,NAME=JENDL-3(40-DEG.)
DATA2,ONES(41093,TOT),INP=2,SYM=0,NAME=TAKAHASHI ET AL.(40-DEG.)
DATA3,ENDF(3411,3,602),INP=1,LINE=2,NAME=JENDL-3(120-DEG.)
DATA4,ONES(41094,TOT),INP=2,SYM=0,NAME=TAKAHASHI ET AL.(120-DEG.)
DATA2,ERR=1
DATA4,ERR=1
PLOT
STOP

```

Fig.A-1 The Sample JCL and Input Data